Utilisation of metabolic resources in *Arabidopsis thaliana* suspension culture



George Dobson

Department of Biology

Linacre College

Thesis submitted for the degree of

Doctor of Philosophy

University of Oxford

Trinity Term 2023

Abstract

Appreciating the relationship between growth rate and metabolism is important for understanding plant growth dynamics in laboratory and agricultural settings. This project uses steady-state ^{13}C-metabolic flux analysis (MFA) to investigate the relationship between growth rate and flux distribution through the network of central carbon metabolism in heterotrophic cells of *Arabidopsis thaliana*.

Two different conditions were used to slow the growth rate of *Arabidopsis* cell suspension cultures; growth at mildly decreased temperatures and growth in medium supplemented with mannose. The results showed that a decreased growth temperature slowed the growth rate and induced minor alterations in flux distribution. Supplementation with mannose also slowed the growth rate and induced a more widespread rearrangement of fluxes through the central network of carbon metabolism. The effect of mannose was likely due to sequestration of inorganic phosphate as mannose 6-phosphate.

The flux solutions also showed that growth at mildly decreased temperature did not alter the relative allocation of ATP and reductant (principally, NAD(P)H) to growth and maintenance processes. In contrast, supplementation with mannose induced a significant increase in the proportion of ATP and reductant available for maintenance processes.

Slowed growth rate was associated with decreased flux through the glucose 6-phosphate dehydrogenase reaction. This effect was independent of the effect of altered allocation of ATP and reductant between growth and maintenance.

This project introduces a novel modelling approach for quantifying ATP and NAD(P)H production/utilisation in plant MFA. The results suggest that the growth rate and the allocation of resources to growth and maintenance have independent effects on the central carbon metabolism. This conclusion highlights the need to consider the general effect of altered growth rates when investigating the specific effects of imposed stress on the metabolic response of plant cell to an environmental perturbation.

Acknowledgments

If I were to thank everyone who helped me get to this point I would have an acknowledgements page as long as the thesis! But without a doubt the biggest thanks has to go to my supervisors Prof. Nicholas J. Kruger and Prof. R. George Ratcliffe. Without their support this project would have been impossible and their constant enthusiasm, support and encouragement has made them the best supervisors a student could ask for.

I would also like extend my thanks to Mr. Pedro Bota, for his technical support in my battles against the GC-MS and his stoic nature in the face of adversity. As well as to Edward Smith, who saw me through the first year of this project. I would also like to thank all the other staff and students of the biochemistry floor, the pleasant atmosphere in the department made this project considerably more enjoyable.

I owe a significant debt my parents. To my dad for his help with proof reading, to my mum for her invaluable help in making figures, and to the rest of my family for pretending they care about plant metabolism.

It would be remise to not acknowledge the impact life outside the DPhil has on the quality of work one can produce. With that in mind, I owe considerable thanks to all the coaches and members of Oxford University Mixed Martial Arts and Jiu-Jitsu Republic Oxford, particularly to Richard Ormiston-Rees, Josh Neale, Big James Halfhide, Josias Gomes, Lee Renault and Snapper (real name) Magor-Elliot. Thank you for giving me a space to release the frustration.

Finally I owe thanks to all the friends who made my time in Oxford enjoyable, to Tom Lewin, Brendan Largey, Christian Harding, Alexandra Bisia and Eve Richardson and to my wonderful girlfriend Rebecca Marston.

Thank you all. It’s been a blast!

List of abbreviations

2OG	2-oxoglutarate
3PGA	3-phosphoglycerate
6PG	6-phosphogluconolactone
6PGp	Plastidic 6-phosphogluconolactone
AcCoAm	Mitochondrial acetyl-coenzyme A
AcCoAp	Plastidic acetyl-coenzyme A
ADP	Adenosine diphosphate
ALA	Alanine
ANOVA	Analysis of variance
ARG	Arginine
ASN	Asparagine
ASP	Aspartate
ATP	Adenosine triphosphate
BCA	Bicinchoninic acid
BSA	Bovine serum albumin
C3P	3-carbon phosphate ester
CC1	Control culture 1
CC2	Control culture 2
CCE	Carbon conversion efficiency
CCM	Central carbon metabolism
CIT	Citrate
CMP	Cytidine monophosphate
COA	Coenzyme A
CO_2	Carbon dioxide

CTP	Cytidine triphosphate
CYS	Cystine
DOF	Degrees of freedom
DHAP	Dihydroxyacetone phosphate
DHAPp	Plastidic dihydroxyacetone phosphate
DW	Dry weight
E4P	Erythrose 4-phosphate
EC	Enzyme component
F6P	Fructose 6-phosphate
F6Pp	Plastidic fructose 6-phosphate
FAD	Flavin adenine dinucleotide
$FADH_2$	Dihydroflavin adenine dinucleotide
FBP	Fructose 1,6-bisphosphate
FBPp	Plastidic fructose 1,6-bisphosphate
FUM	Fumarate
G1P	Glucose 1-phospahte
G6P	Glucose 6-phosphate
G6Pp	Plastidic glucose 6-phosphate
GABA	γ-aminobutyric acid
GAP	Glyceraldehyde 3-phosphate
GAPp	Plastidic glyceraldehyde 3-phosphate
GC-MS	Gas chromatography mass spectrometry
GLU	Glutamate
GLN	Glutamine
GLY	Glycine
GMRP	Growth maintenance respiration paradigm

GMWRP	Growth maintenance wastage respiration paradigm
GOPOD	Glucose oxidase peroxidase
GP	General paradigm
GTP	Guanosine triphosphate
H_2O	Water
HIS	Histidine
ICIT	Isocitrate
ILE	Isoleucine
LEU	Leucine
INCA	Isotopomer network compartmental analysis
LLDAP	L-*meso*-diaminopimilate
LYS	Lysine
MAL	Malate
MET	Methionine
MFA	Metabolic flux analysis
MID	Mass isotopomer distribution vector
MOX-TMS	Methyloxime trimethyl silyl
MS	Murashige and Skoog (medium)
MTBSTFA	N-tert-Butyldimethylsilyl-N-methyltrifluoroacetamide
NAA	1-naphthaleneacetic acid
NAD	Nicotinamide adenine dinucleotide
NADH	Dihydronicotinamide adenine dinucleotide
NADP	Nicotinamide adenine dinucleotide phosphate
NADPH	Dihydronicotinamide adenine dinucleotide phosphate
OAA	Oxaloacetate
OxPPP	Oxidative pentose phosphate pathway

PCA	Principal component analysis
PC	Principal component
PEP	Phospho*enol* pyruvate
PEP	Plastidic phospho*enol* pyruvate
PFK	Phosphofructokinase
PFP	PPi:fructose 6-phosphate phosphotransferase
PHE	Phenylalanine
Pi	Inorganic phosphate
PPi	inorganic pyrophosphate
Pro	Proline
PYR	Pyruvate
PYRm	Mitochondrial pyruvate
PYRp	Plastidic pyruvate
R5P	Ribose 5-phosphate
ROS	Reactive oxygen species
Ru5P	Ribulose 5-phosphate
Ru5Pp	Plastidic ribulose 5-phosphate
S7P	Sedoheptulose 7-phosphate
SEM	Standard error of mean
SER	Serine
SUC	Succinate
SUCCoA	Succinyl coenzyme A
SSR	Sum of squares residual
SSRmax	Maximum acceptable sum of squares residual
SSRmin	Minimum acceptable sum of squares residual
tBDMS	Tert-butyldimethylsilyl ether

TCA	Tricarboxylic acid (cycle)
TFA	Trifluoroacetic acid
THR	Threonine
TP	Triose phosphate
TRP	Tryptophan
TYR	Tyrosine
UDP	Uridine diphosphate
UTP	Uridine triphosphate
VAL	Valine
X5P	Xylose 5-phosphate
X5Pp	Plastidic xylose 5-phosphate

Contents

Abstract ... 2
Acknowledgments ... 3
List of abbreviations ... 4
Chapter 1: Introduction ... 12
1.1 Heterotrophic metabolism in plants ... 12
1.2 Heterotrophic metabolism is a dynamic and stress responsive system ... 14
1.3 Respiration paradigms ... 15
1.4 Experimental approach ... 19
1.5 Project Objectives ... 21
Chapter 2: Materials and methods ... 22
2.1 Cell cultures ... 22
2.2 Growth experiments ... 23
2.2.1 Growth and sampling of Arabidopsis cell suspension cultures ... 23
2.2.2 Quantification of glucose consumption rate ... 23
2.3 Labelling experiments ... 24
2.4 Quantification of biomass outputs ... 26
2.4.1 Quantification of starch and cellulose by anthrone assay ... 26
2.4.2 Quantification of protein by bicinchoninic acid assay ... 28
2.4.3 Quantification of lipids using sulfo-phospho vanillin assay ... 29
2.4.4 Quantification of organic acids and soluble sugars by gas-chromatography mass-spectrometry ... 30
2.5 Extraction of mass isotopomer distribution vectors by gas-chromatography mass-spectrometry analysis ... 31
2.5.1 Preparation and derivatisation of amino acids ... 31
2.5.2 Derivatisation of insoluble carbohydrates ... 32
2.5.3 Gas-chromatography mass spectrometry ... 32
2.5.4 Mass isotopomer distribution vector extraction ... 33
2.6 Metabolic flux analysis ... 33
2.6.1 Model development ... 33
2.6.2 Mass isotopomer distribution vector curation ... 34
2.6.3 Flux estimation ... 34
2.7 Statistical analyses ... 35
Chapter 3: Establishing a robust fluxomic analysis methodology for *Arabidopsis thaliana* suspension cultures ... 37
3.1 Development of a labelling system ... 37
3.2 Validation of GC-MS protocols for biomolecule identification ... 40

3.3 Mass isotopomer distribution vector curation 46
3.4 Model development 52
3.4.1 Initial model 52
3.4.2 Ancillary reactions 56
3.4.3 Assessment and refinement of the modelled CCM 61
3.5 Modelling biosynthetic metabolism 66
3.5.1 Carbohydrate biosynthesis 67
3.5.2 Lipid biosynthesis 71
3.5.3 Protein biosynthesis 74
3.5.4 Organic acid quantification 75
3.5.4 Total biomass equation 76
3.6 Metabolic fluxes under control conditions 76
3.7 Comparison to published flux solutions 82
3.8 The effect of biomass composition on flux distribution 87
3.9 Conclusion 94
Chapter 4: Growth and flux distribution under reduced temperatures 95
4.1 Introduction 95
4.2 Growth profiles 98
4.3 Biomass composition 100
4.4 CCM flux distribution at decreased temperature 102
4.5 Effect of acclimation on Arabidopsis cultures 115
4.5.1 Growth profile of 12°C acclimated cultures 115
4.5.2 Biomass composition of acclimated cultures 117
4.5.3 Metabolic effects of acclimation 118
4.6 Conclusions 127
Chapter 5: Mannose supplementation affects growth and flux distribution in *Arabidopsis* suspension culture independently of osmotic effects 128
5.1 Introduction 128
5.2 Effect of mannose on Arabidopsis cell suspension culture growth 129
5.3 Effect of mannose and mannitol supplementation on biomass composition 132
5.4 Effects of mannose and mannitol on the CCM flux distribution 134
5.4.1 Flux distribution under mild osmotic stress 135
5.4.2 The effect of mannose on flux distribution in the CCM 142
5.5 Conclusions 154
Chapter 6: Growth rate and flux distribution in CCM 155
6.1 Introduction 155
6.2 Growth rates and maintenance costs 155
6.2.1 Metabolic cost of growth 157

6.2.2 Metabolic costs of maintenance 159
6.2.3 Maintenance costs and PEP partitioning 163
6.3 Glucose 6-phosphate utilisation and growth rate 165
6.4 Conclusions 169
Chapter 7: Concluding remarks 170
7.1 Effect of low temperature on the CCM 170
7.2 Effect of mannose supplementation on the CCM 171
7.3 The relationship between growth rate and flux distribution 171
7.4 Future work 173
7.4.1 Building on the conclusions of this thesis 173
7.4.2 Further studies 174
7.5 Summary 176
References 177

Chapter 1: Introduction

Catabolic metabolism is the network of chemical reactions which provides cells with the ATP, reducing power and biosynthetic precursors they need to survive and grow (Noor *et al.,* 2010). This thesis aims to investigate the relationship between growth rate and heterotrophic metabolism in *Arabidopsis thaliana*. Under different growth regimes the requirements of the cell will be different, and so the relative fluxes through metabolic reactions will likely change in order to support growth and homeostasis.

To undertake this investigation metabolic flux analysis (MFA) will be used quantify flux through the reactions of heterotrophic metabolism of *Arabidopsis* cell suspension cultures growing at different rates. Comparison of the relative fluxes through metabolism at different growth rates will give an insight into the difference in demands for metabolic resources, and how flux through metabolism changes to meet these demands.

Metabolism is integral to plant physiology and biochemistry, and understanding how metabolism supports growth is central to predicting growth of crops and natural vegetation in the face of climate change. Further, the results of this study will be useful in providing a framework for separating growth-related from stress-related effects in *Arabidopsis* MFA studies.

1.1 Heterotrophic metabolism in plants

The section of heterotrophic metabolism which produces the vast majority of metabolic resources, and thus the main focus of this project, is the central carbon metabolism (CCM). The CCM in heterotrophic tissues includes the Embden-Meyerhoff pathway (referred to as glycolysis), the oxidative pentose phosphate pathway (OxPPP), the tricarboxylic acid (TCA)

cycle, the anaplerotic reactions replenishing TCA cycle intermediates, and the electron transport chain. The glycolytic pathways (the Embden-Meyerhoff pathway and OxPPP) are two routes for the partial oxidation of respiratory substrate into the three carbon compound, pyruvate. The TCA cycle combines two carbon units derived from pyruvate with oxalacetate (OAA) to form citrate, which is then metabolised though a cycle of eight intermediates to reform OAA and CO_2, thus completing the oxidation of sugars (Sadava *et al*., 2013). Throughout the cycle, metabolites are removed to act as biosynthetic precursors, and anaplerotic reactions replenish the pools of these intermediates. Several reactions in glycolysis and the TCA cycle involve phosphorylation of adenosine diphosphate (ADP) to generate adenosine triphosphate (ATP) through substrate level phosphorylation. Glycolytic, TCA cycle and analerportic reactions can also reduce the co-enzymes nicotinamide adenine dinucleotide (NAD), nicotinamide adenine dinucleotide phosphate (NADP) and flavin adenine dinucleotide (FAD). These reduced co-enzymes can be used as a fuel for oxidative phosphorylation by donating electrons to the electron transport chain, a series of transmembrane protein complexes which use energy from the added electrons to create an electrochemical gradient which drives ATP synthase in the mitochondrial inner membrane (Geigenberger and Fernie, 2014).

Although most of the reactions of CCM required for ATP synthesis can be found in all eukaryotes, plants have evolved a variety of additional enzymes which allow for the bypassing of steps in glycolysis or the TCA cycle (Plaxton and Podestá, 2006; Sweetlove *et al*., 2010). Furthermore, the first reactions of glycolysis and the OxPPP are duplicated in the cytosol and the plastids in plants. This metabolic flexibility is necessary because respiration is used not only to produce ATP but also to fulfil two additional prominent functions of respiration. One is the provision of biosynthetic precursors, which is necessary because plants produce most of their biomass using the intermediates of CCM as a source of carbon skeletons (O'Leary *et al*., 2019). The other is redox balancing, maintaining appropriate concentrations of reactive oxygens species (ROS) and appropriate ratios of

$NADH:NAD^+$ and $NADPH:NADP^+$ is vital for homeostasis (Geigenberger and Fernie, 2014). Plants have several mechanisms to uncouple co-enzyme oxidation from ATP synthesis, including alternative oxidase (Saha *et al*., 2016), alternative dehydrogenases (Rasmusson *et al*., 2008), and uncoupling protein (Smith *et al.,* 2004, Sweetlove *et al*., 2006). These additional enzymes give plants an ability to modulate co-enzyme provision independently of ATP synthesis (Millar *et al*., 2011), so that ROS concentration can be controlled while biosynthesis can be maximised when conditions are optimal. Therefore, not only is the overall rate of respiration variable, but so is the distribution of flux through the reactions of the network of the CCM, which adjusts to vary the relative amounts of biosynthetic precursors, ATP and reduced co-enzymes produced from the CCM.

1.2 Heterotrophic metabolism is a dynamic and stress responsive system

The variable nature of plant CCM conferred by the alternative metabolic pathways as well as duplication of reactions between compartments means that relative flux through CCM can adapt to produce different relative amounts of biosynthetic precursors, ATP, or reducing power as the situation demands (Plaxton and Podestá, 2006; Sweetlove *et al*., 2010; Millar *et al*., 2011; O'Leary *et al*., 2019).

Flux through CCM is regulated by a complex system of enzyme modulation which reconciles the demand for biosynthetic precursors, ATP and reduced co-enzymes for growth and homeostatic processes with the supply of available respiratory substrates (see O'Leary *et al*., 2019 for review). Therefore, any stimulus which can affect the supply of respiratory substrate or the demand for ATP, biosynthetic precursors or reduced co-enzymes for growth and maintaining homeostasis can potentially cause a change in flux distribution in CCM. For example, experiments which manipulated the rate of photosynthesis have shown changes in the fluxes in heterotrophic metabolism in response to carbon excess and carbon limitation in the respiratory supply (Brouquisse *et al*., 1991;

Smith and Stitt, 2007; Leakey *et al*., 2009). There is also evidence that the flux distribution in the CCM can change in response to stimuli which alter the cellular requirements for ATP, biosynthetic precursors or reducing power (Williams *et al.,* 2008; Williams *et al*., 2010; Masakapalli *et al*., 2014a). This could be any stress which causes ROS accumulation (Rhoads *et al.,* 2006) as this would require increased reducing power to resolve. Alternatively, any stress which requires active systems, and thus more ATP, to resolve will also likely induces changes in the flux through the CCM. Finally, any stress promoting increased turnover of biological molecules, which requires more biosynthesis to resolve will also likely have an effect on flux distribution.

Some stresses can also have direct effect on the CCM as well as changing the supply and demand dynamics. For example, reduced temperatures can directly affect the capacity of enzymes in CCM. Individual enzyme respond to reduced temperatures differentially resulting in perturbations in the distribution of flux through CCM (ap Rees *et al.,* 1989; Atkin and Tjoelker, 2003; Atkin *et al*., 2005). In *Arabidopsis* cell suspensions an alternative pathway of glycolytic breakdown through phospho*enol*-pyruvate (PEP) carboxylase and malic enzyme was stimulated in response to phosphate limitation (Plaxton and Tran, 2011; Masakapalli *et al*., 2014a) in order to circumvent phosphate dependent reactions (O'Leary *et al*., 2019). Mutation of the genes that encode CCM enzymes can also perturb flux through the network (McCormick and Kruger, 2015), but duplication of enzymes between compartments means that CCM in plants is robust to some enzymatic loss (van Dongen *et al*., 2011).

1.3 Respiration paradigms

One of the major, ongoing questions in metabolic biology is how the products of the CCM (ATP, NAD(P)H and precursors) are utilised by different biological processes, and what paradigms should be used to discuss this allocation. The first investigations in plants into

the way in which respiratory metabolism interacts with the processes it supports were conducted by K. J. McCree and co-workers, analysing CO_2 exchange data from *Trifolium repens* (McCree and Troughton, 1966 a,b) and C. T. de Wit attempting to quantify respiration, and relate it to other processes in an Elementary Crop Simulator program (de Wit *et al*., 1970). One of the outcomes of these studies was the concept that respiration associated with growth can be separated from respiration associated with maintenance. This work led to McCree publishing the first model describing the relationship between respiration and the processes it supports in (McCree, 1970), as follows:

$$R = R_G + R_M = g_R G + m_R W$$

where R is respiration rate (mol CO_2 s^{-1}), R_G is growth respiration rate (mol CO_2 s^{-1}), R_M is maintenance respiration rate (mol CO_2 s^{-1}), G is growth rate (g new biomass s^{-1}), W is living biomass (g dry mass), g_R is a growth respiration coefficient (amount of CO_2 released due to growth per unit growth e.g. mol CO_2 (g new biomass) $^{-1}$), and m_R is a maintenance respiration coefficient describing the amount of CO_2 released due to maintenance per unit existing biomass per unit time e.g. mol CO_2 (g dry mass)$^{-1}$ s^{-1}). Note that the growth rate is usually quantified as accumulation of biomass and that g_R is a ratio, representing the CO_2 by-product of growth while m_R is a rate associated with maintenance activities.

This equation became known as the growth, maintenance and respiration paradigm (GMRP). The GMRP deals with the two most general processes, growth (addition to the total amount of biomass comprised of protein, lipids, cellulose, minerals, etc.) and maintenance (defined as ‘processes that maintain cellular structures and intracellular gradients of ions and metabolites, along with cellular acclimation (phenotypic adjustment) to environmental changes.’ - Penning de Vries (1975)). The GMRP assumes that all biological processes supported by respiration can be categorised into the ‘growth’ or ‘maintenance’ rubrics. However, the GMRP ignores the fact that some processes, like protein synthesis, are shared by both growth and maintenance (Amthor, 2000).

The GMRP was later extended to include the consideration that 'CO_2 and/or heat may be lost without contributing to plant growth or maintenance' (Amthor, 2000). This is known as the growth, maintenance, wastage and respiration paradigm (GMWRP; Warren Wilson, 1967). The 'wastage' respiration rubric includes futile cycles of ATP production and hydrolysis, or activity of mitochondrial alternative oxidase, alternative dehydrogenases and the uncoupling protein (Thornley, 1971). The term 'wastage' is not entirely accurate and somewhat incompatible with the notion that natural selection has increased efficiency of metabolism. Recent work has suggested that the processes defined as wastage are vital to redox balancing and homeostasis (O'Leary *et al.,* 2019), so wastage might not be the most appropriate name for this group of processes. Perhaps 'balancing respiration' would be a better term.

The GMRP and the GMWRP (in either original or modified form) are useful empirical models for describing respiration. However, they are descriptive rather than explanatory, and to explain the relationship between growth, maintenance and respiration we need a more mechanistic approach, which is provided by the general paradigm (GP, Yemm, 1965). The GP suggests that there is a unique relationship between respiration and each biochemical process it supports. In other words, the rates of every metabolic pathway that uses ATP, biosynthetic precursors and/or NAD(P)H may place different demands on respiration under changing conditions and respond differently to changes in the fluxes through CCM. This approach allows examination of the biochemistry and physiology of plant growth dynamics (Penning de Vries, 1972, 1974). It is important to view each biochemical pathway individually because each pathway may respond uniquely to changes in environment or developmental cues. The general paradigm can be described in the following equation:

$$R=\Sigma_{processes,Y}\, c_Y\, A_Y$$

where Y is a process supported by respiration, c_Y is the metabolic cost of Y (in CO_2 per unit of activity of Y), and A_Y is the rate (activity) of Y. This equation is 'complete' when you consider all quantitatively relevant processes supported by respiration.

Many of the early investigations of metabolic resource allocation were limited by a lack of technologies to investigate *in situ* reaction rates (Amthor, 2000; O'Leary *et al*., 2019). For example, researchers have previously tried to estimate plant maintenance costs by measuring CO_2 release in dark-grown plants (Penning de Vries, 1972; McCree, 1974), or mature tissues (de Wit and Brouwer, 1969; Irving and Silsbury, 1988) where it could be assumed that the growth rate was zero, and all respiration was due to maintenance. However, this proved to be inaccurate because later examples showed that cellular functionality can decline in mature tissues, that growth can continue in dark grown plants (Challa, 1976; Robson and Parsons, 1981; Moser *et al.,* 1982; Breeze and Elston, 1983; Denison and Nobel, 1988), and that respiration in mature tissues can support translocation and senescence as well as maintenance (De Witt and Brouwer, 1969). As a consequence of such considerations, it has been suggested that maintenance respiration rates should be calculated from rates of underlying processes based on the metabolic costs and stoichiometry of the pathways involved (Wohl and James, 1942). In 1975 F. W. T. Penning de Vries was the first to quantitively estimate the costs of maintenance processes, using data from protein turnover and intracellular transport. The following equation was used:

$$m_R = \Sigma_{processes,X}\, m_{R,X} = \Sigma_{processes,X}\, c_X a_X$$

where X is a maintenance process, $m_{R,X}$ is the maintenance respiration coefficient for process X (amount of CO_2 released due to process X per unit of existing biomass per unit of time; mol CO_2 (g living biomass)$^{-1}$ s^{-1}), c_X is the cost of process X (in CO_2 per unit of activity of X), and a_X is the rate of process X per unit biomass (i.e. specific activity; Amthor, 2000).

However, application of this pathway analysis approach is limited. It does not always produce accurate estimates of *in vivo* costs, because it is susceptible to errors introduced by incomplete knowledge of the metabolic network (Amthor, 2000).

1.4 Experimental approach

A potential technology for estimating the allocation of ATP, NAD(P)H and biosynthetic precursors *in situ* is metabolic flux analysis (MFA). MFA is a technique in which ^{13}C isotopic labelling data are fitted to a model of metabolism using an iterative sum of squares minimization algorithm. MFA allows estimation of the *in situ* rates of multiple metabolic reactions and provides confidence intervals for the estimated flux of each reaction (Kruger *et al*., 2012). Over the past 25 years MFA has been used for a variety of purposes (Wiechert, 2001; Crown and Antoniewicz, 2013). In plants, MFA has been applied to quantify fluxes in central metabolism (Rontein *et al.,* 2002; Schwender *et al.,* 2003; Sriram and Shanks 2004), to assess fluxes through parallel pathways in separate compartments (Sriram *et al.,* 2007, Masakapalli *et al.,* 2010) and to identify previously unknown pathways (Schwender *et al.,* 2004), as well as to investigate the rigidity or flexibility of different metabolic nodes (Stephanopoulus and Vallino, 1991; Iyer *et al.,* 2008) and understand the effect of a genetic or environmental perturbation on metabolism such as; phosphate limitation (Masakapalli *et al.,* 2014a), nitrate limitation (Junker *et al*., 2007, Masakapalli *et al*., 2013, Truong *et al.,* 2013, Allen and Young, 2013), increased temperature (Williams *et al*., 2010), oxygenation status (Williams *et al.,* 2008) and osmotic pressure (Williams *et al*., 2010).

This project aims to investigate the relationship between flux through the CCM and the growth rate of cells in *Arabidopsis* suspension cultures by using MFA to estimate reaction rates *in vivo.* From the estimates of flux through CCM and biosynthetic metabolism, the rate of production of ATP, reduced co-enzymes and biosynthetic precursors by CCM can be estimated, as can the rate of utilisation of these resources by biosynthetic metabolism. The remaining ATP and reduced co-enzymes not used for growth represent the maintenance costs, if one is considering the GMRP, the combined costs of maintenance and ‘wastage’ respiration if applying the GMWRP, or simply the costs of any process not included in the model if operating within the GP.

In order to study the relationship between metabolic resource production by the CCM and growth rate, it is necessary to manipulate either the distribution of flux in the CCM, or the growth rate of cultures. The former is technically difficult to achieve in a predictable way and so the culture's growth conditions were perturbed to alter the growth rate. Two conditions were used to slow the growth rate of the cultures; a small drop in temperature from the standard growth temperature of 22°C to 17°C or 12°C (as well as acclimation to growth at 12°C) and supplementation of the cultures with 40mM mannose. These perturbations are less severe than those used in previous studies into the deleterious effects of decreased temperature or mannose supplementation. Most research into cold stress in *Arabidopsis* uses temperatures of 4°C or lower and studies of plant responses to mannose supplementation have used concentrations of at least 50 mM, as these previous studies have aimed to understand the stress responses induced by the perturbations (see chapters 4 and 5 for further detail). The moderate application of the perturbations used in this project was intended to slow the growth rate of the cells without causing major cellular damage.

As well as investigating the relationship between growth and CCM flux distribution this project also provides the opportunity to gain an insight into the effect of mildly decreased growth temperatures and mannose supplementation on flux distribution in CCM. Although multiple studies have investigated the abundance of metabolites and transcripts in response to decreased temperatures in a variety of plant tissues and species, there has been no comprehensive analysis fluxes *in vivo* in response to decreased temperature. Mannose is phosphorylated to mannose 6-phosphate which has been reported to sequester inorganic phosphate and inhibits phosphoglucoisomerase (Sols *et al*., 1960; Goldworthy and Street, 1962). Both inorganic phosphate sequestering and phosphoglucoisomerase inhibition are likely to have a significant effect on fluxes through the CCM. However, no analysis of the effects of mannose on the fluxome has been undertaken so far.

1.5 Project Objectives

From a fluxomic perspective, little is known about the relationship between growth rate and operation of the CCM in plants. MFA provides a useful analytical technique to explore this relationship. Further MFA offers a useful tool for investigating the fluxomic effect of decreased growth temperature and mannose supplementation on *Arabidopsis* suspension cultures. This project aims to:

1. Establish and validate a workflow for ^{13}C-MFA, that builds on the work of previous authors, and allows estimation of metabolic resource partitioning (Chapter 3).
2. Apply ^{13}C-MFA to *Arabidopsis* cultures grown at sub-optimal temperatures (Chapter 4).
3. Use ^{13}C-MFA to investigate the effect of mannose supplementation on CCM fluxes in *Arabidopsis* (Chapter 5).
4. Evaluate the effect of slowed growth rate on the flux distribution in CCM, and how this affects provision and utilisation of ATP, reduced co-enzymes and biosynthetic precursors for different processes (Chapter 6).

Chapter 2: Materials and methods

2.1 Cell cultures

Cell suspensions of *Arabidopsis thaliana* (L.) Heynh. (ecotype Landsberg *erecta*) were taken from a line previously developed in the department (May and Leaver, 1993). Cultures were maintained in liquid 4.4 mg L^{-1} Murashige and Skoog (MS) medium, supplemented with 166.6 mM glucose, 0.5 mg L^{-1} 1-naphthaleneacetic acid (NAA), and 0.05 mg L^{-1} kinetin and set to pH 5.8 with KOH. Cultures were grown in 250 ml Erlenmeyer flasks sealed with a double layer of aluminum foil on an orbital shaker running at 120 rpm at 22°C under a 16-h light, 8-h dark cycle.

Every seven days, cells were sub-cultured by adding 15 ml of 7-d-old culture into 100 ml of fresh MS medium (Williams *et al*., 2008). Heterotrophic cell suspensions were produced by maintaining cultures in the above conditions but in continuous dark.

For low temperature treatments, cells were grown at 12°C or 17°C in an InFors HT Unitron PLUS AJ254 refrigerated incubation chamber. An *Arabidopsis thaliana* suspension culture that was cold acclimated was also established, by transferring 15 ml of 7 d old culture into 100 ml of fresh MS medium and growing this line at 12°C for four weeks, subculturing every 14 d.

The growth rate was altered by supplementing the MS medium (including glucose) with 40 mM mannose. An osmotic control was made by supplementing the growth medium with 40 mM mannitol.

2.2 Growth experiments

2.2.1 Growth and sampling of Arabidopsis cell suspension cultures

Arabidopsis cells were subcultured under sterile conditions and four flasks were incubated under the chosen experimental conditions (2.1).

On day 0 (immediately after the cultures were initiated) 3x10 ml samples were taken from one flask. Subsequently 10 ml samples were taken from each of the other three flasks on days 2, 3, 4, 5, 6, 7, 8 and 10. 10 ml samples were mixed with a vortex and then filtered using a vacuum filtration unit for 30 s. The filtrate was collected and 3x1 ml aliquots were taken from each sample and stored at −20°C for subsequent analysis of glucose concentration. The fresh weight of the filtered cells was determined by scraping the cells off the filter paper into pre-weighed weighing boats and reweighing. Weighing boats containing the filtered cells were covered in aluminium foil and then incubated in a drying oven at 65°C for 24 h before weighing again to determine the dry weight. After weighing, dried cells were transferred to 15 ml falcon tubes and stored at 4°C for subsequent analysis of protein content.

2.2.2 Quantification of glucose consumption rate

A glucose oxidase peroxidase (GOPOD) assay kit (Megazyme Ltd., K-GLUC) was used to quantify the amount of glucose in the culture filtrate obtained from cell samples (2.2.1). The GOPOD assay solution contained glucose oxidase which converted water, oxygen and D-glucose to D-gluconate and hydrogen peroxide. Two molecules of hydrogen peroxide then react with p-hydroxybenzoic acid and 4-aminoantipyrine (both in the assay mixture) in a reaction catalysed by a peroxidase to produce quinoneimine dye and water (Figure 2.1).

Addition of MS media containing glucose to the assay mixture initiated the reactions resulting in the production of the dye and the solution turning pink. The intensity of the colour was measured at 530 nm to determine the amount of glucose in the culture medium.

The frozen filtrate sample was thawed at room temperature and thoroughly mixed by vortexing before being diluted 50-fold in ultrapure water. 5 µl of the diluted sample was then mixed with 150 µl of GOPOD reaction mixture in a pre-measured 96-well plate and incubated at 30°C for 30 min.

A Beckman Coulter DTX 880 multimode detector was used to measure the absorbance of each well at 530 nm. This was compared to a set of standard values made with fresh MS medium diluted in water to calculate the amount of glucose in each well and, from this, the concentration of glucose in each flask at each time point. A range from 0.75 µg to 6 µg of glucose per well was used for the calibration curve.

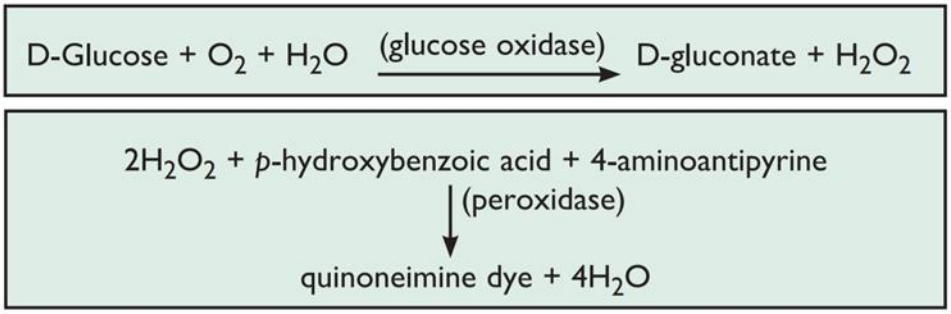


Figure 2.1: *Schematic of GOPOD assay for spectrophotometric quantification of glucose in filtrate.*

2.3 Labelling experiments

Arabidopsis suspension cultures were grown in MS media made with unlabelled glucose, 99% [1-^{13}C] glucose, 99% [2-^{13}C] glucose or a 20% [U-^{13}C] glucose : 80% unlabelled glucose mix.

Media for labelling studies was made by adding MS powder, kinetin and NAA to half the volume of water as in 2.1 (250 ml) and to double the concentration (8.8 g l^{-1} MS powder, 0.25 mg l^{-1} NAA and 0.025 mg l^{-1} kinetin) without glucose. For culture supplemented with

mannose or mannitol these solutes were also added to the media to double the concentration (80 mM) as in 2.1. This medium, without glucose, was sterilized by autoclaving at 121°C and 104 kPa for 1 h. 99% [1-^{13}C] glucose, 99% [2-^{13}C]glucose or a 20% [U-^{13}C] glucose : 80% unlabelled glucose mix was dissolved in 250 ml ultrapure water to 333.2 mM. Under a sterile conditions the labelled glucose solutions were sterilised by passing through a 0.2 µm filter and added to the pre-sterilised MS medium, to produce sterile MS medium containing labelled glucose.

The sterile medium was then separated into three (10 ml) aliquots in 25 ml Erlenmeyer flasks. 1.5 ml of heterotrophically grown *Arabidopsis* culture was added to these flasks before they were placed into the appropriate growth conditions.

Cultures were harvested during mid-exponential growth: for cells grown in the control conditions (22°C, no supplementary solutes), and those supplemented with mannitol this was after 5.5 d; for cultures grown at 17°C this was after 7 d; cultures supplemented with mannose this was after 9 d; for cultures grown at 12°C after 12 d; and for cultures acclimated to growth at 12°C after 14 d.

Biomass was harvested by taking 2.5 ml aliquots of labelled culture or 10 ml of unlabelled culture at mid-exponential growth phase and centrifuging at 4566 x*g* for 30 min in a Sorvall Legend RT centrifuge. The supernatant was decanted and stored for subsequent analysis and the pellet washed with 1 ml MS medium without glucose before centrifuging again at 4566 x*g* for 40 min. The resulting pellets were stored at −80°C.

2.4 Quantification of biomass outputs

10 ml unlabelled samples from 2.3 were placed in pre-weighed falcon tubes, which were centrifuged at 4566 x*g* for 30 min, and the supernatant was discarded. The tops of the falcon tubes were then covered with parafilm and pierced before lyophilisation overnight in a Martin Christ Alpha 2-4 LD Plus freeze dryer. The dry weight of the cells was measured, and they were stored at −20°C for subsequent biomass analysis.

2.4.1 Quantification of starch and cellulose by anthrone assay

2.4.1.1 Chloroform-methanol extraction

Lyophilised culture pellets (from 2.4) were re-suspended in 3 ml of ice-cold methanol and 1.5 ml of ice-cold chloroform for 30 min. Subsequently, 3 ml water was added to generate a biphasic mixture consisting of a lower chloroform layer, and an upper methanol layer, with denatured protein collecting at the interface. Samples were mixed well and centrifuged at 2000 x*g* for 15 min at room temperature to promote phase separation. The upper aqueous phase was collected for analysis of soluble material. Insoluble material was recovered from the combined lower phase and interface material by addition of 3 ml of methanol to reform a secondary chloroform:methanol mixture. This monophasic suspension was split into 1 ml aliquots and centrifuged at 13,000 x*g* for 30 min, and the resulting pellet was recovered for subsequent processing.

2.4.1.2 Solubilisation and degradation of starch

The pellets from 1 ml of secondary chloroform:methanol extract were resuspended in 500 µL 0.2 M sodium acetate buffer (pH 5.8) and then autoclaved for 3 h at 121°C and 104 kPa. After gelatinisation of starch grains, the autoclaved samples were cooled and supplemented with 50 µL 0.2 M sodium acetate buffer containing 2 units of amyloglucosidase from *Aspergillus niger* (Sigma A7420), and 20 units of α-amylase from *Bacillus sp.* (Sigma A6380). Samples were incubated for 16 h at 37°C. After digestion, 1 ml of ethanol was

added to each tube, which was then centrifuged at 13000 x*g* for 15 min (Williams *et al.,* 2008). The supernatant was collected in 250 µl or 150 µl aliquots and evaporated to dryness by vacuum centrifugation prior to analysis of glucose derived from the degraded starch. The remaining insoluble residue was collected by centrifugation and retained for analysis of cell wall components.

2.4.1.3 Hydrolysis of cellulose

The insoluble residue remaining after solubilisation and degradation of starch (2.4.1.2) was washed twice with 1 ml of 70% ethanol. The pellet was then incubated with 1 ml of 2 M trifluoroacetic acid (TFA) in a fume hood at 120°C for 1 h. The hydrolysed sample was centrifuged at 13000 x*g* for 4 min. The resulting supernatant was recovered, and 250 µl or 150 µl aliquots evaporated to dryness by vacuum centrifugation. Samples were retained for subsequent analysis.

2.4.1.4 Anthrone assay

Anthrone reagent was prepared by dissolving 0.5 g of anthrone powder in 10 ml of ethanol followed by addition of 240 ml of 75 % sulfuric acid. Anthrone reagent was stored overnight at 4°C. Glucose was used as a standard at concentrations from 0.54 mM to 5.37 mM.

Starch digest or cell wall hydrolysate (from 2.4.1.2-3) was diluted 10-fold. 500 µl of diluted samples and standards were mixed with 3 ml anthrone reagent in glass tubes before incubation at 100°C for 10 min. The monosaccharides were dehydrated in the acidic conditions to form furfurals, which reacted with the anthrone to form a blue-green complex (Figure 2.2; Seifter *et al*., 1950). Tubes were cooled and absorbance taken at 620 nm in an Evolution 260 Bio UV-visible spectrophotometer.

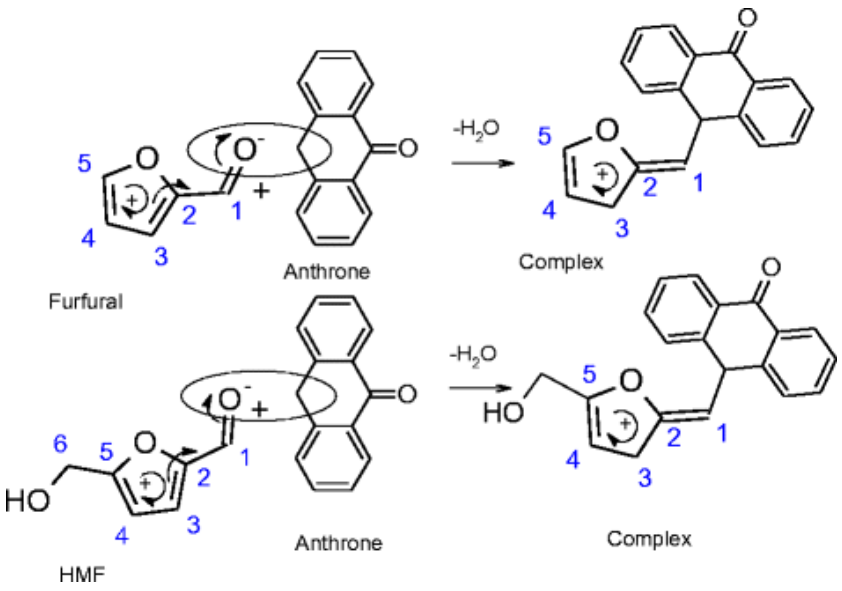


Figure 2.2: *A schematic of reactions between furfurals and anthrone. Reproduced from Haldar et al. (2017).*

2.4.2 Quantification of protein by bicinchoninic acid assay

Bicinchoninic acid (BCA) was used to estimate the protein content in lyophilised cell pellets (from 2.4; Smith *et al.,* 1985). Bovine serum albumin (BSA) was used for production of a standard protein curve. The standards were prepared in 2 M NaOH in a range of concentrations from 0 to 1 mg ml^{-1}. The reagents for the assay were prepared as two solutions for storage. Reagent A (29.04 mM BCA), 188.7 mM sodium carbonate, 8.25 mM sodium tartarate, 100.01 mM sodium hydroxide, 113.1 mM sodium bicarbonate, pH 11.25) and reagent B (250 mM cupric sulphate) mixed in a 50:1 ratio to produce the standard working reagent immediately before use.

The standards and cell pellets were mixed with of 5 ml 2 M NaOH and incubated at 100°C for 10 min. After incubation, the standards were used immediately for the BCA assay while the samples were cooled, centrifuged at 13000 x*g* for 30 min and the supernatant was used for the assay. 2 ml standard working reagent was added to both the 100 µl standards and samples, followed by mixing and incubation at 60°C for 30 min. The sodium salt of BCA reacted with the cuprous ion produced by the biuret reaction under alkaline conditions

(Figure 2.3) to from a complex with a deep blue colour. The absorbance for both the standards and samples was recorded at 562 nm using water as the blank in an Evolution 260 Bio UV-visible spectrophotometer.

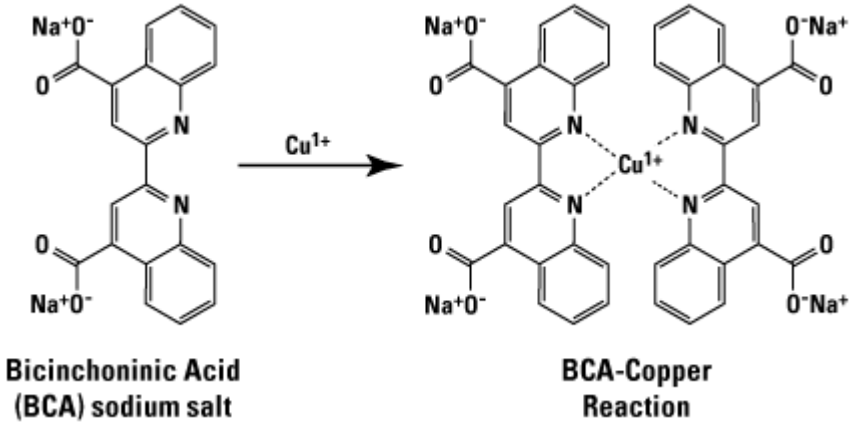


Figure 2.3: *A schematic of the reaction between BCA and cuprous ions.*

2.4.3 Quantification of lipids using sulfo-phospho vanillin assay

The content of lipid in the lyophilised cell pellets (from 2.4) was determined by the sulfo-phospho vanillin assay using linoleic acid as the standard (Izard and Limberger, 2003; Cheng *et al.,* 2011; McMahon *et al.,* 2013). Linoleic acid was dissolved in chloroform and used to prepare the standards in a range from 0 to 1 mg ml^{-1}. These assays were conducted in glass vials. The standards were evaporated to dryness by incubation at 90°C for 10 min. Dry cell pellets were dissolved in phosphate buffered saline (157 mM Na^{+}, 140 mM Cl^{-}, 4.45mM K^{+}, 10.1 mM HPO_4^{2-}, 1.76 mM H_2PO^{4-}) and both the standards and samples were incubated at 95°C for 20 min in 2 ml of 18.4 M sulfuric acid. The acid reacted with the unsaturated lipids to form a carbonium ion. The tubes were cooled on ice, vortexed and the absorbance was recorded at 535 nm in a spectrophotometer.

Phosphoric acid vanillin reagent was prepared by dissolving 0.12 g of vanillin in 20 ml of water, and the volume was adjusted to 100 ml with 85% phosphoric acid. 5 ml of this reagent was added to both standard and samples, mixed well and incubated at 37°C for 10 min in the dark. The phosphoric acid and vanillin reacted to form a phosphovanillin ester which

reacted with the carbonium ions to produce a coloured complex (Knight *et al*., 1972). The absorbance was read again at 535 nm and the increase in absorbance used to quantify the amount of lipid by the phosphoric acid vanillin reagent.

2.4.4 Quantification of organic acids and soluble sugars by gas-chromatography mass-spectrometry

Organic acids were quantified using gas chromatography mass-spectrometry (GC-MS). Lyophilised cell pellets (from 2.4) were resuspended in 1.4 ml methanol and incubated at 70°C for 15 min before centrifugation at 4655 x*g* for 40 min. Samples were then transferred to glass tubes and 750 µl of chloroform and 1.5 ml of water were added. The samples were incubated at room temperature to allow phase separation. The upper phase was split into 150 µl aliquots and dried by vacuum centrifugation.

Samples were then derivatised with methyloxime trimethylsilyl ether (MOX-TMS; section 2.5.2.2) and analysed by GC-MS (section 2.5.3). Agilent Masshunter Quantative Analysis software was used to calculate the concentrations of organic acids based on the area of the relevant peak in the ion chromatogram relative to that in a standard mix of oxalic acid, succinic acid, malic acid, fumaric acid, 2OG and citric acid, as well as the concentration of sucrose and fructose based on separate standard curves.

2.5 Extraction of mass isotopomer distribution vectors by gas-chromatography mass-spectrometry analysis

2.5.1 Preparation and derivatisation of amino acids

Amino acids were extracted from cell pellets and derivatised with tert-butyldimethylsilyl ether (tBDMS), using a method developed from Zamboni *et al*. (2009).

Pellets from 2.3 were each resuspended in 150 µl 100% methanol. The suspensions were incubated at 70°C for 15 min in an Eppendorf thermomixer C shaking at 900 rpm. The suspensions were then centrifuged at 20800 x*g* for 10 min and the supernatant removed. Each pellet was resuspended in 150 µl 100% methanol, and centrifuged at 20800 x*g* for 10 min before the supernatant was discarded.

Acid hydrolysis was conducted by adding 500 µl of 6 M hydrochloric acid to each pellet and incubating at 30°C for 30 min then incubating at 100°C for a further 21-23 h. The hydrolysates were centrifuged for 15 min at 13000 x*g* to remove debris. 2.5 µl of the resulting supernatant was removed and dried by vacuum centrifugation in a Savant Speedvac SPD 120 attached to a Savant RVT 400 refrigerated vapor trap.

25 µl of pyridine was added to each dried sample before incubation at 37°C in a thermomixer shaking at 900 RPM for 30 min. 35 µl of N-tert-butyldimethylsilyl-N-methyltrifluoroacetamide (MTBSTFA) + 1% tBDMS was added before incubation at 60°C in a thermomixer shaking at 900 RPM for 30 min. The samples were finally transferred to glass vials and analysed by GC-MS.

2.5.2 Derivatisation of insoluble carbohydrates

Glucose obtained from starch and cell wall material (see 2.4) was derivatised with MOX-TMS before GC-MS analysis. Several alternative methods for derivatisation were also investigated, but ultimately not used for routine analysis: aldonitrile pentapropionate, methyloxime pentapropionate and 1,2,5,6-di-isopropylidene propionate derivatisations were carried out according to Antoniewicz *et al*. (2011), and diethylacetate acetate derivatisation was carried out according to Price *et al*. (2004).

2.5.2.1 Methyloxime trimethylsilyl ester derivatisation of carbohydrates

150 µl aliquots of starch digest or cell wall hydrolysate were dried by vacuum centrifugation. Each sample was dissolved in 40 µl of 2% (w/v) methyloxime hydrochloride in pyridine and incubated at 37°C for 2 h. Subsequently 70 µl of N-trimethylsilyl-N-methyl trifluoroacetamide was added to each sample before incubation at 37°C for 30 min. Samples were then transferred to glass vials and analysed by GC-MS.

2.5.3 Gas-chromatography mass spectrometry

All GC-MS was conducted on an Agilent Technologies Intuvo 9000 GC system fitted with an Agilent Technologies 59778 MSD.

MOX-TMS derivatised samples (1 µl) entered the GC at an injection port temperature of 230°C (splitless). The oven temperature was constant at 70°C for 5 min, followed by an increase to 330°C at 7.5°C min^{-1}. The temperature was then decreased at 120°C min^{-1} to 70°C where the cycle ended. The carrier gas flow was helium at 1 ml min^{-1}.

tBDMS derivitised samples (1 µl) entered the GC at an injection port temperature of 230°C (1:10 split). The oven temperature was held at 120°C for 5 min before a 4°C min^{-1} increase to 270°C followed by a 20°C min^{-1} increase to 310°C, where the temperature was held for 3 min before the end of the cycle. The carrier gas was helium at a flow rate of 1.2 ml min^{-1}.

2.5.4 Mass isotopomer distribution vector extraction

GC-MS data was visualised using Agilent Masshunter Qualitative Analysis Navigator. Once target molecules had been identified in the chromatogram mass isotopomer distribution data (MIDs) were extracted by exporting the mass spectrum peak list to a text file. RStudio was used to run scripts to round all the peaks to integer m/z values and sum abundance values for each m/z. MSCorr software was used to correct for natural abundance of carbon 13 derived from the derivatising agent and isotopes of all other elements and to normalise the MIDs to one (Wahl *et al*., 2004).

2.6 Metabolic flux analysis

Flux estimates were obtained using the INCA (Isotopomer Network Compartmental Analysis) MatLab package (Young, 2014) for metabolic flux analysis (MFA). INCA uses an elementary metabolite unit framework (Antoniewicz *et al*., 2007) and a highly efficient decomposition algorithm to solve a residual sum of squares minimization problem to produce accurate estimates of fluxes through a metabolic network model.

2.6.1 Model development

The reaction network model was developed from previously published models (Masakapalli *et al*., 2013). The model includes reactions for the Embden-Meyerhoff glycolytic pathway, the OxPPP, the TCA cycle, and biosynthestic pathways for lipids, starch, sucrose and cell wall carbohydrates and individual amino acids. The model takes into account co-enzyme involvement in reactions throughout and the electron transport chain is modelled by allowing all excess NAD(P)H to be converted into ATP. The model was compartmented and reactions for transport between compartments were included (Cheung *et al.,* 2013). Output fluxes for NAD(P)H and ATP are included to estimate coenzyme production in excess of that required by the metabolic network. For labelled molecules fluxes representing the

mixing of labelled and pre-existing pools were included to assess the extent of labelling in these components. A detailed description of the model can be found in Appendix 4.

2.6.2 Mass isotopomer distribution vector curation

A list of amino acid and carbohydrate fragments acceptable for use in MFA was created. This list was based on published analyses of mass spectra (Antoniewicz *et al*., 2011, Laine and Sweeley, 1971, Laine and Sweeley, 1973), if a fragment was excluded by either previous investigation it was deemed unreliable. As well as this an analysis of the mass spectra and the fractional ^{13}C atom abundances of each fragment was conducted. If a fragment had an M+0 peak height of less than $1x10^4$ counts it was deemed unreliable as the smaller isotopomer peaks could exhibit interference from background noise. If the fragments had an M+0 peak greater than $4.5x10^6$ the fragment was deemed unreliable as signal saturation could cap the height of the M+0 peak but not the M+n peaks leading to augmentation of the ratio between the peaks, and an inaccurate MID. If the fractional ^{13}C atom abundance of an unlabelled fragment differed consistently from 0.011 by 0.0011 (10%) or more it was also deemed unreliable. The full list of acceptable fragments is shown in Chapter 3.

2.6.3 Flux estimation

The reaction network (2.6.1), MID data (2.6.2) and biomass composition data (2.4) were entered into INCA. Symmetric molecules were flagged for succinate, fumarate and L-*meso*-diaminopimilate (LLDAP – the immediate precursor to lysine). The flux estimation function in INCA was then used. This function runs a Levenberg-Marquardt optimization algorithm (Levenberg, 1944) to minimise the differences between the measured and simulated MID values by minimising the weighted sum-of-squared residuals (SSR; Young, 2014). The

smaller the SSR the better the fit. The SSR is deemed statistically acceptable when it falls withing the range described by the equation below:

$$\chi^2_{\alpha/2}(n-p), \chi^2_{1-\alpha/2}(n-p)$$

Where n is the number of independent measurements, p is the number of fitted parameters, n−p is the degrees of freedom, and α is the threshold P-value at which the fit is rejected.

2.7 Statistical analyses

For analysis of glucose uptake from the media, the rate of glucose consumption over the exponential growth phase was calculated by linear regression, a two-way analysis of variance was then used to compare the rate of glucose consumption or growth in different cultures. For analysis of the dry weight accumulation the natural logarithm for each data point was taken before linear regression and analysis of variance. The antilogs are reported in the main text. For comparison of control, mannose and mannitol-supplemented cultures after five days of growth Student's t-test (two tailed) was used to compare weights from control and treated cultures.

Confidence intervals for each reaction in the flux solutions were produced by parameter continuation and by Monte Carlo analysis. Parameter continuation assesses the sensitivity of the SSR variation in each parameter (Antoniewicz *et al*., 2006). Monte Carlo analysis uses the best-fit flux estimates to generate multiple synthetic datasets and perturbs them with gaussian noise based on the measurement errors. Refitting each synthetic dataset generates a probability distribution for each parameter (Young, 2014).

Differences between flux solutions made using the same model but MID datasets from different experimental conditions were assessed by checking if the confidence intervals for each reaction overlapped. Comparing two means involves comparing two sources of variability, therefore confidence intervals narrower than 95% need to be compared (Smith

et al., 2023). For reactions with equal variance the 83.4% confidence interval needs to be compared for a 95% probability that the flux through the reactions differ. For reactions with an unequal variances between conditions the appropriate confidence intervals to compare for a 95% probability that the model parameters are different can be calculated by the following equation:

$$\left[1 - 2 \times \Phi\left(-1.96 \times \frac{\sqrt{1+\rho^2}}{1+\rho}\right)\right] \times 100\%$$

Where ρ represents the ratio of standard deviations and Φ represents the standard normal cumulative distribution function. See Knol *et al.* (2011) for a full derivation of this equation.

Appropriate confidence intervals were calculated by ranking the flux estimates from 1000 rounds of Monte Carlo simulation in ascending order for each parameter and discarding the appropriate number at the top and bottom. For example from for the 95% confidence interval the top and bottom 2.5% were discarded and for an 83.4% confidence interval the top and bottom 8.3% were discarded.

Principal component analysis (PCA) were performed on the net fluxes of reactions within the CCM from 1000 Monte Carlo simulations for each condition using MetaboAnalyst, an online implementation of R for metabolomics (Chong *et al.*, 2019; R Core Team, 2020). Free net fluxes were mean-centred and scaled to unit variance before use as variables for PCA.

Chapter 3: Establishing a robust fluxomic analysis methodology for *Arabidopsis thaliana* suspension cultures

Previous MFA studies in *Arabidopsis* cell cultures have developed reliable protocols for labelling of cultures, collection of biomass composition data and mass isotopomer distribution vector (MID) data and *in silico* analysis to produce flux solutions (Kruger *et al*., 2012). This chapter describes the implementation and validation of these protocols as well as their extension in confirming a robust set of GC-MS fragments for MID extraction, refinement of the models used for analysis in terms of subcellular localisation, incorporation of co-enzymes, and addition of ancillary reactions to better define outputs from the CCM. The latter part of this chapter will investigate the reproducibility of the flux solutions made using these methods by comparing independent analyses conducted under similar growth conditions and by comparison to the previously published flux solutions obtained using equivalent approaches. The effect of biomass composition on net flux distribution is also considered.

3.1 Development of a labelling system

The application of MFA to cell cultures typically requires a method for introducing labelled carbon into central metabolism. Designing labelling systems to maximise the information provided by label re-distribution in an affordable and practical way requires careful consideration (Long and Antoniewicz, 2013).

The ^{13}C stable isotope of carbon was selected as a label due the reduced risk compared to that associated with radioactive isotopes and ease of measurement of heavy isotope enrichment using GC-MS. Sugars were chosen as the labelled substrate, because carbohydrates are the major products of photosynthesis supplied to heterotrophic tissues

(Turgeon and Wolf, 2009; O'Leary *et al.,* 2019) and glycolysis is the primary source of pyruvate, the main respiratory substrate in eukaryotes (Le and Millar, 2022). Glucose was used as the specific sugar because it is readily absorbed by the cell cultures and high purity positionally ^{13}C labelled glucose is commercially available. While another option is sucrose, the usual source of carbohydrate for culture systems, sucrose is broken down into hexose units upon absorption (Kruger *et al*., 2012), so there is no need to use more expensive sucrose as the source of ^{13}C. Early MFA studies tended to use only [1-^{13}C]-glucose or [U-^{13}C]-glucose (Wiechert, 2001) but subsequent investigations have shown that a useful labelling strategy in *Arabidopsis* cell cultures is parallel labelling and simultaneous analysis with 99% [1-^{13}C]-glucose, 99% [2-^{13}C]-glucose and 20% [U-^{13}C]-glucose (Masakapalli *et al*., 2010). Combining labelling data, particularly in the combination used in this study, has been shown to improve the reliability of flux estimates in MFA, particularly in the oxidative steps of the OxPPP in the plastid and the cytosol (Masakapalli *et al*., 2010).

Seven-day-old unlabelled *Arabidopsis* suspension cultures were subcultured into MS medium containing labelled glucose and grown as per section 2.4. The assumptions underpinning steady-state MFA require that labelling data needs to be collected while the cultures are at metabolic and isotopic steady state. Growth experiments gave a time frame for the labelling. Growth profiles of *Arabidopsis* suspension cultures under standard conditions were constructed (Figure 3.1). Following subculture the cell suspension passes through a lag phase, which is followed by exponential growth from four to eight days after subculture, and a stationary phase beginning eight days after subculture (Figure 3.1A). The concentration of glucose remaining in the medium remains close to the starting concentration until three days after subculture, after this it declines rapidly, while biomass is accumulating. The glucose concentration of the medium then drops more slowly from seven days after subculture (Figure 3.1B). To ensure measurements were obtained from cultures which were at metabolic and isotopic steady state, cells were harvested during exponential growth, at five days after subculture. A metabolic steady state is achieved when

cells are dividing at a constant rate (exponential growth) and such cultures have previously been shown to have achieved isotopic steady state at five days after subculture (Williams *et al*., 2008).

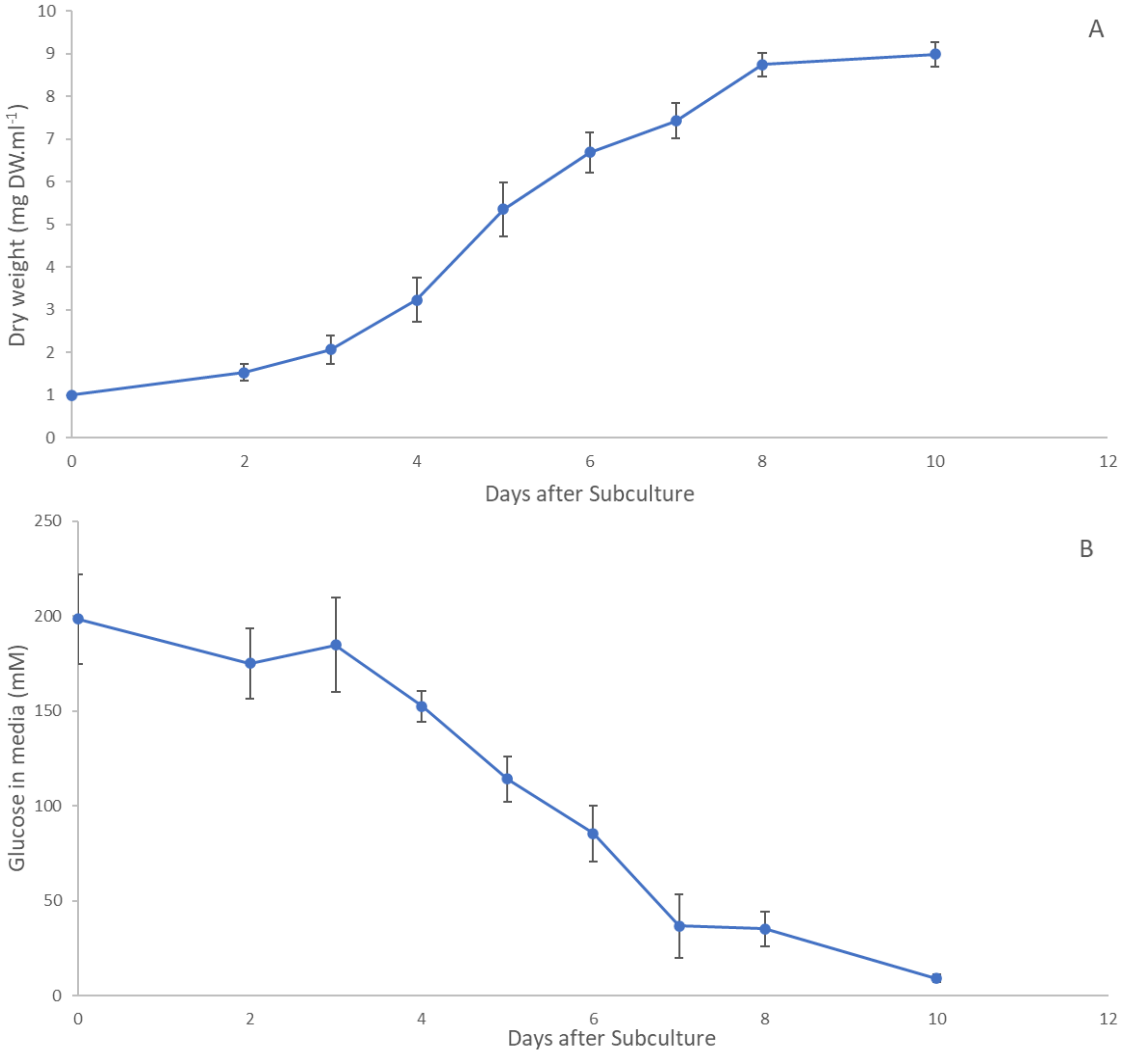


Figure 3.1: *Growth profiles of Arabidopsis cultures. (A) Biomass accumulation and (B) glucose consumption in Arabidopsis suspension cultures grown in control conditions (22°C, MS medium). Points are the mean of three independent culture flasks and error bars represent the standard error of the mean (SEM).*

Figure 3.1B shows some variability in the measured glucose concentration remaining in the medium (large error bars). The variability in the glucose uptake rates is mitigated when MFA is conducted because all fluxes are determined relative to the molar uptake rate of glucose, that is set to 100.

To limit the use of expensive [^{13}C] glucose substrate, labelling experiments were conducted on cells cultures in one tenth the volume of medium normally used to maintain the cell culture. Growth experiments showed that this did not change the growth characteristics of the cell suspension culture (Figure 3.2). Five days after subculture there was no significant difference (*P>0.05*) in mass unit per volume, between the cultures grown in 115 ml total volume and those grown in 11.5 ml total volume (Figure 3.2).

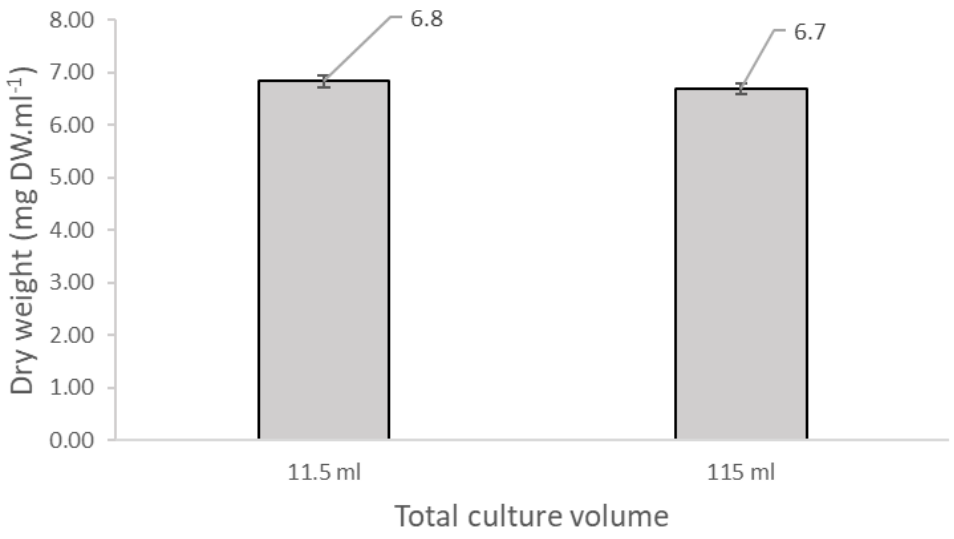


Figure 3.2: *Comparison of cultures grown in 11.5 ml and 115 ml total volume. Bar heights are the mean of three independent culture flasks and error bars represent SEM.*

3.2 Validation of GC-MS protocols for biomolecule identification

GC-MS is a commonly used analytical technique for quantifying the re-distribution of label by the metabolic network, and several well-established derivatisation techniques have been applied in MFA (Kruger *et al*., 2012; Antoniewicz, 2013; Long and Antoniewicz, 2014; Long

and Antoniewicz, 2019). As the GC-MS system intended for use in this project (an Agilent 9000 GC coupled to an Agilent 5977B quadrupole MS) is different from that used in previous MFA studies conducted in the group (an Agilent 7890A GC coupled to an Agilent 5975C quadrupole MS) the suitability of various GC-MS techniques needed to be assessed.

GC-MS protocols were chosen based on previous studies (Zamboni *et al*., 2009; Antoniewicz *et al.,* 2011; Masakapalli *et al*., 2014a; Long and Antoniewicz, 2019) and applied to unlabelled biomass to assess their suitability. Proteogenic amino acids were derivatised using tBDMS. In preliminary analysis carbohydrates were derivatised using aldonitrile pentapropionate, methyloxime pentapropionate, 1,2,5,6-di isopropylidene propionate and diethyldithiolacetal acetate after Antoniewicz *et al*. (2011) and Price (2004). However these methods failed to reliably produce clear, identifiable, glucose chromatogram peaks or mass spectra peaks with fragments suitable for MID extraction and thus the procedures were not developed further. In the final analysis MOX-TMS was used for carbohydrate derivatisation (See Chapter 2).

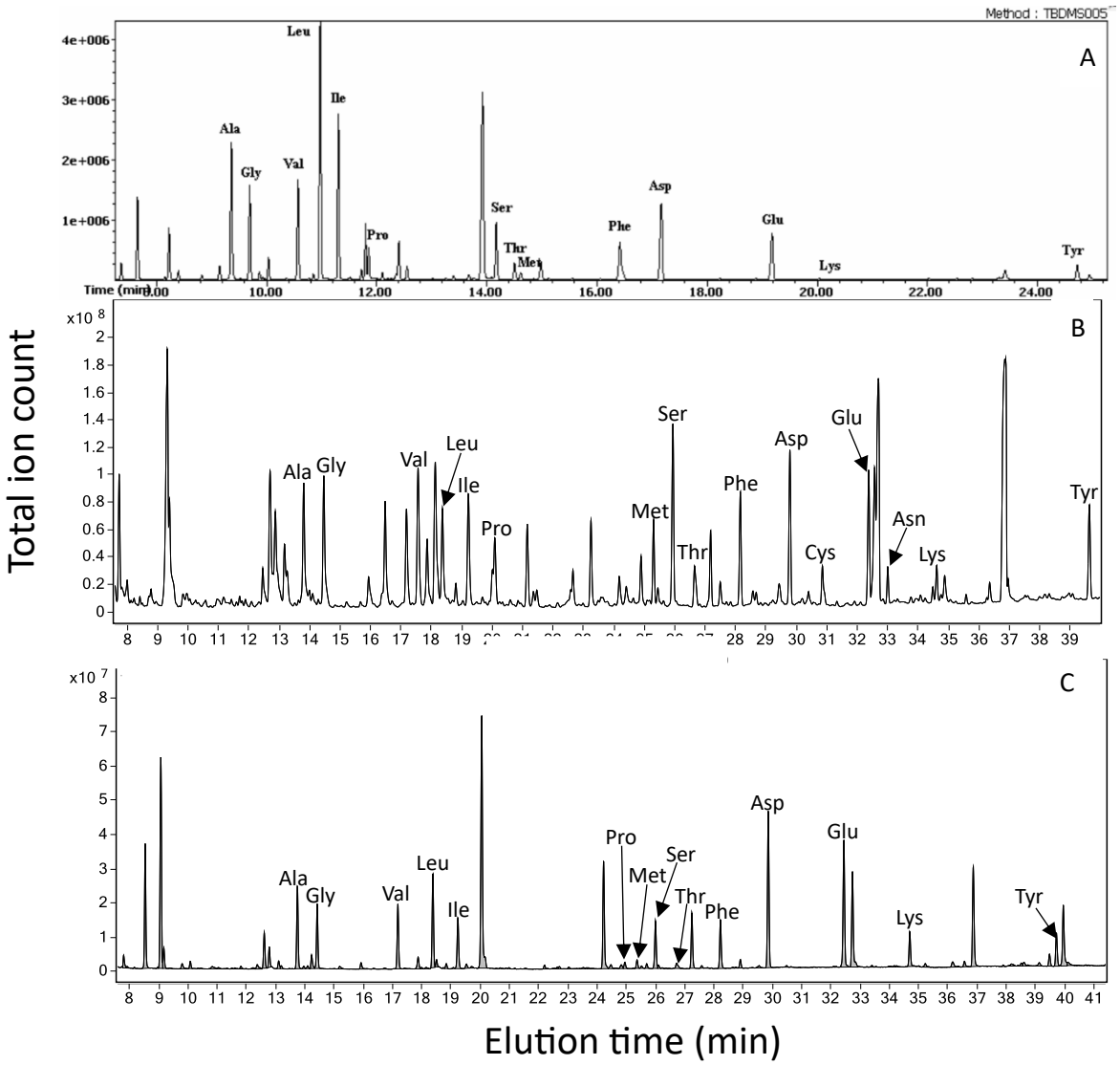


Figure 3.3: *Comparison of total ion chromatograms of tBDMS-derivatised proteogenic amino acids in this project and a published example. (A) Published total ion chromatogram of proteogenic amino acids from E. coli taken from Antoniewicz et al. (2007). (B) Total ion chromatogram of a mix of amino acid standards. (C) Total ion chromatogram of proteogenic amino acids extracted from Arabidopsis.*

Comparison of the total ion counts and mass spectra collected from biological material with those from standards and published examples validated the identification of target molecules. tBDMS-derivatised proteogenic amino acids produced a total ion chromatogram profile which was similar to the one published by Antoniewicz *et al*. (2007) and to that of a mix of amino acids standards (Figure 3.3). The mass spectra of each amino acid also matched those in standard amino acids mixes and in Antoniewicz *et al*. (2007; Appendix 1).

The difference in the elution order of methionine, serine and threonine in this study compared to Antoniewicz *et al*. (2007) probably arises from the difference in columns used for gas chromatography. GC-MS analysis in this study was conducted on an Agilent Technologies Intuvo 9000 GC system fitted with an Agilent DB-5ms Ultra Inert 122-15512UI-INT silica capillary column, while Antoniewicz used a HP5890 Series II GC with a DB-1701 capillary column.

Comparison of mass spectra from MOX-TMS derivatised glucose isolated from starch, sucrose and cell wall material matched with spectra from authentic glucose and from published MOX-TMS derivatised glucose spectra (Figure 3.4, Laine and Sweeley, 1971). All the glucose mass spectra contain diagnostic peaks at m/z 319, 217, 205, 160, 147 and 103. The mass spectra for fructose derived from sucrose and cell wall derived five carbon sugars also matched published spectra (Figure 3.5, 3.6, Laine and Sweeley, 1973); all the fructose mass spectra show diagnostic peaks at m/z 307, 217, 205, 147 and 103 and all the xylose mass spectra show diagnostic peaks at m/z 307, 217, 147 and 103. The comparisons in Figures 3.3 to 3.6 as well as those in Appendix 1 show that the presented amino acids and sugars were accurately identifiable in the GC-MS output, and that they could be used as potential targets for MID extraction.

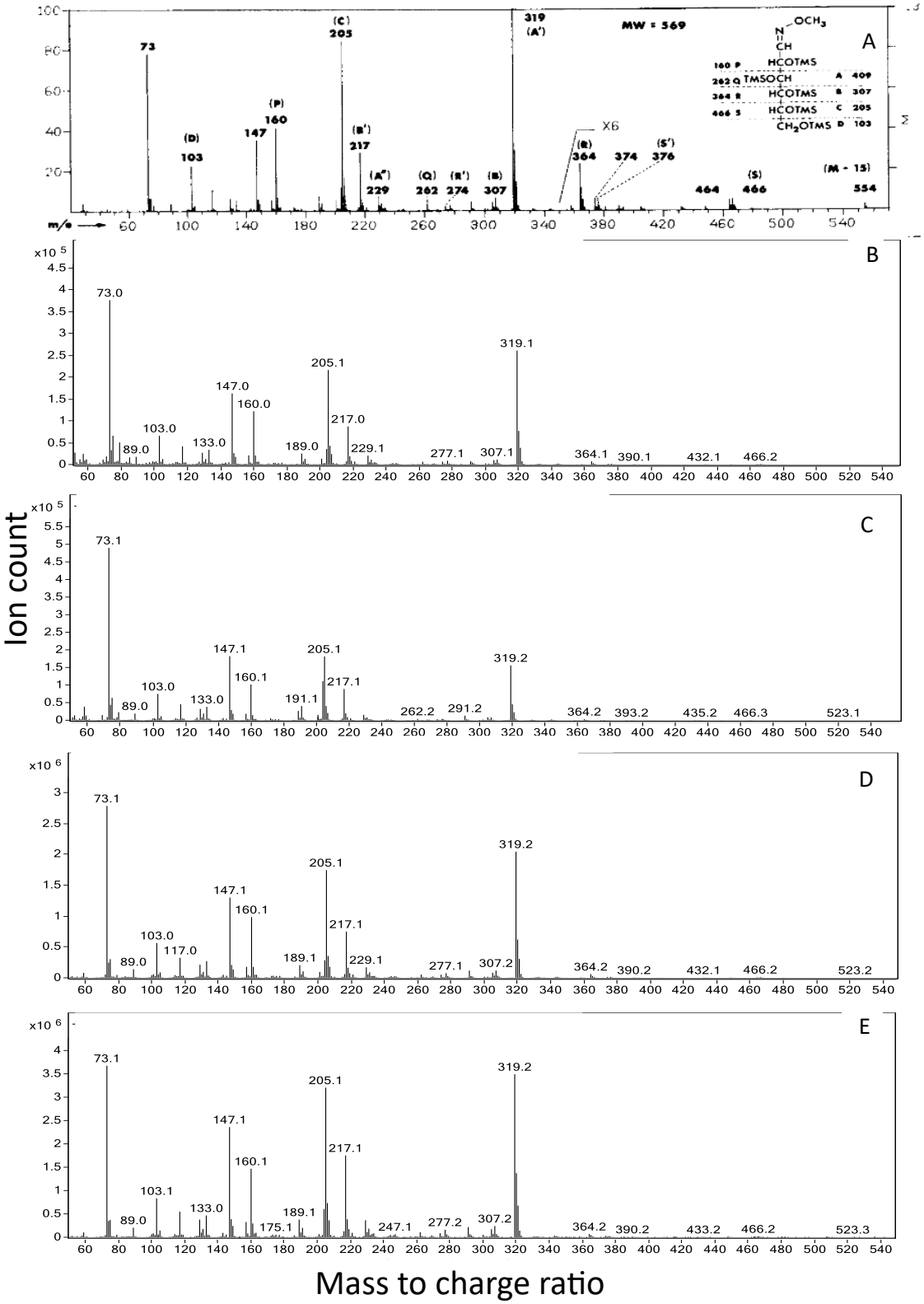


Figure 3.4: *Comparison of mass spectra of MOX-TMS derivatised glucose in this project and published examples. MS spectra of MOX-TMS glucose from (A) Laine and Sweeley (1971), (B) glucose standard, (C) starch-derived glucose, (D) sucrose-derived glucose, (E) cellulose-derived glucose.*

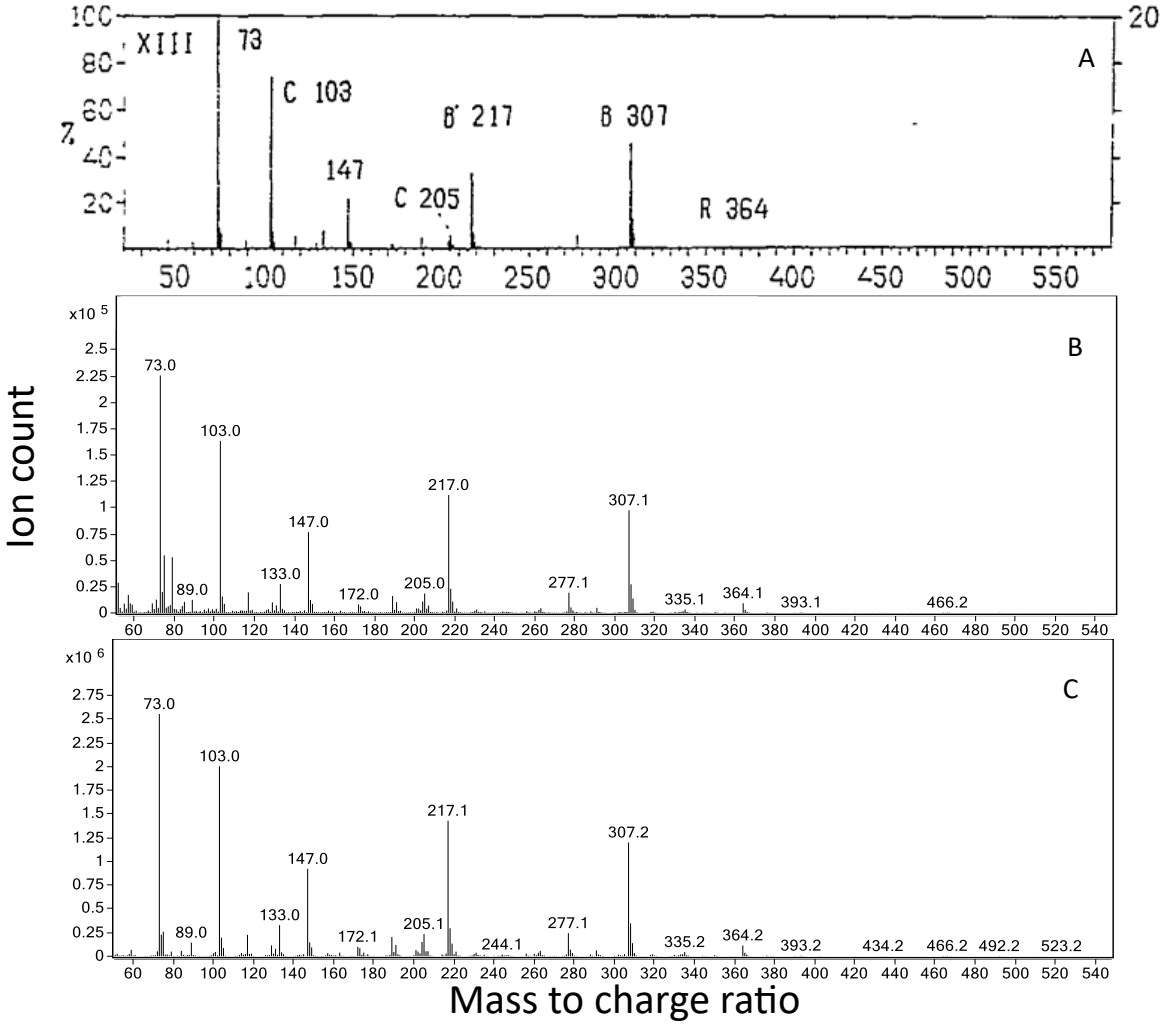


Figure 3.5: *Comparison of mass spectra of MOX-TMS derivatised fructose in this project and published studies. MS spectra of MOX-TMS fructose from (A) Laine and Sweeley (1973), (B) fructose standard, and (C) sucrose-derived fructose.*

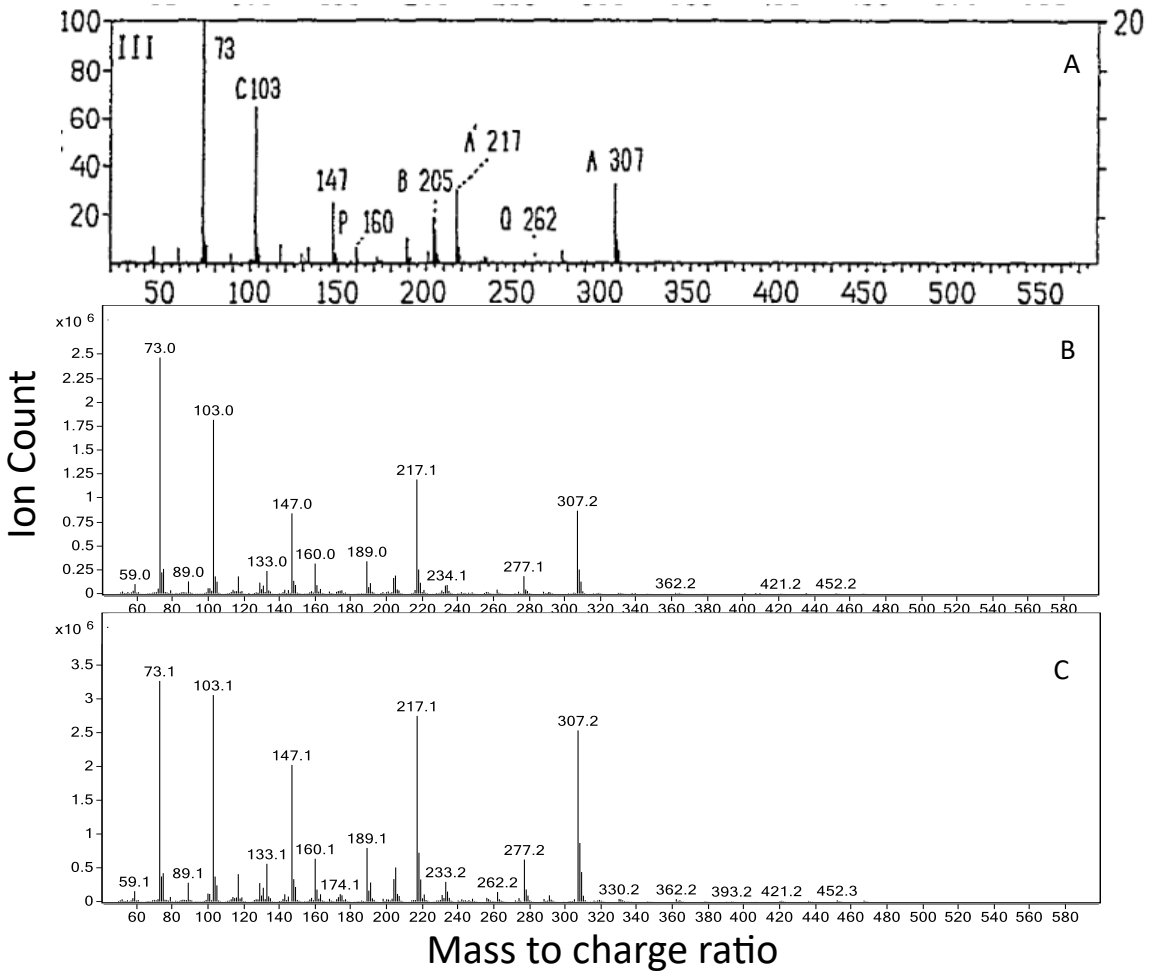


Figure 3.6: *Comparison of mass spectra of MOX-TMS derivatised xylose in this project and published studies. Mass spectra of MOX-TMS xylose from (A) Laine and Sweeley (1973), (B) Authentic xylose, (C) cell wall-derived five carbon sugar.*

3.3 Mass isotopomer distribution vector curation

Once the identification of biomolecules in the GC-MS output was validated, the suitability of individual fragments for extraction of MID vectors needed to be appraised.

Fractional ^{13}C atom abundance in the unlabelled samples was used to assess the accuracy of labelling information. The fractional ^{13}C atom abundance was calculated by dividing the fraction of the fragment in the m+1 peak by the number of carbon atoms in the fragment (See Chapter 2). The natural abundance of ^{13}C is 1.1%. Therefore the m+0 isotopomer of each fragment was expected to make up the vast majority of the fragment population. Additionally, given that the statistical likelihood of an individual molecule of a metabolite

containing two or more ^{13}C atoms is comparatively low (less than 0.08% for a 3-carbon compound), the fractional ^{13}C atom abundance should be close to 0.011 for all unlabelled accurately measured fragments. Fragments which consistently had a fractional ^{13}C atom abundance that differed from 0.011 by 0.005 or more were identified and removed from the analysis, as they were deemed to be an inaccurate description of ^{13}C enrichment in the target molecule (Appendix 2). 0.005 was chosen as an acceptable error level as this is half the default error level used by INCA, the software used for MFA (Young, 2014). Therefore, using a 0.005 error level means that this fragment selection process is more stringent than that expected by INCA.

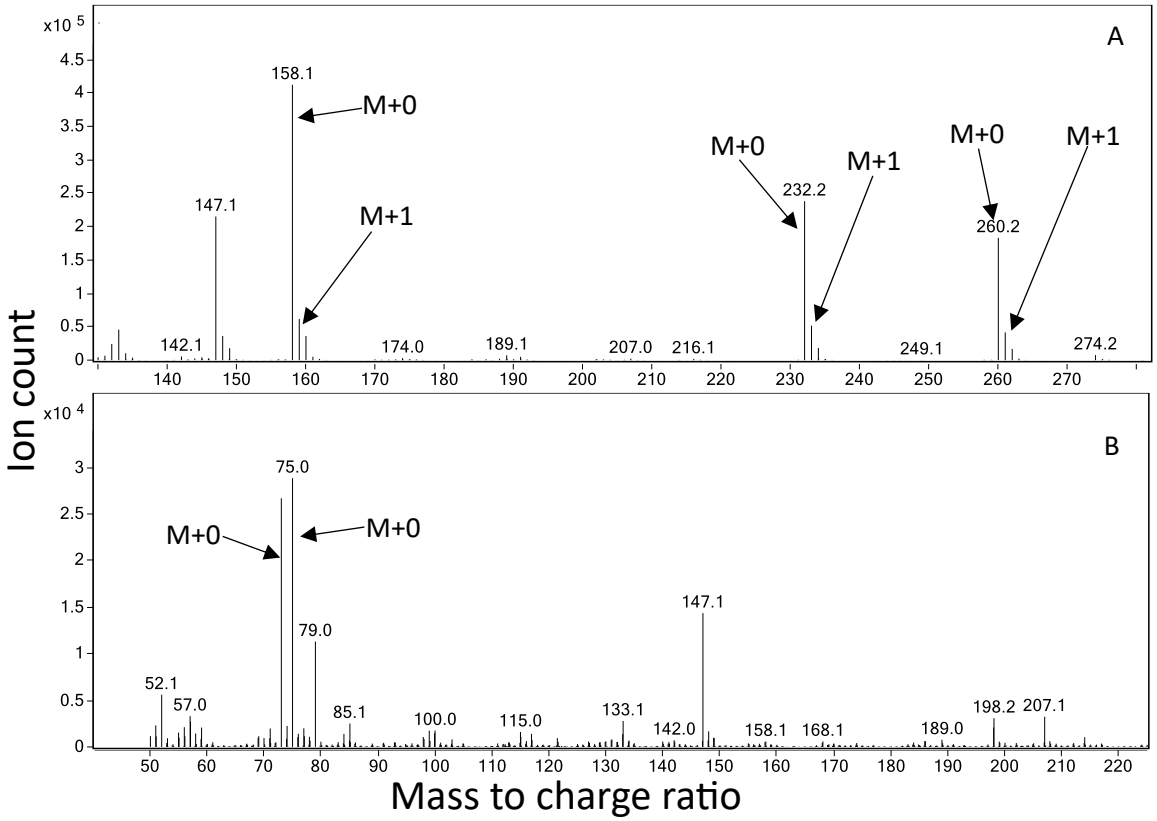


Figure 3.7: *Examples of GC-MS features. (A) Example of clearly defined peaks in the mass spectrum of unlabelled alanine. (B) Overlapping fragments in the mass spectrum of unlabelled proline.*

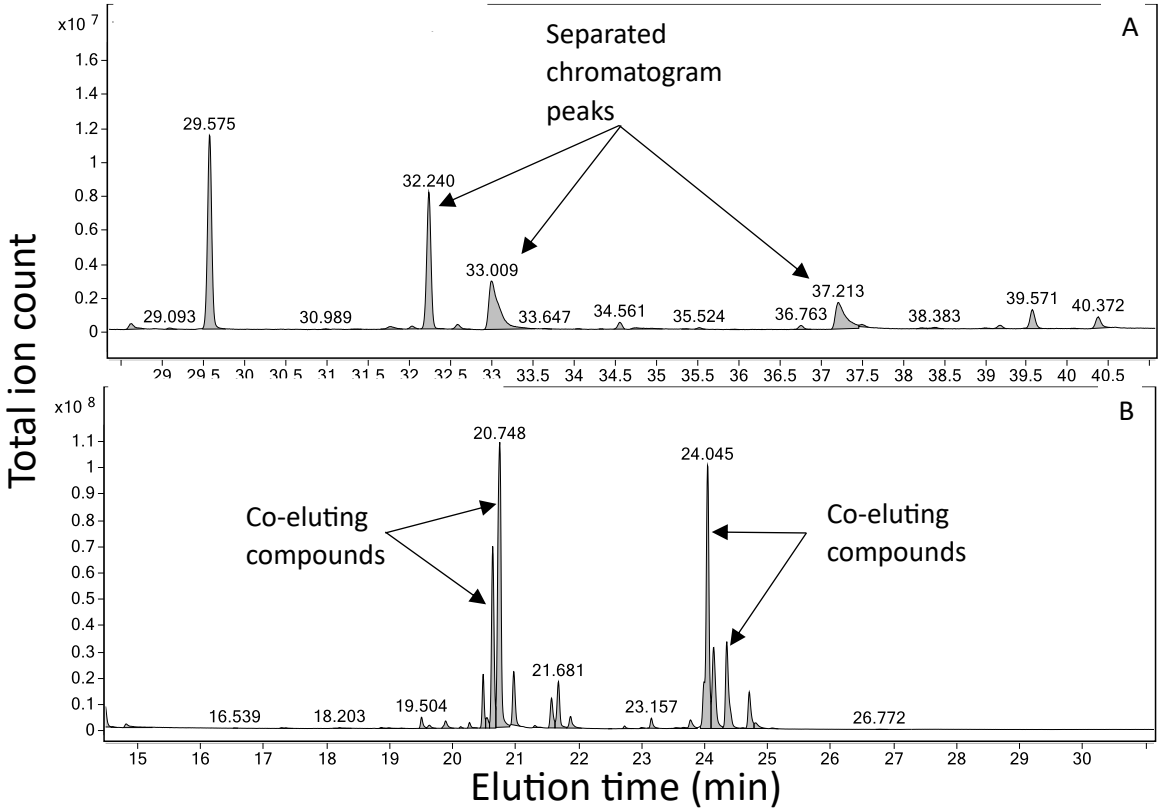


Figure 3.8: *Examples of GC-MS features. (A) Example of clearly defined peaks in the total ion chromatogram from amino acids. (B) Overlapping chromatogram peaks in cell wall samples.*

The main reasons for this inaccuracy included; overlap in the mass spectrum with other fragments (Figure 3.7); co-elution with another compound during GC (Figure 3.8); or mis-assignment of a compound based on an incorrect identification of mass fragments in the spectrum.

Signal saturation is another issue which can cause inaccurate determination of ^{13}C enrichment. If the signal for any peak in a fragment is above the maximum recording threshold of the MS detector, then the signal will be truncated, meaning that of all the less abundant peaks appear larger relative to the saturated peak. Since the lightest mass isotopomer (m+0) predominates in metabolites from unlabelled plant material, this distortion will tend to overestimate the extent of label enrichment. A correlation between inaccurate fractional ^{13}C atom abundance and fragments with total ion chromatogram intensities greater than $5x10^7$ counts was recorded (Figure 3.9) for proteogenic amino acids.

Therefore, fragments from total ion chromatogram peaks greater than $5x10^7$ counts were removed from the analysis. Reducing the amount of sample analysed (2.5 µl rather than 25 µl of hydrolysate) avoided signal saturation in proteogenic amino acids.

A set of acceptable amino acid and carbohydrate fragments was drawn up based on the fractional ^{13}C atom abundance analysis and published analyses of amino acid and carbohydrate GC-MS spectra (Table 3.1). This set of fragments can be used as a guide for future MFA investigations in *Arabidopsis* cell suspension culture, particularly those using an equivalent GC-MS system. The set of amino acids identified was broadly in agreement with those recommended for MFA in *E. coli* (Antoniewicz *et al*., 2007). However, the set here contains an extra fragment of valine (M-159), because the mass spectrum showed a large, non-overlapping family of peaks that produced an MID with an acceptable fractional ^{13}C atom abundance.

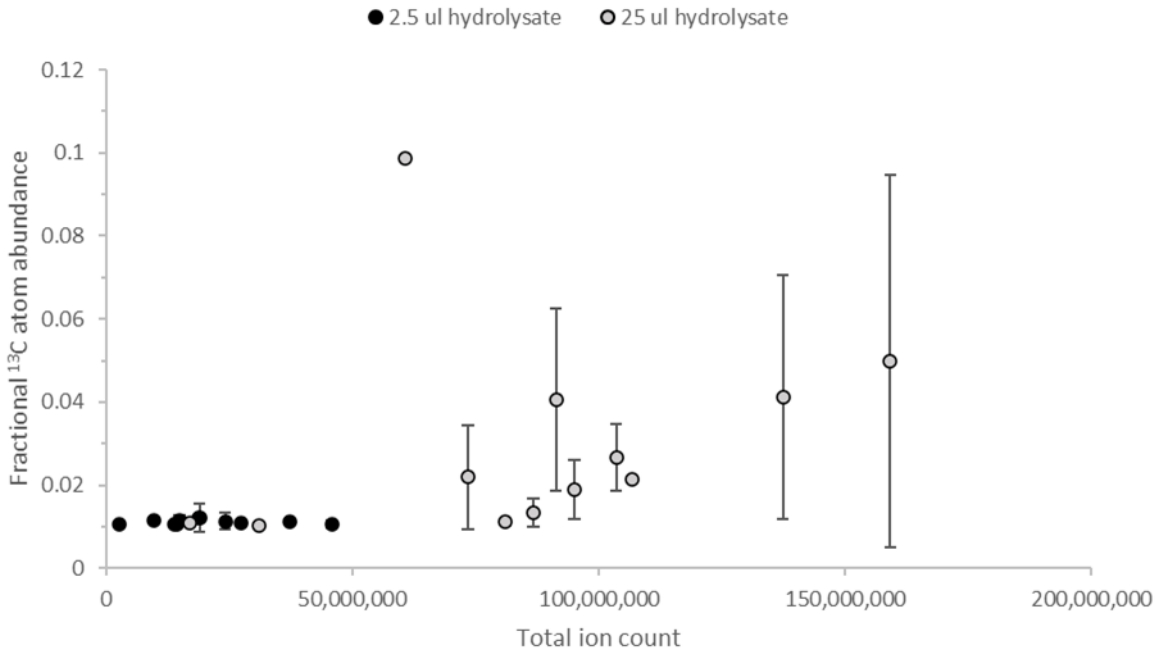


Figure 3.9: *Average ^{13}C atom abundance against total ion count for each proteogenic amino acid detected. Amino acids detected in the analysis of the 25 µl hydrolysate are shown in grey, those detected in the analysis of the 2.5 µl hydrolysate are in black. Each value is the mean ± SD of fractional ^{13}C atom abundance across all fragments analyzed.*

MIDs from glucose derived from starch, sucrose and cell wall material are desirable for resolving the partitioning of carbohydrate metabolism between the cytosol and the plastid (see Section 3.4). This is particularly true of fragments including carbons one and two when using the labelling strategy in this project (see Section 3.1). f160 was the only fragment containing carbons one and two which had a reasonable peak size (the others being the peaks at m/z 262, 274, 364, 674, 376, 464, 466 and 554; Figure 3.4). However, the fractional ^{13}C atom abundance was 0.041-0.054, suggesting that the f160 fragment may not provide a reliable estimate of ^{13}C enrichment. Because of the potential importance of this fragment in resolving compartmentation, f160 MID data were only included in the analysis if the weighted residual for each peak of the f160 fragment in the model fits was less than 5.

A summary of all the fragments that were rejected, along with justification for rejection, is presented in Appendix 2. All the MID data for this project are presented in Appendix 3.

Table 3.1: *Fractional ^{13}C atom abundance in unlabelled proteogenic amino acids and carbohydrates.*

Molecule	Fragment	Mean fractional ^{13}C atom abundance	SEM	Carbon atoms in fragment
Alanine	M-57	0.011	2.8E−04	1, 2, 3
	M-85	0.011	2.7E−05	2, 3
	M-159	0.013	1.0E−03	2, 3
Glycine	M-57	0.011	3.5E−04	1, 2
	M-85	0.009	8.8E−04	2
Valine	M-57	0.010	2.4E−04	1, 2, 3, 4, 5
	M-85	0.012	4.2E−04	2, 3, 4, 5
	M-159	0.010	2.7E−04	2, 3, 4, 5
Leucine	M-85	0.010	1.8E−04	2, 3, 4, 5, 6
Isoleucine	M-85	0.009	1.7E−03	2, 3, 4, 5, 6
	M-159	0.008	2.3E−03	2, 3, 4, 5, 6
Methionine	M-57	0.010	9.0E−04	1, 2, 3, 4, 5
	M-85	0.010	2.7E−04	2, 3, 4, 5
	M-159	0.012	3.3E−04	2, 3, 4, 5
Serine	M-57	0.011	3.4E−04	1, 2, 3
	M-85	0.010	3.7E−04	2, 3
	M-159	0.011	2.8E−04	2, 3
Threonine	M-57	0.013	2.5E−02	1, 2, 3, 4
	M-85	0.013	1.8E−03	2, 3, 4
Phenylalanine	M-57	0.010	7.8E−05	1, 2, 3, 4, 5, 6, 7, 8, 9
	M-85	0.011	2.3E−04	2, 3, 4, 5, 6, 7, 8, 9
	M-159	0.010	1.0E−04	2, 3, 4, 5, 6, 7, 8, 9
	f302	0.010	7.3E−04	1, 2
Aspartate	M-57	0.011	2.8E−04	1, 2, 3, 4
	M-85	0.011	6.5E−04	2, 3, 4
	f302	0.012	1.3E−04	1, 2
Glutamate	M-57	0.010	1.4E−04	1, 2, 3, 4, 5
	M-85	0.009	3.8E−04	2, 3, 4, 5
	M-159	0.010	1.9E−04	2, 3, 4, 5
Starch-derived glucose	f160*	0.041	7.5E−04	1, 2
	f319	0.011	1.5E−04	3, 4, 5, 6
	f307	0.011	1.8E−03	4, 5, 6
Cellulose-derived glucose	f160*	0.054	1.4E−03	1, 2
	f319	0.011	3.7E−04	3, 4, 5, 6
	f307	0.006	2.0E−03	4, 5, 6
Sucrose-derived glucose	f160*	0.041	0.0E+00	1, 2
	f319	0.024	0.0E+00	3, 4, 5, 6
	f307	0.014	0.0E+00	4, 5, 6
Sucrose-derived fructose	f364	0.015	5.6E−04	1, 2, 3, 4
	f307	0.011	1.2E−04	4, 5, 6
	f103	0.013	1.4E−04	6
Cell wall-derived five carbon sugars	f307	0.010	3.3E−04	3, 4, 5
	f103	0.014	2.1E−04	5

Asterisks (*) represent fragments that were used only if they produce a weighted residual of less than 5 during fitting, as described in main text. Amino acids are arranged in order of elution time.

3.4 Model development

MFA hinges on being able to explain the observed redistribution of label into metabolic intermediates and end-products. Therefore, it is necessary to define a model of the steps which are responsible for the observed re-distribution of label, rather than an exhaustive list of every reaction in metabolism (Kruger *et al*., 2012).

3.4.1 Initial model

Initially a model of the *Arabidopsis* metabolic network was constructed that included glycolysis, the OxPPP, the TCA cycle, anaplerotic reactions, uptake fluxes for nitrogen, oxygen and sulfur, an output flux for CO_2 and biosynthetic routes for amino acids, starch, sucrose, five and six carbon cell wall components, and a general lipid synthesis step (see section 3.5). A reaction schematic of this model is shown in Figure 3.10 and a full reaction list and carbon transition mapping is presented in Appendix 4. Details of all models discussed in this chapter are presented in Appendix 5.

In this initial model, hereafter referred to as model 1, it was assumed that the TCA cycle was confined to the mitochondrion, that glycolysis and the oxidative steps of the OxPPP were duplicated in the plastid and cytosol, and that all amino acid and lipid synthesis occurred in the plastid.

The extensive sub-cellular compartmentation of plant metabolism is a non-trivial complicating factor in flux analysis, particularly when pathways are duplicated in two compartments (Kruger and Ratcliffe, 2015). While there have been some attempts to use metabolomic, proteomic or transcriptomic data to constrain compartmentation, these approaches are limited by the observation that changes in metabolite, protein or transcript levels do not necessarily correlate with metabolic flux distribution (Fernie and Stitt, 2012; Chubukov *et al*., 2013). An alternative method for deducing compartmentation in flux maps is to collect MID data which can report on the labelling of intermediates in specific compartments (Ratcliffe and Shachar-Hill, 2006; Allen *et al*., 2012). This approach has been

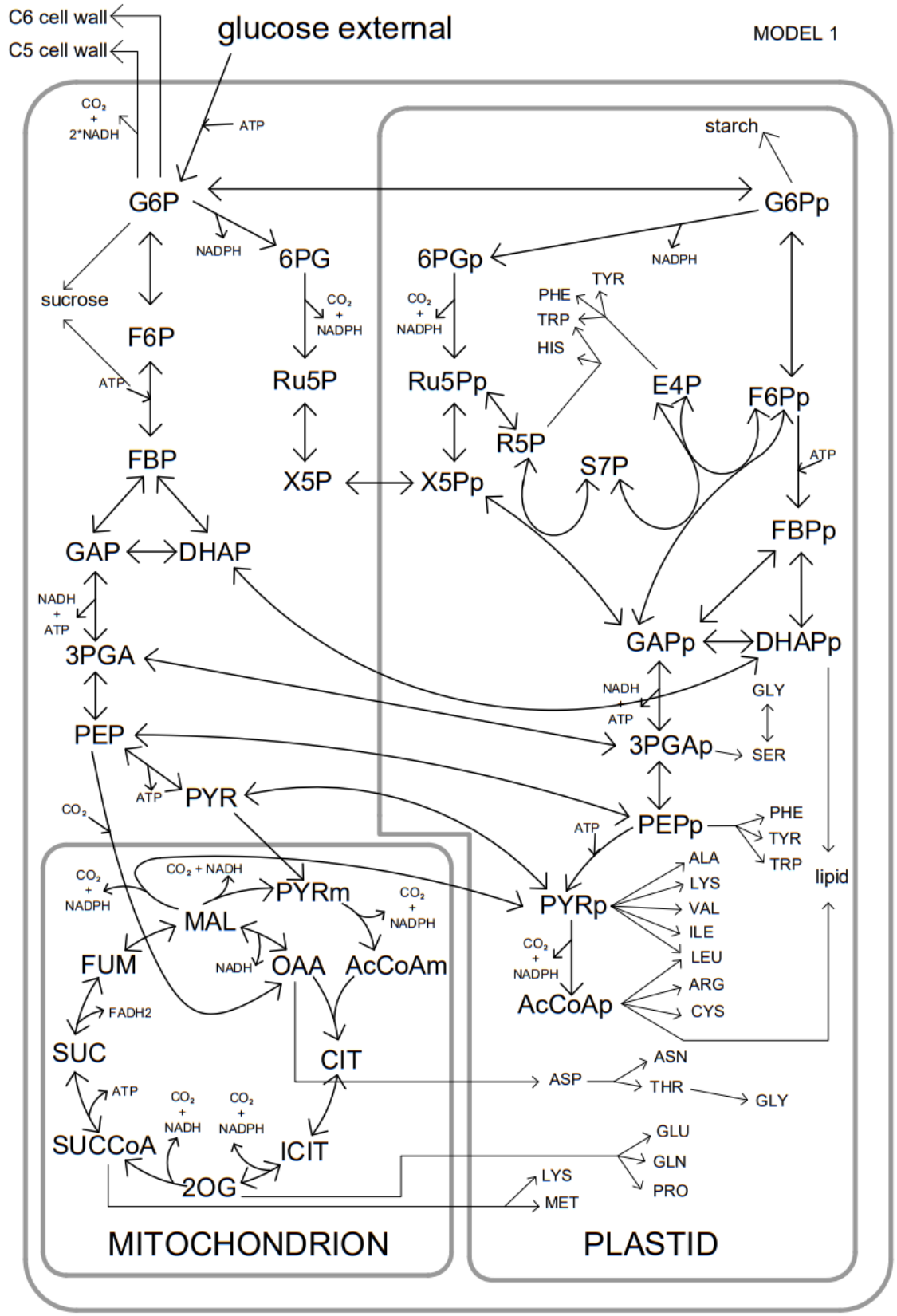


Figure 3.10: *Network topology of the initial model (designated model 1). Reaction fluxes are shown as black arrows. Phospholipid membranes are shown in grey. Double headed arrows represent reactions that were treated as reversible and single headed arrows represent reactions that were treated as irreversible.*

applied to *Arabidopsis* cell cultures, by analysing the labelling patterns in starch, cell wall components and sucrose to deduce the labelling of glucose 6-phosphate G6P pools in the cytosol and plastids (Masakapalli *et al*., 2013, 2014a). The utility of labelling of metabolites from different compartments can become limited when intermediates are in rapid exchange between compartments, in which case the labelling pattern from the two compartmental pools will be identical (Kruger and Ratcliffe, 2015). Some flux maps obtained by MFA use 'transcompartmental' pools which assume the intermediates are in rapid exchange across a membrane, and thus amalgamate the likely net fluxes (William *et al*., 2008). The GC-MS methods in this project allowed the collection of MID data from starch, cell wall carbohydrates and sucrose, therefore compartmentation of glycolysis and the OxPPP in the cytosol and the plastid was included in model 1.

Another element of the model which required consideration was the actions of transketolase and transaldolase in the OxPPP (Schwender *et al*., 2003). Various methods have been used to model the OxPPP in MFA but in this project a method of half reactions proposed by Kleijn *et al*. (2005) was used, as this formulation was able to accommodate the full reaction flexibility displayed by transketolase and transaldolase (R55-R59 in Appendix 5).

PPi:fructose 6-phosphate phosphotransferase (PFP) also needed to be considered, as it causes mixing between cytosolic fructose 6-phosphate (F6P) and fructose 1,6-bisphosphate (FBP) pools. A straightforward approach to encoding this reaction could be to make the phosphofructokinase reaction (PFK; R34) freely reversible, however this could make ATP balancing in the model inaccurate as the PFK reaction requires ATP while the PFP reaction does not. An independent reaction running from FBP to F6P could be included, but this would make flux through PFP/PFK indeterminable and could potentially lead to a futile cycle resulting in loss of ATP. To avoid these issues the reaction was encoded as R35 in Appendix 5 or as below

F6P (abcdef) + FBP (ghijkl) −> FBP (abcdef) + F6P (ghijkl)

This method of defining the exchange reaction catalysed by PFP allows mixing of label between F6P and FBP pools without ATP depletion by futile cycling between F6P and FBP.

It is important to note that while this method of defining the combined effect of PFP and PFK reactions on ^{13}C redistribution can be used to fit labelling data to the model, it does not differentiate between the two enzymatic activities in a way that is typically attempted in other modelling approaches such as flux balance analysis.

Non-phosphorylating glyceraldehyde-3-phosphate dehydrogenase is a distinctive feature of plant metabolism (O'Leary *et al*., 2019). It catalyses conversion of glyceraldehyde 3-phosphate (GAP) to 3-phosphoglycerate (3PGA) without phosphorylation of ADP to ATP, and is thought to play a role in regulating ATP provision. However, it is not possible to distinguish between the phosphorylating and non-phosphorylating GAP dehydrogenases because they affect the distribution of labelled carbon in identical ways. Only the ADP-phosphorylating reaction was included in the model but consideration that the non-phosphorylating reaction might be used needs to be made when analysing estimated levels of substrate level phosphorylation.

The γ-aminobutyric acid (GABA) shunt is another phosphorylation-independent bypass in which 2-oxoglutarate (2OG) is converted to glutamate, then succinate via GABA thus avoiding substrate level phosphorylation by succinyl CoA synthase (Olsen and Delorey, 1999; O'Leary *et al*., 2019). This bypass had to be incorporated into the TCA flux from 2OG to succinate because discrimination between the two pathways is also impracticable in a conventional ^{13}C labelling experiment.

3.4.2 Ancillary reactions

As well as the general network topology, several ancillary reactions were included in the model to expand the scope of the information provided by the flux solution. In this project I used three groups of these ancillary reactions, one group for interpretation of the rates of withdrawal of biomass precursors, another group for summarising the metabolism of ATP and reduced co-enzymes, and a third group for accounting for the contribution of unlabelled material to the measured labelling patterns.

Several metabolic intermediates are removed from glycolysis, OxPPP and the TCA cycle for the synthesise of multiple products. The total rate at which the metabolite is removed from the CCM can be calculated simply by summing the net fluxes through all of the biosynthetic pathways in which that metabolite is involved (Figure 3.11A). However, this method cannot provide an estimate of the precision of the calculated rate of metabolite withdrawal, because even if confidence limits are available for individual products summing these confidence limits does not produce an accurate confidence interval for overall withdrawal of the precursor from the central network. To solve this conundrum, a generic step can be inserted to create a virtual second pool of the metabolite, which is withdrawn from the main pool on demand to act as the precursor for biosynthesis of multiple products (Figure 3.11B). The flux between the two pools (from Metabolite B to Metabolite B.B in Figure 3.11B) provides the overall rate at which that metabolite is withdrawn for biosynthesis and for which an associated confidence interval can be determined.

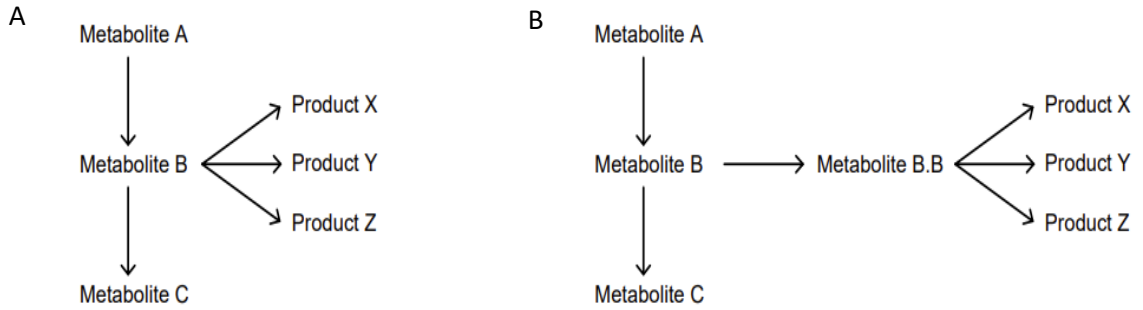


Figure 3.11: *Schematic of the withdrawal for biosynthesis ancillary steps. (A) An example in which is difficult calculate the accuracy of the rate at which metabolite B is withdrawn for biosynthesis. (B) The method used in this project to calculate the rate of withdrawal of metabolite B with an associated confidence interval.*

A variation of this method was also used to sum the flux through reactions that are duplicated in different cellular compartments. A virtual metabolite (a) was included as a by-product of both duplicated reactions in the plastid and the cytosol. An output reaction was then included to give a rate of production of the virtual metabolite with an associated confidence interval. See below;

G6P <–> F6P + a

G6Pp <–> F6Pp + a

a –> a.out

The second group of ancillary reactions included in model 1 were used to track the production of ATP, NADPH, and NADH by the CCM and demand for these coenzymes by biosynthetic metabolism (Figure 3.12). It was assumed that the CCM produces more ATP, NADPH and NADH than it consumes and that the excess ATP, NADPH and NADH are available to support biosynthetic metabolism. Coenzymes produced and consumed by the CCM were assigned to virtual pools defined as ATPi, NADPHi and NADHi (‘i’ standing for ‘internal to CCM’). These could then be passed to a second set of pools, ATPprod, NADPHprod and NADHprod (‘prod’ standing for ‘produced by CCM’), respectively.

The flux from the ‘i' pools to the ‘prod’ pools reports the net production rate of NADPH and NADH by oxidation of metabolites in the CCM and the net production rate of ATP from substrate level phosphorylation in the CCM.

Conversely, coenzymes produced and consumed by biosynthetic metabolism were defined as ATPe, NADPHe and NADHe (‘e’ standing for ‘external to CCM’). The flux from the ‘prod’ pools to the ‘e’ pools gives the net rate of consumption of metabolic resources by biosynthetic metabolism. However, it is likely that the biosynthetic requirement for ATP will be greater than the ATP provision by substrate level phosphorylation alone. ATP can also be produced from reduced coenzymes via the electron transport chain (see O’Leary *et al*., 2019 for review), and this was modelled by including a step in which NADH taken from the NADHprod pool was combined with $0.5*O_2$ to produce 2.5*ATPprod, and $FADH_2$ (produced by succinate dehydrogenase) was combined with $0.5*O_2$ to yield 1.5*ATPprod (see R27 and R28 in Appendix 6). A non-energy linked transhydrogenase step was also included which allowed conversion between NADPHprod and NADHprod (Bykova *et al*., 1999, Cheung *et al*., 2013). Any excess NAD(P)H surplus to the requirements of biosynthetic metabolism was converted into ATPprod which was then exported to an ATPout pool. The flux from ATPprod to ATPout represents the surplus metabolic resources (in excess of requirements for biosynthesis) expressed as ATP equivalents.

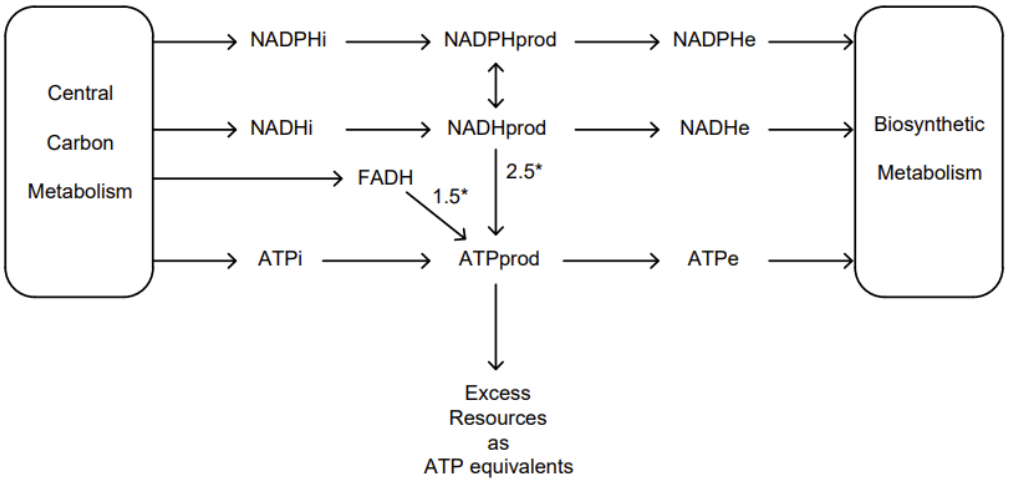


Figure 3.12: *Schematic of the NADPH, NADH and ATP tracking reactions included in the metabolic models in this project to facilitate the analysis of the coenzyme requirements for biosynthesis.*

This system for tracking NADPH, NADH and ATP metabolism is a refinement on previous flux analysis studies. While some MFA studies of *E. coli, Clostridium ljungdhalii* and mammalian adipocyte cultures have tracked metabolic resource production and consumption (Taymaz-Nikerel *et al*., 2010; Antoniewicz, 2021; Oates and Antoniewicz, 2022; Dahle *et al.,* 2022) they have simply summed the flux through multiple reactions which produce or consume NADPH, NADH and/or ATP and thus cannot produce meaningful confidence limits for assessing the accuracy of the estimates.

There are three important considerations that need to be made when interpreting fluxes in this resource tracking system. The first, with reference to earlier discussion, is a consideration of the respiration paradigm used (Amthor, 2000; see Chapter 1 for more details). Use of the GMRP would suggest that the excess resource export is equal to the requirement of maintenance respiration, while the GMWRP would suggest that the excess ATP equivalents is equal to the sum of requirement for maintenance respiration and wastage of metabolic resources in futile cycling. The GP would suggest that excess ATP equivalents is the sum requirement of every biochemical and/or biophysical process that is not included in the model. These processes may contribute to accumulation of new biomass

or homeostasis. The second consideration is that the export of excess resources is quantified as 'ATP equivalents', and so does not necessarily reflect consumption of ATP per se. Whichever respiration paradigm is used it is not possible to identify the specific requirements for NADPH, NADH and ATP for processes that are not included in the model. The third consideration is that the production of ATP by substrate level phosphorylation (ATPi to ATPprod) represents the maximum possible ATP production from substrate level phosphorylation, as any flux through the non-phosphorylating GAP dehydrogenase and/or GABA shunt would decrease the yield of ATP relative to that determined by the model.

A group of ancillary reactions was also included to account for the effect of unlabelled material on the MID measurements. In labelling experiments *Arabidopsis* suspension culture is transferred to MS medium containing ^{13}C labelled glucose. The ^{13}C will be distributed around metabolism, but there will be some pre-existing biomass which will not contain ^{13}C label. To account for this, ancillary reactions were included in which the main pool of a metabolite (A) was combined with a pool containing only natural abundance ^{13}C to create the measured metabolite (A.s) pool (Figure 3.13). Flux from the .s pool into the Sink was fixed at 100 so that the contributions from labelled and pre-existing pools to the analysed pool are presented as a percentage.

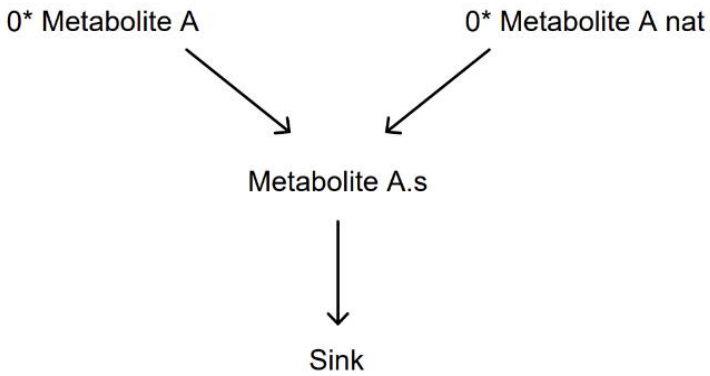


Figure 3.13: *Schematic of the unlabelled contribution ancillary reactions. The 0* multiplier ensures that no material is withdrawn through this reaction which would otherwise have distorted the deduced fluxes in the network.*

The ancillary reactions recorded here allow the flux solutions to offer greater insight into the biosynthetic demands for specific precursors, the production of ATP, NADPH and NADH metabolism, and the contribution of unlabelled material to the labelling pattern. This expanded utility of MFA will assist in addressing the main goal of this project, to assess the relationship between growth and metabolism in *Arabidopsis* cell suspension cultures.

3.4.3 Assessment and refinement of the modelled CCM

The flux solutions produced in this project needed to provide a precise estimate of flux distribution though the CCM. To test the utility of model 1, flux estimation was used to calculate the best fit solution based on MID data from cultures grown at 22°C in MS medium and the 95% confidence intervals for each flux estimate was determined by parameter continuation. To assess how well fluxes through the network could be defined the size of the confidence interval for each reaction was calculated and the mean confidence interval size for all net reactions in the CCM was determined. A small confidence interval for a reaction would indicate that the reaction was well defined and a small mean confidence interval for the CCM would indicate that the model was providing a precise description of the flux distribution. Despite being a statistically acceptable fit to the labelling data the mean confidence interval for model 1 was infinite (Table 3.2), due to reactions for transport of PEP and 3PGA between plastid and cytosol as well as conversion of PEP to 3PGA by phosphglycerate mutase and enolase having undefinable fluxes (Figure 3.14, Appendix 5).

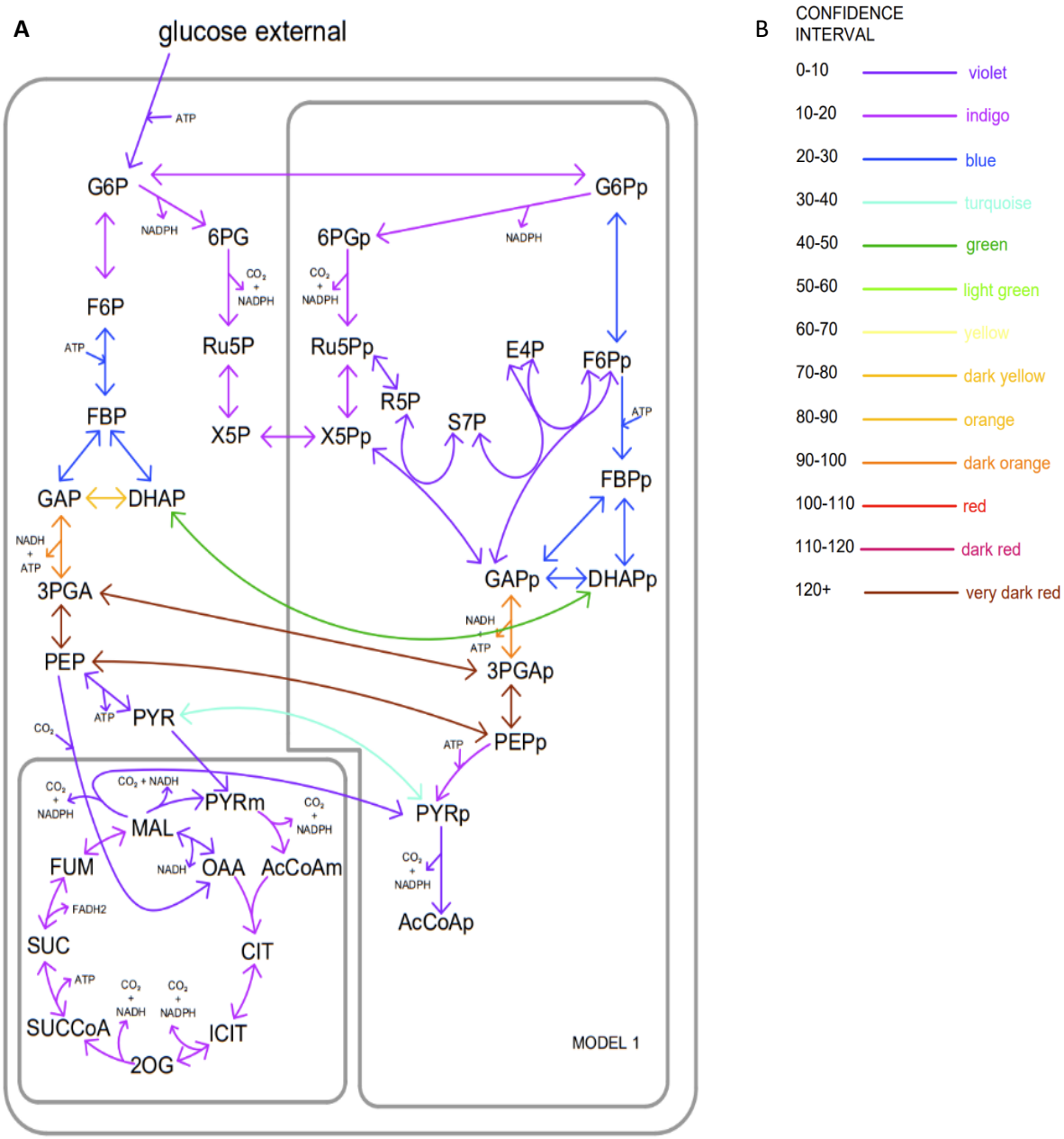


Figure 3.14: *Definition of the CCM reactions in model 1. (A) Schematic of the CCM element of the model colour coded to indicate the size of the 95% confidence interval for each reaction. (B) Key: blue and purples indicate small 95% confidence intervals, a well-defined reaction; while reds indicate large 95% confidence intervals, a poorly defined reaction.*

Twelve potential configurations of the network were assessed with the aim of minimising the mean confidence interval and hence improving the precision of the deduced fluxes through the network (Table 3.2). Details of each model are presented in Appendix 5. Combining the 3PGA and PEP pools into a single three carbon phosphate ester (C3P) pool in both the cytosol and the plastid reduced the mean confidence interval to 19.5 (model 2) and combining the cytosolic and plastidic C3P pools into a single transcompartmental pool reduced the mean confidence interval to 18.8 (model 3). Combining dihydroxyacetone phosphate (DHAP) and GAP, individually, into single transcompartmental pools further reduced the mean confidence interval to 11.9 if the C3P pool was used (model 4), or 11.5 if separate transcompartmental 3PGA and PEP pools were retained (model 5).

Table 3.2: *Summary statistics and mean confidence intervals for twelve different network topologies. See Appendix 5 for diagrams and reaction lists for each model.*

Model	SSR	DOF	SSR min	SSR max	Mean confidence interval	Description
1	1126.1	1210	1115.5	1308.3	Infinite	Original model (Figure 3.10).
2	1111.7	1213	1118.4	1311.4	19.5	As model 1 but 3PGA and PEP pools combined into C3P pools.
3	1131.9	1216	1121.3	1314.5	18.8	As model 2 but C3P and C3Pp combined into transcompartmental pool.
4	1184.6	1220	1125.1	1318.7	11.9	As model 3 but DHAP and GAP pools made transcompartmental.
5	1184.6	1221	1126.1	1319.7	11.5	As model 4 but C3P separated into transcompartmental 3PGA and PEP pools.
6	1184.4	1219	1124.1	1317.7	10.5	As model 4 but FBP transcompartmental pool.
7	1184.4	1220	1125.1	1318.7	10	As model 5 but FBP transcompartmental pool.
8	1124.5	1215	1120.3	1313.5	18.5	As model 3 but C3P split into transcompartmental 3PGA and PEP pools.
9	1126.1	1216	1121.3	1314.5	19.2	As model 8 but with transcompartmental DHAP.
10	1228.1	1218	1123.2	1316.6	9.1	As model 3 but DHAP and GAP combined into TP pool.
11	1229.8	1217	1122.2	1315.6	9	As model 10 but with C3P separated into 3PGA and PEP.
12	1295.1	1220	1125.1	1318.7	6.8	As model 11 but with a transcompartmental TP pool.

Including FBP in the transcompartmental pool further reduced the mean confidence interval to 10.5 and 10.0, depending on whether C3P (model 6) or 3PGA and PEP (model 7) pools was used. However, including more metabolite pools in the transcompartmental part of the

model meant that the initial reactions of glycolysis became less well defined. Reverting to model 3, but separating the transcompartmental C3P pool into distinct 3PGA and PEP pools gave a mean confidence interval of 18.5 (model 8), slightly lower than 18.8 for model 3. In model 8, DHAP transport between cytosol and plastid was poorly defined as was conversion between DHAP, GAP and 3PGA. However, including DHAP as a single transcompartmental pool which could exchange with both plastidic and cytosolic GAP pools increased the mean confidence interval to 19.2 (model 9).

A more useful solution was obtained by combining DHAP and GAP into triose phosphate (TP) pools in cytosol and plastid. This reduced the mean confidence interval to 9.1 or 9.0 depending on the use of C3P or 3PGA and PEP (model 10 and model 11). Including TP as a transcompartmental pool further reduced the mean confidence interval to 6.8 in the final model, model 12 (Figure 3.15). Model 12 was selected for MFA, the and carbon atom transitions for model 12 are shown in Appendix 4.

The degrees of freedom (DOF) is the difference between the number of independent measurements and the number of reactions in the model. Therefore, since all of the analytical variants described above involved the same MID dataset, the changes in the DOF seen in Table 3.2 are due to the different numbers of reactions in the different models.

Analysis of these different reaction network topologies suggests that the available MID data are unable to define the transport of 3PGA and PEP across the plastid membrane or the interconversion of GAP and DHAP by triose phosphate isomerase. This could be because the MID datasets do not contain sufficient information on metabolites derived from cytosolic 3PGA and PEP to be able to differentiate between the compartmental pools of these intermediates. Resolution of the reactions surrounding TP, 3PGA and PEP has been limited in other steady-state MFA studies of *Arabidopsis* (Williams *et al*., 2008, 2010; Masakapalli *et al*., 2013, 2014a) although resolution of compartmentation was possible in a similar model in a recent study using isotopically non-stationary MFA based on analysis of the labelling patterns of metabolic intermediates rather than end products (Smith *et al*., 2023).

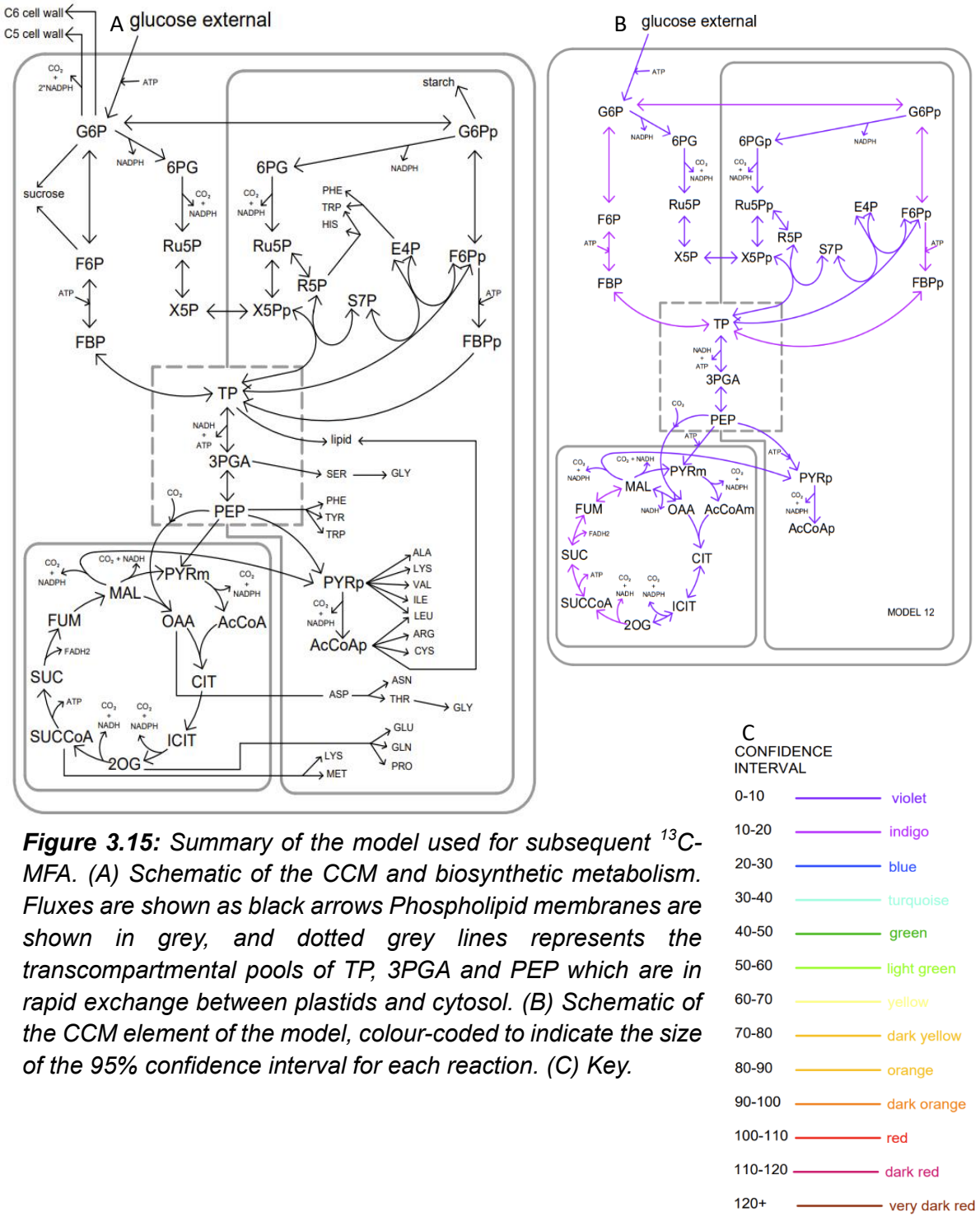


Figure 3.15: *Summary of the model used for subsequent ^{13}C-MFA. (A) Schematic of the CCM and biosynthetic metabolism. Fluxes are shown as black arrows Phospholipid membranes are shown in grey, and dotted grey lines represents the transcompartmental pools of TP, 3PGA and PEP which are in rapid exchange between plastids and cytosol. (B) Schematic of the CCM element of the model, colour-coded to indicate the size of the 95% confidence interval for each reaction. (C) Key.*

3.5 Modelling biosynthetic metabolism

The CCM functions to provide ATP, reduced co-enzyme and biosynthetic precursors for growth and maintenance. Therefore, a model of the CCM needs to take into account the removal of intermediates to act as precursors for biomass, and measured biomass composition can be used to constrain fitting of MID data to the model (Kruger *et al*., 2012). Biomass constraints were implemented in this project by encoding biosynthetic equations for soluble and insoluble carbohydrates (sucrose, starch and cell wall material), individual amino acids, and lipids. An overall biomass equation was then encoded to define the relative accumulation of these different biomass components and convert them into a 'Biomass' sink. Nucleic acid synthesis was not included in the model because previous studies have shown that nucleic acids accounts for only a negligible proportion of biomass production in this line of *Arabidopsis* cultures (Masakapalli *et al*., 2010, 2013, 2014a).

An approach similar to Sriram *et al.* (2006) was chosen. In this method cell cultures were grown under experimental conditions, before harvesting, lyophilisation, fractionation and analysis using a series of biochemical assays for quantification of carbohydrates, proteins and lipids. Soluble metabolites were quantified using GC-MS. This approach is used routinely in determination of biomass compositions for flux analysis in microbial systems (Long and Antoniewicz, 2019). For more methodological details refer to Section 2.4. Radioisotopometric methods present an alternative approach for collecting information on biomass composition (Masakapalli *et al*., 2010) but time and practical constraints meant that this was not explored.

3.5.1 Carbohydrate biosynthesis

Defining carbohydrates synthesised in the plastid and in the cytosol is important for determining subcellular compartmentation of metabolic flux (see Section 3.4). Starch is synthesised from G6P in the plastid, initially G6P is converted to glucose-1-phosphate (G1P) by phosphoglucomutase, before conversion to ADP-glucose and PPi by ADP-glucose pyrophosphorylase followed by addition of the glucosyl unit to an extending amylose or amylopectin chain by starch synthase (Fünfgeld *et al*., 2022; Figure 3.16).

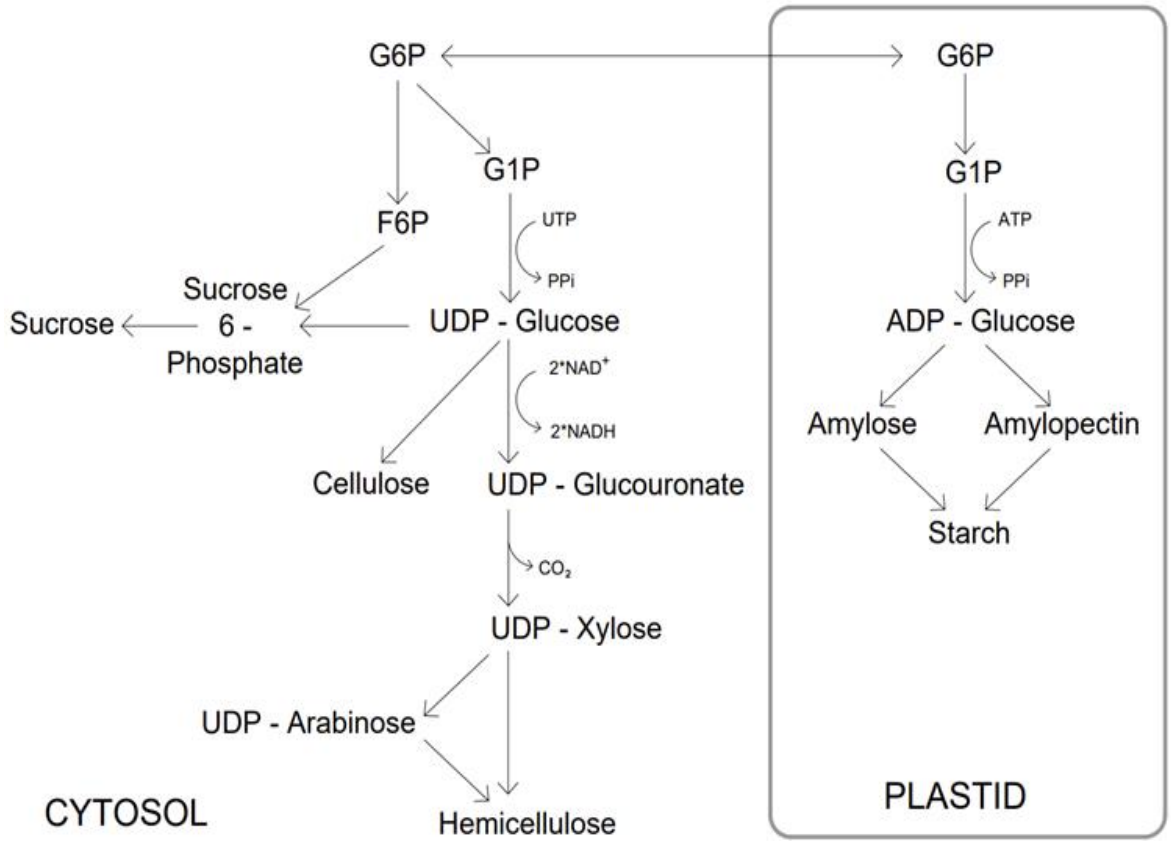


Figure 3.16: *Schematic of starch, sucrose and hemicellulose synthesis in heterotrophic Arabidopsis suspension cultures.*

These three enzymatic reactions were combined into one step in the MFA model using the equation below (R82 in model 12).

G6Pp + ATP −> STARCH + PPi + ADP

Cellulose and hemicellulose are synthesised in the cytosol. Like starch, cellulose is derived from G1P. which is converted to UDP-glucose by UDP-glucose pyrophosphorylase, before addition to an extending cellulose chain catalysed by a membrane bound cellulose synthase complex (Cosgrove, 2005; Polko and Kieber, 2019). The five carbon sugar components of the cell wall are derived from UDP-glucose undergoing dehydrogenation by UDP-glucose dehydrogenase and then decarboxylation by UDP-glucuronate decarboxylases, producing CO_2 and NADH as by-products (Harper and Bar-Peled, 2002). The equations for cell wall biosynthesis in the model (R83 and R83 in Appendix 5) were therefore as follows:

G6P + ATP −> C6CELLWALL + PPi + ADP

*G6P + ATP −> C5CELLWALL + CO_2 + 2*NADH + PPi + ADP*

In which UTP is generated from ATP via:

ATP + UDP <−> UTP +ATP

Sucrose is also synthesised in the cytosol from the combination of UDP-glucose and F6P by sucrose phosphate synthase, followed by dephosphorylation by sucrose phosphate phosphatase, and thus the equations used in the model for the fructose and glucose moieties of sucrose (R81 and R82 in appendix 5) were:

G6P + ATP −> GSUC + PPi + PPi

F6P −> FSUC + Pi

For determination of insoluble carbohydrate content, starch and cell wall carbohydrates were separated and hydrolysed into component monosaccharides. An anthrone assay was then used to quantify the amount of sugars relative to a glucose standard (see section 2.4 for details).

Sucrose was measured using quantitative GC-MS analysis. In both biological samples and authentic sucrose, most of the of sucrose broke down during the derivatisation process into its component sugar moieties; glucose and fructose (Figure 3.17). Consequently measuring the size of the small peak for sucrose would not give an accurate estimate of the actual

sucrose content, while measurement of the glucose peak may be distorted by residual glucose from the MS medium. Therefore, the concentration of fructose was used to estimate the sucrose content, since each sucrose unit is made up of one molecule of fructose and one of glucose, the amount of glucose derived from sucrose will be equal to the amount of fructose present in the chromatogram.

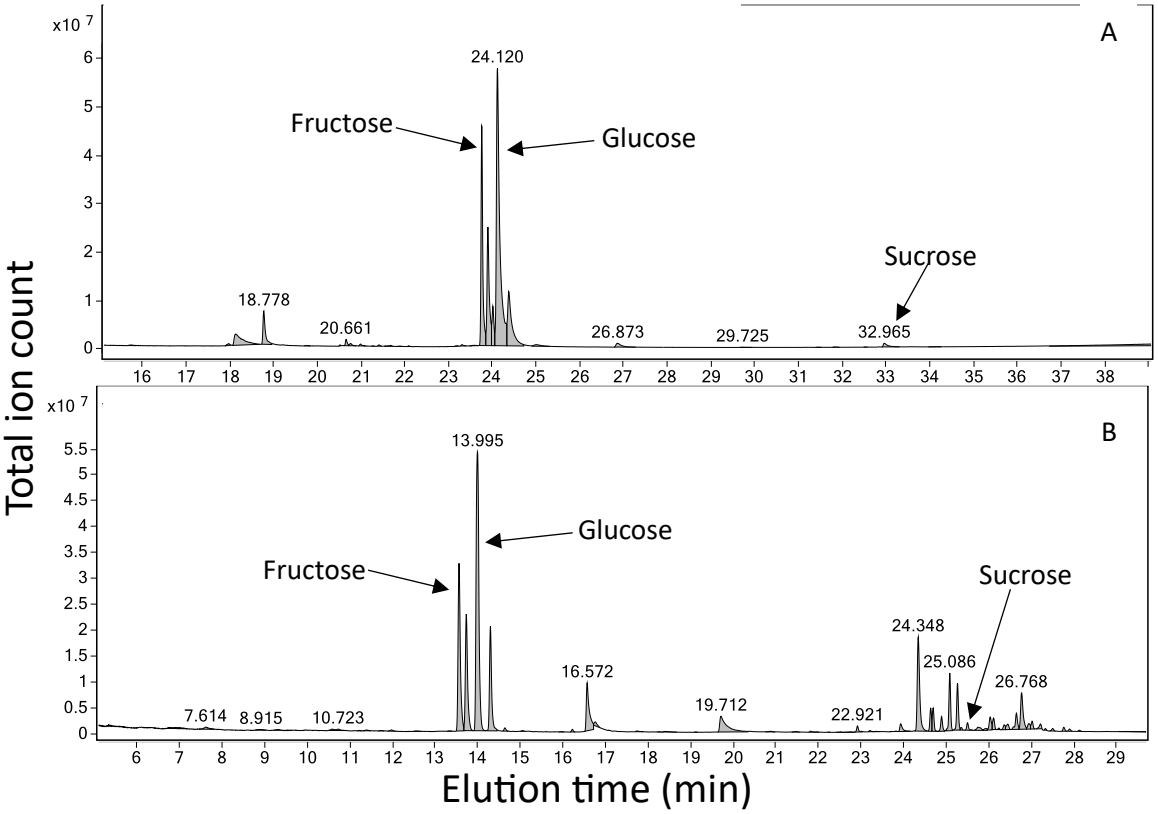


Figure 3.17: *Total ion chromatogram of (A) soluble carbohydrates derived from unlabelled cell culture, and (B) from authentic sucrose. Most of the sucrose breaks down into glucose and fructose during derivatisation.*

The anthrone assay and quantitative GC-MS analysis provided information on the amount of each carbohydrate as a proportion of biomass (i.e. g.gDW^{-1}). Dividing these by the molecular weight of glucose (180.156) gives the molar abundance of the carbohydrates as mol of glycosyl equivalent per gram of dry biomass (Table 3.3).

Table 3.3: *Carbohydrates content in Arabidopsis cell suspension cultures grown in MS medium at 22°C*

Carbohydrate	Content (mmol glycosyl equivalent.gDW^{-1})	SEM
Starch	0.106	0.006
Cell wall carbohydrates	0.082	0.014
Sucrose fructosyl	0.119	0.005
Sucrose glucosyl	0.119	0.005

The anthrone assay cannot distinguish between different sugars, but the cell wall is made up of six carbon glucose as well as various five carbon sugars and the production of both five and six carbon cell wall carbohydrates was accounted for in the model. Therefore, a consideration had to be made of the composition of the cell wall carbohydrates. The exact composition of the cell walls is variable (Draeger *et al*., 2015) but principally cell wall sugars contain either five or six carbons and the bulk of the cell wall is made up of cellulose and hemicellulose backbones. Cellulose is (1,4) linked β-D-glucan, and hemicellulose is made up of xyloglucan, a (1,4) linked β-D-glucan back bone with xylose branches, and arabinoxylan, a (1,4) linked β-D-xylan back bone with arabinose and glucuronic acid branches. So all the cellulose derived sugars will be 6-carbon glucose while approximately half of the hemicellulose derived sugars will be six-carbon glucose or glucouronic acid, while the remainder will be five-carbon xylose and arabinose. Thus the biomass composition of cell wall carbohydrates was assumed to be 75% six-carbon cell wall components (all of cellulose and half of hemicellulose) and 25% five-carbon cell wall components (half of hemicellulose). Pectins, although only a minority component of cell wall, also comprise a roughly 3:1 ratio of six-carbon to five-carbon sugars (Cosgrove, 2005). The total cell wall carbohydrate content was 0.015 g.gDW^{-1}, with the assumption that 75% of cell wall carbohydrates are six carbon and 25% five carbon sugars, the contents are 0.011 g.gDW^{-1} and 0.004 g.gDW^{-1} respectively. Dividing these values by the molecular weight gave 0.062 and 0.025 mmol.gDW^{-1} respectively (Table 3.4).

Table 3.4: *Estimated cell wall composition of Arabidopsis cultures grown in MS medium at 22°C*

Cell wall carbohydrate content ($g.gDW^{-1}$)	Sugars	Proportion of total cell wall carbohydrate	Molecular weight ($g.mol^{-1}$)	Sugar content ($mmol.gDW^{-1}$)
0.015 (0.003)				
	Six carbon	0.75	180.16	0.062
	Five Carbon	0.25	150.13	0.025

The small grey bracketed number represents the standard error based on 15 measurements.

3.5.2 Lipid biosynthesis

The lipid content of cell cultures was quantified using a sulfo-phospho vanillin assay, in which a carbonium ion is formed at carbon-carbon double bonds in fatty acid chains which then reacts with a phosphovanillin ester to produce a pink dye (see Section 2.4 for details). The more carbon-carbon double bonds present in the sample the higher the absorbance at 535 nm. The standard curve in this assay was made with linoleic acid (18:2), but the assumption was made that the majority of fatty acids in higher plants are monounsaturates, therefore the increase in absorbance made by one mole of the standard would be equal to the increase in absorbance caused by two moles of culture derived fatty acids and a correction needed to be made (multiplication by two) to the lipid component of biomass in $mmol.gDW^{-1}$. The lipid content in of *Arabidopsis* cultures is shown in Table 3.5.

Table 3.5: *Lipid content in Arabidopsis cell suspension cultures grown in MS medium at 22°C*

Fatty acid content ($g.gDW^{-1}$)	Linolate molecular weight ($g.mol^{-1}$)	Fatty acid content (mmol linolate equivalent.gDW^{-1})	Fatty acid content corrected for 18:2 to 18:1
0.025 (0.001)	280.45	0.086	0.172

The small grey bracketed number represents the standard error based on 15 measurements.

In the model used in this study a single pool of lipids was encoded (see Section 3.4). It was assumed that the majority of lipids in the cultures were in the form of phospholipids (forming membrane lipid bilayers). Therefore, reactions defining lipid synthesis had to include not only fatty acids, directly measured by the sulfo-phospho vanillin assay, but also the other precursors needed for production of the rest of the phospholipid molecules. So, the lipid synthesis equation had to take into account the relative amounts of precursors required to produce one mole of lipid quantified as fatty acid equivalents. The main fatty acids in *Arabidopsis* are 18 carbon chains (olelate, linoleate and α-linolenate; Harwood, 1988) produced from acetyl-CoA by the action of ATP-dependent acetyl-CoA carboxylase and NADPH-dependent fatty acid synthase (He *et al.*, 2020), followed by aerobic desaturation catalysed by NADPH-dependent desaturases (Figure 3.18). Therefore, producing one mole of C18:1 fatty acid will require nine moles of acetyl-CoA, eight moles of ATP, seventeen moles of NADPH and one mole of oxygen (for desaturation). While eight moles of ADP and seventeen moles of $NADP^+$ are generated as by-products. Fatty acids exist in the form of phospholipids so the lipid synthesis equation also needs to consider the biosynthetic requirements for the precursors of phospholipids associated with each mole of fatty acids. Glycerol 3-phosphate, which provides the three carbon glycerol backbone of all phospholipids is synthesised by NADH dependent hydrogenation of DHAP, which is included in the triose phosphate pool in the metabolic model (see Section 3.4). Glycerol-3-phosphate then has two fatty acid chains added to it by acyl transferases to form phosphatidic acid. Phosphatidic acid is then combined with CTP (generated from CDP using ATP) to prime it for synthesis of phosphatidylglycerol, phosphatidylserine and phosphatidylethanolamine. Phosphatidylserine and phosphatidylethanolamine are synthesised by the addition of serine to phosphatidic acid, while addition of a second glycerol-3-phosphate forms phosphatidylglycerol.

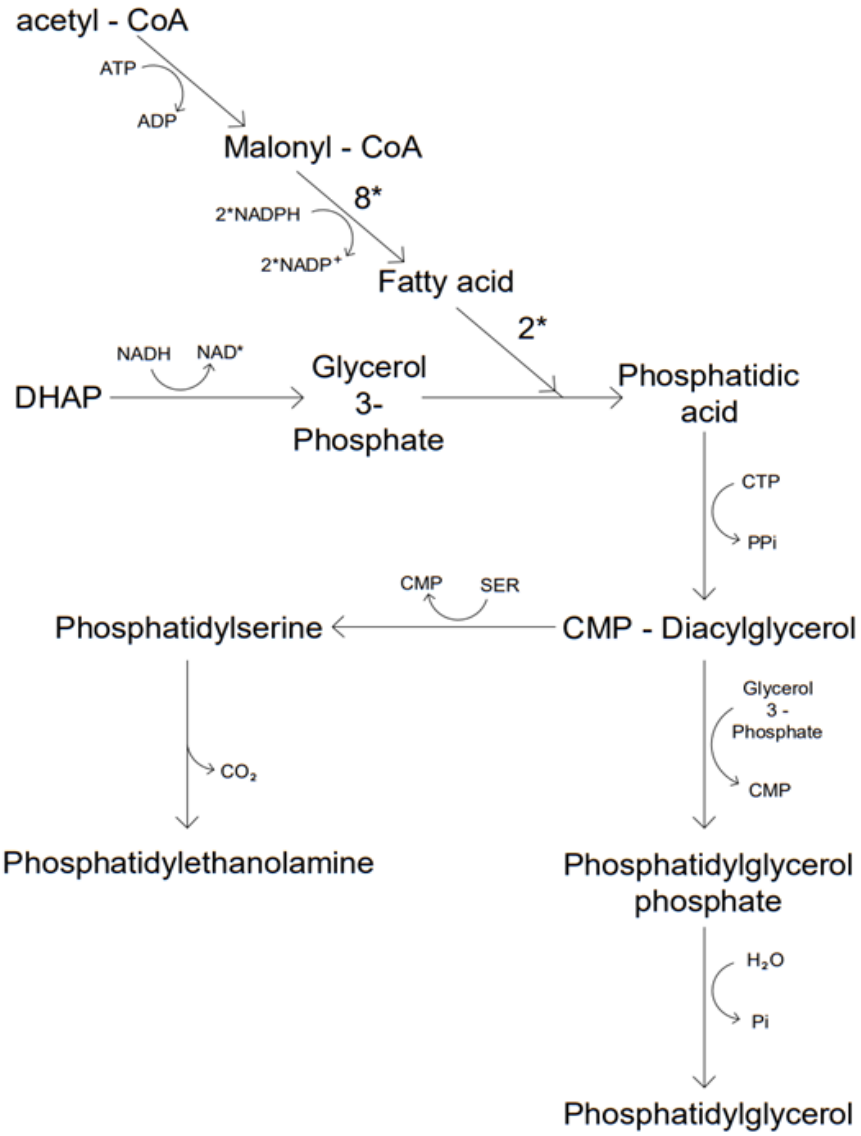


Figure 3.18: *Schematic of lipid synthesis in heterotrophic Arabidopsis suspension cultures.*

It was assumed that that all phosphatidylserine was decarboxylated to phosphatidylethanolamine and that phosphatidylethanolamine and phosphatidylglycerol exist in a 3:1 ratio. Therefore, synthesis of each mole of fatty acid in a phospholipid form would require the nine moles of acetyl-CoA, eight moles of ATP, seventeen moles of NADPH and one mole of oxygen to form one mole of monounsaturated fatty acid, as well as 0.875 moles of glycerol-3-phosphate (0.5 moles to make phosphatidic acid and 0.375 moles to make phosphatidylglycerol) 0.5 moles of ATP equivalent (CTP), and 0.125 moles of serine to make phosphatidylserine and phosphatidylethanolamine. It would produce an

extra 0.5 moles of ATP and 0.125 moles of CO_2 as byproducts. This yields the final lipid synthesis equation (R79 in Appendix 5) shown below:

9 acetyl CoA + 0.875 triose phosphate + 0.125 serine + 8.5 ATP + 17 NADPH + 0.5 NADH + O_2 −> Lipid + 0.125 CO_2 + 8.5 ADP + 17 $NADP^+$ + 0.5 NAD^+

3.5.3 Protein biosynthesis

The protein content of unlabelled *Arabidopsis* suspension cultures was assessed using a BCA assay which yielded a value of 0.434 g.gDW^{-1} (± 0.03). Protein consists of twenty different amino acids but the BCA assay cannot distinguish between the different amino acids. However, discrimination between the production rates of the twenty amino acids is necessary because they are produced by different biosynthetic pathways involving different precursors and amounts of ATP and reductant. Therefore, the approach taken by Schulte *et al*. (2021) was used, and the amino acid composition of cellular protein was calculated based on the published amino acid composition from Long and Antoniewicz (2014).The relative molar abundance of the individual amino acids is shown in Table 3.6. The biosynthesis of each amino acid was defined by a series of reaction (R85-R108 in Appendix 5) to account for the requirement for metabolic precursors, ATP and reductant. The reference amino acid composition from Long and Antoniewicz (2014) was from *E. coli*, but was used because the only available amino acid compositions for *Arabidopsis* are based on GC-MS analysis with external standards, which is an unreliable technique. Further, as discussed on page 90 the distribution of fluxes in CCM is shown to be relatively insensitive to changes in the amino acid composition.

Table 3.6: *Amino acid content in Arabidopsis cell suspension cultures grown in MS medium at 22°C. The relative molar abundance of individual amino acids in protein was taken from Long and Antoniewicz (2014)*

Protein content ($g.gDW^{-1}$)	Amino acid	Amino acid (mmol.g $protein^{-1}$)	Amino acid content ($mmol.gDW^{-1}$)
0.434 (0.03)			
	Alanine	1.103	0.479
	Arginine	0.633	0.275
	Asparagine	0.557	0.242
	Aspartate	0.557	0.242
	Cysteine	0.197	0.085
	Glutamate	0.655	0.284
	Glutamine	0.655	0.284
	Glycine	1.015	0.441
	Histidine	0.197	0.085
	Isoleucine	0.502	0.218
	Leucine	0.884	0.384
	Lysine	0.655	0.284
	Methionine	0.251	0.109
	Phenylalanine	0.360	0.156
	Proline	0.415	0.180
	Serine	0.546	0.237
	Threonine	0.568	0.246
	Tryptophan	0.120	0.052
	Tyrosine	0.306	0.133
	Valine	0.742	0.322

3.5.4 Organic acid quantification

The accumulation of organic acids generated by the TCA cycle was assessed using quantitative GC-MS analysis of soluble extracts of the cell suspension. The calculated organic acid contents are shown in Table 3.7.

Table 3.7: *Organic acid content in Arabidopsis cell suspension cultures grown in MS medium at 22°C*

Organic acid	Mean content ($mmol.gDW^{-1}$)
Succinate	0.036 (0.017)
Fumarate	0.092 (0.033)
Malate	0.194 (0.039)
2-oxoglutarate	0.002 (0.001)
Citrate	0.062 (0.021)

3.5.4 Total biomass equation

Sections 3.5.1-3.5.4 have described the equations included in the model to account for production of soluble and insoluble carbohydrates, lipids, individual amino acids and organic acids. The quantification of these biomass components by biochemical assays and quantitative GC-MS was used to constrain the relative molar contributions of each biomass component to one unit mass of dry biomass, by introduction of an overall biomass equation. Based on these measurements the final biomass equation for *Arabidopsis* suspension cultures grown in MS medium at 22°C is shown below (the biomass equations for all other conditions are presented in Appendix 6):

*0.479*Alanine + 0.275*Arginine + 0.242*Asparagine + 0.242*Aspartate + 0.085*Cystine + 0.284*Glutamate + 0.284*Glutamine + 0.441*Glycine + 0.085*Histidine + 0.218*Isoleucine + 0.384*Leucine + 0.284*Lysine + 0.109*Methionine + 0.156*Phenylalanine + 0.18*Proline + 0.237*Serine + 0.246*Threonine + 0.052*Tryptophan + 0.133*Tyrosine + 0.322*Valine + 18.95*ATP + 0.172*Lipid + 0.062*6-Carbon cell wall carbohydrate + 0.025*5-Carbon cell wall carbohydrate + 0.106*Starch + 0.036*Succinate + 0.092*Fumarate + 0.19*Malate + 0.002*2-oxoglutarate + 0.062*Citrate + 0.119*Sucrose fructosyl + 0.119*Sucrose glucosyl −> Biomass*

The coefficients represent the relative molar abundance of each component per unit weight of biomass.

The ATP and reductant costs for synthesis of each biomass component were included in the individual equations, but the energy cost of protein elongation was considered in this final biomass equation, and is based on the assumption that four molecules of ATP equivalents (two molecules of ATP and two of GTP) are required per peptide bond.

3.6 Metabolic fluxes under control conditions

Once methodologies for collecting and curating MID and biomass composition data had been established and a model defined, it was necessary to test the reproducibility of the results. Practical considerations meant that many of the labelling experiments had to be done sequentially, alongside an appropriate control. So it was important to establish if

Arabidopsis cultures grown under the same conditions at different times would produce similar flux solutions. Two cultures were grown at 22°C in MS media containing labelled glucose, one month apart. MID datasets were extracted from each and used to produce flux solutions (See Appendix 3 for the full MID datasets). The two flux solutions obtained from the separate MID datasets will be referred to as control 1 and control 2. The flux solutions were compared to assess the reproducibility of the methodology used in this project.

The full flux solutions are presented in Appendix 7, and summaries of the net fluxes through the CCM are shown in tables 3.8 and 3.7. Both the flux solutions were statistically acceptable. The control 1 flux distribution produced an SSR of 1188.3, with 1190 DOF and a range of statistically acceptable SSR values of 1096.3-1287.5, while the control 2 flux solution produced an SSR of 1135.1 with 1166 DOF and a critical SSR range of 1073.3-1262.5. Comparison of the flux solutions was conducted by assessing the extent of overlap of the appropriate confidence intervals for individual net fluxes (as described in section 2.7). The results of this analysis (Table 3.8, Figure 3.19) show that the control 1 and control 2 had very similar net flux distributions, with the majority of reactions of the central network of the CCM having overlapping confidence intervals. The only net fluxes that were significantly different between control 1 and control 2 were in the OxPPP, through phosphopentose isomerase, transketolase and transaldolase, which differed by about 10%. These reactions were well defined, so the confidence intervals do not overlap, but the general distribution of flux through the CCM was otherwise not significantly different. This observation suggests that caution will need to be exercised when it comes to comparing these reactions between control and experimental conditions, because although there may be statistically significant differences in net fluxes in the OxPPP, the biological relevance of these differences will need to be considered.

Table 3.8: *Comparison of control 1 and control 2 flux solutions.*

Reaction	Control 1	Control 2
GLCext + ATP −> G6P	100.0 (n/a, n/a)	100.0 (n/a, n/a)
G6P <−> F6P	1.2 (1.2, 36.8)	1.2 (1.1, 40.2)
F6P + ATP −> FBP	0.0 (0.0, 35.6)	0.0 (0.0, 39.)
FBP <−> TP + TP	0.0 (0.0, 35.6)	0.0 (0.0, 39.)
G6P <−> G6Pp	96.6 (55.8, 96.8)	96.8 (50.0, 96.9)
G6Pp <−> F6Pp	47.6 (11.1, 52.1)	43.5 (2.3, 47.6)
F6Pp + ATP −> FBPp	77.4 (41.6, 78.9)	76.3 (36.4, 77.7)
FBPp <−> TP + TP	77.4 (41.6, 78.9)	76.3 (36.4, 77.7)
G6P −> 6PG + NADPH	0.0 (0.0, 22.0)	0.0 (0.0, 23.6)
6PG −> RU5P + CO_2 + NADPH	0.0 (0.0, 22.0)	0.0 (0.0, 23.6)
RU5P <-> X5P	0.0 (0.0, 22.0)	0.0 (0.0, 23.6)
G6Pp −> 6PGp + NADPH	47.9 (21.3, 50.4)	52.3 (24.1, 55.6)
6PGp −> RU5Pp + CO_2 + NADPH	47.9 (21.3, 50.4)	52.3 (24.1, 55.6)
RU5Pp <−> X5Pp	29.8 (4.9, 31.5)	32.8 (6.2, 35.0)
RU5Pp <−> R5Pp	**18.1 (16.4, 18.9)**	**19.5 (18.0, 20.6)**
X5P <−> X5Pp	0.0 (0.0, 22.0)	0.0 (0.0, 23.6)
X5Pp <−> TP + EC2	**29.8 (26.6, 31.5)**	**32.8 (29.9, 35.1)**
F6Pp <−> E4Pp + EC2	**−13.2 (−14.0, −11.5)**	**−14.7 (−15.9, −13.2)**
S7Pp <−> R5Pp + EC2	**−16.7 (−17.5, −15.1)**	**−18.1 (−19.2, −16.6)**
F6Pp <−> TP + EC3	**−16.7 (−17.5, −15.1)**	**−18.1 (−19.2, −16.6)**
S7Pp <−> E4Pp + EC3	**16.7 (17.5, 15.1)**	**18.1 (19.2, 16.6)**
TP <−> 3PGA + NADH + ATP	167.0 (166.1, 168.9)	166.4 (165.0, 168.1)
3PGA <−> PEP	156.1 (154.8, 158.8)	155.8 (153.5, 158.3)
PEP −> PYRm + ATP	76.0 (73.4, 80.6)	78.8 (74.0, 82.4)
PEP −> PYRp + ATP	43.0 (39.4, 44.5)	40.2 (36.9, 42.8)
PYRm −> ACoAm + CO_2 + NADH	77.4 (74.2, 84.7)	81.0 (75.2, 87.7)
PYRp −> ACoAp + CO_2 + NADH	20.0 (18.5, 20.7)	19.0 (17.7, 20.0)
OAA + ACoAm −> CIT	77.4 (72.6, 83.9)	81.0 (75.0, 88.0)
CIT <−> ICIT	76.8 (71.9, 83.3)	80.4 (74.4, 87.4)
ICIT <−> 2OG + $CO2_2$+ NADPH	76.8 (71.9, 83.3)	80.4 (74.4, 87.4)
2OG −> SUCCoA + CO_2 + NADH	66.2 (60.8, 73.3)	70.3 (63.7, 78.0)
SUCCoA <−> SUC + ATP	62.1 (56.6, 69.4)	66.4 (59.6, 74.4)
SUC <−> FUM + $FADH_2$	65.8 (63.3, 75.5)	69.9 (63.3, 77.7)
FUM <−> MAL	68.6 (63.3, 75.5)	72.6 (66.1, 80.2)
MAL <−> OAA + NADH	65.0 (6.1, 69.1)	67.6 (63.5, 71.9)
PEP + CO_2 −> OAA	30.1 (28.0, 34.1)	30.1 (27.6, 34.2)
MAL −> PYRm + CO_2 + NADH	1.4 (0.0, 6.4)	2.2 (0.0, 7.4)
MAL −> PYRp + CO_2 NADPH	0.2 (0.0, 1.1)	0.8 (0.0, 1.7)

The values in grey brackets are the 95% confidence limits calculated by parameter continuation. Net fluxes which are significantly different between the two conditions are shown in boldface.

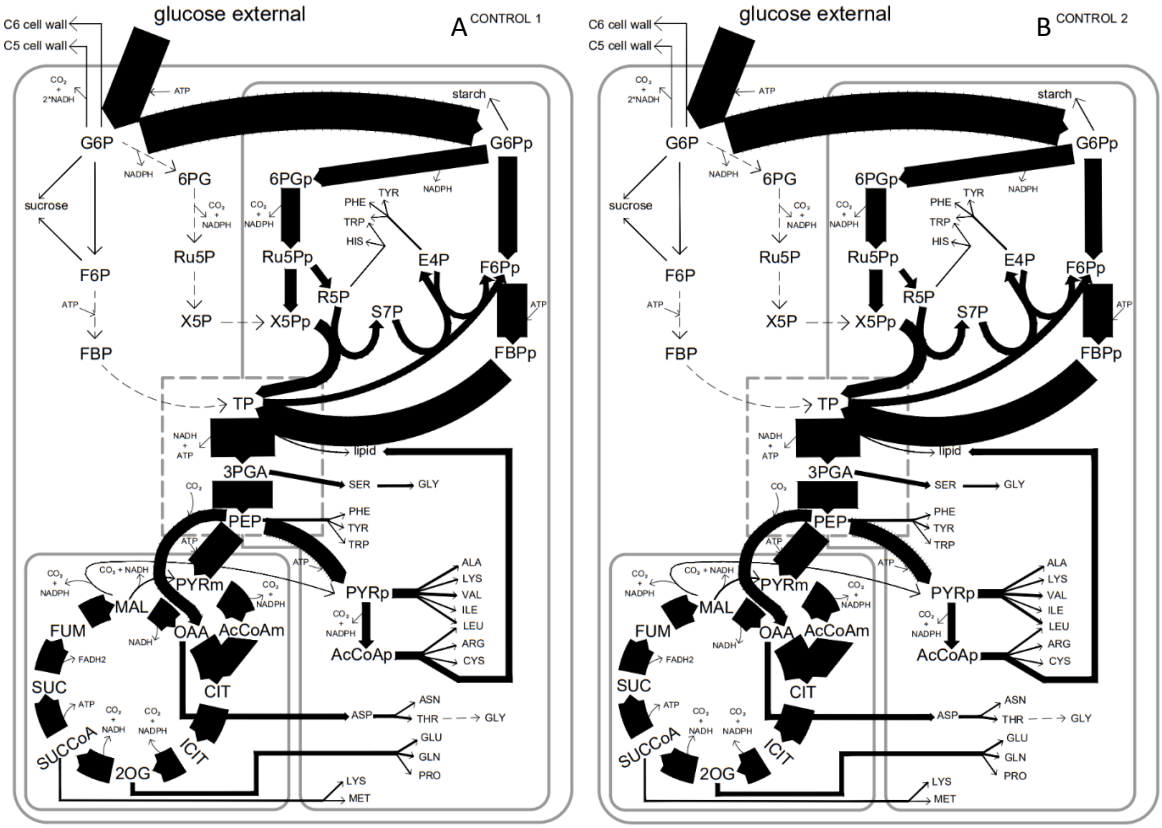


Figure 3.19: *Flux maps of control 1 and control 2. The thickness of lines indicates the relative flux of the reactions, dotted lines represent fluxes less than 0.009 relative to a glucose uptake of 100.*

In the model used in this study a reaction of CO_2 release was included (R18 in model 12), since the rate of carbon uptake (in the form of glucose) was fixed the carbon lost as CO_2 could be calculated as a percent of carbon uptake, the remainder is the carbon invested in biomass as a percentage of carbon uptake, the carbon conversion efficiency (CCE). In control 1 and control 2 the CCE was very similar at 53.6% and 51.0% respectively (Figure 3.20). Comparison of the calculated confidence intervals showed there was no significant difference. The ancillary reactions for combining flux through duplicated reactions (Sections 3.4.2) showed that the utilisation of G6P between glycolysis and the OxPPP was not significantly different in the two solutions (Figure 3.21). The slight difference in the amount of carbon entering the OxPPP between the control 1 and control 2 is likely the cause of the later reactions of the pentose phosphate pathway having non-overlapping confidence intervals (Table 3.8).

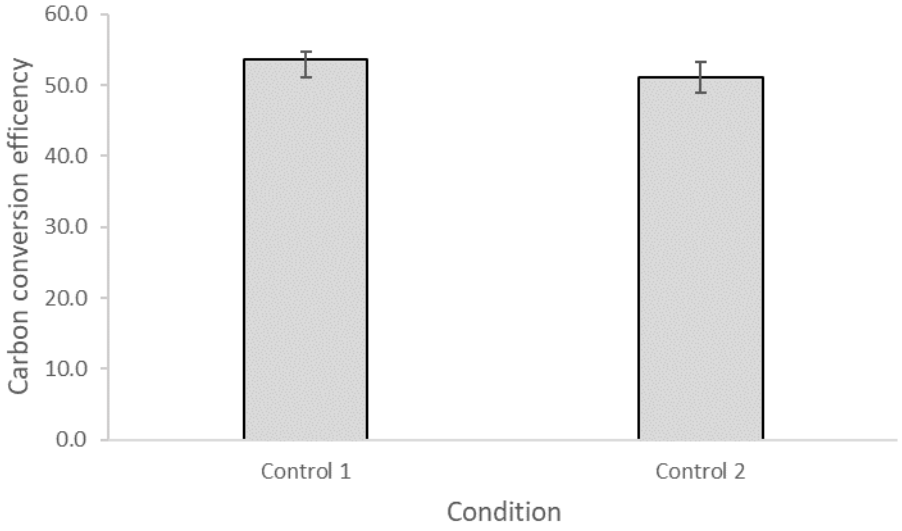


Figure 3.20: *Carbon conversion efficiency of Arabidopsis cell culture grown in MS medium at 22°C. Error bars represent 95% confidence interval calculated by parameter continuation.*

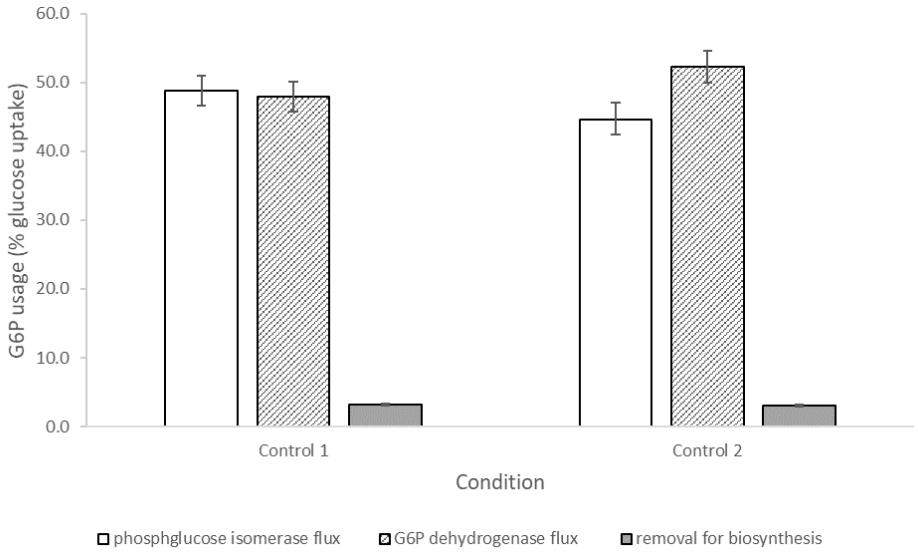


Figure 3.21: *Utilisation of the combined plastidic and cytosolic G6P pool in Arabidopsis cell cultures grown under control conditions. The flux of G6P through phosphoglucoisomerase, (white), G6P dehydrogenase (hatched), and the combined sucrose, cell wall and starch synthesis enzymes (grey) is shown. Error bars represent 95% confidence interval calculated by parameter continuation.*

The utilisation of PEP was also not significantly different in control 1 and control 2 (Figure 3.22). Around two thirds of PEP entered the TCA cycle, primarily via mitochondrial pyruvate while one third entered biosynthetic metabolism, primarily via plastidic pyruvate. The observations that that there was no significant difference in CCE, and flux distribution at the G6P and PEP metabolic hubs suggests that the overall flux distribution was not significantly different between control 1 and control 2.

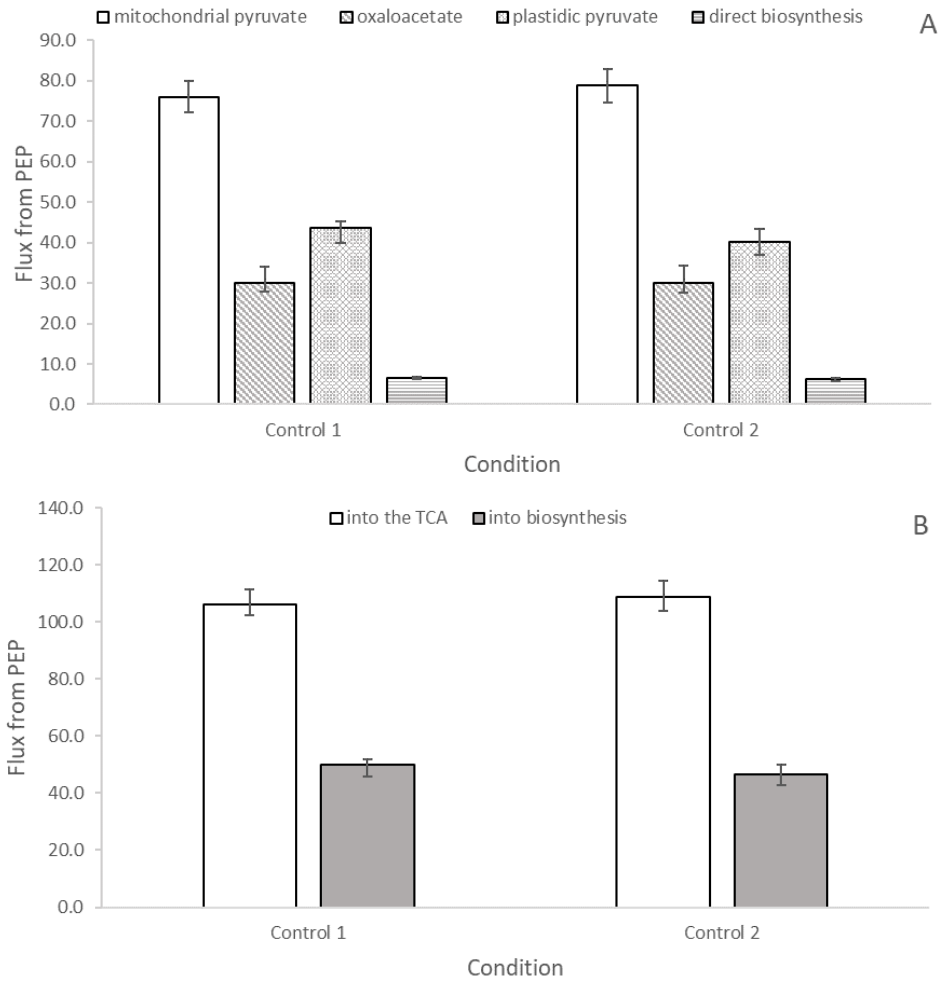


Figure 3.22: *Metabolic fate of PEP in Arabidopsis cell culture under control conditions. Error bars represent 95% confidence interval calculated by parameter continuation.*

Further comparison of the control 1 and control 2 flux solutions was provided by performing PCA on synthetic datasets produced by 1000 rounds of Monte Carlo simulations (Figure 3.23). The 95% confidence ellipses overlap for the control 1 and control 2 suggesting that there are no major differences between the two flux distributions.

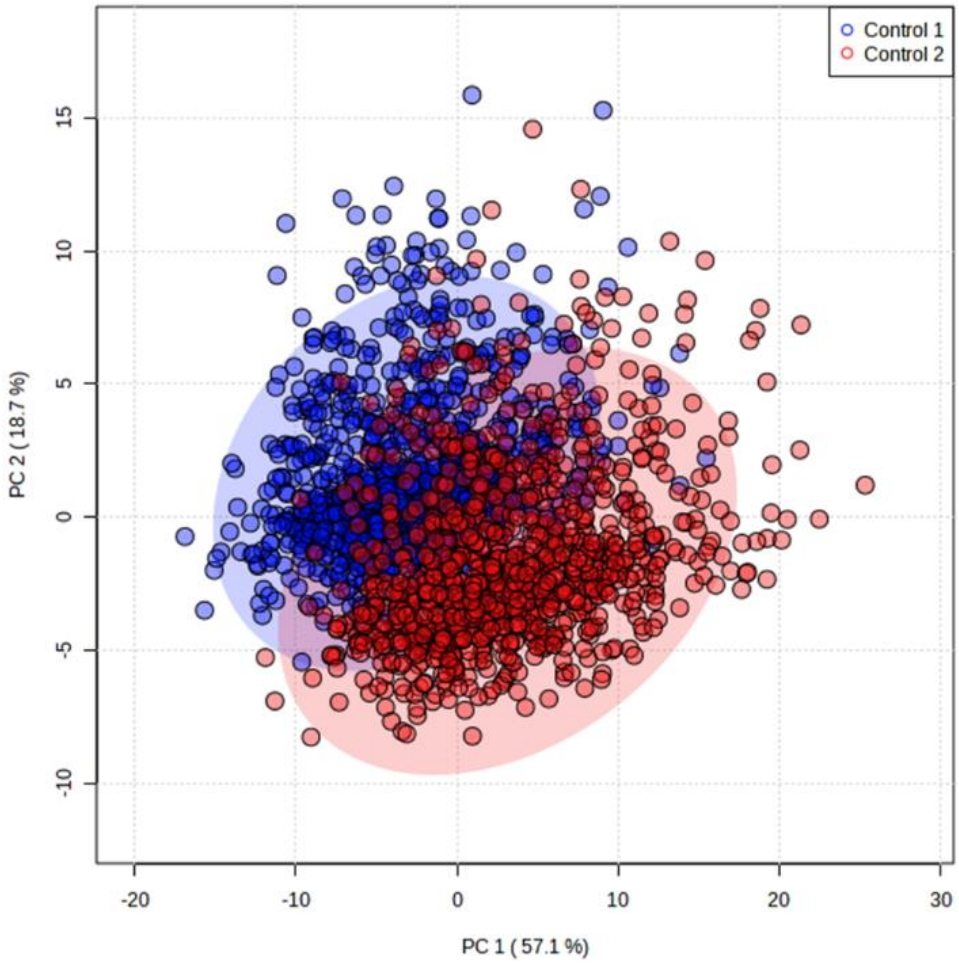


Figure 3.23: *Principal component analysis of net fluxes of reactions in the CCM from the control 1 (blue) and control 2 (red) flux solutions. Synthetic data sets derived from 1000 rounds of Monte Carlo simulation of the control 1 and control 2 flux solutions.*

3.7 Comparison to published flux solutions

The flux solutions produced from *Arabidopsis* suspension cultures grown in standard conditions (22°C, MS medium) a month apart in this project were very similar and can be used as the basis for comparison with the flux solutions from cultures grown under other conditions. However, several other flux solutions have been generated for the same *Arabidopsis* culture grown under equivalent conditions over the past 15 years (Williams *et*

al., 2008, 2010; Masakapalli *et al*., 2013, 2014a; Smith *et al*., 2023). The flux solutions in this project and the solutions from published MFA studies were compared (Table 3.9).

There were some striking differences between the flux solutions produced in this project and those in the literature. There were also significant differences in the biomass composition measured in different studies, and some of the differences in flux distribution could potentially be due to the different biomass compositions. For example, the flux solutions reported by Masakapalli *et al*. (2013, 2014a) were constrained by biomass compositions consisting of a significantly larger proportion of starch, cell wall and sucrose than the flux solutions in this project or reported by Williams *et al*. (2008, 2010). This meant that there was a considerably greater flux of G6P removal for biosynthesis in the flux solutions deduced by Masakapalli *et al*. (2013, 2014a). Further, the net flux through phosphoglucoisomerase was increased and net flux through G6P dehydrogenase was lower in both studies by Masakapalli *et al*. (2013, 2014a) Smith *et al.* (2023) used identical biomass constraints as Masakapalli *et al*. (2014a). The same pattern of greater biomass contribution, and phoshoglucoisomerase flux but lower G6P dehydrogenase flux was seen in a much more pronounced manner in Smith *et al*. (2023).

The relative partitioning of PEP into plastidic and mitochondrial pyruvate pools was similar in the flux solutions from this project and those reported in Williams *et al*. (2008, 2010), while those of Masakapalli *et al.* (2013, 2014a) and Smith *et al*. (2023) showed a relative partitioning toward mitochondrial pyruvate (the best fit values from Masakapalli *et al*. (2013, 2014a) for conversion of PEP into mitochondrial pyruvate were above the maximum 95% confidence interval from the equivalent reactions in this study, while the best fit values for conversion of PEP into plastidic pyruvate are less than the lower 95% confidence limit identified in this study. The same pattern is seen in Smith *et al*. (2023) and the 95% confidence intervals from this experiment and from Smith *et al*. (2023) do not overlap. This is likely a consequence of the lower protein content in the biomass composition reported by Masakapalli *et al*. (2013, 2014a) and Smith *et al*. (2023). The effect of the PEP partitioning

between plastidic and mitochondrial pyruvate has a knock on effect on TCA cycle fluxes, which are slightly higher (often just above the upper 95% confidence interval) in the flux solutions which have larger flux from PEP to mitochondrial pyruvate.

However, there are some differences between the flux solutions which cannot readily be explained by changes in the biomass composition. For example, the compartmentation of glycolysis and the OxPPP and the highly variable net fluxes through OxPPP between studies. In this project a preference for plastidic glycolysis over cytosolic glycolysis was seen, this feature was seen in Williams *et al*. (2010) and Masakapalli *et al*. (2013), but not in Williams *et al*. (2008), Masakapalli *et al*. (2014a) and Smith *et al*. (2023). Flux through the OxPPP in the Williams *et al*. (2010) flux solution was also above the upper 95% confidence limit calculated in this study, but all other flux solutions reported considerably lower flux through the OxPPP, (with Masakapalli *et al*. (2013, 2014a) and Smith *et al*. (2023) showing fluxes less than the lower 95% confidence limits in this study). In this study, the flux through combined plastidic and cytosolic phosphoglucoisomerase and through combined plastidic and cytosolic G6P dehydrogenase were very similar implying approximately equal flux through glycolysis and the OxPPP (Figure 3.21).

Further evidence of the differences in flux distribution in the various studies is provided by PCA (Figure 3.24). The two flux solutions produced in this study (red and green) are very close to each other while the flux solutions produced by other studies are clearly separated from each other and from the solutions produced in this study. This suggests that it would be inappropriate to use the published solutions as a basis for comparing the impact of altered growth conditions on flux solutions which is to be done in the following chapters.

Table 3.9: *Flux solutions for cultures in standard conditions in this project and in published Arabidopsis MFA studies*

Reaction	Control 1	Relative flux in specified study				
		Williams *et al.* (2008)	Williams *et al.* (2010)	Masakapalli *et al.* (2013)	Masakapalli *et al.* (2014a)	Smith *et al.* (2023)
GLCext + ATPi −> G6P	100.0	100.0	100.0	100.0	100.0	100.0
G6P <−> F6P	1.2 (1.2, 36.8)	0.8	25.9	−15.3	18.6	59.9 (55.5, 64.6)
F6P + ATP −> FBP	0.0 (0.0, 35.6)					54.0 (48.6, 60.6)
FBP <−> TP + TP	0.0 (0.0, 35.6)	−0.2		−23.2	12.1	54.0 (48.6, 60.6)
G6P <−> G6Pp	96.6 (55.8, 96.8)	69.7	44.6	95.9	58	30.3 (25.9, 34.6)
G6Pp <−> F6Pp	47.6 (11.1, 52.1)		22.5	67.3	35.7	23.7 (19.9, 27.9)
F6Pp + ATPi −> FBPp	77.4 (41.6, 78.9)					23.7 (19.9, 27.4)
FBPp <−> TP + TP	77.4 (41.6, 78.9)	56.9		86.1	53.9	23.7 (19.9, 27.4)
G6P −> 6PG + NADPH	0.0 (0.0, 22.0)			7.9	12.9	0.0 (0.0, 0.0)
6PG −> RU5P + CO_2 + NADPH	0.0 (0.0, 22.0)					0.0 (0.0, 0.0)
RU5P <−> X5P	0.0 (0.0, 22.0)					
G6Pp −> 6PGp + NADPH	47.9 (21.3, 50.4)	30.4	62.8	21.2	15.5	0.4 (0.2, 2.2)
6PGp −> RU5Pp + CO_2 + NADPH	47.9 (21.3, 50.4)					0.4 (0.2, 2.2)
RU5Pp <−> X5Pp	29.8 (4.9, 31.5)					−0.4 (−0.7, 0.8)
RU5Pp <−> R5Pp	18.1 (16.4, 18.9)					0.9 (0.6, 1.4)
X5P <−> X5Pp	0.0 (0.0, 22.0)					
X5Pp <−> TP + EC2	29.8 (26.6, 31.5)	19.3	41.1	18.8	18.3	−0.4 (−0.7, 0.8)
F6Pp <−> E4Pp + EC2	−13.2 (−14.0, −11.5)	8.6	19.6	8.9	8.6	0.8 (0.2, 1.0)
S7Pp <−> R5Pp + EC2	−16.7 (−17.5, −15.1)	10.7	21.4	9.9	9.7	−0.4 (−1.0, −0.2)
F6Pp <−> TP + EC3	−16.7 (−17.5, −15.1)	10.7	21.4	9.9	9.7	−0.4 (−1.0, −0.2)
S7Pp <−> E4Pp + EC3	16.7 (17.5, 15.1)	10.7	21.4	9.9	9.7	0.4 (0.2, 1.0)
TP <−> 3PGA + NADHi + ATP	167.0 (166.1, 168.9)	118.8	113.7			153.7 (127.7, 178.9)
3PGA <−> PEP	156.1 (154.8, 158.8)					146.0 (123.0, 171.6)
PEP −> PYRm + ATP	76.0 (73.4, 80.6)	60.9	65.3	92.5	101	47.7 (38.0, 63.3)
PEP −> PYRp + ATP	43.0 (39.4, 44.5)	31.9	25.6	8.4	4.7	12.1 (0.0, 15.1)
PYRm −> ACoAm + CO_2 + NADH	77.4 (74.2, 84.7)	58.5	61.3	94.8	86.2	89.8 (86.2, 113.1)
PYRp −> ACoAp + CO_2 + NADH	20.0 (18.5, 20.7)					9.0 (5.8, 12.4)
OAA + ACoAm −> CIT	77.4 (72.6, 83.9)	58.5	61.3	94.8	86.1	96.4 (85.8, 111.1)
CIT <−> ICIT	76.8 (71.9, 83.3)	55.0				94.3 (82.9, 1083.0)
ICIT <−> 2OG + CO_2 + NADPH	76.8 (71.9, 83.3)		60.1	92	83.2	94.3 (82.9, 1083.0)
2OG −> SUCCoA + CO_2 + NADH	66.2 (60.8, 73.3)	49.1	26.5	82.4	70	81.1 (69.5, 95.3)
SUCCoA <−> SUC + ATP	62.1 (56.6, 69.4)	49.1				81.1 (69.5, 95.3)
SUC <−> FUM + $FADH_2$	65.8 (63.3, 75.5)	49.1		81.8	68.9	80.1 (68.4, 94.1)
FUM <−> MAL	68.6 (63.3, 75.5)	24.4	26.9	82.2	69.3	80.4 (68.7, 94.4)
MAL <−> OAA + NADH	65.0 (6.1, 69.1)	24.4				
PEP + CO_2 −> OAA	30.1 (28.0, 34.1)	21.6	19.2	27.2	26	83.8 (76.9, 102.6)
MAL −> PYRm + CO_2 + NADH	1.4 (0.0, 6.4)	1.4		6.3	0.9	62.5 (54.1, 76.9)
MAL −> PYRp + CO_2 + NADPH	0.2 (0.0, 1.1)	0.0	2.9	0.8	0.8	0.0 (0.0, 7.1)

The values in grey brackets are the 95% confidence limits calculated by parameter continuation.

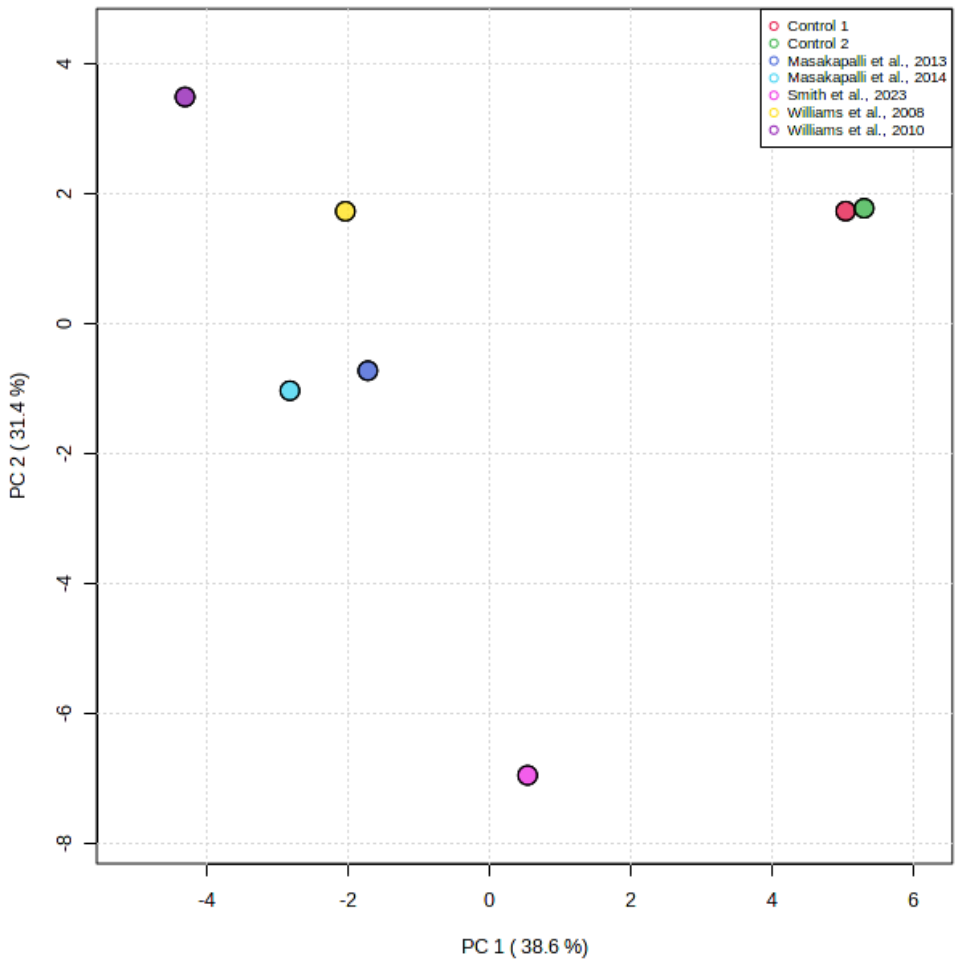


Figure 3.24: *Principal component analysis of net fluxes of reactions in the CCM from the control 1 and control 2 flux solutions from this project and from five published flux solutions.*

3.8 The effect of biomass composition on flux distribution

Some of the differences in flux between the flux solutions presented in section 3.7 are potentially attributable to changes in the measured biomass composition, despite the conclusion by William *et al.* (2010) that biomass composition does not significantly affect the flux distribution in the CCM. This prompts a re-consideration of the role of biomass composition in metabolic modelling.

Figure 3.25 compares the biomass composition measurements in this study and those recorded by Masakapalli *et al*. (2013, 2014a). Although the lipid and organic acid contents are similar in all three studies (Figure 3.25A,D), the protein and carbohydrate contents are not (Figure 3.25B,C). The protein content was considerably greater in the current study compared to other studies of *Arabidopsis* (Williams *et al*., 2008, 2010; Masakapalli *et al*., 2013, 2014a) and biomass compositions from *Nicotiana tabacum* and *Catharanthus roseus* hairy root cells (Sriram *et al*., 2006, Masakapalli *et al.,* 2014b). In contrast he carbohydrate content identified in this project was lower than other *Arabidopsis* studies, though the relative amounts of different carbohydrates are similar in this project and in Masakapalli *et al.* (2013, 2014a) with starch contributing the most and cell wall carbohydrates the least. It is unclear why biomass compositions obtained in this project differ from those of Masakapalli *et al*. (2013, 2014a). However, the studies by Masakapalli *et al.* (2013, 2014a) employed a radioisotopometric method, which reported only on the biosynthetic activity during the labelling period, whereas the biochemical methods used here integrate biosynthesis over the entire growth phase from subculture until the time of harvest, five days later. Further, the radioactive ^{14}C glucose labelling period used by Masakapalli *et al*. (2013, 2014a) was only 48 hours, and it has not been confirmed if this is sufficient time for the cultures to reach isotopic steady state (Williams *et al*., 2008). Since products derived from intermediates close to glucose in the network (such as carbohydrates derived from G6P and F6P) are likely to become labelled much more quickly than those derived from intermediates more distant in the network (like amino acids derived from three carbon

phosphate esters, acetyl CoA and TCA cycle intermediates) It is possible that the radioisotopometric method might over-estimate the proportion of carbohydrates synthesised from glucose phosphates and correspondingly underestimate the contribution of amino acids to the biomass composition.

Interestingly Williams *et al*. (2008, 2010) recorded protein contents of 19.1% and 20% respectively, considerably lower than the protein content measured in this study. However, Williams *et al*. used a Bradford assay with a BSA standard to quantify protein content. The Bradford assay is a common technique for protein measurements, however the response produced by BSA in the assay is approximately twice that of most proteins thereby potentially halving the estimated protein content when used as a calibration standard (Kruger, 2009). Therefore, the protein contents reported by Williams *et al*. may be inaccurately low by a factor of approximately two which would bring them into the range determined in the current study.

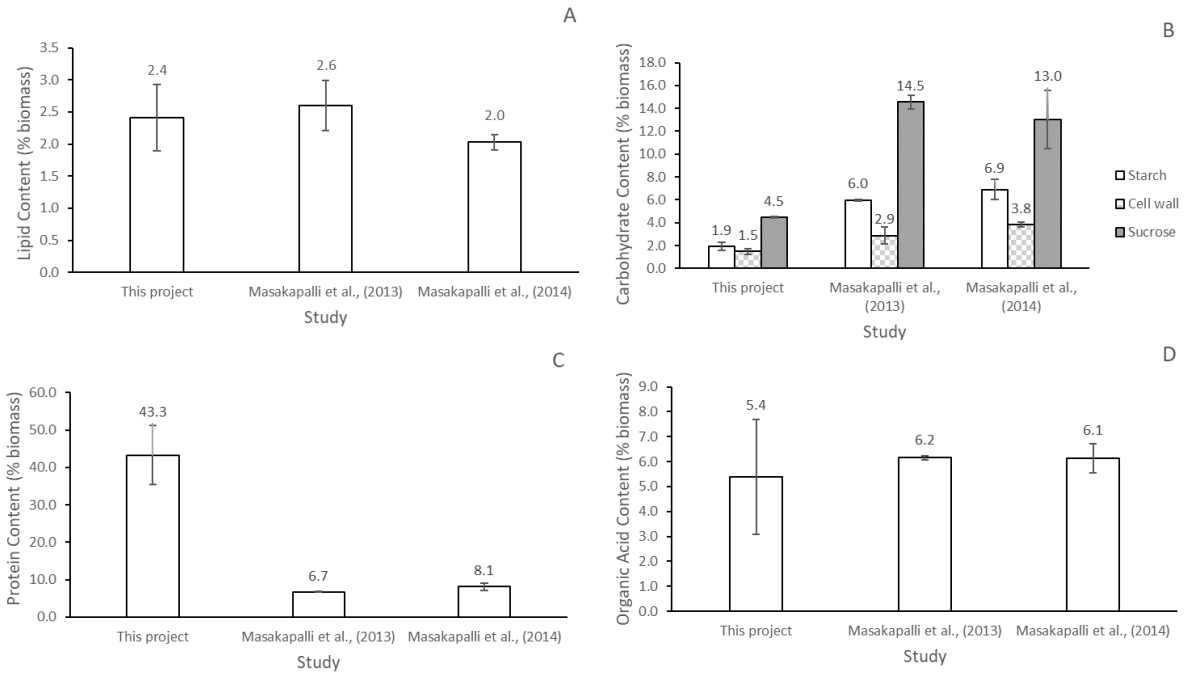


Figure 3.25: *Biomass composition from three MFA studies of Arabidopsis. In this project biomass composition data was collected by colorimetric assays and quantitative GC-MS analysis; in Masakapalli et al. (2013, 2014a) biomass composition data was collected by radioisotopometric methods.*

To assess the impact of the differences in biomass composition on the contrasting flux solutions a biomass equation derived from the biomass measurements in Masakapalli *et al*. (2014a; Appendix 6) was used to calculate a flux solution with model 12 (see Section 3.5) and the MID data from the control 1 labelling experiment (see Section 3.3). This flux solution produced a statistically acceptable SSR of 1153 (based on a 95% $\chi 2$ confidence interval of 1096.3-1287.5 for 1190 DOF) (see Appendix 7 for full flux distribution). Comparison of the flux solutions obtained from the same labelling dataset but produced using the biomass equations derived from either the composition measurements in this study or those from Masakapalli *et al*. (2014a), showed significant differences in fluxes through some reactions (Table 3.10).

Use of the biomass equation derived from Masakapalli *et al*. (2014a) produced a flux solution with a significantly lower flux through the TCA cycle as well as smaller flux through GAP dehydrogenase and enolase (Table 3.10). It is likely that the reduced flux of triose phosphates through GAP dehydrogenase and enolase, reflects the increased biosynthetic demand for G6P. Indeed fluxes through plastidic phosphoglucoisomerase, phosphfructokinase and aldolase were considerably lower when the biomass composition from Masakapalli *et al*. (2014a) was applied. However, partitioning between the cytosol and the plastid reactions was associated with relatively large confidence intervals thus obscuring any statistical significance of these potential differences.

Interestingly, the flux through G6P dehydrogenase and 6-phosphoglucolactonase/dehydrogenase are not significantly different between the two solutions. OxPPP products ribose 5-phosphate (R5P) and erythrose 4-phosphate (E4P) are required for synthesis of phenylalanine, tyrosine, tryptophan and histidine, so the biosynthetic requirement for R5P and E4P was greater when the biomass equation from this study was used, rather than that of Masakapalli *et al*. (2014a). The lack of a correlation between the R5P/E4P requirement and flux through the OxPPP suggests that flux through the OxPPP might not be tightly correlated with the demands for precursors for biomass production. This is considered further in Chapter 6.

The proportion of PEP partitioned into the TCA cycle and into biosynthesis was unchanged between the two solutions. However, the smaller absolute flux to PEP via enolase when the Masakapalli *et al.* (2014a) biomass equation was used resulted in less mitochondrial pyruvate being available to enter the TCA cycle. Consequently, TCA cycle fluxes were significantly lower. This mirrors the decreased demand for amino acids derived from 2OG, succinyl-CoA (SuccCoA), and OAA in the solution using the Masakapalli *et al*. (2014a) derived biomass equation.

Use of the biomass equation defined by Masakapalli *et al*. (2014a) produced a flux solution with a statistically significantly higher CCE (65.1 ± 2.2 % compared to 53.6 ± 2.9%). The increased CCE implies that a greater proportion of the carbon entering the network as glucose is incorporated into biomass when the Masakapalli *et al*. (2014a) biomass equation is applied. This is likely due to the lower protein content in the Masakapalli *et al*. (2014a) biomass equation which causes the biosynthetic requirement for ATP and NAD(P)H to be smaller, and so less glucose needs to be completely oxidised to produce these resources (Figure 3.26).

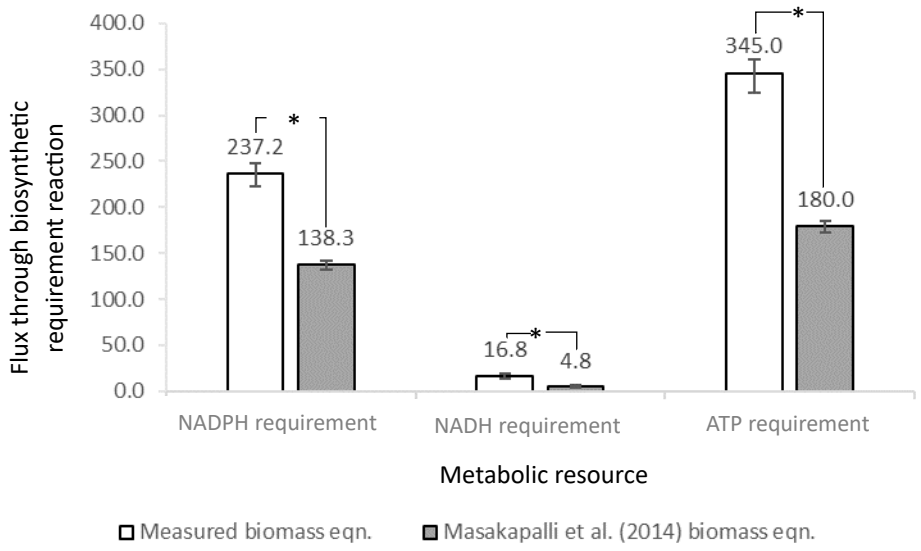


Figure 3.26: *Biosynthetic requirement of NAD(P)H and ATP in flux solutions produced using the same model and MID data set but different biomass equations. Error bars represent 95% confidence interval calculated by parameter continuation. An asterisk (*) indicates a statistically significant difference between the two solutions calculated by confidence interval comparison.*

The changed flux distribution in response to an altered biomass composition brings into question the assertion that the flux through the CCM is not affected by the biomass composition (Williams *et al*., 2010). The previous assertation was based on the observation that analysis of *Arabidopsis* suspension cultures grown under normal conditions (22°C, MS medium) and an experimental condition (MS medium supplemented with 171 mM mannitol) yielded the same flux distribution even though there were significant differences in the biomass composition between the two cultures. However, the differences in biomass composition reported by Williams *et al*. (2010) were considerably smaller than the differences between the biomass compositions in this study and in Masakapalli *et al*. (2014a). Williams *et al*. (2010) reported a 40% increase in protein content, a 28% increase in cell wall carbohydrates and a 50% decrease in of soluble metabolites, while relative to the biomass composition in this study the biomass composition reported by Masakapalli *et al*. (2014) displayed a protein content 81% lower, a lipid content 17% lower, a cell wall carbohydrate content 153% higher, a starch content 263% higher, a sucrose content 189% higher and an organic acid content 13% higher.

Interestingly, when the biomass composition from Masakapalli *et al*. (2014a) is used but the amino acids are split according to the amino acid composition used in section 3.5.3 another statistically acceptable flux solution is produced, with an SSR of 1155 and 1190 DOF and a critical SSR range of 1096.3-1287.5. In this distribution the fluxes in CCM are not significantly different from the flux solution produced when the amino acid composition measured by Masakapalli *et al*. (2014a) is applied. No fluxes differ by more than 2.7% of glucose uptake rate (Appendix 7). This suggests that the flux solution is relatively insensitive to variations in amino acid composition. This insensitivity could be due to the fact that all amino acids are derived from nine precursors and all nine precursors are produced by relatively large fluxes.

It is likely that biomass constraints play a role in determining flux distributions. However, this role may be limited, and the influence is only discernible if flux solutions using radically different biomass compositions are compared. In this context it is notable that the differences in biomass composition between this study and Masakapalli *et al*. (2014a) were considerably larger than the differences in cell wall, protein and soluble metabolite content reported by Williams *et al*. (2010).

The conclusion that the effect of the biomass composition on flux distribution is limited is supported by Yuan *et al*. (2016), in which three large scale models of *Arabidopsis* CCM and three different biomass compositions were assessed using flux balance analysis. The authors concluded that flux through *Arabidopsis* CCM is relatively robust to changes in the biomass composition, but sensitive to changes in the model structure.

Table 3.10: *Comparison of flux solutions constrained by the biomass measurements in this study and those in Masakapalli et al. (2014a)*

Reaction	Measured biomass eqn.	Masakapalli *et al*., (2014a) biomass eqn.
GLCext + ATPi −> G6P	100.0 (n/a, n/a)	100.0 (n/a, n/a)
G6P <−> F6P	1.2 (1.2, 36.8)	7.9 (7.6, 17.6)
F6P + ATP -> FBP	0.0 (0.0, 35.6)	0.0 (0.0, 9.7)
FBP <−> TP + TP	0.0 (0.0, 35.6)	0.0 (0.0, 9.7)
G6P <−> G6Pp	96.6 (55.8, 96.8)	79.2 (69.2, 80.1)
G6Pp <−> F6Pp	47.6 (11.1, 52.1)	29.2 (19.2, 31.7)
F6Pp + ATPi −> FBPp	77.4 (41.6, 78.9)	55.9 (46.1, 57.2)
FBPp <−> TP + TP	77.4 (41.6, 78.9)	55.8 (46.0, 57.2)
G6P −> 6PG + NADPH	0.0 (0.0, 22.0)	0.0 (0.0,9.2)
6PG −> RU5P + CO_2 + NADPH	0.0 (0.0, 22.0)	0.0 (0.0, 9.2)
RU5P <−> X5P	0.0 (0.0, 22.0)	0.0 (0.0, 9.2)
G6Pp −> 6PGp + NADPH	47.9 (21.3, 50.4)	41.7 (30.4, 43.7)
6PGp −> RU5Pp + CO_2 + NADPH	47.9 (21.3, 50.4)	41.7 (30.4, 43.7)
RU5Pp <−> X5Pp	29.8 (4.9, 31.5)	26.6 (16.0, 27.9)
RU5Pp <−> R5Pp	**18.1 (16.4, 18.9)**	**15.1 (14.3, 15.8)**
X5P <−> X5Pp	0.0 (0.0, 22.0)	0.0 (0.0, 9.2)
X5Pp <−> TP + EC2	**29.8 (26.6, 31.5)**	**26.6 (24.9, 27.9)**
F6Pp <−> E4Pp + EC2	−13.2 (−14.0, −11.5)	−12.3 (−13.0, −11.5)
S7Pp <−> R5Pp + EC2	**−16.7 (−17.5, −15.1)**	**−14.3 (−14.9, −13.4)**
F6Pp <−> TP + EC3	**−16.7 (−17.5, −15.1)**	**−14.3 (−14.9, −13.4)**
S7Pp <−> E4Pp + EC3	**16.7 (17.5, 15.1)**	**14.3 (13.4, 14.9)**
TP <−> 3PGA + NADHi + ATP	**167.0 (166.1, 168.9)**	**121.6 (119.9, 124.2)**
3PGA <−> PEP	**156.1 (154.8, 158.8)**	**115.2 (113.3, 118.2)**
PEP −> PYRm + ATP	**76.0 (73.4, 80.6)**	**52.3 (49.3, 56.0)**
PEP −> PYRp + ATP	**43.0 (39.4, 44.5)**	**37.1 (35.0, 38.3)**
PYRm −> ACoAm + CO_2 + NADH	**77.4 (74.2, 84.7)**	**53.0 (49.4, 58.4)**
PYRp −> ACoAp + CO_2 + NADH	**20.0 (18.5, 20.7)**	**29.8 (28.6, 30.7)**
OAA + ACoAm −> CIT	**77.4 (72.6, 83.9)**	**53.0 (49.4, 58.4)**
CIT <−> ICIT	**76.8 (71.9, 83.3)**	**50.4 (46.8, 55.9)**
ICIT <−> 2OG + CO_2 + NADPH	**76.8 (71.9, 83.3)**	**50.4 (46.8, 55.9)**
2OG −> SUCCoA + CO_2 + NADH	**66.2 (60.8, 73.3)**	**46.1 (42.3, 51.8)**
SUCCoA <−> SUC + ATP	**62.1 (56.6, 69.4)**	**43.5 (39.7, 49.3)**
SUC <−> FUM + $FADH_2$	**65.8 (63.3, 75.5)**	**45.2 (41.4, 50.9)**
FUM <−> MAL	**68.6 (63.3, 75.5)**	**43.6 (39.8, 49.4)**
MAL <−> OAA + NADH	**65.0 (6.1, 69.1)**	**37.3 (34.1, 41.1)**
PEP + CO_2 −> OAA	**30.1 (28.0, 34.1)**	**22.0 (20.9, 25.0)**
MAL −> PYRm + CO_2 + NADH	1.4 (0.0, 6.4)	0.6 (0.0, 4.1)
MAL −> PYRp + CO_2 + NADPH	0.2 (0.0, 1.1)	0.2 (0.0, 1.0)

The values in grey brackets are the 95% confidence limits calculated by parameter continuation. Fluxes which are significantly different between the two conditions are shown in bold

3.9 Conclusion

This chapter has discussed the development and assessment of a methodology for producing flux solutions of the CCM from steady-state MFA of *Arabidopsis* suspension cultures. The reproducibility of flux distributions produced by this method and the effect biomass constrains can have on flux estimates was also assessed. From the analyses and comparisons of the flux maps reported in this chapter the following can be concluded;

1. The methodology adopted for this study can generate precise and reproducible flux solutions.

2. There is relatively poor agreement between flux distributions deduced in independent MFA studies. Thus, solutions from other studies should not be used as a quantitative basis for comparison of flux solution under different conditions.

3. The biomass constraints used for fitting the data can affect the calculated flux distributions, particularly if the biomass compositions are radically different.

Chapter 4: Growth and flux distribution under reduced temperatures

4.1 Introduction

To achieve the main objective of this thesis, to assess net fluxes in the CCM at slowed growth rates, it is necessary to grow cell cultures in conditions which impair the rate at which biomass can accumulate. Low temperature is an important, and well-studied environmental factor which affects plant physiology (Boyer, 1982; Stitt and Hurry, 2002), and limits the growth rate of *Arabidopsis* (Antoun and Ouellet, 2013), making it a potentially useful treatment for this study.

Arabidopsis has been used extensively as a model in studies of plant responses to low temperature (Hannah *et al*., 2006). The majority of the work on low temperature carried out in *Arabidopsis* has focused on comparatively large decreases from 22°C to 4°C (Thomashow *et al*., 1999). The main themes of this research have been genomic regulation by cold responsive transcription factors, alteration of membrane fluidity and production of compatible solutes to act as osmolytes and cryoprotectants (Aslam *et al*., 2022; Satyakam *et al*., 2022).

In this project, decreases in temperature from the standard growth temperature of 22°C to 17°C or 12°C were used. There are strong theoretical reasons for anticipating that the growth rate and metabolic flux distribution of the cultures will change in response to a small change in temperature. First, all absolute reactions rates will decrease as the temperature is lowered, due to the physical effects of temperature on chemical reactions described by the Arrhenius equation, which results in all reactions being slower and the growth rate decreasing (Laidler, 1984). Furthermore, different enzymes are likely to respond differently to the temperature change depending on their physical properties and their regulation *in*

vivo, thereby changing the relative fluxes through different sections of the metabolic network (ap Rees *et al.,* 1988). Although the growth response of *Arabidopsis* at 4°C is well characterised, a drop in temperature of eighteen degrees is likely to decrease the growth rate of the cell culture so much as to make growth and labelling experiments impractical.

There is also indirect evidence of slowed growth rate and potential flux re-arrangement in *Arabidopsis* and other plants in response to mild temperature drops. Hasdai *et al.* (2006) identified morphological changes, pigmentation changes and slowed flowering in *Arabidopsis* plants grown at 14°C. Further morphological changes and growth regime changes were reported by Antoun and Ouellet (2013) when *Arabidopsis* plants were grown at a variety of temperatures including 12°C and 17°C. Khavari-Nejad *et al*. (2013) exposed *Arabidopsis* plants to growth at 13°C and recorded increased proline content and evidence of increased oxidative stress (increased malondialdehyde level and increased superoxide dismutase activity) relative to plants grown at 22°C. Iyer *et al.* (2008) used a temperature decrease of 7°C or 8°C, from 27°C/20°C (day/night) to 20°C/12°C, while investigating the metabolism of developing soybean (*Glycine max*) cotyledons. They found that this small decrease in growth temperature increased carbon partitioning from the plastidic pyruvate pool into oil synthesis and that flux through the OxPPP was decreased in response to the temperature decrease, but only if the temperature change happened early in the development of the cotyledon. They further identified increased flux through the anaplerotic reactions catalysed by PEP carboxylase and malic enzyme at lower temperature. These papers suggest that a small temperature decrease, similar to those planned in the current study, can affect the growth regime and physiology of whole plants. However, it is unclear if these changes are associated with changes in flux through the CCM.

Relatively little work has been done to investigate small temperature drops in *Arabidopsis* cell suspension cultures, but there is strong evidence of proteomic and transcriptomic changes in *Arabidopsis* suspension cultures in response to 4°C (Sasaki *et al.,* 2008; Chiba *et al.,* 2008; Miniami *et al.,* 2009; Li *et al.,* 2012; Li *et al.,* 2020). The only study to grow

Arabidopsis suspension cultures at 12°C was an investigation into the phosphoproteome which found unique phosphorylation patterns in cultures grown at 22°C, 12°C and 4°C (El-Khatib *et al*., 2007), suggesting some regulatory change in response to the reduction in temperature.

Taken together the literature suggests that *Arabidopsis* plants and cell suspension cultures respond to mild reductions in temperature across multiple levels of cellular organisation. There is therefore a likelihood of some metabolic re-arrangement in *Arabidopsis* suspension cultures in response to mildly reduced temperatures. Applying MFA to cultures grown at 17°C and 12°C, will give an insight into the CCM response to chilling temperatures and slowed growth rate.

Cold acclimation is the process of physiological adjustment in plants exposed to cold but not freezing temperatures which allows for the development of freezing tolerance (Thomashow *et al.,* 1999). There is strong evidence that cold acclimation and the associated metabolic changes occur in whole *Arabidopsis* plants (Guy *et al.,* 1992; Gilmore *et al.,* 2000; Hannah *et al.,* 2006; Kaplan *et al.,* 2007; Nägele *et al.,* 2011; Töpfer *et al.,* 2013; Kazemi-Shahandashti and Maali-Amiri, 2018) and in *Arabidopsis* suspension cultures (Sasaki *et al.,* 2008; Chiba *et al.,* 2008; Miniami *et al.,* 2009; Li *et al.,* 2012; Li *et al.,* 2020). To separate the early metabolic effects of reduced temperature from the metabolic effects of acclimation a line of culture was acclimated to growth at 12°C for one month prior to the initiation of labelling experiments.

4.2 Growth profiles

There is evidence of altered growth dynamics in response to 12°C and 17°C in *Arabidopsis* plantlets, but this needed to be confirmed for suspension cultures.

Suspension cultures were grown in a total volume of 115 ml at 22°C, 17°C or 12°C over a period of 10-30 days with samples taken at frequent time points (Figure 4.1). The culture grown at 22°C began to grow rapidly after three days whereas it was five and six days after subculture before the 17°C and 12°C cultures, respectively, entered a rapid growth phase. The 22°C culture entered a stationary phase eight days after subculture, while the 12°C entered a stationary phase at 18 days after subculture and the 17°C culture later than ten days after subculture (Figure 4.1A). Further, linear regression of the natural logarithm of each data point over the exponential growth phase followed by single factor analysis of variance (ANOVA) suggested significantly different rates of biomass accumulation at the different temperatures *(P<0.01)*. The antilogs of the gradients calculated from linear regression are 1.51 ± 0.05 mg DW.ml^{-1}.d^{-1} (mean ± SEM) for the 22°C culture, 1.32 ± 0.02 mg DW.ml^{-1}.d^{-1} for the 17°C culture and 1.13 ± 0.01 mg DW.ml^{-1}.d^{-1} for the 12°C culture.

Due to the different growth rates of the cultures the labelled biomass had to be harvested at different times. Steady state MFA works when a constant specific growth rate can be assumed, i.e. the system is at steady state and biomass is accumulating exponentially. Typically these conditions are achieved in the mid-exponential phase of the culture cycle. Therefore the control condition cultures were harvested after 5.5 d growth, the 17°C cultures were harvested after 7 d growth and the 12°C cultures after 12 d growth.

In terms of glucose consumption over the 10 d growth period the 22°C culture decreased the residual glucose in the medium to 9 mM, while the 17°C culture only decreased it to 123 mM and the 12°C culture to 156 mM (Figure 4.1B). Linear regression showed that the culture growing at 22°C reduced the glucose concentration in the medium by 29.46 ± 1.56 mM.d^{-1} from three days after subculture to six days after subculture, while the 17°C grown

culture reduced the glucose concentration by only 8.72 ± 8.22 mM d^{-1} from five to eight days after subculture and the 12°C grown culture by 8.64 ± 1.48 mM d^{-1} from 9 to 15 days after subculture. Analysis of variance showed significant difference between the 22°C culture and the 17°C and 12°C cultures *(P<0.05)*, but in this case there was no significant difference between the 17°C and 12°C cultures.

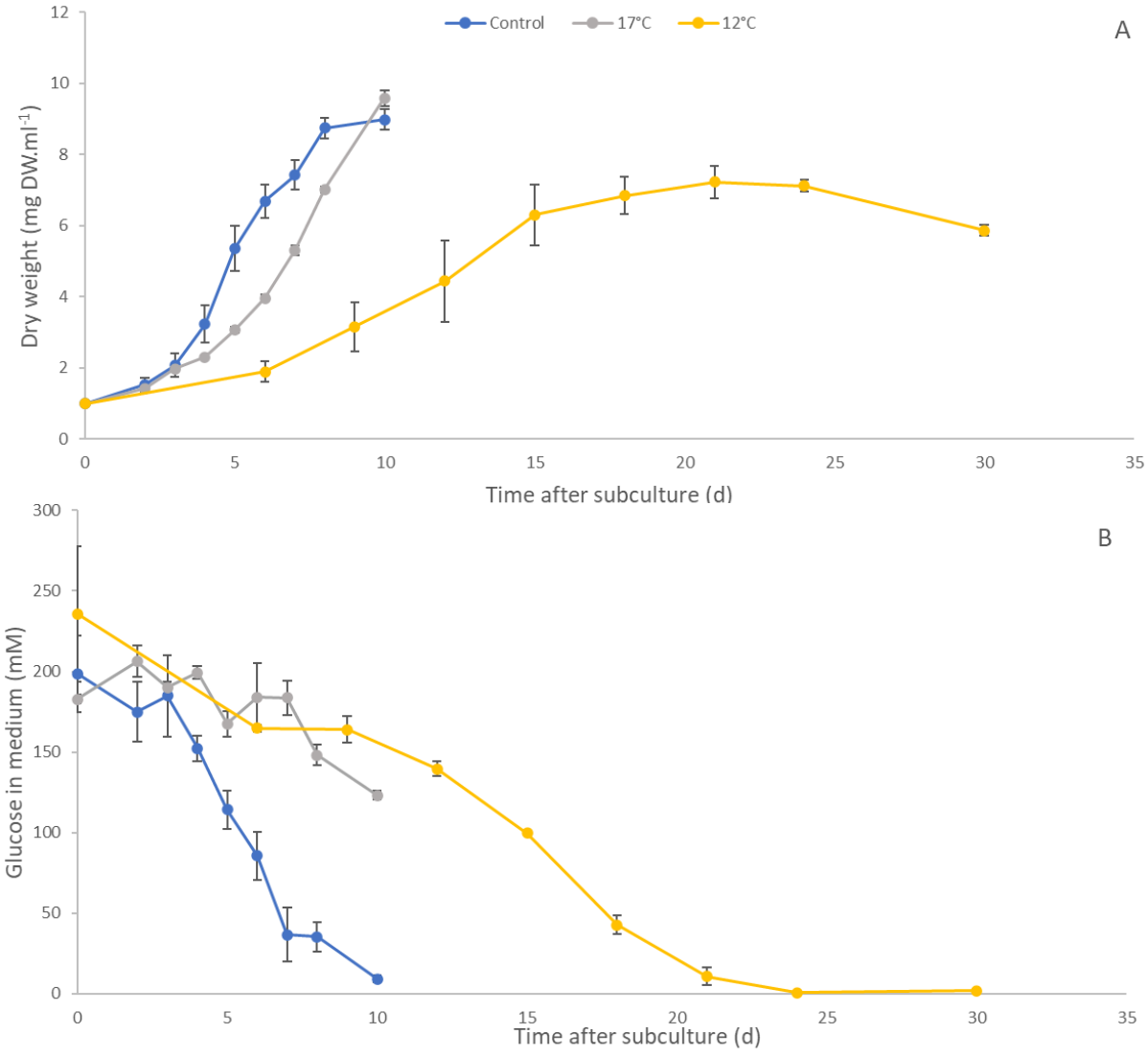


Figure 4.1: *Growth profiles of Arabidopsis suspension cultures grown at different temperatures. (A) dry weight accumulation, and (B) glucose consumption for cultures grown at different temperatures. Each point is the mean of three different flasks, error bars represent ± one SEM. In the labelling experiments biomass was harvested at mid-exponential phase, this was after 5.5 d of growth for the control conditions cultures, 7 d of growth for the 17°C cultures, and 12d of growth for the 12°C cultures.*

These data show that a decreased temperature slows growth and the rate of glucose uptake from the medium in *Arabidopsis* suspension cultures, making growth at mildly reduced temperatures an appropriate perturbation for investigating the relationship between growth rate and flux distribution. This is consistent with the altered growth regimes seen on whole *Arabidopsis* plants at low temperatures by Hasdai *et al*. (2006), Antoun and Ouellet (2013) and Khavari-Nejad *et al*. (2013).

The longer time course for the 12°C grown cultures shows that cold grown cultures do eventually consume a similar amount of glucose as cultures grown at 22°C, but take considerably longer to do so, and convert this into less biomass. This could reflect glucose accumulation in the cells or increased senescence and apoptosis in the 12°C culture.

4.3 Biomass composition

Biomass composition was quantified in cultures grown in 22°C, 17°C and 12°C as per section 2.4 and 3.4 (Figure 4.2). These biomass compositions were used to constrain the MFA by defining biomass equations, which are presented in Appendix 6. The lipid content in the 17°C grown cultures was significantly lower than that of the 22°C grown cultures while the lipid content of the 12°C cultures was significantly greater than both (Figure 4.2A). There was no significant difference in the starch and cell wall content between the 22°C and 17°C grown cultures, although the 22°C grown cultures had a much greater sucrose content. The 12°C grown cultures had a significantly greater starch content and lower cell wall content than the 22°C grown cultures as well as a much smaller sucrose content (Figure 4.2B). The majority of biomass in all conditions was protein, although the protein content of the 17°C grown cultures was significantly lower than the 22°C or 12°C grown cultures (Figure 4.2C). The 22°C grown culture had a considerably greater total organic acid content but the only significant difference between the 22°C and reduced temperature grown cultures was that the 17°C grown culture had a significantly lower succinate content.

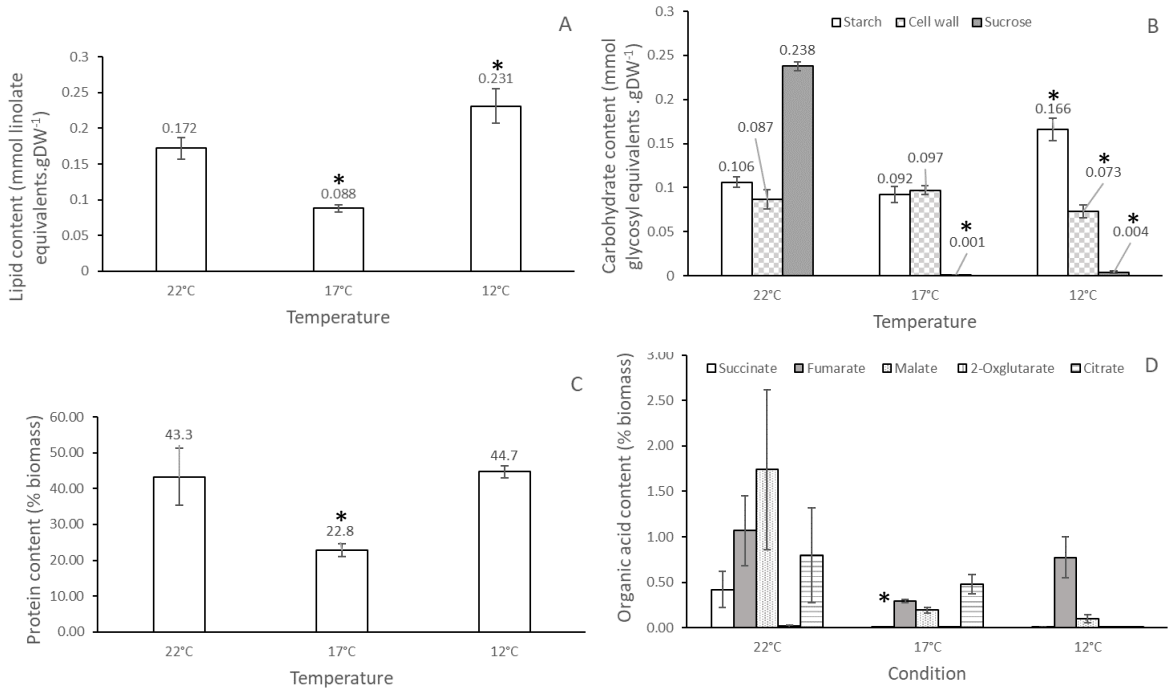


Figure 4.2: *Biomass composition of Arabidopsis cell suspension cultures grown at 22°C, 17°C or 12°C. Panels show the content of: (A) lipids; (B) insoluble carbohydrates and sucrose; (C) protein and (D) various organic acids. Points are means of 3-15 independent repeats, error bars show ± 1 SEM and asterisks (*) represent values which differed significantly from those in the 22°C culture.*

Sasaki *et al.* (2008) found an increased carbohydrate content in *Arabidopsis* cultures which had been exposed to 4°C. However whether the glucose observed by Sasaki *et al.* (2008) was derived from starch, cell wall carbohydrates, sucrose or free glucose pools was unclear. Dynamic modelling of *Arabidopsis* carbohydrate metabolism in response to 4°C and direct measurement of starch content of *Arabidopsis* plants also showed increased starch accumulation as well as a small increase in sucrose content (Nägele *et al.,* 2011; Herrmann *et al*., 2021). Increased carbohydrate content as well as increased content of some amino acids and organic acids has been reported in whole *Arabidopsis* plants exposed to 4°C (Cook *et al.,* 2004; Kaplan *et al*., 2004), and these likely operate as compatible solutes, or precursors for defence against opportunistic infection by pathogens (Guy *et al.,* 1992; Uemura *et al*., 2003; Kaplan *et al.,* 2004). Interestingly, Kaplan *et al*. (2004) noted an increase in the content of TCA cycle intermediates succinate, malate, fumarate, 2OG, and citrate associated with growth at 4°C while the content of most of these

organic acids measured in this study showed no significant change in response to growth at 17°C or 12°C. It is possible that the content of TCA cycle intermediates and sucrose is only affected at a temperature lower than 12°C.

Iyer *et al*. (2008) also performed flux analysis under mildly reduced temperatures, in soybean cotyledons and found decreased oil and starch content. The trends in biomass composition with decreased temperature identified in this study differ from those of Iyer *et al*. (2008), likely because of the different species and tissue type, and while cells in suspension culture are continually dividing the biological role of differentiated developing cotyledons is to accumulate protein and oils to provide storage reserves in mature seeds.

The results discussed here show that growth of *Arabidopsis* cultures at moderately decreased temperatures can affect the biomass composition, notably increased lipid and starch content. These changes in biomass composition could be related to changes in flux distribution in the CCM, which will be elucidated by MFA.

4.4 CCM flux distribution at decreased temperature

^{13}C MFA was applied to *Arabidopsis* cultures grown at 12°C and 17°C as well as under standard growth temperature (22°C). Cultures grown at 12°C were grown in parallel to Control 1 from Chapter 3 and the cultures grown at 17°C were grown at the same time as Control 2. Flux solutions were generated for all four cultures, flux maps are shown in Figure 4.3 and summaries of the net fluxes through the CCM are shown in Tables 4.1 and 4.2, full solutions are presented in Appendix 7. Both the decreased temperature cultures produced statistically acceptable flux solutions. The 17°C culture produced a flux solution with an SSR of 893.8 with 820 DOF and a critical SSR range of 742.5-901.2, and the 12°C culture produced a flux solution produced an SSR od 1058.8 with 987 DOF and a critical SSR range of 901-1079. The two cultures grown at 22°C yielded very similar flux solutions (see

Chapter 3) while the two cultures grown at lower temperature yielded solutions which showed some significant differences compared to the 22°C culture.

As described in Chapter 3, INCA can perform Monte Carlo analysis using a method described by Press *et al*. (1992), in which the optimal set of parameters are used to produce many synthetic datasets containing Gaussian noise, based on the defined experimental error. These synthetic datasets are then used to re-estimate the model parameters thus creating a probability distribution for each parameter. Performing 1000 rounds of Monte Carlo simulation on the best-fit solutions for each of the cultures provided a probability distribution for each reaction. These 1000 flux solutions were extracted and used for PCA . The scores plot shows clustering of the two 22°C cultures together and, separately, clustering of the 17°C and 12°C cultures together, with moderate separation between the two clusters (Figure 4.4A). This suggests some difference in flux distribution between the 22°C cultures and the decreased temperature cultures.

The flux solutions for the 22°C cultures are concentrated in the upper left sector of the plot in Figure 4.4A while the solutions for the lower temperature cultures predominate in the lower right. The loading of each reaction calculated in PCA describes the extent to which each reaction influences each principal component and thus contributes to the separation between groups in the scores plot. A biplot superimposes the distribution of the loadings (red arrows) onto the scores plot (Figure 4.4B). The loadings which spread from the origin along the axis of maximum separation between the two groups of flux solutions are the reactions which contribute to the separation. In Figure 4.4B the loadings which contribute to the separation between the groups are highlighted by the blue rings. Flux through plastidic G6P dehydrogenase, phosphopentose epimerase, phosphopentose isomerase, transketolase and transaldolase reactions in the OxPPP decreased, while flux through the transcompartmental GAP dehydrogenase/phosphoglycerate kinase reaction, moving from the upper left to the lower right sections of the plot increased (Figure 4.4B; R50-R59 and R38 in Appendix 7).

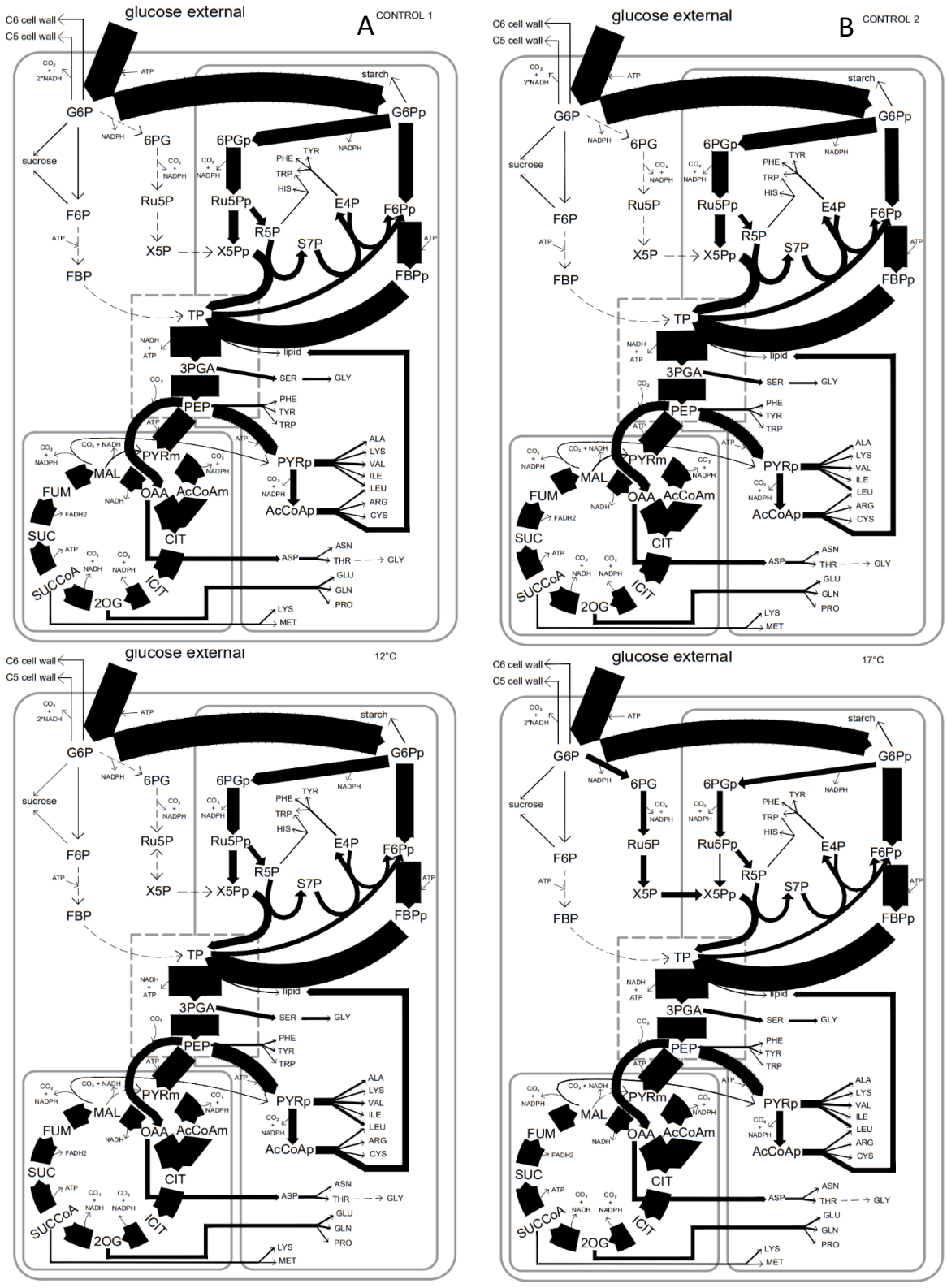
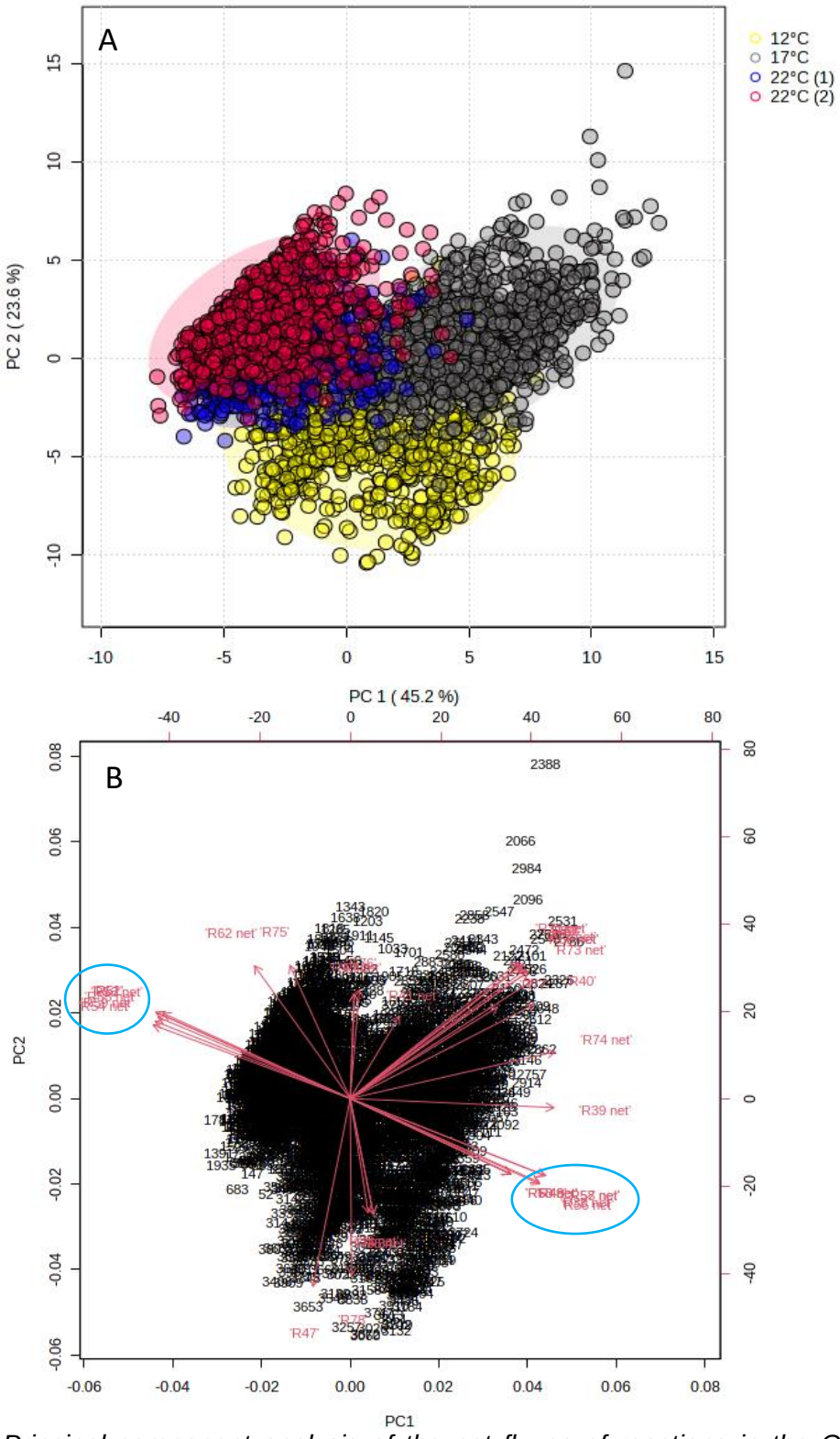


Figure 4.3: *Flux maps derived from MFA for Arabidopsis cultures grown at different temperatures. (A) comparison of 22°C grown culture (top) and parallel-grown 12°C culture (bottom, see Table 4.1 for further detail); (B) comparison of second 22°C grown culture (top) and parallel-grown 17°C culture (bottom, see table 4.2 of further detail). The thickness of lines indicates the relative flux of the reactions, dotted lines represent fluxes less than 0.009 relative to a glucose uptake of 100.*



.***Figure 4.4:*** *Principal component analysis of the net fluxes of reactions in the CCM in cultures grown at different temperatures. (A) Scores plots of flux solutions for two cultures grown at 22°C (blue and red), one culture grown at 17°C (grey) and one culture grown at 12°C (yellow). (B) Biplot of PCA with loadings indicated in red. The blue rings highlight the fluxes which exerted the greatest influence on the separation of the two clusters of flux solutions along the axis of maximum separation. Synthetic datasets were derived from 1000 rounds of Monte Carlo simulation for each of the four flux solutions.*

To further investigate the differences between individual net fluxes the overlap in appropriate confidence intervals of each flux between flux solutions was analysed (see section 2.7; Tables 4.1 and 4.2). Confidence interval overlap analysis supports the biplot analysis; in the 12°C grown culture fluxes through phosphopentose isomerase, transketolase and transaldolase decreased while flux through GAP dehydrogenase/phosphoglycerate kinase and plastidic pyruvate dehydrogenase was significantly increased relative to the 22°C grown culture.

Similar to the 12°C culture, the flux solution for the 17°C grown culture showed significantly lower flux through phosphopentose isomerase, transketolase and transaldolase, and significantly increased flux through GAP dehydrogenase/phosphoglycerate kinase, enolase, cytosolic pyruvate kinase and malate dehydrogenase relative to the 22°C culture.

If all the reactions in the metabolic network decreased with temperature as described by the Arrhenius equation, then flux through the network would slow approximately uniformly and the relative fluxes estimated by MFA would not be significantly different at different temperatures. However, the PCA and confidence interval overlap analysis suggest that growth at decreased temperatures induces some small, but significant changes to the relative flux distribution in the CCM. Notably, decreased flux through the OxPPP and increased flux through the later reactions of glycolysis, indicating that reactions in the CCM do not respond uniformly to temperature. This could either be because of differential sensitivity of the individual enzymes to low temperatures, because of a temperature induced change in regulation of the enzymes at a transcriptional, translational or post-translational level, because of a change in the concentrations of substrates or products, or because of a combination of factors. El-Khatib *et al*. (2007) showed that the phoshoproteome of *Arabidopsis* cell suspension cultures changes in response to growth at 12°C so it is possible that some of the low temperature induced changes in flux distribution in the CCM are related to the change in phosphorylation status of proteins. Further, evidence from MFA studies in other organisms has shown that changes in relative flux distribution in response to small

changes in temperature are seen in other plants (Iyer *et al*., 2008) and in yeast grown at 16°C rather than 28°C (Quirós *et al*., 2013).

As discussed in Chapter 3, the biomass equation used to constrain MFA can have some effect on the flux estimates, and so some of the altered fluxes may be linked to the altered biomass composition recorded at 12°C and 17°C. The increased plastidic acetyl-CoA production in the 12°C grown culture may be to accommodate increased lipid and protein production, while the increase in net flux through phosphoglycerate kinase/enolase, cytosolic pyruvate kinase and malate dehydrogenase in the 17°C grown cultures may be related to the reduced protein content of these cultures because a smaller proportion of the 3PGA, PEP and plastidic pyruvate produced are required for biosynthesis.

Table 4.1: *Comparison of flux solutions from Arabidopsis cultures grown at 22°C and 12°C.*

Reaction	Relative flux at specific temperature	
	22°C (Control 1)	12°C
GLCext + ATPi −> G6P	100.0 (n/a, n/a)	100.0 (n/a, n/a)
G6P <−> F6P	1.2 (1.2, 36.8)	0.0 (0.0, 66.9)
F6P + ATP −> FBP	0.0 (0.0, 35.6)	0.0 (0.0, 66.9)
FBP <−> TP + TP	0.0 (0.0, 35.6)	0.0 (0.0, 66.9)
G6P <−> G6Pp	96.6 (55.8, 96.8)	99.2 (31.9, 99.2)
G6Pp <−> F6Pp	47.6 (11.1, 52.1)	57.4 (−9.7, 60.1)
F6Pp + ATPi −> FBPp	77.4 (41.6, 78.9)	81.9 (15.0, 82.8)
FBPp <−> TP + TP	77.4 (41.6, 78.9)	81.9 (15.0, 82.8)
G6P −> 6PG + NADPH	0.0 (0.0, 22.0)	0.0 (0.0, 14.7)
6PG −> RU5P + CO_2 + NADPH	0.0 (0.0, 22.0)	0.0 (0.0, 14.7)
RU5P <−> X5P	0.0 (0.0, 22.0)	0.0 (0.0, 22.0)
G6Pp −> 6PGp + NADPH	47.9 (21.3, 50.4)	40.1 (24.1, 42.8)
6PGp −> RU5Pp + CO_2 + NADPH	47.9 (21.3, 50.4)	40.1 (24.1, 42.8)
RU5Pp <−> X5Pp	29.8 (4.9, 31.5)	24.5 (9.0, 26.4)
RU5Pp <−> R5Pp	**18.1 (16.4, 18.9)**	**15.5 (14.7, 16.4)**
X5P <−> X5Pp	0.0 (0.0, 22.0)	0.0 (0.0, 14.7)
X5Pp <−> TP + EC2	**29.8 (26.6, 31.5)**	**24.5 (22.7, 26.4)**
F6Pp <−> E4Pp + EC2	**−13.2 (−14.0, −11.5)**	**−10.4 (−11.4, −9.5)**
S7Pp <−> R5Pp + EC2	**−16.7 (−17.5, −15.1)**	**−14.1 (−15.0, −13.3)**
F6Pp <−> TP + EC3	**−16.7 (−17.5, −15.1)**	**−14.1 (−15.0, −13.3)**
S7Pp <−> E4Pp + EC3	**16.7 (17.5, 15.1)**	**14.1 (13.2, 15.0)**
TP <−> 3PGA + NADHi + ATP	**167.0 (166.1, 168.9)**	**172.7 (171.8, 173.8)**
3PGA <−> PEP	156.1 (154.8, 158.8)	158.9 (153.8, 161.5)
PEP −> PYRm + ATP	76.0 (73.4, 80.6)	76.8 (71.9, 82.3)
PEP −> PYRp + ATP	**43.0 (39.4, 44.5)**	**49.0 (45.6, 51.7)**
PYRm −> ACoAm + CO_2 + NADH	77.4 (74.2, 84.7)	76.8 (71.8, 82.3)
PYRp −> ACoAp + CO_2 + NADH	**20.0 (18.5, 20.7)**	**25.6 (23.9, 26.8)**
OAA + ACoAm −> CIT	77.4 (72.6, 83.9)	76.8 (71.8, 82.3)
CIT <−> ICIT	76.8 (71.9, 83.3)	76.8 (71.8, 82.3)
ICIT <−> 2OG + CO_2 + NADPH	76.8 (71.9, 83.3)	76.8 (71.8, 82.3)
2OG −> SUCCoA + CO_2 + NADH	66.2 (60.8, 73.3)	65.9 (60.6, 72.0)
SUCCoA <−> SUC + ATP	62.1 (56.6, 69.4)	61.7 (56.3, 68.0)
SUC <−> FUM + $FADH_2$	65.8 (63.3, 75.5)	65.9 (60.6, 72.0)
FUM <−> MAL	68.6 (63.3, 75.5)	69.4 (64.3, 75.3)
MAL <−> OAA + NADH	65.0 (6.1, 69.1)	69.0 (64.2, 74.5)
PEP + CO_2 −> OAA	30.1 (28.0, 34.1)	25.9 (24.5, 27.7)
MAL −> PYRm + CO_2 + NADH	1.4 (0.0, 6.4)	0.0 (0.0, 2.0)
MAL −> PYRp + CO_2 NADPH	0.2 (0.0, 1.1)	0.3 (0.0, 1.5)

The values in grey brackets are the 95% confidence limits. Fluxes which are significantly different between the two conditions are shown in bold.

Table 4.2: *Comparison of flux solutions from Arabidopsis cultures grown at 22°C and 17°C.*

Reaction	Relative flux at specific temperature	
	22°C (Control 2)	17°C
GLCext + ATPi −> G6P	100.0 (n/a, n/a)	100.0 (n/a, n/a)
G6P <−> F6P	1.2 (1.1, 40.2)	0.0 (0.0, 35.9)
F6P + ATP −> FBP	0.0 (0.0, 39.0)	0.0 (0.0, 35.9)
FBP <−> TP + TP	0.0 (0.0, 39.0)	0.0 (0.0, 35.9)
G6P <−> G6Pp	96.8 (50.0, 96.9)	80.3 (36.9, 98.2)
G6Pp <−> F6Pp	43.5 (2.3, 47.6)	61.1 (23.5, 65.3)
F6Pp + ATPi −> FBPp	76.3 (36.4, 77.7)	82.4 (46.1, 83.8)
FBPp <−> TP + TP	76.3 (36.4, 77.7)	82.4 (46.1, 83.8)
G6P −> 6PG + NADPH	0.0 (0.0, 23.6)	17.8 (0.0, 34.9)
6PG −> RU5P + CO_2 + NADPH	0.0 (0.0, 23.6)	17.8 (0.0, 34.9)
RU5P <−> X5P	0.0 (0.0, 23.6)	17.8 (0.0, 34.9)
G6Pp −> 6PGp + NADPH	52.3 (24.1, 55.6)	17.3 (0.0, 40.1)
6PGp −> RU5Pp + CO_2 + NADPH	52.3 (24.1, 55.6)	17.3 (0.0, 40.1)
RU5Pp <−> X5Pp	32.8 (6.2, 35.0)	3.5 (−13.7, 24.6)
RU5Pp <−> R5Pp	**19.5 (18.0, 20.6)**	**13.8 (12.5, 15.5)**
X5P <−> X5Pp	0.0 (0.0, 23.6)	17.8 (0.0, 34.9)
X5Pp <−> TP + EC2	**32.8 (29.9, 35.1)**	**21.3 (18.4, 24.7)**
F6Pp <−> E4Pp + EC2	**−14.7 (−15.9, −13.2)**	**−8.9 (−10.6, −7.4)**
S7Pp <−> R5Pp + EC2	**−18.1 (−19.2, −16.6)**	**−12.4 (−14.1, −11.0)**
F6Pp <−> TP + EC3	**−18.1 (−19.2, −16.6)**	**−12.4 (−14.1, −11.0)**
S7Pp <−> E4Pp + EC3	**18.1 (19.2, 16.6)**	**12.4 (11.0, 14.1)**
TP <−> 3PGA + NADHi + ATP	**166.4 (165.0, 168.1)**	**172.8 (171.1, 174.5)**
3PGA <−> PEP	**155.8 (153.5, 158.3)**	**160.5 (157.5, 163.2)**
PEP −> PYRm + ATP	**78.8 (74.0, 82.4)**	**84.9 (79.2, 90.8)**
PEP −> PYRp + ATP	40.2 (36.9, 42.8)	41.0 (37.3, 44.1)
PYRm −> ACoAm + CO_2 + NADH	81.0 (75.2, 87.7)	84.9 (79.2, 92.7)
PYRp −> ACoAp + CO_2 + NADH	19.0 (17.7, 20.0)	19.6 (18.6, 20.7)
OAA + ACoAm −> CIT	81.0 (75.0, 88.0)	84.9 (79.2, 92.7)
CIT <−> ICIT	80.4 (74.4, 87.4)	84.4 (78.7, 92.2)
ICIT <−> 2OG + CO_2 + NADPH	80.4 (74.4, 87.4)	84.4 (78.7, 92.2)
2OG −> SUCCoA + CO_2 + NADH	70.3 (63.7, 78.0)	73.8 (67.6, 82.4)
SUCCoA <−> SUC + ATP	66.4 (59.6, 74.4)	69.7 (63.3, 78.6)
SUC <−> FUM + $FADH_2$	69.9 (63.3, 77.7)	73.8 (67.6, 82.4)
FUM <−> MAL	72.6 (66.1, 80.2)	77.0 (71.0, 85.4)
MAL <−> OAA + NADH	**67.6 (63.5, 71.9)**	**75.0 (69.6, 80.8)**
PEP + CO_2 −> OAA	30.1 (27.6, 34.2)	27.5 (26.4, 31.3)
MAL −> PYRm + CO_2 + NADH	2.2 (0.0, 7.4)	0.0 (0.0, 4.7)
MAL −> PYRp + CO_2 + NADPH	0.8 (0.0, 1.7)	1.8 (0.7, 2.8)

The values in grey brackets are the 95% confidence limits. Fluxes which are significantly different between the two conditions are shown in bold.

Interestingly, the CCE was unchanged for the reduced temperature grown cultures compared to those at 22°C (Figure 4.5). This suggests that, although there were changes in biomass composition and significant changes in flux through some of the reactions in the CCM at decreased temperature, the partitioning of absorbed carbon into biomass or CO_2 remained unchanged by the growth temperature. This is consistent with the proposal suggested by Hansen *et al*. (2009), that the CCE only decreases when plants are grown at temperatures approaching the limits of their tolerance, and that 12°C and 17°C are both within the tolerable temperatures of the Landsberg-*erecta* ecotype of *Arabidopsis* (Hannah *et al*., 2006).

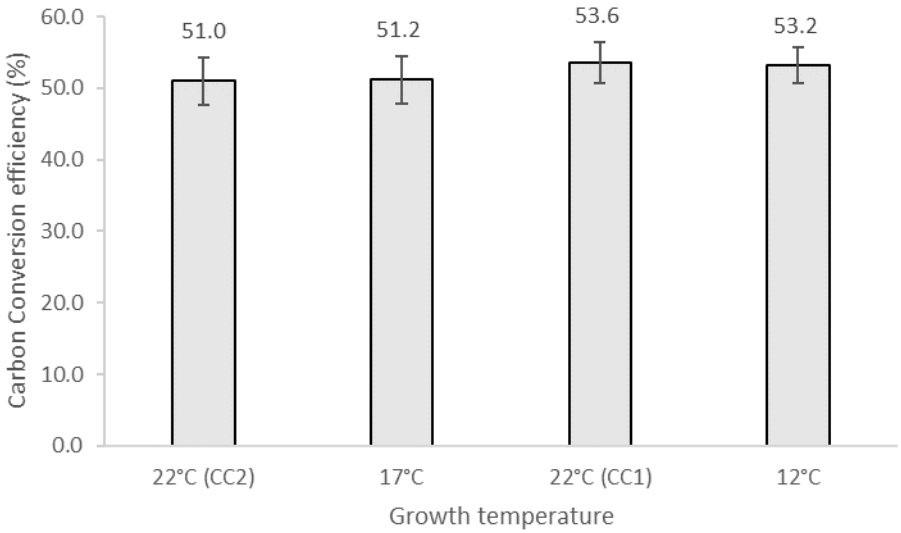


Figure 4.5: *Carbon conversion efficiency of Arabidopsis cell culture grown in MS medium at 22°C, 17°C or 12°C. Error bars represent 95% confidence interval calculated by parameter continuation. Control 1 (CC1) was grown parallel to the 12°C culture and control 2 (CC2) was grown in parallel with the 17°C culture.*

Some of the changes in net fluxes between the 22°C cultures and decreased temperature cultures cannot immediately be explained by changes in biomass composition. Both the 12°C and the 17°C cultures show significantly decreased flux through transketolase, transaldolase, and phosphopentose isomerase relative to the parallel grown 22°C cultures despite the lack of significant change in the demand for E4P and R5P in protein production in the 12°C culture. The comparisons presented in Chapter 3 indicate the tendency of MFA to over-estimate the significance of differences in flux through the non-oxidative steps of OxPPP. So, the biological relevance of the apparent decreased fluxes through the non-oxidative steps of OxPPP is unclear (Tables 4.1 and 4.2).

Closer inspection of the OxPPP in the flux maps shows that the duplication of G6P dehydrogenase reactions between the plastid and the cytosol increased the size of the confidence intervals. This potentially obscures the significance of the differences in these reactions between solutions (Tables 4.1 and 4.2). G6P utilisation represents an important metabolic hub (Jiang *et al*., 2022), so to make a more detailed analysis of G6P utilisation, the variation of the biomass output ancillary reactions for summing duplicated reactions was employed (Section 3.4.2). This allowed quantification of the total flux from cytosolic and plastidic G6P dehydrogenase, from cytosolic and plastidic phosphoglucoisomerase and the combined contribution of cytosolic and plastidic G6P to biomass, with associated confidence intervals.

Figure 4.6 shows that in cultures grown at 22°C there was similar net flux through the combined plastidic and cytosolic phosphoglucoisomerase and combined G6P dehydrogenase, meaning that similar proportions of the combined G6P pool enter glycolysis and the OxPPP. However, in cultures grown at 17°C, or 12°C a significantly larger proportion of the G6P pool flowed through phosphoglucoisomerase while a significantly smaller proportion was used by G6P dehydrogenase and entered the OxPPP.

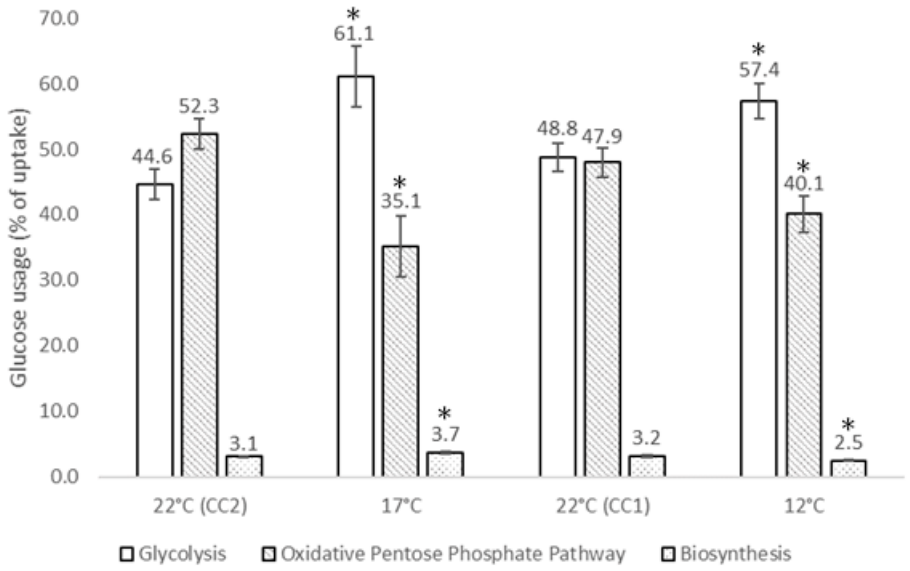


Figure 4.6: *Utilisation of the combined plastidic and cytosolic G6P pool in Arabidopsis cell suspension cultures grown under different temperatures. Flux through phosphoglucoisomerase (white), through G6P dehydrogenase (hatched) and flux to the biosynthetic pool (grey) are shown. Error bars represent 95% confidence intervals calculated by parameter continuation and asterisks (*) refer to statistically significantly differences between the decreased temperature cultures and the 22°C cultures calculated by confidence interval overlap.*

Previous MFA studies at low temperatures have shown different effects on OxPPP flux. Soybean cotyledons grown at 12°C showed an increased flux through the OxPPP and anaplerotic reactions while winemaking strains of *Saccharomyces cerevisiae* grown at mildly decreased temperatures also showed increased OxPPP flux (Iyer *et al*., 2008, Quirós *et al*., 2013). The precise reason for the difference in OxPPP response to temperature is unclear but it is important to note that both Iyer *et al*. (2008) and Quirós *et al*. (2013) investigated different species growing in different conditions. As mentioned previously Iyer *et al*. (2008) investigated soybean cotyledons, in which metabolism was likely carrying out a different biological function (accumulation of oils and proteins) compared to *Arabidopsis* suspension cultures (growth and cell division). Quirós *et al*. (2013) investigated an *S. cerevisiae* strain used for wine making, again, obviously a different species from *Arabidopsis* and the *S. cerevisiae* were grown on synthetic grape must (freshly crushed grape juice containing skin, stem and seeds), in bioreactors for fermentation, rather than

continuous growth. It is possible that the different species and growth conditions used by Iyer *et al*. (2008) and Quirós *et al*. (2013) were responsible for the different response to OxPPP from that seen in this study.

The reason for the change in G6P utilisation noted in this study could be that the enzymes which utilise G6P and partition it through the OxPPP (G6P dehydrogenase) or glycolysis (phoshpglucoisomerase) are differentially sensitive to decreased temperature. G6P dehydrogenase has been shown to be responsive to various stimuli (Jiang *et al*., 2022), but recent reports have shown that G6P dehydrogenases in strawberry (*Fragaria x ananassa*) and winter wheat (*Triticum aestivum*) are actually transcriptionally upregulated and show increased maximum capacity in response to temperatures of 4°C or lower (Zhang *et al*., 2020; Tian *et al*., 2021; Lei *et al*., 2022). Similarly, earlier studies showed the transcriptional upregulation of G6P dehydrogenase in rice (*Oryza sativa*), poplar (*Populus suaveolens)* and sugarcane (*Saccharum officinarum*) in response to temperatures of 4°C (Hou *et al*., 2007; Lin *et al*., 2013; Yang *et al*., 2014). Research into the role of temperature in regulating *Arabidopsis* G6P dehydrogenase is limited, but Landi *et al.* (2021) showed that different isoforms of G6P dehydrogenase in *Arabidopsis* respond differently to growth at 4°C. While the cytosolic isoform showed increased catalytic capacity under cold stress, a chloroplastic isoform showed a decrease in capacity. However, the G6P dehydrogenase isoform that showed decreased capacity only exhibited this response under short term cold stress (4°C for less than seven days) and was only expressed in photosynthetically active plastids, which are not present in a heterotrophic suspension culture.

These studies suggest that G6P dehydrogenase transcription is probably upregulated in *Arabidopsis.* However, an increase in transcription will not necessarily produce a change in enzyme activity *in vivo*, and even if G6P dehydrogenase activity is increased in response to decreased temperature it is unclear if this will compensate for the inherent effect of temperature on reaction rates as captured by the Arrhenius equation.

Despite its importance in the CCM, the regulation of phosphoglucoisomerase is not fully understood (Bahaji *et al*., 2015; Preiser *et al*., 2020). There is some evidence that the kinetic parameters of phosphoglucoisomerase isolated from rabbit muscle tissue are affected by temperature (Dyson and Noltmann, 1967), but this has not been confirmed in plants. Although there have been no reported investigations on the effects of temperature on plant phosphoglucoisomerase, studies in *Arabidopsis* and spinach (*Spinacia oleracea*) have shown that phosphoglucoisomerase is competitively inhibited by E4P and 6-phosphogluconate (6PG; Backenhausen *et al*., 1997, Preiser *et al*., 2020). Both E4P and 6PG are intermediates in the OxPPP, which could explain the negative correlation in flux between G6P dehydrogenase and phosphoglucoisomerase. Published information on the regulations of G6P dehydrogenase and phosphoglucoisomerase cannot explain the change G6P utilisation in response to decreased temperatures seen in this study. Nor can published transcriptomic and metabolomic analysis of cold grown *Arabidopsis* plants (Kaplan *et al.,* 2004) or previously published MFA studies. Further analysis of this effect is discussed in Chapter 6.

Considering the results in Figures 4.3-4.7, it can be concluded that growth of *Arabidopsis* suspension cultures at mildly reduced temperatures slows the growth rate and glucose uptake rate as well as altering the biomass composition of the cultures. Statistically significant changes were observed in the net fluxes for only a few reactions, some of which could be attributed to the change in biomass composition. A previously unreported effect of temperature on the utilisation of G6P is also seen, in which G6P is preferentially partitioned into glycolysis rather than the OxPPP.

4.5 Effect of acclimation on Arabidopsis cultures

A central goal of contemporary studies of plant response to cold is to understand cold acclimation; exposure to cold temperatures which then increases the ability of plants to withstand freezing temperatures. Studies of cold acclimation in whole *Arabidopsis* plants are myriad and have shown that acclimation induces unique changes in the transcriptome and the metabolome, as well as some changes in the fluxome (Guy *et al.,* 1992; Thomashow, 1999; Gilmore *et al.,* 2000; Hannah *et al.,* 2006; Kaplan *et al.,* 2007; Nägele *et al.,* 2011; Töpfer *et al.,* 2013; Kazemi-Shahandashti and Maali-Amiri, 2018, Herrmann *et al*., 2021). While there are fewer studies of cold acclimation in *Arabidopsis* cell suspension cultures, they have provided evidence that *Arabidopsis* suspensions can cold acclimate and that acclimation is associated with changes in sugar content, the transcriptome, the proteome and membrane dynamics (Sasaki *et al.,* 2008; Chiba *et al.,* 2008; Miniami *et al.,* 2009; Li *et al.,* 2012; Li *et al.,* 2020). With cold acclimation inducing changes at multiple levels of cellular physiology it is reasonable to expect that cold acclimation might also affect the fluxome. To examine the extent of such effects a line of *Arabidopsis* suspension cultures was grown for one month at 12°C, prior to labelling and MFA as described in chapters 2 and 3.

4.5.1 Growth profile of 12°C acclimated cultures

Growth profiles showed that acclimation did not significantly affect rate of biomass accumulation (Figure 4.7A), or glucose consumption (Figure 4.7B) compared to non-acclimated growth at 12°C. The acclimated cultures had a growth rate of 1.16 ± 0.01 mg $DW.ml^{-1}.d^{-1}$ and a glucose uptake rate of 1.51 ± 0.26 mM d^{-1} compared to 1.13 ± 0.01 mg $DW.ml^{-1}.d^{-1}$ and 1.56 ± 0.28 mM d^{-1} respectively, for the non-acclimated 12°C culture.

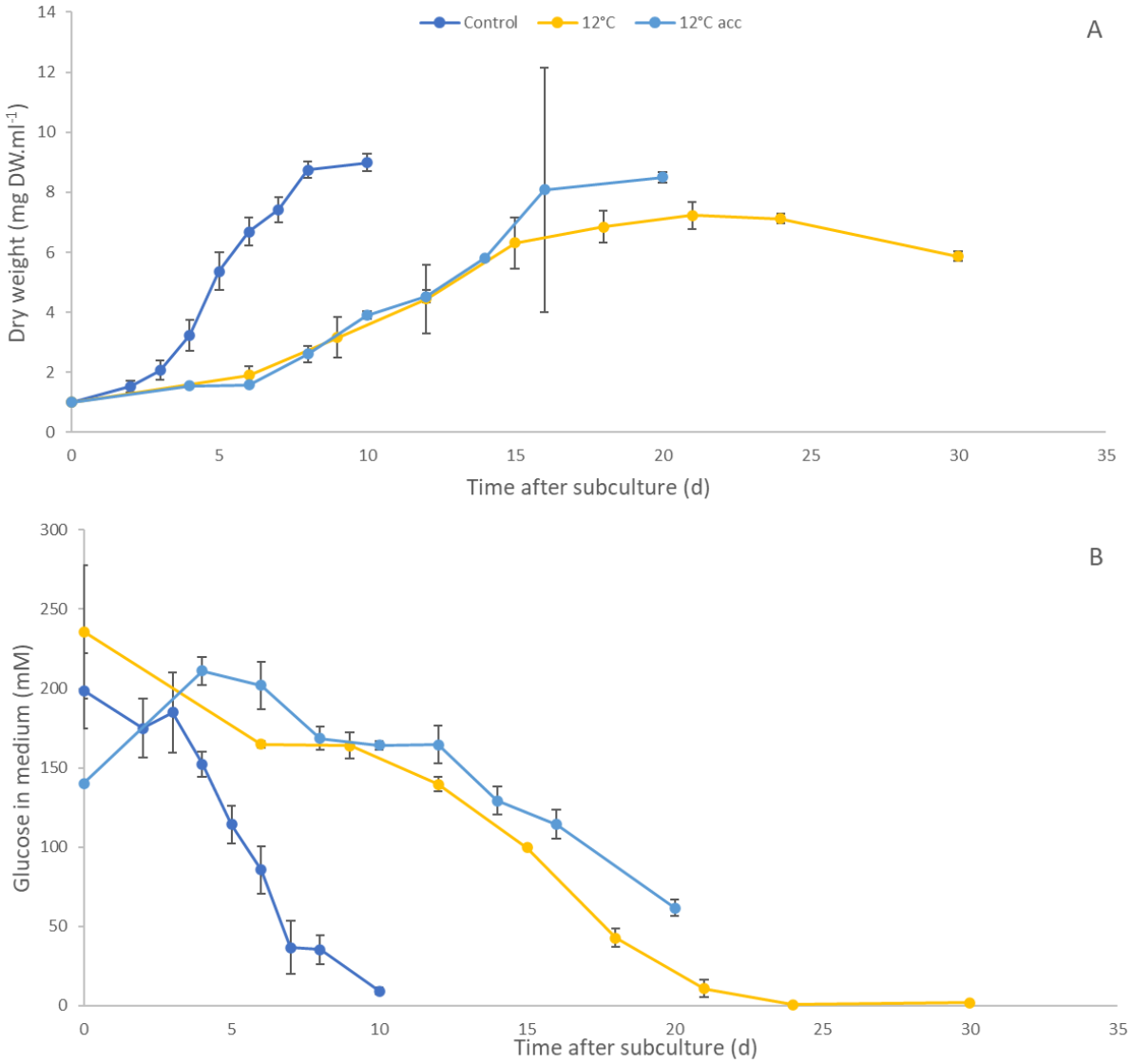


Figure 4.7: *Effect of cold acclimation on the growth profiles of Arabidopsis suspension cultures at 12°C (A) dry weight accumulation of cultures grown under different conditions. (B) Glucose consumption of cultures grown under different conditions. Control 1 cultures grown at 22°C are shown in dark blue, non-acclimated cultures grown at 12°C are shown in yellow and cultures acclimated to growth at 12°C are shown in light blue. Each point is a mean of three different flasks, error bars represent ± one SEM. 12°C acc = culture acclimated to growth at 12°C. In the labelling experiment biomass was harvested at mid exponential phase, this was after 5.5 d of growth for the control conditions cultures, after 12 d for the non-acclimated 12°C cultures and after 14 d of growth for the acclimated 12°C culture*

4.5.2 Biomass composition of acclimated cultures

Biomass composition analysis of cell cultures acclimated to growth at 12°C showed that the acclimated cell line had reduced lipid, protein and organic acid contents but significantly increased starch and cellulose content compared to the 22°C and the non-acclimated 12°C (Figure 4.8). This finding is consistent with previous research on cold acclimation in *Arabidopsis,* which noted an increased carbohydrate content (Cook *et al*., 2004; Kaplan *et al*., 2004; Sasaki *et al*., 2008; Nägele *et al.,* 2011; Herrmann *et al*., 2021).

However, the decreased protein and low sucrose content differ from a previous report of the effect of low temperatures (Kaplan *et al*., 2007), which showed significant increases in the transcript abundance and metabolite abundance of enzymes and intermediate in the biosynthetic pathways for 18 amino acids and sucrose. However, in Kaplan *et al.* (2007) whole *Arabidopsis* plants were grown at 4°C for four days. After two days the sucrose content began decreasing, likely as sucrose was converted to raffinose. The smaller sucrose content recorded for the acclimated 12°C cultures presented in Figure 4.8 could be a result of sucrose conversion to raffinose. Further, It is possible that growth at 12°C rather than 4°C is not cold enough to affect the accumulation of amino acids or sucrose, or that the accumulation of these metabolites happens in whole plants but not cell cultures. The biomass composition data presented here was used to constrain MFA by defining a biomass, shown in Appendix 6.

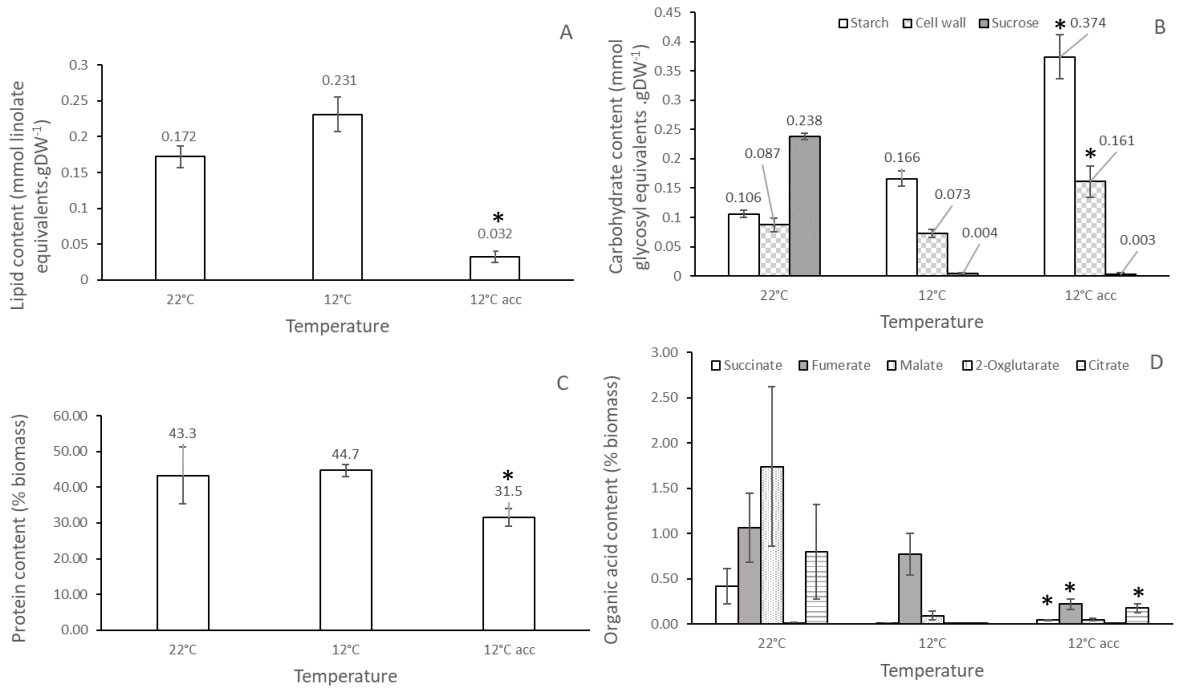


Figure 4.8: *Biomass composition of Arabidopsis cell suspension cultures grown at 22°C, 12°C or 12°C after acclimation . Panels show the content of: (A) lipids; (B) insoluble carbohydrates and sucrose; (C) protein content; and (D) content of various organic acids. Points are means of 3-15 independent repeats, error bars show SEM and asterisks (*) represent values that differed significantly from those in the non-acclimated 12°C culture.*

4.5.3 Metabolic effects of acclimation

The 12°C acclimated cell culture was used to produce a flux solution using the methodology described in Chapter 2 (Appendix 7; Table 4.3). The 12°C acclimated culture produced a statistically acceptable SSR of 573.7 (based on a 95% $\chi 2$ confidence interval of 450.3-575.5 for 1190 DOF). Flux maps are presented in Figure 4.9 The net fluxes through the CCM for the 22°C, non-acclimated 12°C and acclimated 12°C grown cultures from 1000 rounds of Monte Carlo were used for PCA. The PCA scores plot in Figure 4.10A showed non-overlapping confidence ellipses, indicating a significant difference in the flux distribution in the 12°C acclimated line compared to the 22°C and 12°C non-acclimated cultures. Analysis of the loading of reactions in PCA show that the reactions contributing most the difference were increased flux through the steps of glycolysis catalysing conversion of TP to PEP, the TCA cycle and anaplerotic reactions, and decreased in the

phosphopentose isomerase, transketolase and transaldolase reactions in the OxPPP and the conversion of PEP to pyruvate (Figure 4.9B).

Extraction of usable GC-MS data from 12°C acclimated cultures proved difficult. It was not possible to get MID vectors for methionine, threonine, fructose or five carbon cell wall sugars under any labelling strategy, as the total ion chromatogram peaks were too small to be identified or reliably measured. The consequence of the reduced constraint on the flux solution meant that many reactions were only poorly resolved and so the size of the 95% confidence intervals increased. This increased the likelihood of concluding a false negative (erroneously assuming there is no significant difference) from confidence interval overlap analysis. None the less, despite these limtations confidence interval overlap was able to identify significantly decreased net fluxes in the OxPPP, and significantly increased net fluxes in the later reactions of glycolysis, the TCA cycle and anaplerotic reactions in the acclimated culture (Table 4.3, Figure 4.9). This is consistent with conclusions based on the interpretation of the PCA.

Taken together the results of these analyses showed that acclimation to growth at 12°C over a period of one month induced a significant change in flux distribution which was not seen in non-acclimated cultures grown at 12°C. This is likely a part of the cold acclimation process which also induces considerable changes in metabolomic, transcriptomic and proteomic organisation in plants. Understanding the specific changes in net fluxes will require careful examination.

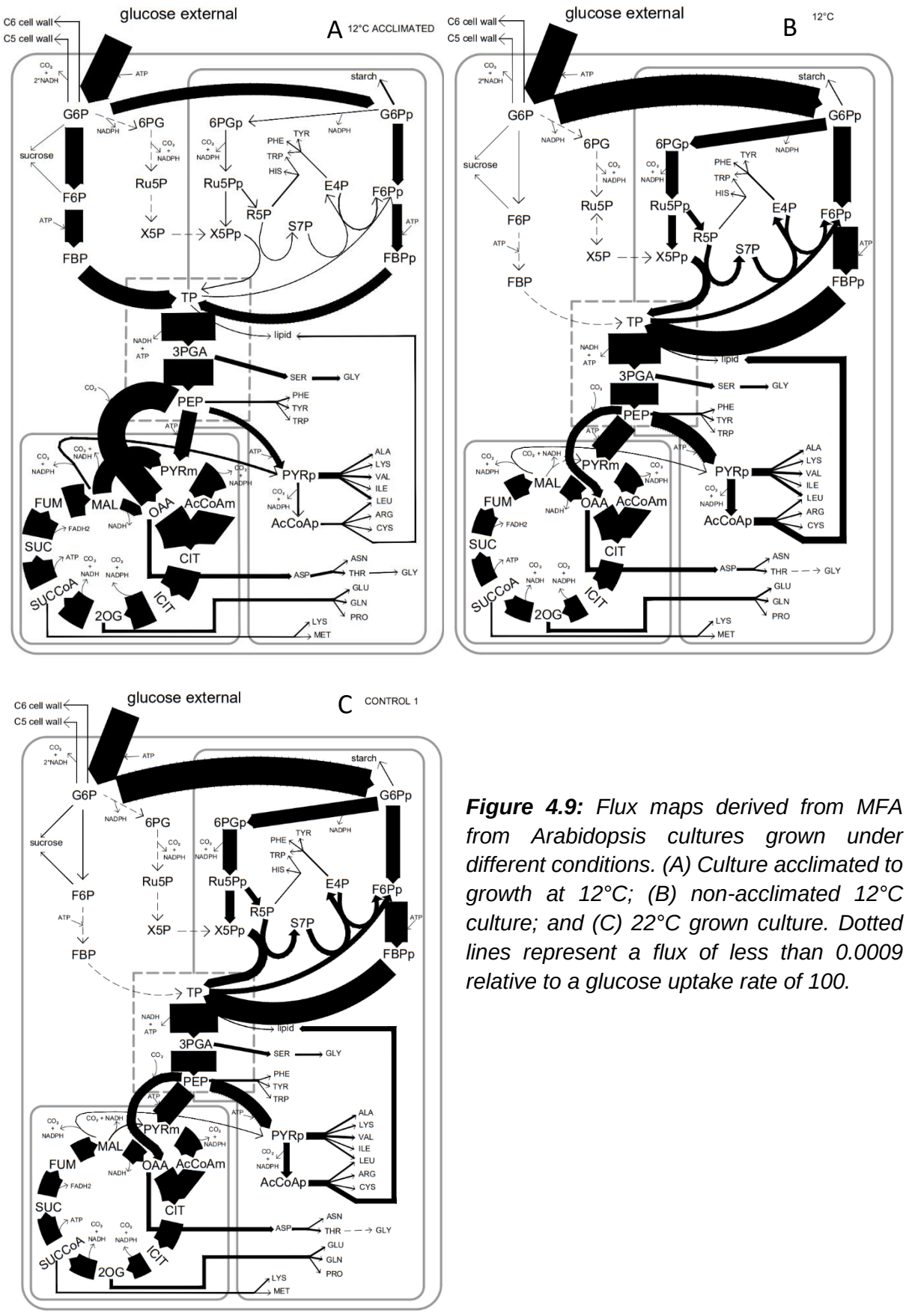


Figure 4.9: *Flux maps derived from MFA from Arabidopsis cultures grown under different conditions. (A) Culture acclimated to growth at 12°C; (B) non-acclimated 12°C culture; and (C) 22°C grown culture. Dotted lines represent a flux of less than 0.0009 relative to a glucose uptake rate of 100.*

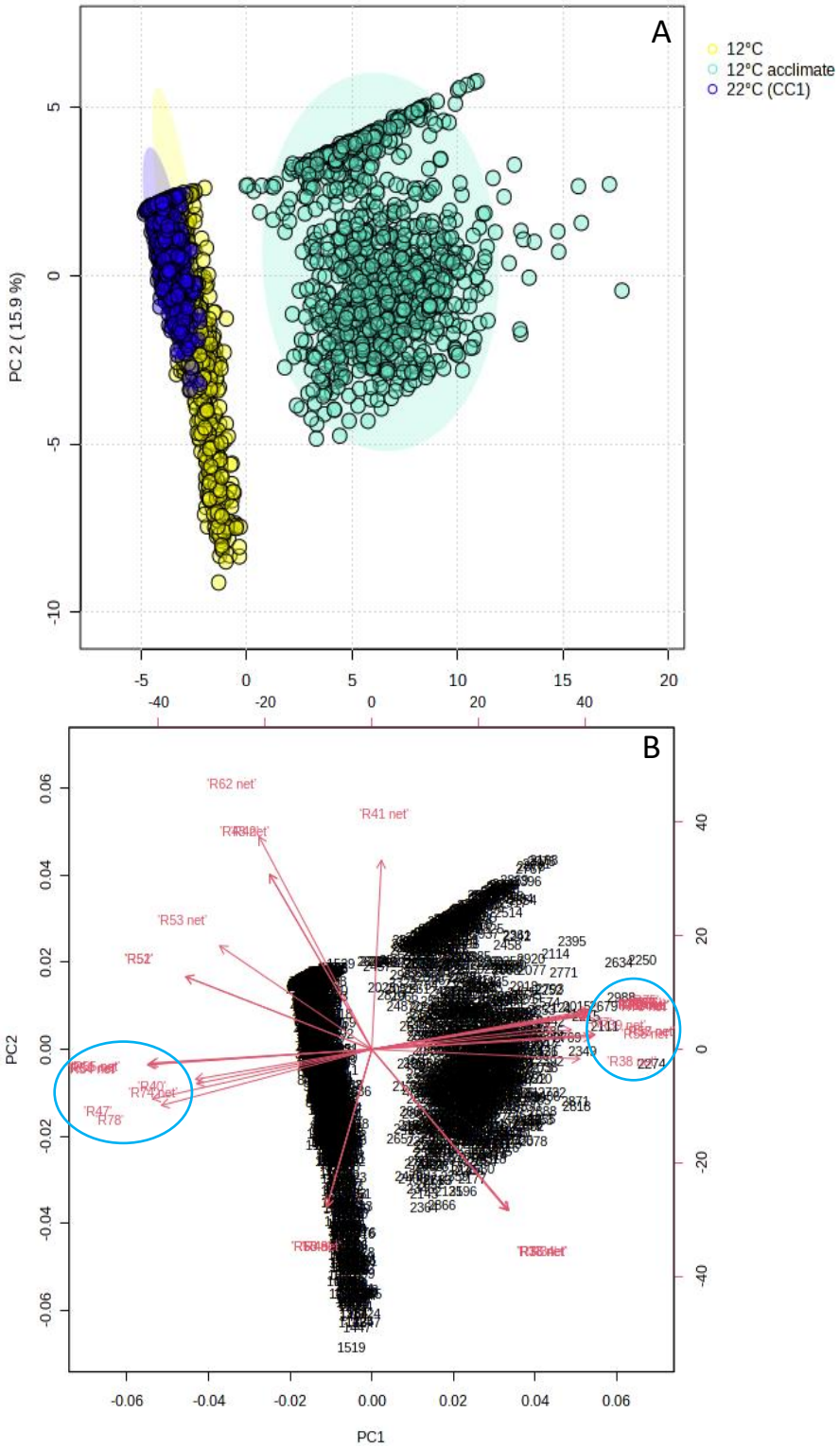


Figure 4.10: *Principal component analysis of the net fluxes of reactions in the CCM in cultures grown at different temperatures. (A) Scores plots of flux solutions for a control culture grown at 22°C (blue), a non-acclimated culture grown at 12°C (yellow) and a culture acclimated to growth at 12°C (turquoise). (B) Biplot of PCA with loadings indicated in red. The blue rings highlight the fluxes which exerted the greatest influence on the separation of the two clusters of flux solutions along the axis of maximum separation. Synthetic datasets were derived from 1000 rounds of Monte Carlo simulation for each of the four flux solutions.*

Table 4.3: *Comparison of flux solutions from Arabidopsis cultures grown in non-acclimated 12°C and acclimated 12°C cultures*

Reaction	Relative flux under specific condition	
	12°C	12°C acclimated
GLCext + ATPi −> G6P	100.0 (n/a, n/a)	100.0 (n/a, n/a)
G6P <−> F6P	0.0 (0.0, 66.9)	59.5 (0.0, 83.1)
F6P + ATP −> FBP	0.0 (0.0, 66.9)	59.5 (0.0, 83.1)
FBP <−> TP + TP	0.0 (0.0, 66.9)	59.5 (0.0, 83.1)
G6P <−> G6Pp	99.2 (31.9, 99.2)	38.5 (10.5, 98.9)
G6Pp <−> F6Pp	57.4 (−9.7, 60.1)	33.4 (6.2, 96.2)
F6Pp + ATPi −> FBPp	81.9 (15.0, 82.8)	31.9 (8.4, 95.6)
FBPp <−> TP + TP	81.9 (15.0, 82.8)	31.9 (8.4, 95.6)
G6P −> 6PG + NADPH	0.0 (0.0, 14.7)	0.0 (0.0, 13.6)
6PG −> RU5P + CO_2 + NADPH	0.0 (0.0, 14.7)	0.0 (0.0, 13.6)
RU5P <−> X5P	0.0 (0.0, 22.0)	0.0 (0.0, 13.6)
G6Pp −> 6PGp + NADPH	40.1 (24.1, 42.8)	0.5 (0.0, 13.9)
6PGp −> RU5Pp + CO_2 + NADPH	40.1 (24.1, 42.8)	0.5 (0.0, 13.9)
RU5Pp <−> X5Pp	24.5 (9.0, 26.4)	−1.5 (−6.4, 7.5)
RU5Pp <−> R5Pp	**15.5 (14.7, 16.4)**	**2.0 (0.9, 6.4)**
X5P <−> X5Pp	0.0 (0.0, 14.7)	0.0 (0.0, 13.6)
X5Pp <−> TP + EC2	**24.5 (22.7, 26.4)**	**−1.5 (−2.4, 7.3)**
F6Pp <−> E4Pp + EC2	**−10.4 (−11.4, −9.5)**	**2.3 (−2.4, 7.3)**
S7Pp <−> R5Pp + EC2	**−14.1 (−15.0, −13.3)**	**−0.8 (−5.2, −0.3)**
F6Pp <−> TP + EC3	**−14.1 (−15.0, −13.3)**	**−0.8 (−5.2, −0.3)**
S7Pp <−> E4Pp + EC3	**14.1 (13.2, 15.0)**	**0.8 (0.3, 5.2)**
TP <−> 3PGA + NADHi + ATP	172.7 (171.8, 173.8)	180.7 (172.8, 190.1)
3PGA <−> PEP	158.9 (153.8, 161.5)	166.5 (152.9, 184.0)
PEP −> PYRm + ATP	76.8 (71.9, 82.3)	50.6 (11.7, 86.1)
PEP −> PYRp + ATP	**49.0 (45.6, 51.7)**	**18.6 (8.8, 86.1)**
PYRm −> ACoAm + CO_2 + NADH	**76.8 (71.8, 82.3)**	**112.2 (81.6, 154.5)**
PYRp −> ACoAp + CO_2 + NADH	**25.6 (23.9, 26.8)**	**5.3 (0.0, 9.3)**
OAA + ACoAm −> CIT	**76.8 (71.8, 82.3)**	**112.2 (81.6, 154.5)**
CIT <−> ICIT	**76.8 (71.8, 82.3)**	**112.1 (81.4, 154.5)**
ICIT <−> 2OG + CO_2 + NADPH	**76.8 (71.8, 82.3)**	**112.1 (81.4, 154.5)**
2OG −> SUCCoA + CO_2 + NADH	**65.9 (60.6, 72.0)**	**103.0 (69.5, 149.7)**
SUCCoA <−> SUC + ATP	61.7 (56.3, 68.0)	99.5 (64.9, 147.9)
SUC <−> FUM + $FADH_2$	**65.9 (60.6, 72.0)**	**102.9 (69.4, 149.7)**
FUM <−> MAL	**69.4 (64.3, 75.3)**	**105.9 (73.3, 151.2)**
MAL <−> OAA + NADH	**69.0 (64.2, 74.5)**	**37.7 (−2.8, 64.2)**
PEP + CO_2 −> OAA	**25.9 (24.5, 27.7)**	**91.2 (56.5, 136.2)**
MAL −> PYRm + CO_2 + NADH	**0.0 (0.0, 2.0)**	**61.6 (27.1, 112.4)**
MAL −> PYRp + CO_2 + NADPH	0.3 (0.0, 1.5)	6.5 (0.4, 14.7)

The values in grey brackets are the 95% confidence limits calculated by parameter continuation. Fluxes which are significantly different between the two conditions are shown in bold.

A potential example of confidence interval overlap suggesting a false negative is the estimated CCE for the 12°C acclimated culture (Figure 4.11). Confidence interval overlap analysis registered no significant difference between the CCE of the acclimated and non-acclimated cultures despite it being 8.7% lower in the acclimated culture. This is a consequence of the poor definition of the CO_2 output flux. If this is a false negative and the CCE of the acclimated culture is significantly lower than the non-acclimated culture, this would likely be due to increased flux through several reactions that produce CO_2 Including UDP-glucuronate decarboxylase, pyruvate decarboxylase, isocitrate dehydrogenase, 2OG dehydrogenase, and malic enzyme (Table 4.3).

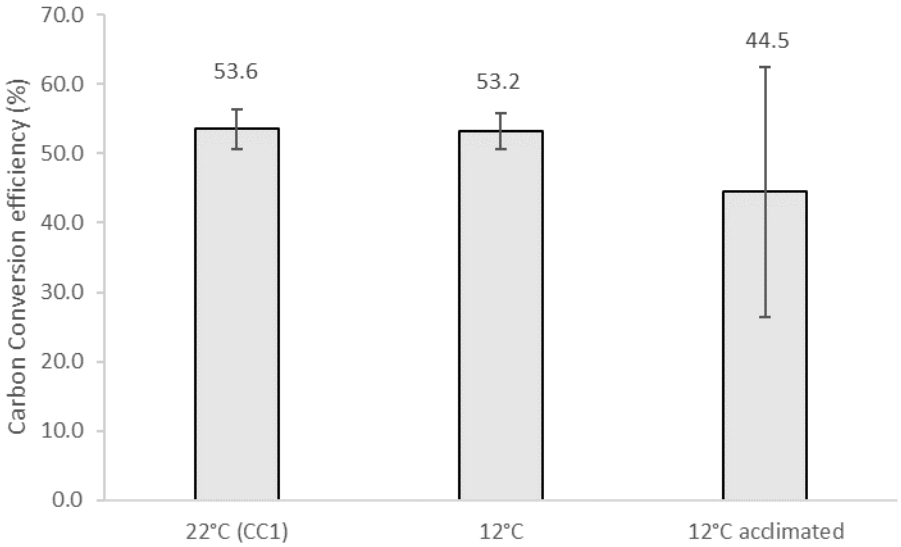


Figure 4.11: *Carbon conversion efficiency of Arabidopsis cell culture grown in MS medium at 22°C, 12°C or acclimated for 12°C. Error bars represent 95% confidence interval calculated by parameter continuation.*

The duplicated plastidic and cytosolic reactions in the first steps of the OxPPP and glycolysis (Table 4.3) were also susceptible to false negatives. Here the problem was exacerbated by difficulty in resolving compartmentation. To circumvent this problem and to investigate the effects of acclimation on G6P utilisation the virtual metabolite method described in Section 3.4.2 was applied to estimate the overall flux through these reactions across both cytosol and plastids (Figure 4.12).

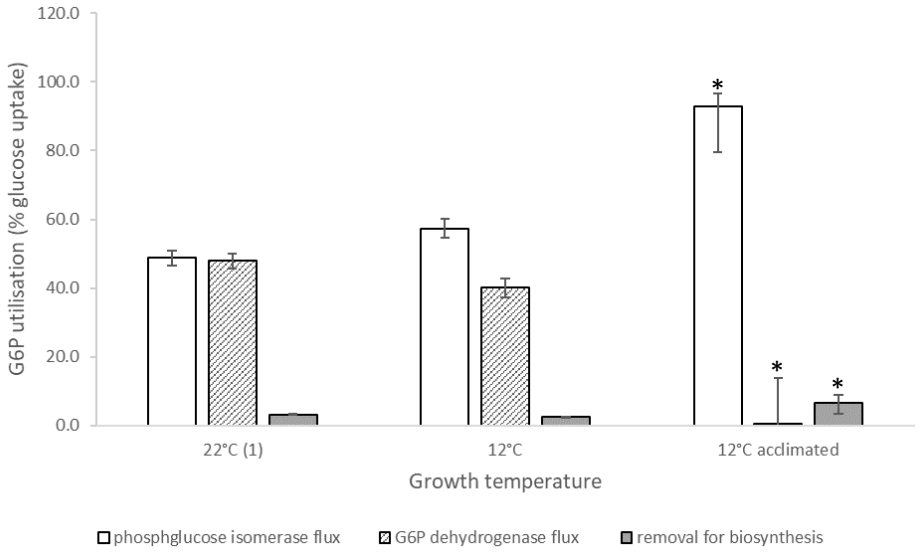


Figure 4.12: *Utilisation of the combined plastidic and cytosolic G6P pool in Arabidopsis cell suspension cultures grown under different conditions. Flux through phosphoglucoisomerase (white), through G6P dehydrogenase (hatched) and flux to the biosynthetic pool (grey) are shown. Error bars represent 95% confidence intervals calculated by parameter continuation and asterisks refer to statistically significantly different net fluxes between the 12°C acclimated and non-acclimated cultures as calculated by confidence interval overlap.*

The flux of G6P removed for biosynthesis of starch, cell wall components and sucrose was significantly higher in the 12°C acclimated cultures compared to the non-acclimated 12°C grown culture and the 22°C grown culture. This was clearly a result of the increased starch and cell wall carbohydrate content of the acclimated culture (Figure 4.8). The trend of an increased net flux through the combined plastidic and cytosolic phosphoglucoisomerase and decreased net flux through the combined G6P dehydrogenase is significantly more pronounced in the 12°C acclimated culture compared to the non-acclimated 12°C grown culture. The reasons for this effect are unclear. From the data presented here it might appear that the OxPPP:glycolysis ratio is correlated with the insoluble carbohydrate content. However, the 17°C grown culture did not have an increased carbohydrate content relative to the 22°C culture, but still had altered OxPPP:glycolysis ratio.

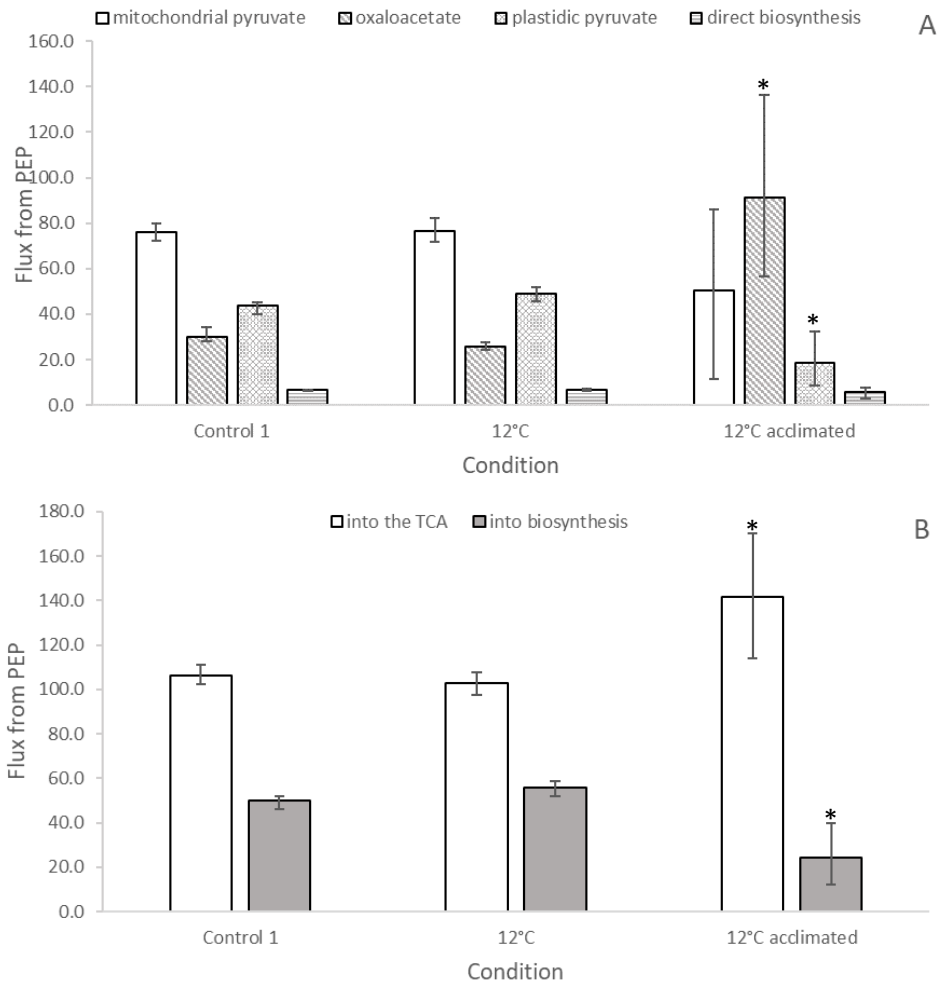


Figure 4.13: *Utilisation of PEP in Arabidopsis suspension cultures grown at 22°C, at 12°C without acclimation and at 12°C with one month of acclimation. (A) Partitioning of PEP into mitochondrial pyruvate, OAA, plastidic pyruvate, or into the PEP.B pool in Arabidopsis suspension cultures grown under each condition. (B) Partitioning of PEP into the TCA cycle (combined net flux from PEP to mitochondrial pyruvate and OAA) and into biosynthesis (combined net flux into plastidic pyruvate and the PEP.B pool). Error bars represent 95% confidence intervals calculated by parameter continuation and asterisks refer to statistically significantly different net fluxes between the 12°C acclimated and non-acclimated cultures as calculated by appropriate confidence interval overlap.*

Another difference between the acclimated and non-acclimated cell cultures was the partitioning of PEP into mitochondrial and plastidic pyruvate, OAA or direct removal for biosynthesis (Figure 4.13A). PEP that is converted to mitochondrial pyruvate or OAA ultimately enters the TCA cycle, while PEP can be partitioned to biosynthesis directly, or via plastidic pyruvate. The virtual metabolite method was used to calculate combined fluxes from PEP into the TCA cycle or into biosynthesis (Figure 4.13B).

Figure 4.13 shows that PEP partitioning into the TCA cycle was significantly increased by acclimation to 12°C, while partitioning to biosynthesis was significantly decreased. These changes are due to the significantly increased flux through PEP carboxylase and cytosolic pyruvate kinase and correlate with the decreased protein content in the acclimated cells, and thus reduced demand for PEP and pyruvate as precursors for amino acid synthesis. It is possible that the changes in PEP carboxylase and pyruvate kinase flux are due to the altered biomass composition, but it is equally possible that the increased TCA cycle flux is a response to increased demand for reductants as cold stress is associated with oxidative stress (Khavari-Nejad *et al*., 2013; Kazemi-Shahandashti and Maali-Amiri, 2018; Landi *et al*., 2021).

From the data presented here it is clear that acclimation of *Arabidopsis* cell suspension cultures to growth at 12°C did not affect the rate of biomass accumulation or glucose uptake, but did cause a significant change in the biomass composition and in the flux distribution in the CCM. Specifically, cold acclimation significantly increased the content of insoluble carbohydrates and stimulated increased flux through glycolysis, the TCA cycle and anaplerotic reactions, and decreased flux through the OxPPP. The altered biomass composition has been recorded previously in response to cold acclimation. The increased flux through the TCA cycle and anaplerotic reactions may be a result of the reduced demand for lipids and amino acids, or the result of increased requirements for ATP or reducing power to maintain homeostasis in cold induced oxidative stress. The altered OxPPP:glycolysis ratio is an augmentation of the results seen in non-acclimated cultures grown at 17°C and 12°C, the mechanism or consequences of which are unclear.

4.6 Conclusions

This chapter has presented an investigation into the effect of mildly reduced temperatures on flux through the CCM of *Arabidopsis* suspension cultures. The metabolic effects of acclimation to growth at 12°C were also investigated. From the analyses presented in this chapter it can be concluded that:

1. Growth at mildly reduced temperature caused a change in growth rate and biomass composition in *Arabidopsis* suspension cultures with relatively little effect on the flux distribution.

2. Of the few CCM net fluxes that were affected by growth at mildly reduced temperatures, some are likely consequences of the altered biomass composition.

3. Growth at reduced temperatures caused a significant change in the OxPPP:glycolysis ratio, an effect which requires further research.

4. Acclimation to growth at 12°C did not affect the growth rate, but did affect the biomass composition and induces a significant global change in flux distribution in the CCM.

5. Acclimation to 12°C decreased the OxPPP:glycolysis ratio further, as well as increasing flux through the TCA cycle and anaplerotic reactions which may be related to the biomass composition and/or demand for metabolic resources from maintenance metabolism.

Chapter 5: Mannose supplementation affects growth and flux distribution in *Arabidopsis* suspension culture independently of osmotic effects

5.1 Introduction

Mannose is a hexose sugar and the C2 epimer of glucose. It exists primarily as the pyranose (six-membered ring) form, with 67% of naturally occurring mannose in the α-anomer and 33% as the β- anomer (Figure 5.1; Steinhardt *et al*., 1962; Stewart *et al*., 1971). Mannose is present in most organisms as part of glycoproteins, glycolipids and as storage and structural mannan polymers (Herold and Lewis, 1977). In humans mannose is used to treat congenital disorders of glycosylation and prevent urinary tract infections (Sharma *et al*., 2014).

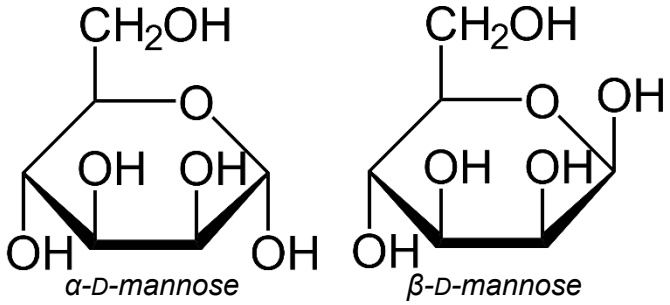


Figure 5.1: *Hawthorn projections of α-D-mannose and β-D-mannose.*

In plants, free mannose only exists during the break down of storage mannans (Herold and Lewis, 1977), and free mannose is metabolised quickly to sucrose, starch or other products (Reid, 1971; McCleary and Matheson, 1976). In plants supplemented with exogenous mannose, the carbohydrate affects stem and root growth as well as oxygen, nitrogen and chloride uptake (Stenlid, 1954, 1959, 1971; Herold and Lewis, 1977).

The identification of mannose as a growth inhibitor makes it a treatment that could potentially be used to slow the growth rate and thus allow investigation of the relationship between growth and the flux distribution in the CCM. Growth studies were used to identify an appropriate concentration of mannose to slow the growth rate of *Arabidopsis* cultures before ^{13}C MFA was used to determine the effect of mannose on the CCM flux distribution.

5.2 Effect of mannose on Arabidopsis cell suspension culture growth

Previous studies of plant responses to mannose have used a wide range of concentrations (Herold and Lewis, 1977). To find a mannose concentration which could mildly affect the growth rate, *Arabidopsis* suspension cultures were grown in MS medium containing up to 40 mM mannose and cultured for 10 d (Figure 5.2A). The cultures supplemented with 5 mM, 10 mM or 20 mM mannose did not show a significant difference in dry weight accumulation relative to the unsupplemented culture, but the culture supplemented with 40 mM mannose showed a significantly lower growth rate (linear regression over natural logarithm followed by ANVOVA and Student's t-test, $P<0.01$), and a lower rate of glucose uptake (Student's t-test; $P<0.05$; Figure 5.2B). The unsupplemented culture had a growth rate of 1.49 ± 0.07 mg $DW.ml^{-1}.d^{-1}$ (mean ± SEM) and a glucose uptake rate of 37.57 ± 0.28 $mM.d^{-1}$ while the 40 mM mannose culture had a growth rate of 1.26 ± 0.01 mg $DW.ml^{-1}.d^{-1}$ and a glucose uptake rate of 1.24 ± 1.87 $mM.d^{-1}$.

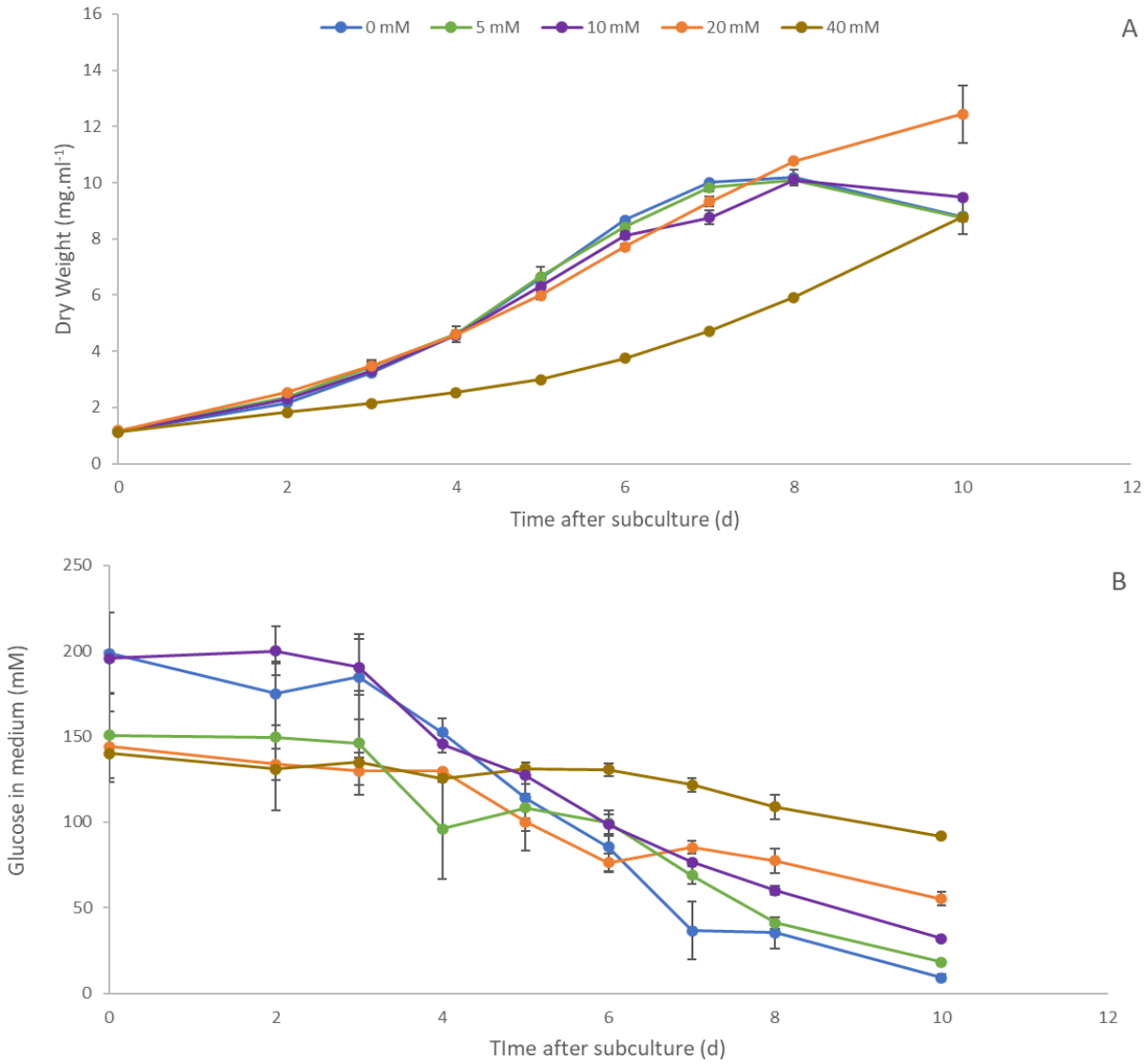


Figure 5.2: *Growth profiles of Arabidopsis suspension cultures grown in media containing different concentrations of mannose. (A) Dry weight accumulation and (B) glucose remaining in medium for Arabidopsis cultures. Each point is the mean of three independent flasks and error bars represent the SEM.*

There are several possible explanations for the effect of free mannose on the growth rate. There is evidence for mannose distorting the growth of various plants and tissues by sequestering inorganic phosphate and thus limiting ATP availability, and also that mannose competitively inhibits phosphoglucoisomerase thus blocking glycolysis (Sols *et al*., 1960; Goldsworthy and Street, 1965; Herold and Lewis, 1977).

It is also possible that the slowed growth rate and rate of glucose uptake in the 40 mM mannose supplemented medium is due to the osmotic effect of having a more concentrated medium. To investigate this further *Arabidopsis* cultures were grown in MS medium containing 40 mM mannitol. Mannitol is a polyol that is commonly used in studies of osmotic stress (Figure 5.3). After five days of growth the mannitol supplemented cultures showed no significant difference in dry weight (Student's t-test, *P>0.05*) from the unsupplemented cultures, while mannose supplemented cultures had a significantly lower dry weight (Figure 5.4). This suggests that the decreased growth rate seen in the 40 mM mannose cultures was not due to increased osmotic pressure.

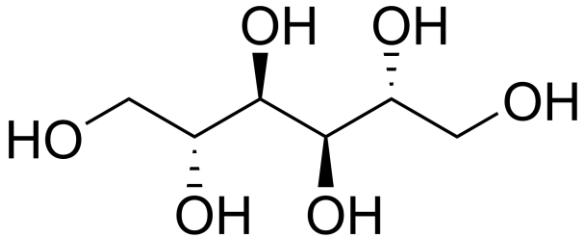


Figure 5.3: *Chemical structure of mannitol.*

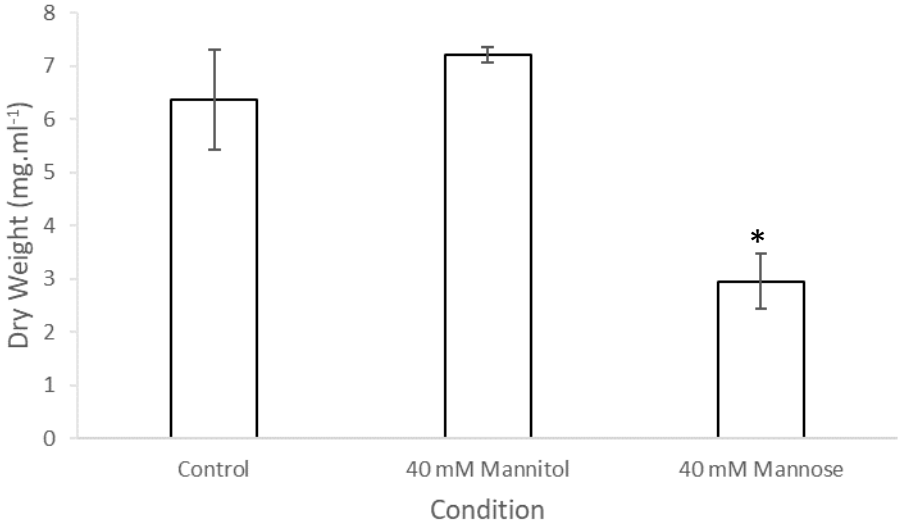


Figure 5.4: *Effect of supplementation of the growth medium by 40 mM mannose and 40 mM mannitol on biomass accumulation in Arabidopsis cell suspension cultures after 5 d of growth at 22°C. Each point is the mean of four independent flasks and the error bars represent SEM. An asterisk (*) represents a statistically significant difference from the control (unsupplemented) culture according to Student's t-test.*

5.3 Effect of mannose and mannitol supplementation on biomass composition

Biomass composition was measured for *Arabidopsis* cultures grown in MS medium and medium supplemented with 40 mM mannose or 40 mM mannitol as per section 3.4 (Figure 5.5). The presence of 40 mM mannitol in the culture medium did not significantly affect the protein or lipid content of the cultures, but did decrease the cell wall, sucrose and fumarate content and increase the starch content relative to the unsupplemented culture. These results are similar to those in a study of *Arabidopsis* leaves exposed to 25 mM mannitol, which showed an increase in starch content quantified by Lugol's staining, transcriptomic and metabolomic data, as well as transcriptomic and metabolomic evidence for alterations in cell wall metabolism (Skirycz *et al*., 2009). Usually starch content decreases in response to abiotic stress, but studies of osmotic stress have shown starch accumulation in *Arabidopsis* leaves in response to 25 mM mannitol (Skirycz *et al*., 2009), 150 mM mannitol (Zanella *et al.,* 2016), 200 mM mannitol (Monroe *et al*., 2014), as well as in *Arabidopsis* seedlings exposed to 200 mM mannitol (Liu *et al*., 2019). Only mannitol concentrations higher than 300 mM produce a decrease in starch accumulation in *Arabidopsis* leaves (Valerio *et al*., 2011) and whole plants (Thalmann *et al*., 2016). No explanation for this pattern of starch content is presented in the literature but these dynamics highlight the plasticity of starch and suggest that it should not be seen as merely a storage compound (see Thalmann and Santelia, 2017 for further review). It is possible that the altered cell wall carbohydrate content is a part of cell wall loosening to facilitate growth at low turgor pressure (Wu and Cosgrove, 2000; Sharp *et al*., 2004; Zhu *et al*., 2007; Moore *et al*., 2008; Skirycz *et al*., 2009).

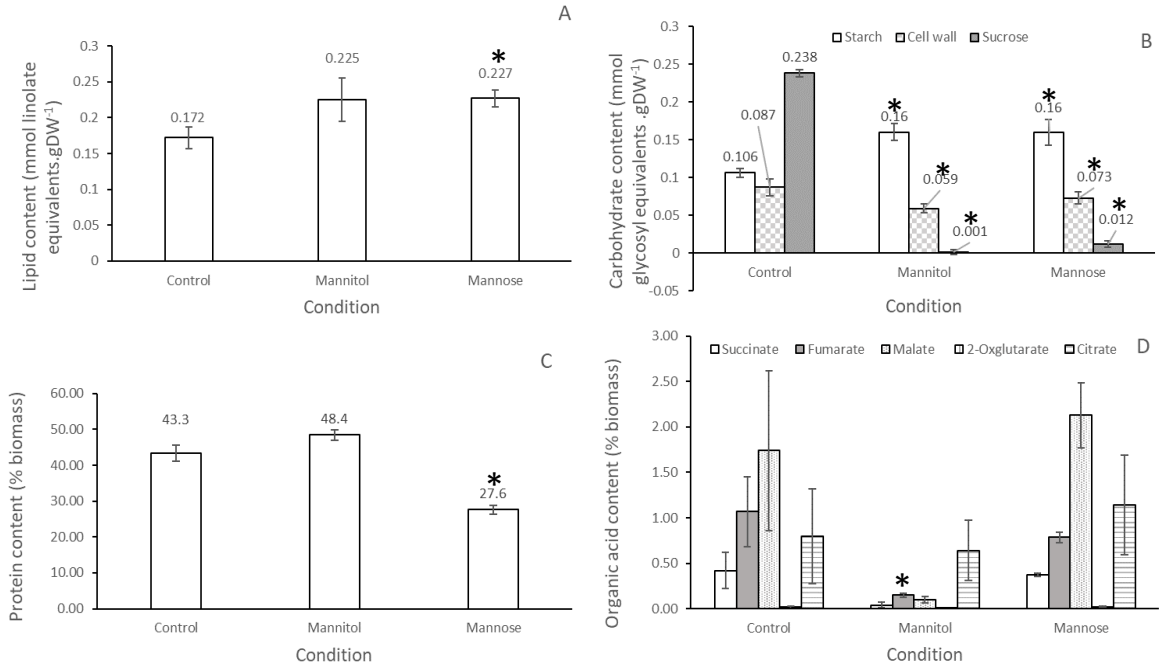


Figure 5.5: *Biomass composition of Arabidopsis cell suspension cultures grown in MS medium and MS media supplemented with either 40 mM mannitol or 40 mM mannose. Panels show the content of: (A) lipids; (B) insoluble carbohydrates and sucrose; (C) protein; and (D) various organic acids. Points are the means of 3-15 independent repeats error bars show SEM and asterisks (*) represent values that differed significantly from those in the unsupplemented culture.*

The cultures supplemented with 40 mM mannose showed the same increase in starch content and decrease in cell wall and sucrose content as the cultures supplemented with 40 mM mannitol. Although, they also displayed a significantly increased lipid content and decreased protein content. Decreased protein content has been noted in previous studies: Pathirana *et al*. (2016) found a decreased soluble protein content in *Arabidopsis* cell suspension cultures supplemented with 100 mM mannose and Stenlid *et al*. (1959) noted a decreased nitrate uptake when Garden Cress (*Lepidium sativum*) was grown on mannose, which could be related to decreased protein content.

The consistent changes in starch, cell wall and sucrose composition could be due to osmotic pressure caused by mannose supplementation. However, the significant change in lipid and protein content suggests that supplementation with mannose does have an additional effect on the biomass composition beyond that of mannitol.

It is interesting that the sucrose content decreased when 40 mM mannose or mannitol was added to the growth medium. There is extensive literature from other plant systems and Arabidopsis calli that would suggest that an increased osmotic pressure would increase sucrose accumulation in the cells (Morgan, 1984; Quick *et al*., 1989; Cocucci *et al*., 1993; Wang *et al*., 2000; Zhao *et al*., 2009; Krasavina *et al*., 2014). However, none of these studies used Arabidopsis suspension culture. When the same line of suspension cultures as used in this study were exposed to 171 mM mannitol a significant decrease in soluble metabolites was noted (Williams *et al*., 2008). It is possible that even the control cultures in this study and in Williams et al. (2008) experienced considerable external osmotic pressure due to the concentrations of the components in MS medium, and that sucrose accumulated in the cells to counteract this osmotic pressure. But, when mannitol or mannose are added they are absorbed but not rapidly metabolised (Thompson *et al*., 1986) and so mannitol and mannose counteract the osmotic pressure and sucrose does not need to accumulate.

5.4 Effects of mannose and mannitol on the CCM flux distribution

^{13}C MFA was applied to *Arabidopsis* cultures grown in MS medium or MS medium supplemented with 40 mM mannitol or 40 mM mannose (the culture grown in unsupplemented media was the Control 1 culture in Chapter 3). The culture grown in the presence of 40 mM mannitol served as an osmotic control: any changes in the flux distribution between the control and mannitol containing cultures would be due to the osmotic effect of the mannitol and any further changes in the mannose-supplemented culture would be due to the specific effects of mannose. The model was not extended to include mannose or mannitol metabolism because, mannitol is not metabolised by *Arabidopsis* and 40 mM mannose is unlikely to represent a significant respiratory substrate (Todd and Tague, 2001). Further, the dilution of the input labelled sugar with unlabelled substrate did not indicate a substantial change in the supply of respiratory substrate (Appendix 7).

5.4.1 Flux distribution under mild osmotic stress

As well as acting as an osmotic control the mannitol flux solution could give an insight into the effect of mild osmotic stress on *Arabidopsis* metabolism. Skirycz *et al*. (2009) conducted transcriptomic and metabolomic studies on *Arabidopsis* leaves exposed to 25 mM mannitol, and suggested that a metabolic alteration in response to mild osmotic stress was likely. However, Williams *et al*. (2010) conducted ^{13}C MFA on *Arabidopsis* suspension cultures exposed to 171 mM mannitol and concluded that a severe osmotic stress had no significant effect on the relative flux distribution. A flux map for cultures grown in the presence of 40 mM mannitol is presented in Figure 5.6 and a summary of the net fluxes through the reactions of the CCM is presented in Table 5.1. The full flux solution can be found in Appendix 7. This flux solution had a statistically acceptable SSR of 1154.3 with 1141 DOF and a critical SSR range of 1049.3-1236.5.

Interestingly, in the flux solutions calculated here, there were some significantly different fluxes between the unsupplemented and 40 mM mannitol cultures. The PCA scores plot for the net fluxes through the CCM shows clear separation of the 95% confidence ellipses for the two conditions (Figure 5.7A). The PCA biplots show that this separation was due to differences in fluxes in transketolase, transaldolase and phosphopentose isomerase in the OxPPP (R54-R59 in Appendix 7) as well as the fluxes converting TP into mitochondrial and plastidic pyruvate (R38-40), and the TCA cycle fluxes (R66-74; Figure 5.7B).

Analysis of the flux maps (Figure 5.6) using confidence interval overlap (Table 5.1) showed that supplementation with 40 mM mannitol caused an increase in flux from TP to PEP, increased partitioning of pyruvate into the plastid and a lower flux through the TCA cycle. Although, only the 2OG dehydrogenase, succinyl-CoA synthase, fumarate dehydrogenase and citrate synthase reactions in the TCA cycle registered as significantly decreased. Mannitol supplementation also caused a decreased flux through the OxPPP, as suggested by the biplot in Figure 5.7, but only the flux though one transketolase half reaction was significantly different.

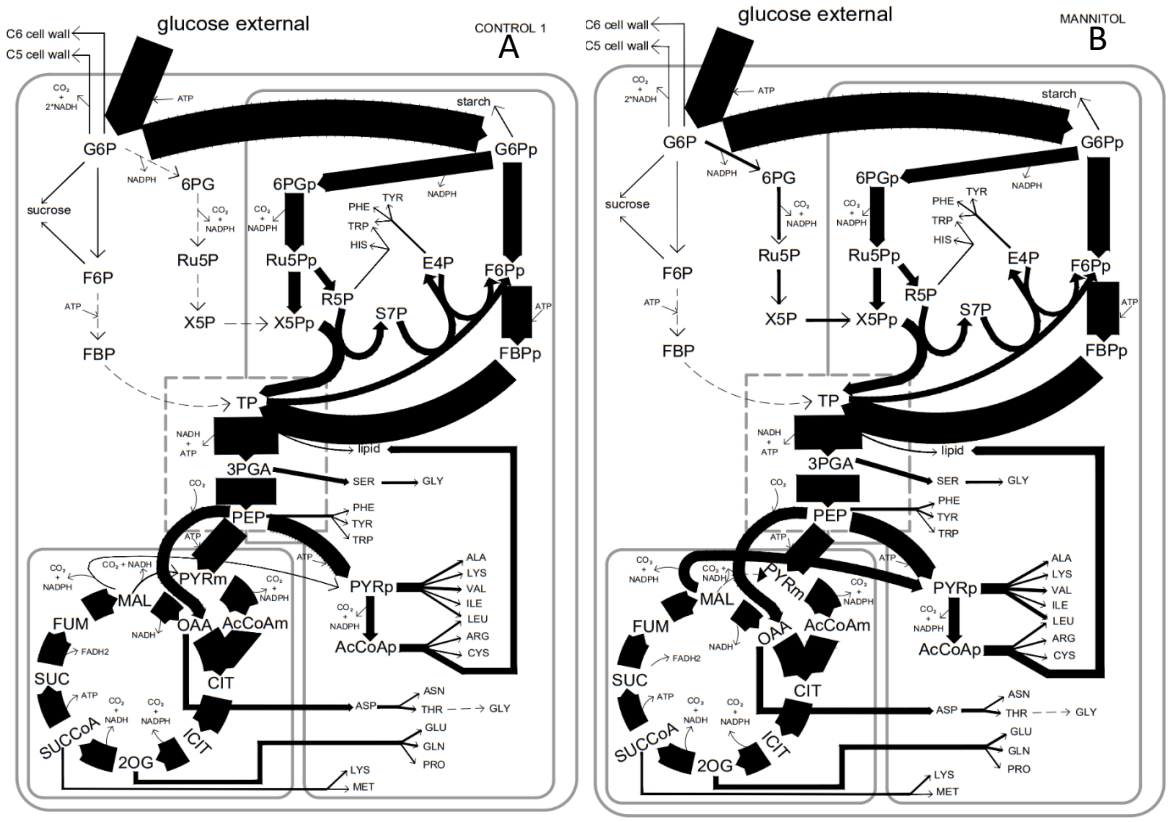


Figure 5.6: *Flux maps derived from MFA for Arabidopsis cultures grown in different media. (A) culture grown in standard MS medium; (B) parallel-grown culture grown in MS medium supplemented with 40 mM mannitol. Dotted lines represent a flux of less than 0.0009 relative to a glucose uptake rate of 100.*

Table 5.1: *Comparison of the net CCM fluxes in flux solutions from Arabidopsis suspension cultures grown in unsupplemented MS medium or medium supplemented with 40 mM mannitol*

Reaction	Relative flux in specific culture	
	Unsupplemented (Control 1)	Mannitol supplemented
GLCext + ATPi −> G6P	100.0 (n/a, n/a)	100.0 (n/a, n/a)
G6P <−> F6P	1.2 (1.2, 13.4)	0.0 (0.0, 16.7)
F6P + ATP −> FBP	0.0 (0.0, 12.2)	0.0 (0.0, 16.7)
FBP <−> TP + TP	0.0 (0.0, 12.2)	0.0 (0.0, 16.7)
G6P <−> G6Pp	96.6 (84.5, 96.8)	92.6 (74.4, 99.4)
G6Pp <−> F6Pp	47.6 (35.1, 49.7)	56.0 (38.7, 59.9)
F6Pp + ATPi −> FBPp	77.4 (65.2, 78.2)	81.3 (64.5, 82.6)
FBPp <−> TP + TP	77.4 (65.2, 78.2)	81.9 (64.5, 82.6)
G6P −> 6PG + NADPH	0.0 (0.0, 4.1)	6.7 (0.0, 15.5)
6PG −> RU5P + CO_2 + NADPH	0.0 (0.0, 4.1)	6.7 (0.0, 15.5)
RU5P <−> X5P	0.0 (0.0, 4.1)	6.7 (0.0, 15.5)
G6Pp −> 6PGp + NADPH	47.9 (42.7, 50.1)	34.9 (22.6, 45.7)
6PGp −> RU5Pp + CO_2 + NADPH	47.9 (42.7, 50.1)	34.9 (22.6, 45.7)
RU5Pp <−> X5Pp	29.8 (25.0, 31.3)	18.6 (7.5, 28.1)
RU5Pp <−> R5Pp	18.1 (17.4, 18.8)	16.3 (15.0, 17.7)
X5P <−> X5Pp	0.0 (0.0, 4.1)	6.7 (0.0, 15.5)
X5Pp <−> TP + EC2	29.8 (28.4, 31.3)	25.3 (22.7, 28.1)
F6Pp <−> E4Pp + EC2	**−13.2 (−13.9, −12.4)**	**−10.6 (−12.0, −9.3)**
S7Pp <−> R5Pp + EC2	−16.7 (−17.4, −16.0)	−14.7 (−16.0, −13.4)
F6Pp <−> TP + EC3	−16.7 (−17.4, −16.0)	−14.7 (−16.0, −13.4)
S7Pp <−> E4Pp + EC3	16.7 (16.0, 17.4)	14.7 (13.2, 16.0)
TP <−> 3PGA + NADHi + ATP	**167.0 (166.0, 168.0)**	**171.8 (170.4, 173.3)**
3PGA <−> PEP	**156.1 (154.2, 158.2)**	**160.1 (158.2, 162.1)**
PEP −> PYRm + ATP	**76.0 (73.4, 80.6)**	**70.7 (66.7, 74.9)**
PEP −> PYRp + ATP	**43.0 (39.4, 44.5)**	**51.7 (48.5, 54.4)**
PYRm −> ACoAm + CO_2 + NADH	**77.4 (72.6, 83.9)**	**70.7 (66.7, 76.4)**
PYRp −> ACoAp + CO_2 + NADH	**20.0 (18.8, 21.0)**	**26.1 (24.9, 27.0)**
OAA + ACoAm −> CIT	**77.4 (72.6, 83.9)**	**70.7 (66.7, 76.4)**
CIT <−> ICIT	76.8 (71.9, 83.3)	70.3 (66.3, 76.0)
ICIT <−> 2OG + CO_2 + NADPH	76.8 (71.9, 83.3)	70.3 (66.3, 76.0)
2OG −> SUCCoA + CO_2 + NADH	**66.2 (60.8, 73.3)**	**58.2 (53.8, 64.4)**
SUCCoA <−> SUC + ATP	**62.1 (56.6, 69.4)**	**53.5 (49.0, 59.9)**
SUC <−> FUM + $FADH_2$	**65.8 (60.4, 72.9)**	**58.2 (53.7, 64.4)**
FUM <−> MAL	68.6 (63.3, 75.5)	62.3 (58.0, 68.3)
MAL <−> OAA + NADH	65.0 (61.1, 69.1)	61.3 (57.5, 65.3)
PEP + CO_2 −> OAA	30.1 (28.0, 34.1)	29.6 (28.6, 33.3)
MAL −> PYRm + CO_2 + NADH	1.4 (0.0, 6.4)	0.0 (0.0, 4.3)
MAL −> PYRp + CO_2 + NADPH	0.2 (0.0, 1.1)	0.9 (0.0, 2.1)

The values in grey brackets are the 95% confidence limits calculated by parameter continuation. Fluxes which are significantly different between the two conditions are shown in bold.

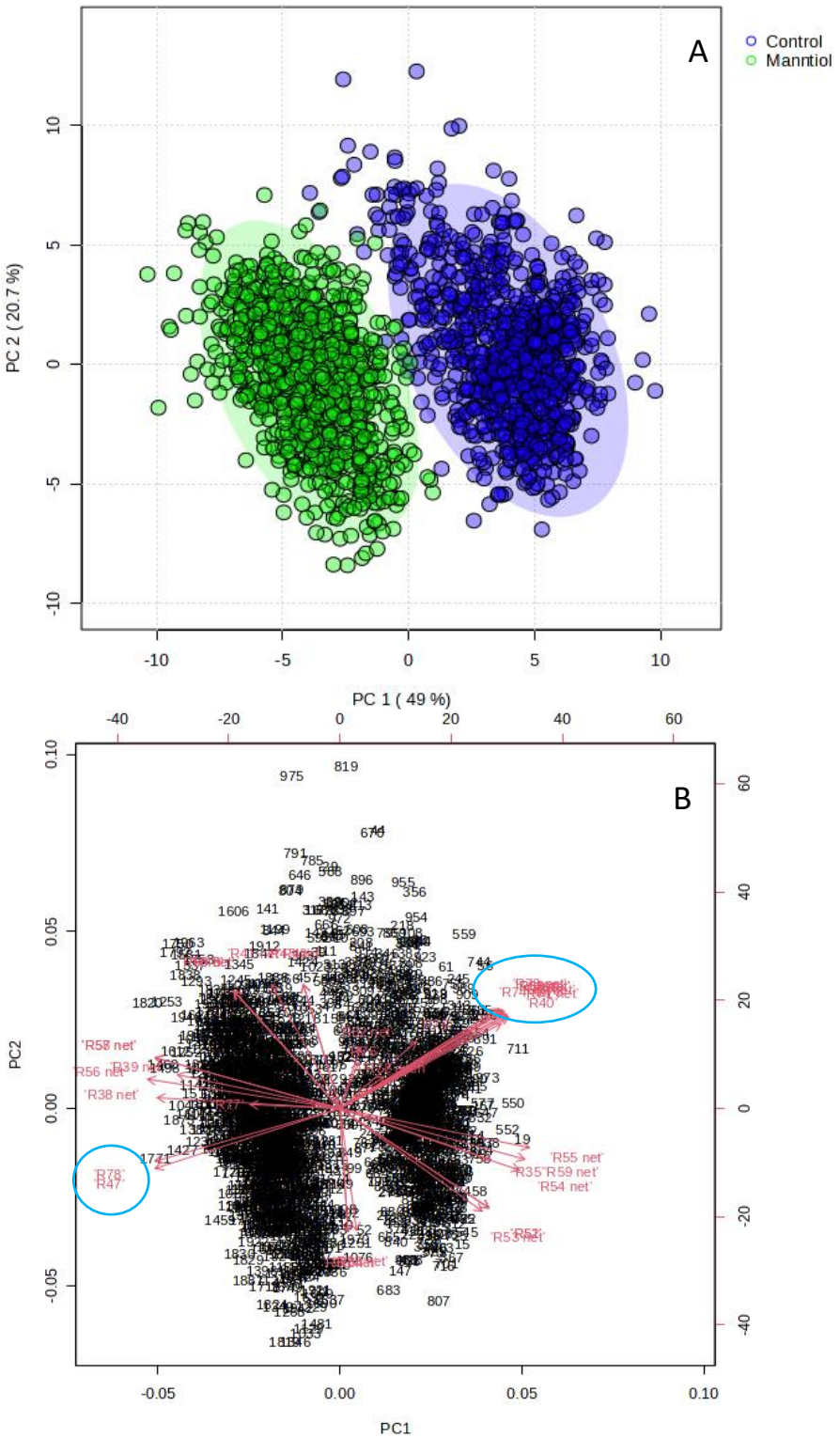


Figure 5.7: *Principal component analysis of the net fluxes of reactions in the CCM in cultures grown in MS medium or medium supplemented with 40 mM mannitol (A) Scores plot of flux solution for unsupplemented cultures (blue), and cultures supplemented with mannitol (green). (B) Biplot of PCA with the loadings indicated in red. The blue rings highlight the fluxes which exerted the greatest influence on the separation of the two clusters of flux solutions along the axis of maximum separation. Synthetic datasets were derived from 1000 rounds of Monte Carlo simulation for each of the two flux solutions.*

Some of the changes in flux could be due to the change in biomass composition. Both protein and lipid content increased when cultures were supplemented with 40 mM mannitol, although these changes were slight (Figure 5.5). Lipid is synthesised from plastidic acetyl CoA which is derived from plastidic pyruvate, and some amino acids are derived from plastidic pyruvate while others are derived from PEP directly. In the flux solutions for mannitol-supplemented cultures there was a significantly greater biosynthetic output flux from PEP (to the PEP.B pool) and into plastidic pyruvate, and a significantly decreased flux from PEP to mitochondrial pyruvate (Figure 5.8). Lower flux to mitochondrial pyruvate could also explain the lower estimates of the TCA cycle fluxes in the presence of mannitol.

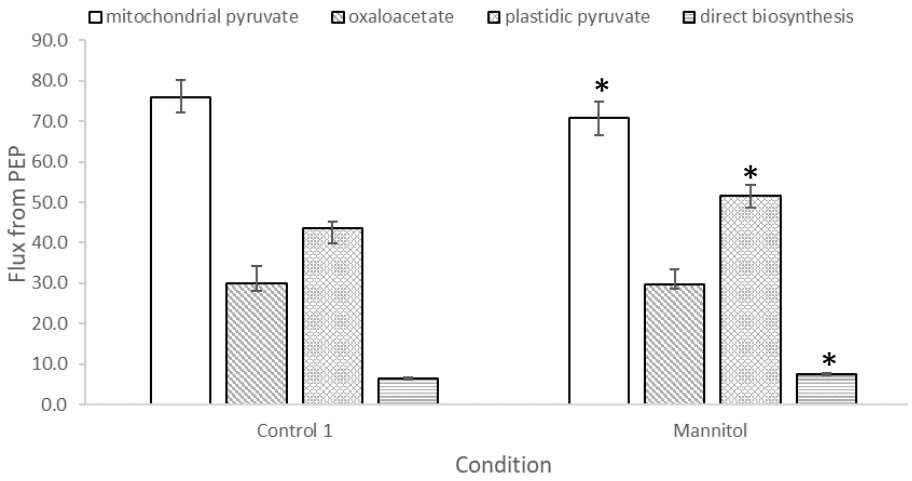


Figure 5.8: *Utilisation of PEP in Arabidopsis suspension cultures grown in MS medium or MS medium supplemented with mannitol. Asterisks (*) represent fluxes which differ significantly from those of the control.*

The increased net fluxes from TP to PEP in the mannitol-supplemented medium, cannot be explained by changes in the biomass composition. It is likely that this increase in fluxes is a result of a change in relative usage of G6P by phosphoglucoisomerase and G6P dehydrogenase (Figure 5.9). In the unsupplemented culture flux through the combined plastidic and cytosolic phosphoglucose isomerase was 48.8 (95% confidence interval 46.7 – 51.0) relative to a glucose uptake rate of 100 and the combined G6P dehydrogenase flux was 47.9 (45.8 – 50.1). In contrast, in the mannitol-supplemented culture the phosphoglucoisomerase flux increased to 56.0 (52.0 – 60.0) and G6P dehydrogenase flux

decreased to 41.6 (37.7 – 45.7). In the OxPPP carbon was removed from the CCM as CO_2, R5P and E4P, so a smaller proportion of the absorbed glucose entering the OxPPP means that less carbon will be removed from the CCM and more will be available to be converted to TP and then PEP. This mannitol associated alteration of the OxPPP:glycolysis ratio does not result in statistically significant differences in the phosphoglucoisomerase and G6P dehydrogenase reactions themselves but has an amplified effect on the well-defined reactions lower in the network, which do register as statistically significantly different (Figure 5.9, Table 5.1).

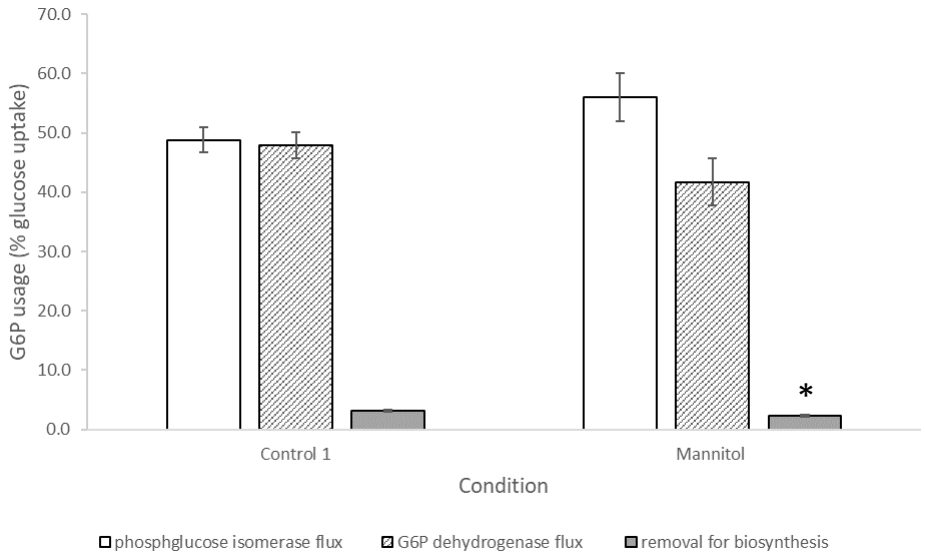


Figure 5.9: *Utilisation of the combined plastidic and cytosolic G6P pool in Arabidopsis cell suspension cultures grown under different conditions. Error bars represent 95% confidence intervals calculated by parameter continuation. Asterisks (*) represent fluxes which differ significantly from those of the control.*

The flux solutions from unsupplemented cultures and cultures supplemented with 40 mM mannitol suggest that the mild osmotic stress caused by mannitol induced an alteration in the contribution of carbohydrates to biomass composition, a statistically significant increase in net flux to TP and PEP and a decrease in relative flux through some TCA cycle reactions. However, these results contrast with an earlier MFA study investigating osmotic stress. Williams *et al*. (2010), supplemented *Arabidopsis* suspension cultures with 171 mM

mannitol and did not see the increased starch content which is noted in this study, as well as noting no significant difference in the flux distribution between unsupplemented and 171 mM mannitol supplemented cultures.

The reason that Williams *et al*. (2010) noted no significant changes in the flux distribution could be due to the difference in the methods used for assessing the significance of differences between flux solutions. Williams *et al*. (2010) compared the overlap of local standard deviations for each reaction (Wiechert and de Graff, 1997), which assumes that changes in one reaction will not have any effect on the other reactions in the model (Antoniewicz *et al*., 2006). In contrast the flux solutions presented here were compared with the more appropriate confidence interval overlap method (see Section 2.7). There are considerable differences in the flux through some reactions between the unsupplemented and 171 mM mannitol supplemented cultures in Williams *et al*. (2010). For example, the 171 mM mannitol-supplemented culture in Williams *et al*. (2010) showed a 36-42% decrease in fluxes through the TCA cycle relative to the unsupplemented culture. The statistically significant decrease in TCA cycle fluxes between the mannitol-supplemented and unsupplemented cultures in this study was only a 13-16% decrease.

If the reliability of the flux estimates in Williams *et al*. (2010) was similar to those of the flux estimates obtained in the 40 mM mannitol study, then application of the statistical methods used here could well register many reactions in the flux solutions estimated by Williams *et al*. (2010) as significantly different. This suggests that increasing mannitol concentrations might decrease the TCA flux, potentially by increasing pyruvate partitioning into protein biosynthesis.

This study and Williams *et al*. (2010) show opposite effects on glycolysis and the OxPPP in response to mannitol. The increase in OxPPP flux in response to 171 mM could be in response to an increase in the demand for NADPH due to oxidative stress caused by the more severe osmotic stress (Borsani *et al*., 2001).

Conducting MFA on cultures supplemented with 40 mM mannitol provides an osmotic control for separating effects of adding 40 mM extra solute in the MS medium from the specific effects of mannose on the CCM in the following section. MFA on mannitol supplemented cultures also confirms that mild osmotic stress can induce some metabolic rearrangement as suggested by Skirycz *et al*. (2009), and allows comparison with the more severe osmotic stress investigated by Williams *et al*. (2010).

5.4.2 The effect of mannose on flux distribution in the CCM

Arabidopsis cultures grown in MS medium supplemented with 40 mM mannose showed a flux distribution that was statistically acceptable (SSR of 1212.8 with 1133 DOF and critical SSR range of 1041.6-1228.2) but was significantly different to cultures grown in normal MS medium and medium supplemented with mannitol. Flux maps are presented in Figure 5.10 and a summary of the net CCM reactions in Table 5.2. Full flux solutions are available in Appendix 7. PCA was conducted based on the net fluxes of the CCM derived from 1000 Monte Carlo simulations of the best-fit estimates of each flux solution (Figure 5.11A).

The PCA scores plot shows that the flux distribution in the CCM of the mannose-supplemented culture was significantly different from the flux distributions in the unsupplemented or mannitol-supplemented cultures. Further, the mannose-supplemented cultures exhibited a greater difference from the unsupplemented cultures than the mannitol-supplemented cultures did. Analysis of the PCA loadings in the biplot (Figure 5.11B) showed that the reactions which contribute to the difference between the cultures containing mannose and the control or mannitol containing cultures were; the reactions of the TCA cycle, anaplerotic fluxes, flux from TP to pyruvate and the phosphopentose isomers/epimerase, transketolase and transaldolase reactions in OxPPP.

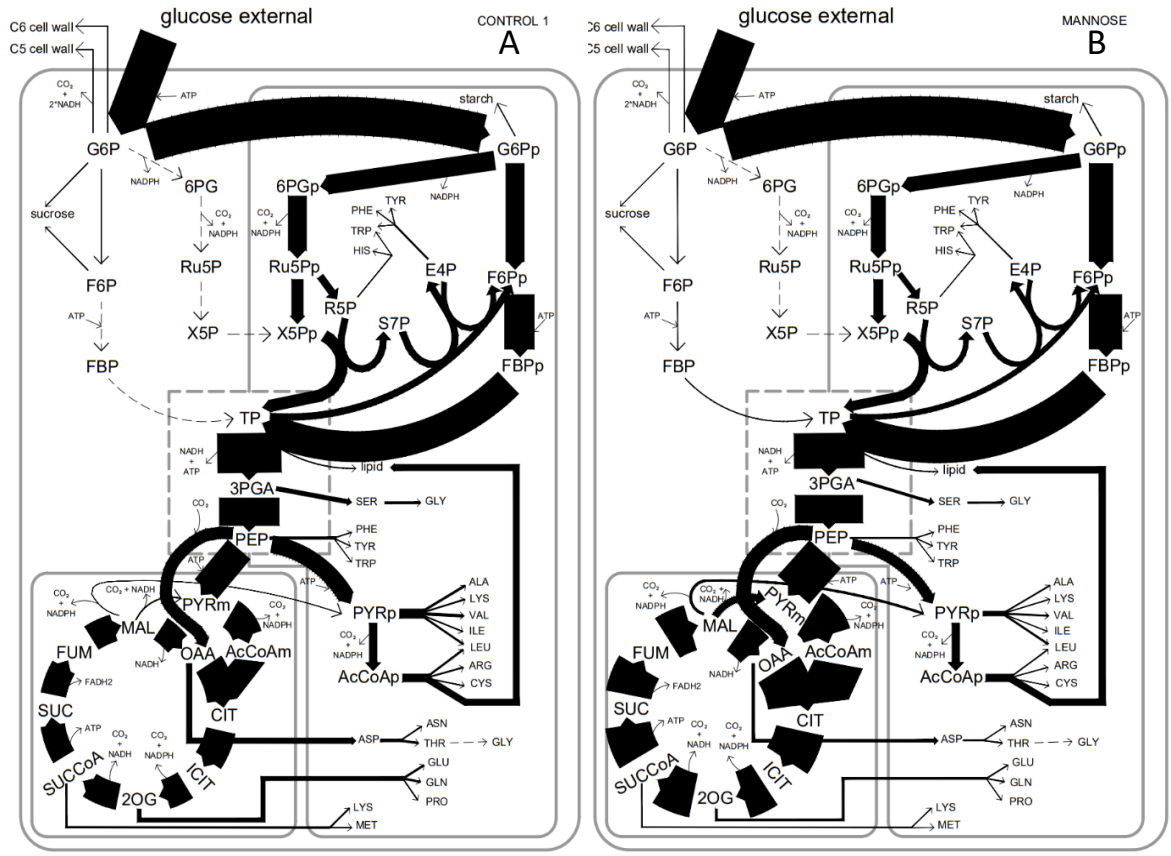


Figure 5.10: *Flux maps derived from MFA for Arabidopsis cultures grown in different media. (A) culture grown in standard MS medium; (B) parallel-grown culture grown in MS medium supplemented with 40 mM mannose. The thickness of the lines represents the relative flux through each reaction. Dotted arrows represent a flux less than 0.0009 relative to a glucose uptake rate of 100.*

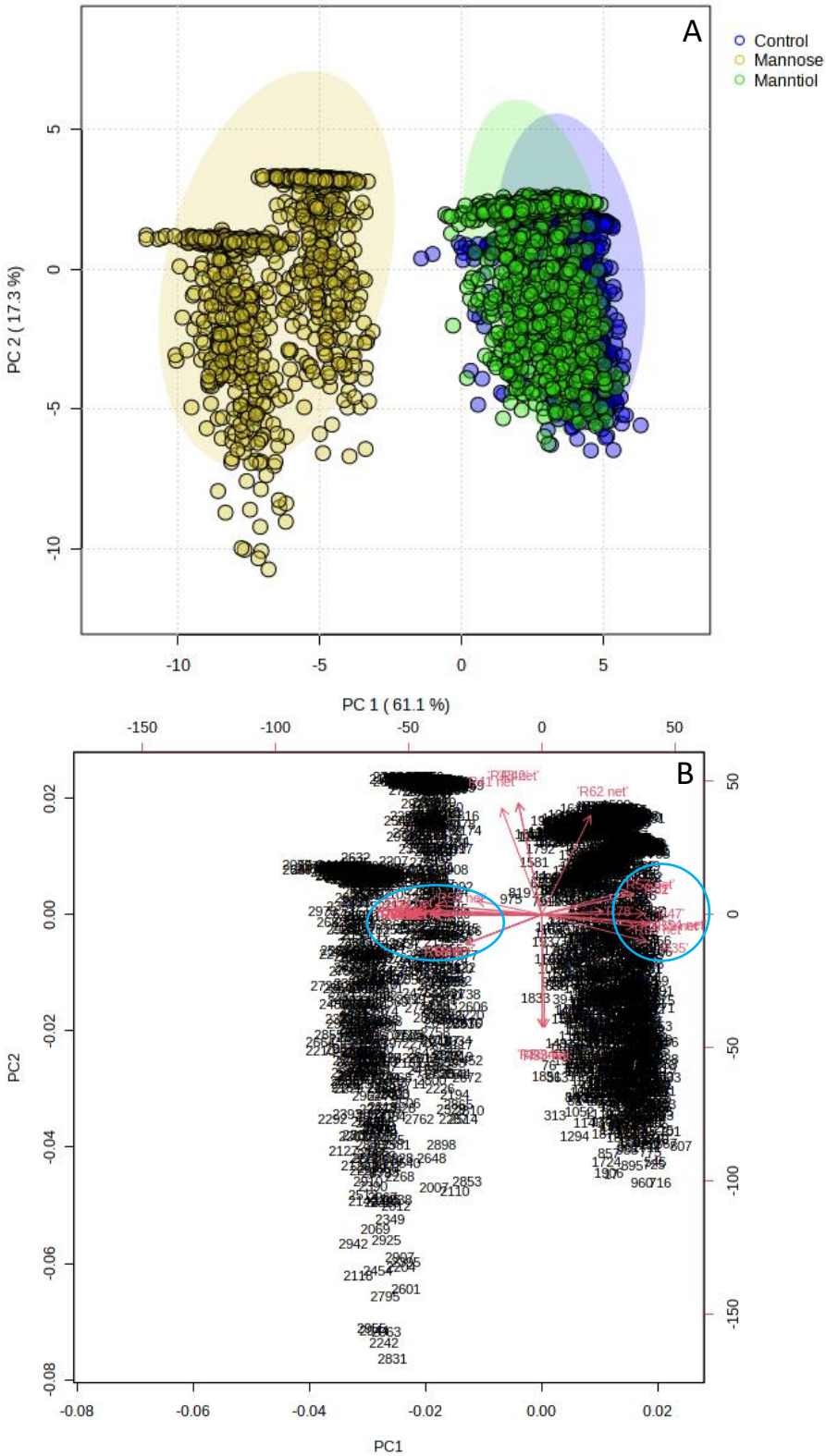


Figure 5.11: *Principal component analysis of the net fluxes of reactions in the CCM in cultures grown in MS medium or medium supplemented with 40 mM mannose (A) Scores plot of flux solution for unsupplemented cultures (blue), and cultures supplemented with mannitol (green) or with mannose (gold). (B) Biplot of PCA loadings indicated in red. The blue rings highlight the fluxes which exerted the greatest influence on the separation of the two clusters of flux solutions along the axis of maximum separation. Synthetic datasets were derived from 1000 rounds of Monte Carlo simulation for each of the two flux solutions.*

The flux maps in Figure 5.10 and confidence interval overlap showed that all the TCA cycle fluxes increased significantly in the mannose-supplemented culture (Table 5.2). The fluxes through plastidic and cytosolic malic enzyme, GAP dehydrogenase/phosphoglycerate kinase, phosphoglycerate mutase/enolase, mitochondrial pyruvate kinase and mitochondrial pyruvate dehydrogenase also increased in the mannose-supplemented culture, while flux through plastidic pyruvate dehydrogenase decreased. Flux through phosphopentose isomerase, phosphopentose epimerase, transketolase and transaldolase significantly decreased in the mannose-supplemented cultures.

The decreased protein content in the mannose supplemented culture could be a contributing factor to the decreased flux from PEP to plastidic pyruvate and the increase in flux from PEP to mitochondrial pyruvate (Figure 5.12). Several amino acids are derived from PEP, pyruvate or acetyl-CoA in the plastid, thus a decreased protein content is associated with a reduced requirement for PEP, pyruvate and acetyl-CoA for biosynthesis. Therefore, a greater proportion of PEP may be available to form mitochondrial pyruvate and acetyl-CoA to enter the TCA cycle.

Table 5.2: *Comparison of the net CCM fluxes in flux solutions from Arabidopsis suspension cultures grown in MS medium or medium supplemented with 40 mM mannose*

Reaction	Relative flux in specific culture	
	Unsupplemented (Control 1)	Mannose supplemented
GLCext + ATPi −> G6P	100.0 (n/a, n/a)	100.0 (n/a, n/a)
G6P <−> F6P	1.2 (1.2, 13.4)	1.2 (0.0, 45.3)
F6P + ATP −> FBP	0.0 (0.0, 12.2)	1.1 (0.0, 45.2)
FBP <−> TP + TP	0.0 (0.0, 12.2)	1.1 (0.0, 45.2)
G6P <−> G6Pp	96.6 (84.5, 96.8)	98.1 (16.3, 99.3)
G6Pp <−> F6Pp	47.6 (35.1, 49.7)	60.5 (15.0, 62.6)
F6Pp + ATPi −> FBPp	77.4 (65.2, 78.2)	83.6 (39.0, 85.3)
FBPp <−> TP + TP	77.4 (65.2, 78.2)	83.6 (39.0, 85.3)
G6P −> 6PG + NADPH	0.0 (0.0, 4.1)	0.0 (0.0, 1.9)
6PG −> RU5P + CO_2 + NADPH	0.0 (0.0, 4.1)	0.0 (0.0, 1.9)
RU5P <−> X5P	0.0 (0.0, 4.1)	0.0 (0.0, 1.9)
G6Pp −> 6PGp + NADPH	47.9 (42.7, 50.1)	36.3 (0.0, 38.2)
6PGp −> RU5Pp + CO_2 + NADPH	47.9 (42.7, 50.1)	36.3 (0.0, 38.2)
RU5Pp <−> X5Pp	29.8 (25.0, 31.3)	23.1 (22.5, 24.4)
RU5Pp <−> R5Pp	**18.1 (17.4, 18.8)**	**13.2 (12.8, 13.8)**
X5P <−> X5Pp	0.0 (0.0, 4.1)	0.0 (0.0, 1.9)
X5Pp <−> TP + EC2	**29.8 (28.4, 31.3)**	**23.1 (23.0, 24.4)**
F6Pp <−> E4Pp + EC2	**−13.2 (−13.9, −12.4)**	**−10.7 (−11.3, −10.2)**
S7Pp <−> R5Pp + EC2	**−16.7 (−17.4, −16.0)**	**−12.5 (−13.1, −12.4)**
F6Pp <−> TP + EC3	**−16.7 (−17.4, −16.0)**	**−12.5 (−13.1, −12.4)**
S7Pp <−> E4Pp + EC3	**16.7 (16.0, 17.4)**	**12.5 (12.4, 13.1)**
TP <−> 3PGA + NADHi + ATP	**167.0 (166.0, 168.0)**	**178.7 (177.2, 180.3)**
3PGA <−> PEP	**156.1 (154.2, 158.2)**	**172.3 (169.5, 175.1)**
PEP −> PYRm + ATP	**76.0 (73.4, 80.6)**	**106.7 (169.5, 175.1)**
PEP −> PYRp + ATP	**43.0 (39.4, 44.5)**	**25.6 (21.2, 29.8)**
PYRm −> ACoAm + CO_2 + NADH	**77.4 (72.6, 83.9)**	**123.0 (113.0, 134.0)**
PYRp −> ACoAp + CO_2 + NADH	20.0 (18.8, 21.0)	18.9 (15.7, 21.7)
OAA + ACoAm −> CIT	**77.4 (72.6, 83.9)**	**123.0 (113.0, 134.0)**
CIT <−> ICIT	**76.8 (71.9, 83.3)**	**122.6 (112.5, 133.6)**
ICIT <−> 2OG + CO_2 + NADPH	**76.8 (71.9, 83.3)**	**122.6 (112.5, 133.6)**
2OG −> SUCCoA + CO_2 + NADH	**66.2 (60.8, 73.3)**	**117.2 (106.3, 129.1)**
SUCCoA <−> SUC + ATP	**62.1 (56.6, 69.4)**	**115.1 (103.9, 127.4)**
SUC <−> FUM + $FADH_2$	**65.8 (60.4, 72.9)**	**116.9 (106.0, 128.9)**
FUM <−> MAL	**68.6 (63.3, 75.5)**	**118.2 (107.5, 130.0)**
MAL <−> OAA + NADH	**65.0 (61.1, 69.1)**	**95.6 (87.9, 103.7)**
PEP + CO_2 −> OAA	30.1 (28.0, 34.1)	36.4 (31.8, 41.4)
MAL −> PYRm + CO_2 + NADH	**1.4 (0.0, 6.4)**	**16.3 (10.0, 23.3)**
MAL −> PYRp + CO_2 + NADPH	**0.2 (0.0, 1.1)**	**5.0 (4.2, 5.7)**

The values in grey brackets are the 95% confidence limits calculated by parameter continuation. Fluxes which are significantly different between the two conditions are shown in bold.

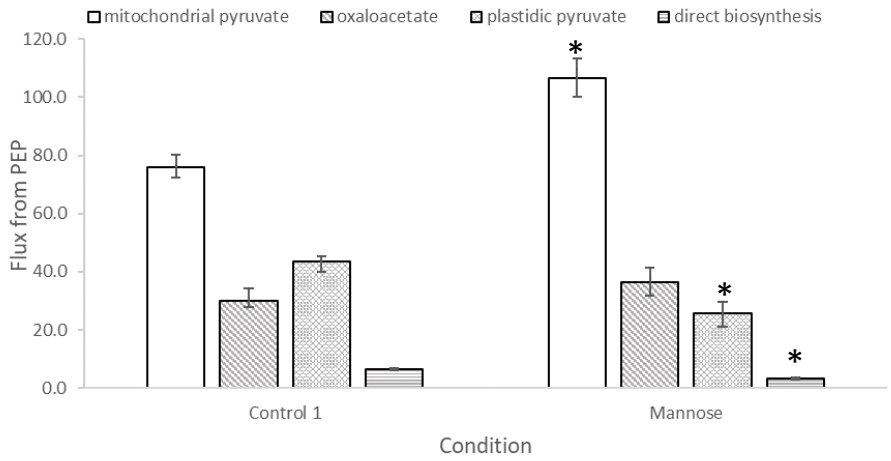


Figure 5.12: *Utilisation of PEP in Arabidopsis suspension cultures grown in MS medium or MS medium supplemented with mannose. Error bars represent 95% confidence intervals calculated by parameter continuation and asterisks (*) represent fluxes which differ significantly from those of the control.*

The increased flux from TP to PEP and decreased flux through the OxPPP is likely related to the utilisation of G6P. Figure 5.13 shows that supplementation with mannose significantly increased the proportion of the combined cytosolic and plastidic G6P which goes through phosphoglucoisomerase thus entering glycolysis and significantly decreased the proportion that entered the OxPPP via G6P dehydrogenase. This change in G6P utilisation could be a specific effect of mannose on either phosphoglucoisomerase or G6P dehydrogenase. However, a very similar change in flux distribution was seen in the reduced temperature cultures in Chapter 4, suggesting that this change in G6P utilisation may be a response to the slowed growth rate or glucose utilisation rate (further discussion in Chapter 6).

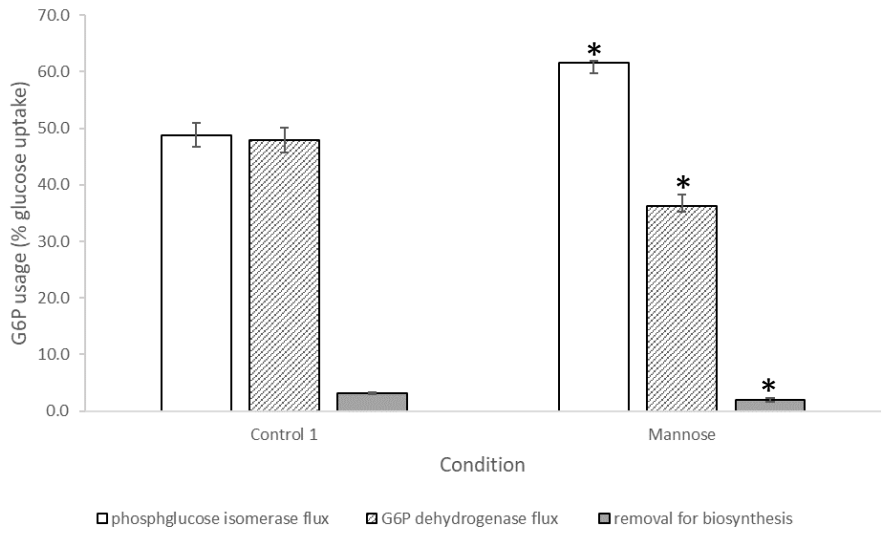


Figure 5.13: *Utilisation of the combined plastidic and cytosolic G6P pool in Arabidopsis cell suspension cultures grown in unsupplemented MS medium or MS medium supplemented with 40 mM mannose. Error bars represent 95% confidence intervals calculated by parameter continuation. Asterisks (*) represent fluxes which differ significantly from those of the control.*

The statistically significant changes in flux distribution between the control and mannose-containing cultures suggests that mannose supplementation affected the flux distribution in the CCM of *Arabidopsis* suspensions. Further, there are clear differences in the flux solutions produced from cultures supplemented with 40 mM mannose and 40 mM mannitol. The mannitol-supplemented cultures had decreased flux through the TCA cycle and no change in the anaplerotic reactions while the mannose-supplemented cultures had significantly increased flux through the TCA cycle and the anaplerotic reactions. Both the mannose and mannitol supplemented cultures showed increased flux from TP to PEP, decreased flux through the OxPPP and altered patterns of G6P utilisation. However, the magnitude of these changes in the mannose-supplemented culture relative to the unsupplemented cultures were considerably larger than those in the mannitol-supplemented culture relative to the unsupplemented culture (Table 5.1, 5.2, Figure 5.9, 5.13). The observation that mannose and mannitol affect CCM flux distribution in different ways suggests that although supplementation with mannose may cause some mild osmotic stress it had a specific effect beyond that of osmotic stress alone.

Mannose was first characterised as ‘toxic’ in 1917 and exogenous mannose has been shown to affect the growth characteristics of many plants (Knudson, 1917; Stenlid, 1954, 1959, 1971). In *Arabidopsis* supplementation with mannose has been associated with the inhibition of seed and pollen germination, hypocotyl elongation, root growth and rosette growth, in addition to decreased chlorophyll content and increased anthocyanin accumulation (Pego *et al*., 1999; Baskin *et al*., 2001; Todd and Tague, 2001; Stevenson and Harrigton, 2009; Hirsche *et al*., 2017). Mannose supplementation has also caused disturbed actin cytoskeleton and apoptosis linked DNA fragmentation, membrane permeability and cytoplasmic retraction (Stein and Hanson, 1999; Banaś *et al*., 2010: Pathirana *et al*., 2017). This study has now added an altered biomass composition and a significant rearrangement of flux through the CCM to the list of effects of mannose supplementation on *Arabidopsis.*

The deleterious effects of mannose supplementation are reliable enough to make growth on mannose a common selection marker for transgenic *Arabidopsis.* In which *E. coli* phosphomannoisomerase is used to confer resistance to the normal inhibitory effects of mannose (Todd and Tague, 2001; Reed *et al*., 2001). Early analyses assumed that *Arabidopsis* could not metabolise mannose. However, subsequent studies have identified the phosphomannoisomerase and phosphomannomutase genes required to detoxify mannose in *Arabidopsis* (Qian *et al*., 2007; Maruta *et al*., 2008). These studies showed that the enzymes are produced in *Arabidopsis* tissues and that they are active *in vitro* but the activity of the enzymes *in vivo* could not be measured. Presumably using growth on mannose as a selection marker for *Arabidopsis* works because, although phosphomannoisomerase and phosphomannomutase are present in *Arabidopsis* cells their capacity is insufficient to prevent mannose induced growth inhibition.

There is debate as to the mechanism by which mannose causes its deleterious effects (Stevenson and Harrington, 2009). It is confirmed that mannose is absorbed into plant cells and is phosphorylated by hexokinase to produce mannose 6-phosphte (Saltman, 1953; Goldsworthy and Street, 1965; Higgins and Easterby, 1974; Herold and Lewis, 1977;

Truenit *et al*., 1999; Büttner *et al*., 2000). There is evidence that mannose 6-phosphate then accumulates and sequesters inorganic phosphate, thus limiting ATP production (Street and Lowe, 1959; Stenlid, 1959; Goldsworthy and Street, 1965; Sheu-Hwa *et al*., 1975; Herold *et al*., 1976; Herold and Lewis, 1977; Loughman *et al*., 1989; Ciersko and Kleczkowski, 2001; Maleszewski *et al*., 2004) and further evidence that accumulated mannose 6-phosphate competitively inhibits phosphoglucoisomerase, thus blocking glycolysis (Slein *et al*., 1950; Sols *et al*., 1960; Goldsworthy and Street, 1965, Herold and Lewis, 1977). Another line of investigation has shown that mannose can interfere with sugar signalling and can alter gene expression via a hexokinase-mediated signalling pathway (Jang and Sheen, 1994; Pego *et al*., 1999; Baskin *et al*., 2001; Ciereszko and Kleczkowski, 2002, Hirsche *et al*., 2017). The extent to which these three mechanisms contribute to the physiological effects of exogenous mannose on plants is unclear.

As Figure 5.13 shows, when *Arabidopsis* cultures were supplemented with mannose, the relative flux through phosphoglucoisomerase increased significantly. The increased flux associated with mannose supplementation suggests that, in this instance, mannose was not inhibiting the conversion of G6P to F6P. A possible explanation is that mannose 6-phosphate is likely to accumulate in the cytosol while the majority of the phosphoglucoisomerase activity is in the plastid (Table 5.2).

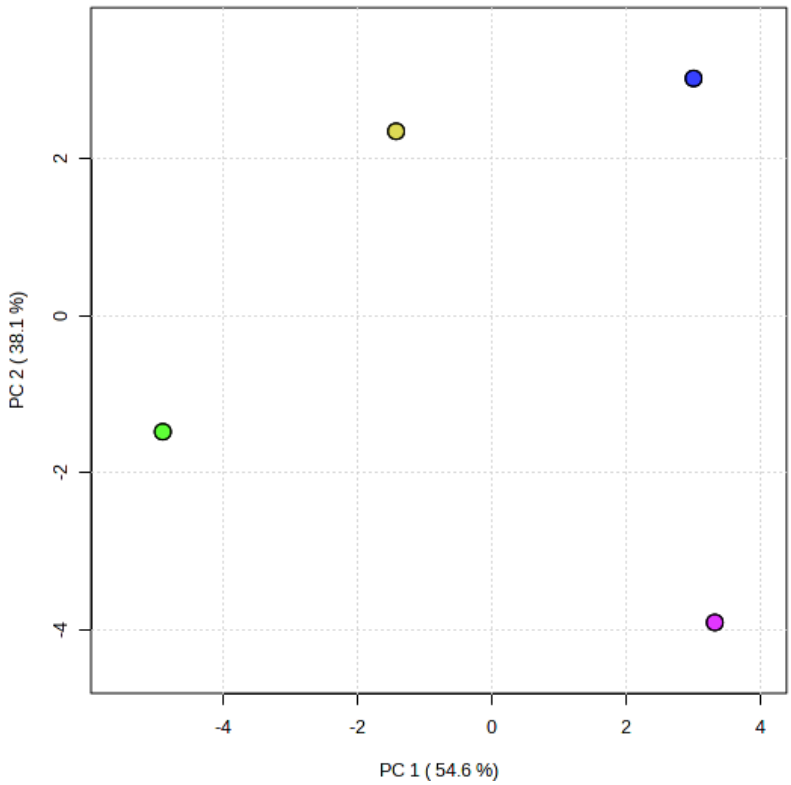


Figure 5.14: *PCA scores plot of best-fit flux solutions from; the control from this study (blue), the mannose supplemented cultures from this study (gold), the control cultures from Masakapalli et al. (2014a; pink) and the phosphate deprived cultures from Masakapalli et al. (2014a; green)*

However, it does seem likely that mannose 6-phosphate sequestered phosphate in this study. A previous MFA study investigated the effect of phosphate deprivation on *Arabidopsis* cell suspension cultures (Masakapalli *et al*., 2014a). PCA was conducted on the best-fit solutions for the control and phosphate-deprived cultures from Masakapalli *et al*. (2014a) and the control and mannose-supplemented cultures from this study. The scores plot showed that both phosphate deprivation and mannose supplementation caused a decrease in PC1 (Figure 5.14). Furthermore, comparison of the flux solutions showed that both phosphate deprivation and mannose supplementation increased the in fluxes in TCA cycle and anaplerotic reactions, as well as decreased flux through the OxPPP (Table 5.3).

Table 5.3: *Flux solutions for cultures grown under standard and experimental conditions in this study and in Masakapalli et al. (2014a)*

Reaction	Relative flux in specific study and condition			
	This study Control	This study Mannose supplemented	Masakapalli *et al*. (2014a) Control	Masakapalli *et al*. (2014a) −Pi
GLCext + ATPi −> G6P	100.0 (n/a, n/a)	100.0 (n/a, n/a)	100.0	100.0
G6P <−> F6P	1.2 (1.2, 13.4)	1.2 (0.0, 45.3)	18.6	−2.4
F6P + ATP −> FBP	0.0 (0.0, 12.2)	1.1 (0.0, 45.2)		
FBP <−> TP + TP	0.0 (0.0, 12.2)	1.1 (0.0, 45.2)	12.1	−4.9
G6P <−> G6Pp	96.6 (84.5, 96.8)	98.1 (16.3, 99.3)	58	97.6
G6Pp <−> F6Pp	47.6 (35.1, 49.7)	60.5 (15.0, 62.6)	35.7	83.7
F6Pp + ATPi −> FBPp	77.4 (65.2, 78.2)	83.6 (39.0, 85.3)		
FBPp <−> TP + TP	77.4 (65.2, 78.2)	83.6 (39.0, 85.3)	53.9	91.1
G6P −> 6PG + NADPH	0.0 (0.0, 4.1)	0.0 (0.0, 1.9)	12.9	0.0
6PG −> RU5P + CO_2 + NADPH	0.0 (0.0, 4.1)	0.0 (0.0, 1.9)		
RU5P <−> X5P	0.0 (0.0, 4.1)	0.0 (0.0, 1.9)		
G6Pp −> 6PGp + NADPH	47.9 (42.7, 50.1)	36.3 (0.0, 38.2)	15.5	12.2
6PGp −> RU5Pp + CO_2 + NADPH	47.9 (42.7, 50.1)	36.3 (0.0, 38.2)		
RU5Pp <−> X5Pp	29.8 (25.0, 31.3)	23.1 (22.5, 24.4)		
RU5Pp <−> R5Pp	**18.1 (17.4, 18.8)**	**13.2 (12.8, 13.8)**		
X5P <−> X5Pp	0.0 (0.0, 4.1)	0.0 (0.0, 1.9)		
X5Pp <−> TP + EC2	**29.8 (28.4, 31.3)**	**23.1 (23.0, 24.4)**	18.3	7.3
F6Pp <−> E4Pp + EC2	**−13.2 (−13.9, −12.4)**	**−10.7 (−11.3, −10.2)**	8.6	3.3
S7Pp <−> R5Pp + EC2	**−16.7 (−17.4, −16.0)**	**−12.5 (−13.1, −12.4)**	9.7	4.1
F6Pp <−> TP + EC3	**−16.7 (−17.4, −16.0)**	**−12.5 (−13.1, −12.4)**	9.7	4.1
S7Pp <−> E4Pp + EC3	**16.7 (16.0, 17.4)**	**12.5 (12.4, 13.1)**	9.7	4.1
TP <−> 3PGA + NADHi + ATP	**167.0 (166.0, 168.0)**	**178.7 (177.2, 180.3)**		
3PGA <−> PEP	**156.1 (154.2, 158.2)**	**172.3 (169.5, 175.1)**		
PEP −> PYRm + ATP	**76.0 (73.4, 80.6)**	**106.7 (169.5, 175.1)**	101	142.3
PEP −> PYRp + ATP	**43.0 (39.4, 44.5)**	**25.6 (21.2, 29.8)**	4.7	0.0
PYRm −> ACoAm + CO_2 + NADH	**77.4 (72.6, 83.9)**	**123.0 (113.0, 134.0)**	86.2	153.7
PYRp −> ACoAp + CO_2 + NADH	20.0 (18.8, 21.0)	18.9 (15.7, 21.7)		
OAA + ACoAm −> CIT	**77.4 (72.6, 83.9)**	**123.0 (113.0, 134.0)**	86.1	153.7
CIT <−> ICIT	**76.8 (71.9, 83.3)**	**122.6 (112.5, 133.6)**		
ICIT <−> 2OG + CO_2 + NADPH	**76.8 (71.9, 83.3)**	**122.6 (112.5, 133.6)**	83.2	152.8
2OG −> SUCCoA + CO_2 + NADH	**66.2 (60.8, 73.3)**	**117.2 (106.3, 129.1)**	70	143.1
SUCCoA <−> SUC + ATP	**62.1 (56.6, 69.4)**	**115.1 (103.9, 127.4)**		
SUC <−> FUM + $FADH_2$	**65.8 (60.4, 72.9)**	**116.9 (106.0, 128.9)**	68.9	142.3
FUM <−> MAL	**68.6 (63.3, 75.5)**	**118.2 (107.5, 130.0)**	69.3	143.1
MAL <−> OAA + NADH	**65.0 (61.1, 69.1)**	**95.6 (87.9, 103.7)**		
PEP + CO_2 −> OAA	30.1 (28.0, 34.1)	36.4 (31.8, 41.4)	26	30.1
MAL −> PYRm + CO_2 + NADH	**1.4 (0.0, 6.4)**	**16.3 (10.0, 23.3)**	0.9	16.3
MAL −> PYRp + CO_2 + NADPH	**0.2 (0.0, 1.1)**	**.0 (4.2, 5.7)**	0.8	0.0

The values in grey brackets are the 95% confidence limits calculated by parameter continuation. Fluxes which are significantly different between the two conditions are shown in bold.

The hexokinase-mediated effect of mannose on gene regulation has not been investigated here, because MFA is not the appropriate tool for assessing gene regulation. However, the MS medium used in this study contained 166.7 mM glucose, a concentration that ensures that exponential growth of the cell suspension is not limited by glucose availability. Since hexokinase phosphorylates both glucose and mannose the hexokinase mediated sugar signalling pathway is probably fully saturated in both the control and experimental conditions in this study and therefore is unlikely to be responsible for any of the differences between the unsupplemented and mannose supplemented cultures.

To summarise: supplementation of *Arabidopsis* cell suspension cultures with 40 mM mannose caused an increased contribution of lipid and insoluble carbohydrates to biomass and a decreased contribution of protein and sucrose. This was accompanied by significant rearrangement of the flux distribution in the CCM, comprising increased flux through glycolysis and the TCA cycle and decreased flux through the OxPPP. These changes in flux distribution are distinct from the effects of supplementation with 40 mM mannitol suggesting that the effect of mannose is not merely an osmotic effect. Further, the changes in flux distribution are consistent with the notion that mannose is phosphorylated to mannose 6-phosphate, which accumulates and sequesters phosphate.

5.5 Conclusions

In this chapter ^{13}C MFA has been used to study the effect of supplementation with 40 mM mannose on the flux distribution in the CCM of *Arabidopsis* suspension cultures. The metabolic effect of the mildly increased osmotic pressure of an extra 40 mM of solute was also investigated using mannitol. From this work three conclusions can be drawn:

1. Mild osmotic stress did not affect the growth rate but did slightly alter the biomass composition as well as causing some significant changes in flux distribution, notably a decrease in TCA cycle and OxPPP fluxes and an increase in glycolytic fluxes.

2. Supplementation with 40 mM mannose significantly slowed the growth rate, altered the biomass composition and induced a significant re-arrangement of fluxes in the CCM, including a decrease in the OxPPP flux and considerable increases in the TCA cycle and anaplerotic reaction fluxes.

3. The mannose induced flux rearrangement is likely a response to phosphate sequestration by mannose 6-phosphate rather than inhibition of glycolysis or an osmotic effect.

Chapter 6: Growth rate and flux distribution in CCM

6.1 Introduction

MFA has been conducted on *Arabidopsis* cell suspension cultures to produce flux maps of cultures grown under various conditions. These flux distributions, as well as previously published distributions can be interrogated to explore the relationship between growth and flux distribution in the CCM.

6.2 Growth rates and maintenance costs

Arabidopsis suspension cultures were grown in various conditions. Control cultures were grown under standard growth conditions (MS medium, 22°C), while other experimental cultures were grown in medium supplemented with 40 mM mannose or mannitol, or at decreased temperature (17°C or 12°C). A cell suspension culture was also acclimated to growth at 12°C over a period of one month. As discussed in previous chapters, cultures grown at decreased temperature or supplemented with 40 mM mannose showed a significant decrease in the rate of biomass accumulation (Figure 6.1A). The differences in growth rate between these cultures were accompanied by changes in the rate of glucose uptake (Figure 6.1B). In contrast, cultures grown in MS medium supplemented with 40 mM mannitol did not display a significantly different dry weight to the control cultures after five days of growth (See sections 4.2, 4.5 and 5.2 for further details).

The slowed growth rate in certain cultures could be due to a change in the allocation of carbon, ATP and/or reductant to the biophysical/biochemical processes that contribute to growth or to other processes that do not contribute to growth. As discussed in Chapters 1 and 3, proposals about the nature of these non-growth related processes depend on the respiration paradigm that is being considered. The GMRP would suggest that these non-growth processes contribute only to homeostasis, the GMWRP would suggest that these

non-growth processes include homeostatic processes and wastage of resources by futile cycling, and the GP would suggest that these non-growth processes may contribute to homeostasis or to growth and include any cellular process not included in the model. For simplicity I will refer to the cost of these non-growth processes as 'maintenance costs' for the rest of this chapter. To confirm if slowed growth rate is related to altered partitioning between growth and maintenance costs, the relative costs of these processes need to be quantified.

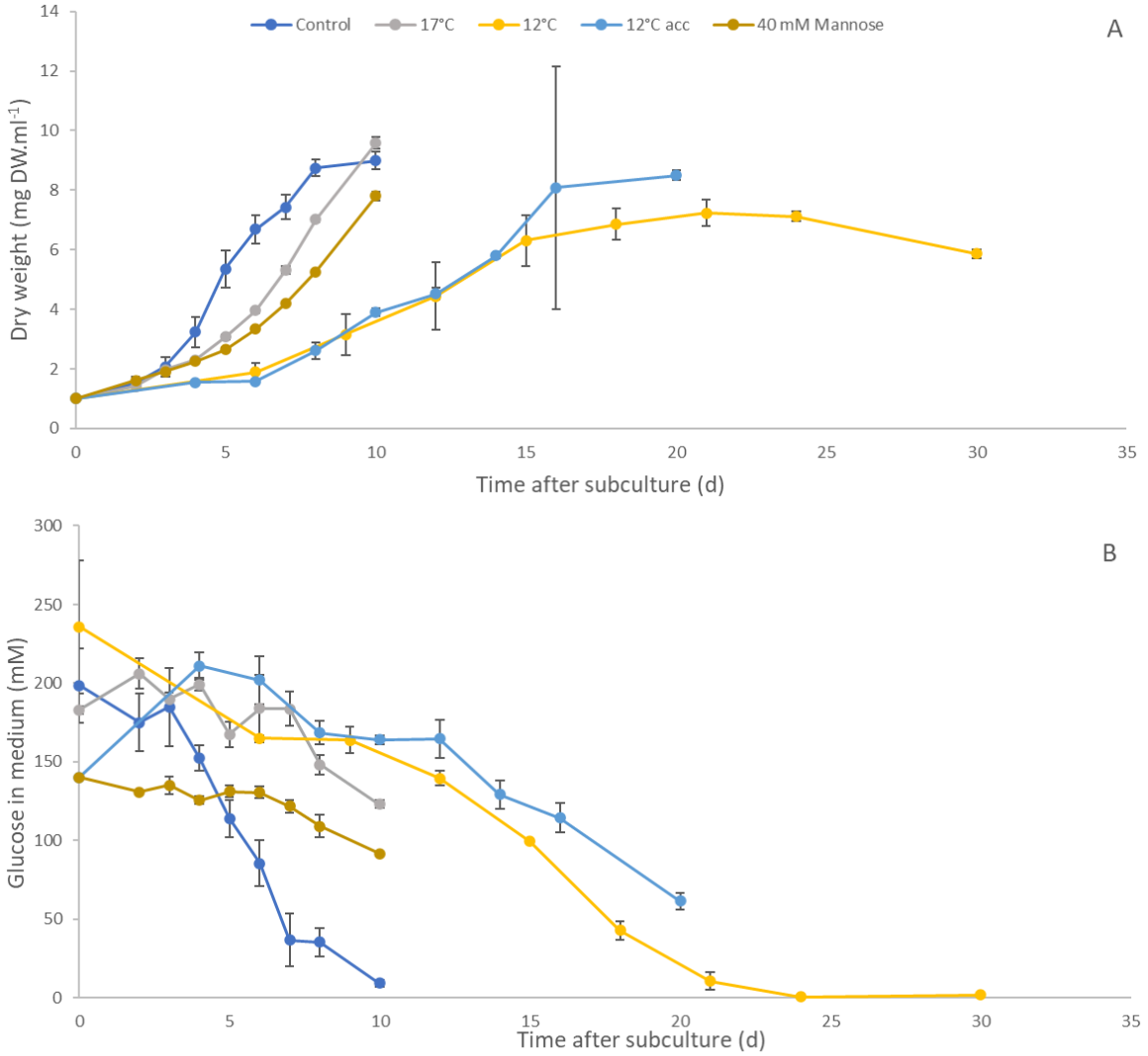


Figure 6.1: *Growth profiles of Arabidopsis suspension cultures grown under different conditions. (A) Dry weight accumulation and (B) glucose remaining in medium for Arabidopsis cultures. Each point is the mean of three independent flasks and error bars represent the SEM. In the labelling experiments biomass was harvested at mid-exponential phase, this was after 5.5 d of growth for the control conditions cultures, 7d of growth for the 17°C cultures, 12d of growth for the 12°C cultures, 14d of growth for the 12°C acclimated culture and 7d of growth for the mannose supplemented culture.*

6.2.1 Metabolic cost of growth

The metabolic costs associated with biomass production can be calculated from the flux distributions directly because biosynthetic metabolism for amino acids, lipids, and carbohydrates were included in the model, as were ancillary reactions that quantify the total requirement of ATP, reductant and each biosynthetic precursor (see Section 3.4 and 3.5). These costs will be referred to as the growth costs for the rest of this chapter. The production and biosynthetic requirements for ATP, NAD(P)H and $FADH_2$ are presented in Table 6.1 and the full flux distributions are presented in Appendix 7.

The two control cultures produced similar amounts of NADH and $FADH_2$ but control 2 produced a significantly higher amount of NADPH. This is probably a consequence of the increased flux through G6P dehydrogenase in control 2 (See Chapter 3). The 17°C and 12°C grown cultures produced less NADPH than the control cultures, likely due to decreased G6P dehydrogenase flux (Table 6.1). In the 12°C grown cultures the production of NADPH by the CCM was decreased enough to cause a significant increase in the transhydrogenase flux converting NADH to NADPH to meet biosynthetic requirement (Bykova *et al*., 1999, Cheung *et al*., 2013). The fact that the relative requirements for reductant and ATP for growth did not significantly change in the decreased temperature cultures suggests that although the absolute growth rate is reduced, the proportion of resources required for this growth does not change.

The acclimated 12°C culture had considerably different rates of production and requirement of ATP and reductant compared to the control cultures (Table 6.1). The decreased flux through G6P dehydrogenase and increased flux through succinate dehydrogenase caused significantly decreased production of NADPH and significantly increased production of $FADH_2$ respectively. However, the differences in the other parameters do not register as statistically significant due to large confidence intervals in the acclimated culture, and thus could be false negatives.

Therefore, although the results from 12°C acclimated culture are presented in figures and tables, this is for reference only. Due to the susceptibility of the acclimated culture to type 2 errors, the data obtained with the acclimated culture are not included in the analysis for the remainder of this chapter.

Table 6.1 *Production of and biosynthetic demand for ATP and reduced co-enzymes in cultures under different conditions*

Reaction	Relative flux under specified condition						
	Control 1	Control 2	17°C	12°C	12°C acclimated	Mannose	Mannitol
NADPH production by CCM	172.9 (165.6, 181.1)	**185.8 (177.1, 194.6)**	**156.4 (144.6, 168.3)**	**157.2 (148.4, 166.6)**	**119.7 (86.9, 160.8)**	**200.2 (190.2, 211.0)**	**154.6 (147.8, 161.6)**
NADPH requirement for biosynthesis	237.2 (222.9, 284.2)	225.8 (210.2, 239.3)	237.6 (220.1, 250.4)	255.9 (242.5, 267.3)	193.6 (99.7, 260.3)	**137.7 (114.5, 158.8)**	**277.1 (276.0, 278.8)**
NADH production by CCM	397.0 (382.0, 417.1)	406.5 (388.2, 428.5)	426.0 (388.2, 428.5)	409.9 (395.6, 426.3)	500.4 (396.4, 644.8)	**549.7 (518.8, 583.8)**	388.1 (381.5, 394.3)
NADH requirement for biosynthesis	16.8 (13.5, 19.4)	15.5 (12.2, 18.1)	13.2 (7.8., 16.8)	12.4 (0.0, 18.1)	0.0 (0.0, 23.0)	**7.2 (5.0, 9.1)**	**21.1 (18.4, 23.2)**
Trans-hydrogenase	64.3 (42.5, 82.0)	40.0 (16.3, 61.6)	81.2 (54.2, 103.0)	**98.7 (77.0, 117.8)**	73.9 (−61.5, 169.1)	**−62.4 (−96.3, −31.8)**	**122.5 (115.1, 129.7)**
Net NADPH production	0.0 (0.0, 0.0)	0.0 (0.0, 0.0)	0.0 (0.0, 0.0)	0.0 (0.0, 0.0)	0.0 (0.0, 61.0)	**62.4 (31.8, 96.3)**	0.0 (0.0, 0.0)
Net NADH production	351.0 (310.9, 397.0)	351.0 (310.9, 397.0)	331.7 (294.5, 381.8)	298.8 (266.7, 336.5)	426.5 (239.4, 702.8)	**542.5 (510.8, 577.5)**	**244.5 (240.2, 248.0)**
Net $FADH_2$ production	65.8 (60.4, 72.9)	69.9 (63.3, 77.7)	73.8 (67.6, 82.4)	65.9 (60.6, 72.0)	**102.9 (69.4, 149.7)**	**116.9 (106.0, 128.9)**	**58.2 (56.3, 59.9)**
Substrate level phosphorylation by CCM	170.6 (167.2, 178.9)	175.5 (167.2, 184.3)	185.9 (176.1, 197.0)	178.2 (169.3, 187.8)	157.9 (103.0, 226.8)	**241.5 (227.7, 256.1)**	166.49 (162.3, 169.8)
ATP requirement for biosynthesis	345.0 (324.3, 361.1)	328.3 (305.7, 347.9)	346.4 (320.9, 365.1)	361.1 (341.9, 377.4)	303.1 (155.7, 410.3)	**184.2 (153.2, 212.3)**	**396.3 (341.9, 377.4)**

The values in grey brackets are the 95% confidence limits calculated by parameter continuation. Fluxes which are significantly different from the control conditions are shown in bold.

The mannose-supplemented cultures had a significantly decreased relative growth requirement for ATP and reductant and a significantly increased relative production rate of NAD(P)H, $FADH_2$ and ATP. This allowed the entire growth requirement for ATP to be supplied by substrate level phosphorylation (Note that the extent to which the non-phosphorylating GAP dehydrogenase and the GABA shunt are active is not estimated here) and the transhydrogenase reaction to run in the direction of conversion of NADPH into NADH, to enter the electron transport chain reaction. This reveals that in mannose-supplement cultures the slowed growth rate is accompanied by a change in the allocation of resources between growth and maintenance.

The mannitol-supplemented culture had increased biosynthetic requirements for ATP and reductant, as well as significantly decreased production of NADPH and $FADH_2$ and increased transhydrogenase flux.

6.2.2 Metabolic costs of maintenance

The flux distributions offer two potential ways to estimate the maintenance costs (or, more precisely, the costs of any process not included in the model):

- Firstly, the flux distributions can be used to calculate the CCE. This describes the percentage of carbon taken up and metabolised by the cultures as glucose that is converted to new biomass. A low CCE means that only a small proportion of the metabolised carbon is used for growth and a large proportion is oxidised to produce ATP and/or reductant.

- Secondly, the ancillary reactions which track NADPH, NADH, $FADH_2$ and ATP production and consumption (Table 6.1), also allow for the estimation of the maximum potential production of ATP and reductant in excess of the requirement for biosynthesis. This excess is most conveniently expressed in terms of ATP equivalents, and increased production of excess ATP equivalents implies a larger maintenance cost. Note that these ancillary reactions quantify ATP equivalents because the specific requirements for NAD(P)H and ATP for maintenance cannot be determined separately. Moreover, these estimated ATP equivalents represent the maximum potential production of ATP equivalents, because the ATP bypasses (including metabolic futile cycles) that do not contribute to labelling cannot be defined in MFA (See Chapter3).

Figure 6.2 shows the CCE for each culture. The CCE for the cultures grown at 17°C or 12°C or in mannitol-supplemented medium were not significantly different from the CCE of the cultures grown under standard conditions. In contrast the culture grown in mannose-supplemented medium had a CCE significantly lower than that of the control cultures.

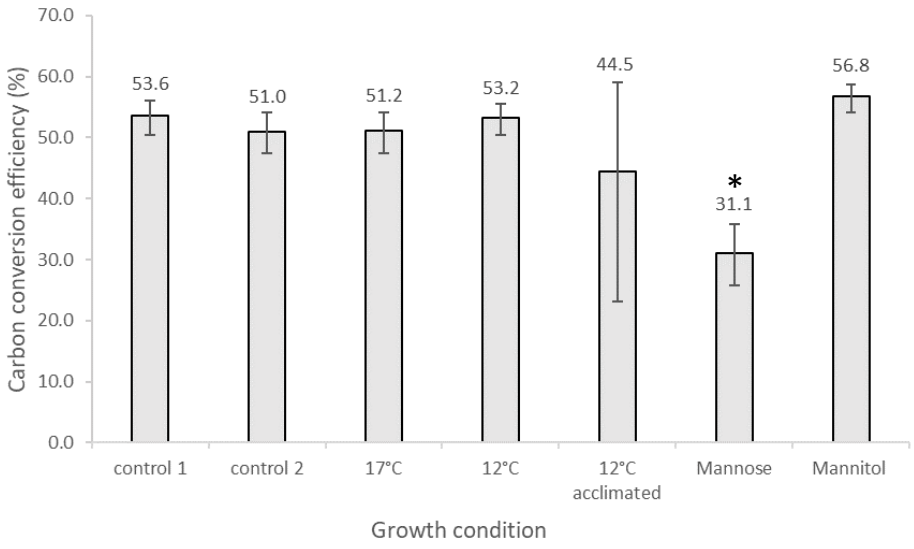


Figure 6.2: *Carbon conversion efficiency of Arabidopsis cell culture grown under different conditions. Error bars represent 95% confidence interval calculated by parameter continuation. Asterisks (*) represent significantly different CCE calculated by confidence interval overlap of net CO_2 production.*

The excess ATP and reductant export from the model is shown in Figure 6.3. The cultures grown at 17°C and 12°C did not produce a significantly different surplus of ATP equivalents relative to the control cultures. The mannose-supplemented cultures produced a significantly larger excess of ATP equivalents, and the mannitol supplemented cultures produced a significantly smaller excess of ATP equivalents than the control culture. The culture acclimated to growth at 12°C produces a larger excess of ATP and reductant but the significance of this difference is obscured by the large confidence intervals. (Figure 6.3).

Previous discussion has highlighted that:

- The changes in the flux distribution within the CCM at low temperature were limited to relatively few reactions (Chapter 4).
- The biosynthetic requirements for NAD(P)H and ATP were not significantly different between low temperature and control cultures (Table 6.1).
- There was no significant change in the CCE or excess ATP equivalents available for maintenance between low temperature and control cultures (Figures 6.2 and 6.3).

This suggests that extensive rearrangement of flux distribution in the CCM is not required for *Arabidopsis* suspension cultures to grow at temperatures as low as 12°C, at least for the duration of the labelling periods used here. This is not surprising considering that both 17°C and 12°C are well within the tolerable growth temperatures for the Landsberg *erecta* ecotype from which this suspension culture was first isolated (May and Leaver, 1993; Hannah *et al*., 2006).

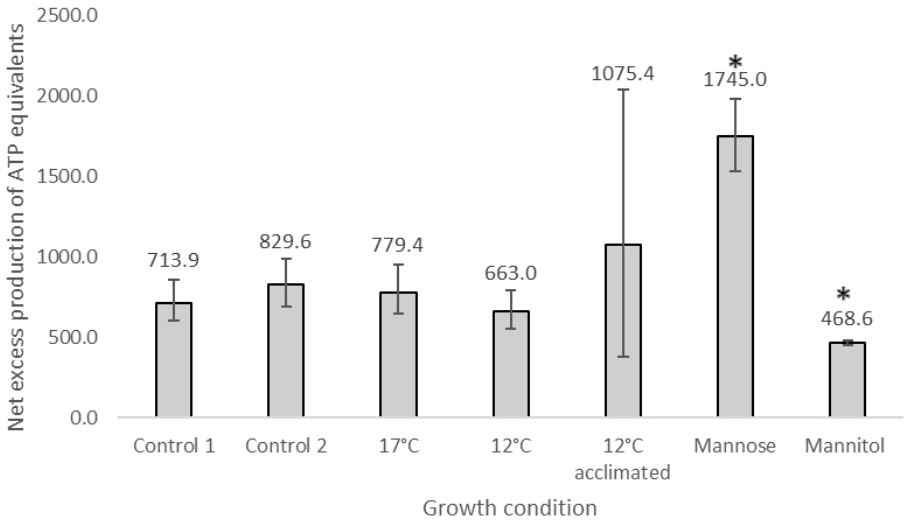


Figure 6.3: *Production of excess ATP and reductants as ATP equivalents in Arabidopsis cell suspension cultures grown under different conditions. Error bars represent 95% confidence interval calculated by parameter continuation. Asterisks (*) represent significantly different flux calculated by confidence interval overlap.*

In contrast the mannose-supplemented culture did exhibit a significant rearrangement of flux through the CCM (Chapter 5), decreased relative growth requirements (Table 6.1), a decreased CCE and an increased relative production rate of ATP equivalents. This implies that a larger proportion of all metabolic resources are being partitioned into maintenance and a correspondingly smaller proportion into growth, probably a consequence of the phosphate sequestering effect of mannose (see Chapter 5). The mechanism underlying this change in partitioning is unclear, but is consistent with the idea that under phosphate-limited conditions, cells are likely to have evolved to conserve ATP by reducing the growth rate, resulting in an increase in the relative allocation of resources to maintenance. The absolute maintenance costs may also be increased due to disruption of processes by the limited ATP availability.

It has been suggested that 'stress' could be defined as conditions that cause a rearrangement of flux distribution in the CCM (Williams *et al*., 2010). Based on this definition, mannose supplementation and a decreased growth temperature could be considered as stress conditions. However, later authors suggest that stress could be

defined as any condition which causes a diversion of metabolic resources from growth to maintenance (Cheung *et al*., 2013). By this definition of stress the mannose-supplemented cultures are stressed, while the 12°C or 17°C grown cultures are merely slow growing.

6.2.3 Maintenance costs and PEP partitioning

In previous chapters PCA has been conducted on synthetic datasets based on 1000 rounds of Monte Carlo simulation of the flux distributions from each condition. These synthetic datasets can be used to investigate the flux distributions further by plotting the estimated fluxes through individual reactions from each Monte Carlo simulation.

In Figure 6.4 the CCE for each of the 6000 Monte Carlo simulated flux solutions (1000 from each culture condition) are plotted against the excess production of ATP and NAD(P)H as ATP equivalents from each simulated flux distribution. This shows an inverse relationship between the two (r^2=0.99).

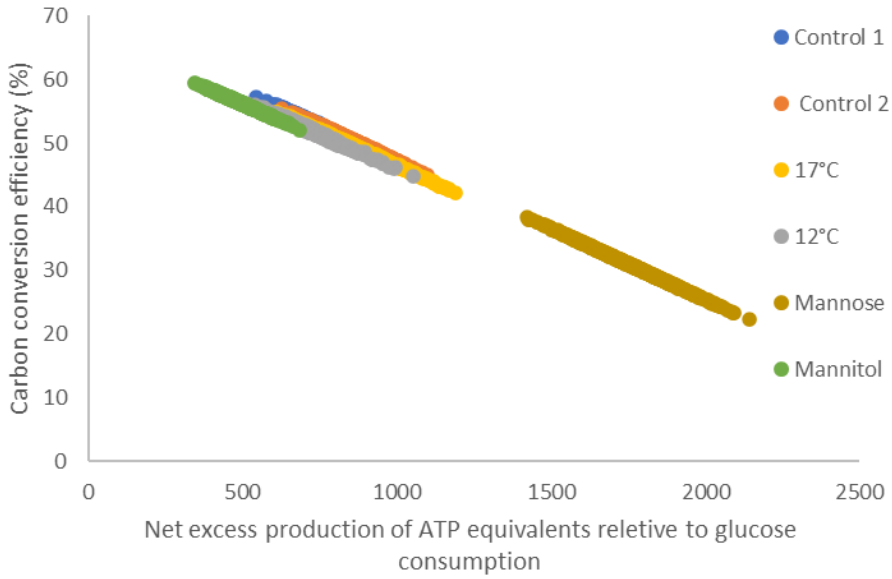


Figure 6.4: *Scatter plot derived from Monte Carlo analysis of synthetic data sets showing the inverse relationship between the CCE and the production of excess ATP and NAD(P)H as ATP equivalents.*

The Monte Carlo simulations from 12°C acclimated cultures were removed from Figure 6.4 because they obscured the differences between the different conditions discussed above, but the 12°C acclimated flux distributions still fit the same line (r^2=0.99) when 12°C acclimated Monte Carlos were included).

The inverse relationship between the CCE and excess production of ATP equivalents suggest that the two methods for estimating the cost of maintenance respiration are equivalent, and this may be an axiomatic consequence of the model. The separation of the Monte Carlo simulations from the mannose supplemented flux distributions mirrors the decreased CCE and increased excess ATP equivalent production in the mannose-supplemented cultures.

Slight shifting of the 17°C, 12°C and mannitol-supplemented cultures along the vertical axis in figure 6.4 can be seen. This shifting is likely a consequence of the differences in biomass composition altering the amount of CO_2 released per unit of biomass produced. The altered biomass composition could also explain the observation that both the CCE and the excess ATP equivalent production are marginally higher in control one than in the 12°C culture.

The results in Sections 6.2.1 and 6.2.2 show that growth rates might slow as a consequence of increased allocation of resources to maintenance, or due to other factors, such as a lower growth temperature. Thus, the growth rate does not necessarily correlate with the growth and maintenance costs. However, the relative cost of growth and maintenance did correlate with the partitioning of PEP into the TCA cycle (via mitochondrial pyruvate kinase or PEP carboxylase) or into biosynthesis (Figure 6.5). It is unsurprising that a greater carbon partitioning into the TCA cycle results in a greater potential excess of ATP and reductant being produced. The non-linearity of the relationship is likely because multiple reactions throughout the CCM produce and consume ATP, reductant or CO_2, so the relative production rates are unlikely to be described by a simple linear relationship.

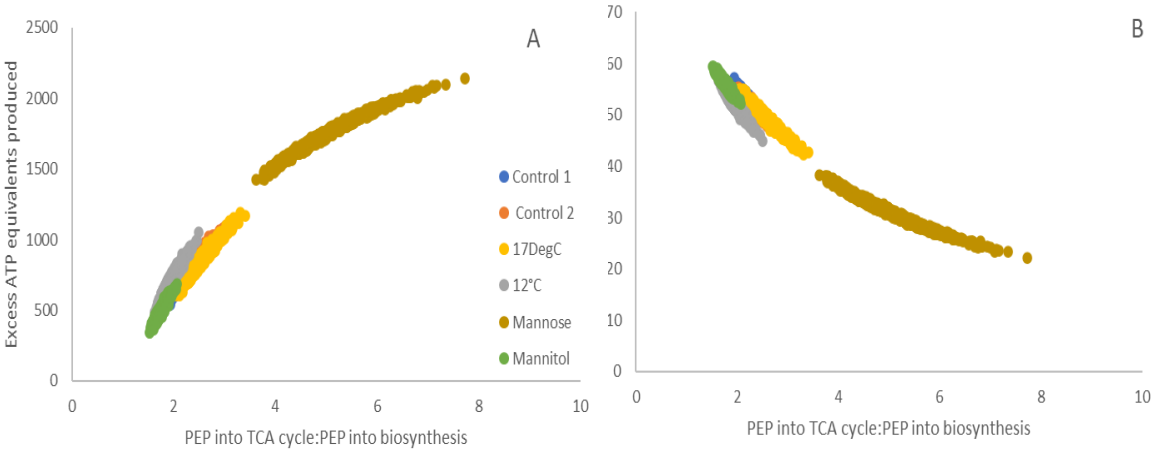


Figure 6.5: *Correlation between the ratio of PEP partitioning into the TCA cycle and biosynthesis and either (A) the excess production of ATP equivalents or (B) CCE. 12°C are not included because they obscured the rest of the graph.*

6.3 Glucose 6-phosphate utilisation and growth rate

Section 6.2 shows that the maintenance costs do not correlate with growth rate. However, all the cultures that displayed slowed growth rates also displayed an altered pattern of G6P utilisation. The cultures grown at 17°C and 12°C and the mannose-supplemented cultures showed significantly increased relative flux through phosphoglucoisomerase, the first step of glycolysis, and significantly decreased relative flux through G6P dehydrogenase, the first step of the OxPPP (Figure 6.6). Chapters 4 and 5 argue that this change in the utilisation of glucose is unlikely to be a kinetic effect of decreased temperature or of phosphate sequestration by mannose.

This change in the OxPPP:glycolysis ratio is also seen in *Arabidopsis* suspension cultures exposed to increased temperature (Williams *et al*., 2010) and phosphate deprivation (Masakapalli *et al*., 2014a). Moreover, the same effect has been recorded in *E. coli* and *Bacillus* species in continuous cultures growing at decreased rates (Nanchen *et al*., 2006; Tännler *et al*., 2008; Valgapea *et al*., 2011) as well as *Saccharomyces cerevisiae* during fermentation (Li *et al*., 2015).

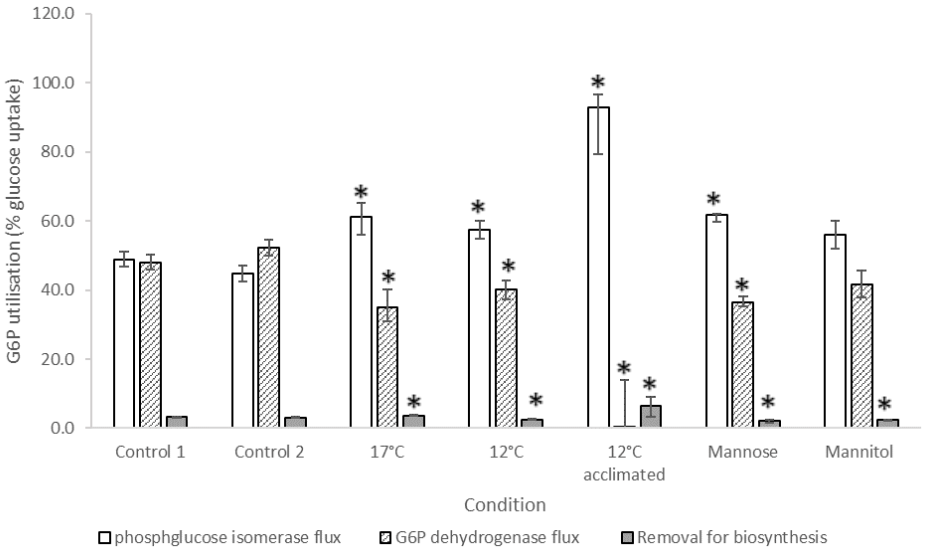


Figure 6.6: *Utilisation of the combined plastidic and cytosolic G6P pool in Arabidopsis cell suspension cultures grown under different conditions. Error bars represent 95% confidence intervals calculated by parameter continuation. Asterisks (*) represent fluxes significantly different from the relevant control.*

The OxPPP is a source of NADPH, as well as aromatic amino acid precursors E4P and R5P (Jiang *et al*., 2022). It is possible that the relative increase in the proportion of G6P entering the OxPPP in faster growing cultures is related to the increased biosynthetic requirements for NADPH, E4P and R5P. However, plotting the biosynthetic requirement for E4P, R5P or NADPH against the OxPPP:glycolysis ratio from each Monte Carlo simulation shows that there is no correlation between the requirement for OxPPP products and the OxPPP:glycolysis ratio (Figure 6.7).

Moreover, there is a negative correlation between the NADPH production by the CCM and the NADPH requirement for biosynthesis, as observed by Masakapalli *et al*. (2013). This suggests that the function of the OxPPP in *Arabidopsis* cell suspension culture is not solely to provide NADPH, E4P and R5P for growth. If this was the case, a positive correlation between the supply and the demand would be seen.

It is possible that the OxPPP provides NADPH for maintenance processes. However, plotting scatter graphs from the Monte Carlo simulations shows that NADPH production by the OxPPP does not change with the excess ATP equivalents produced (Figure 6.8), suggesting that OxPPP flux does not influence the amount of ATP equivalents available for maintenance.

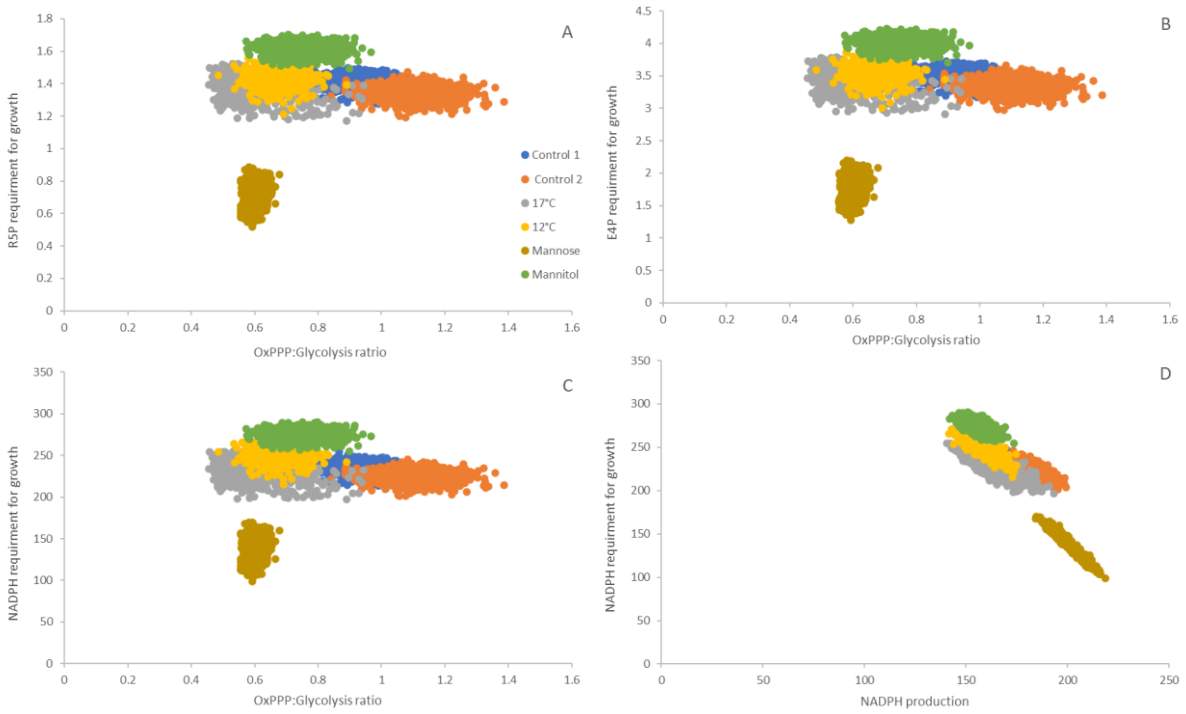


Figure 6.7: *Scatter plots derived from Monte Carlo analysis of synthetic data sets showing the relationship between the OxPPP:glycolysis flux ratio and the growth requirement for (A) E4P, (B) NADPH, and (C) R5P. (D) Analysis of the same datasets showing the inverse relationship between NADPH production and the growth requirement for the coenzyme.*

Previous thinking would suggest that all changes in the flux distribution in the CCM are related to an alteration in the relative requirements for ATP, reductant and biosynthetic precursors for growth and maintenance processes. However, flux through the OxPPP is not strongly correlated with growth requirements for E4P, R5P or NADPH, nor by the maintenance requirement for NADPH, and yet relative flux through the OxPPP varies with the growth rate and the rate of glucose uptake. The role of the OxPPP in metabolism is therefore unclear. It is possible that flux through the OxPPP is related to the growth rate in a way which is independent of requirements for NADPH, E4P or R5P. Further research is

required to fully explain the changes in OxPPP flux with growth rate. Flux through the OxPPP might be better defined if MID data from histidine, tyrosine and tryptophan were available.

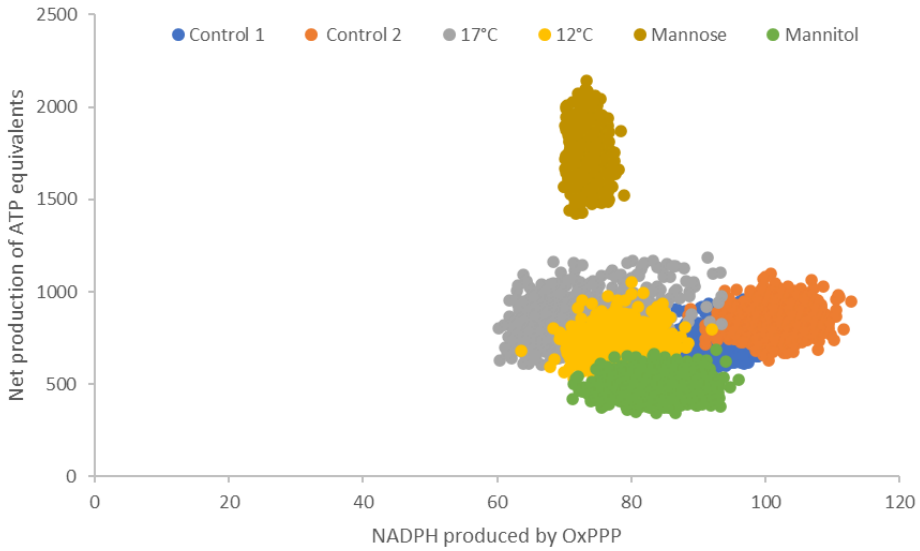


Figure 6.8: *Scatter plot derived from Monte Carlo analysis of synthetic data sets showing the lack of correlation between NADPH production by OxPPP and the production of excess ATP equivalents.*

Another important consideration is the extent to which this OxPPP and growth rate correlation occurs in whole plants. In the MS medium used for cell suspension cultures the glucose concentration is very high (166.7 mM in this project). In heterotrophic tissues in plants it is unlikely that the intercellular sugar concentrations would be this large. Therefore *in planta* the rate of sugar uptake and phosphorylation may be lower and thus the availability of G6P will be lower than in this study, which, in turn may affect the relative flux through phosphoglucoisomerase and G6P dehydrogenase.

6.4 Conclusions

Based on the flux distributions for *Arabidopsis* cell suspension cultures grown at different rates obtained in chapters 3, 4 and 5 this chapter presents an analysis of the relationship between growth rate, resource allocation between growth and maintenance and flux distribution through the CCM. The analysis conducted here provides the following conclusions:

1. Decreased growth rate can be associated with a decrease in the relative allocation of resources to growth.

2. The growth rate can also slow independently of the relative allocation of ATP and reductant.

3. The growth rate is associated with an altered utilisation of G6P, with decreased flux through the OxPPP at slower growth rates. Previous thinking about the role of the OxPPP cannot explain the dynamics noted here.

Chapter 7: Concluding remarks

The main aim of this project was to use MFA to investigate the relationship between the growth rate and flux distribution in the CCM, and its ability to provide ATP, reductant and biosynthetic precursors to support growth and maintenance processes. Two different conditions were chosen to slow the growth rate of *Arabidopsis* suspension cultures; mildly decreased temperatures and medium supplemented with mannose. Both conditions slowed the growth rate of the cell cultures to similar extents, therefore allowing the aim to be achieved by conducting MFA under the chosen conditions.

The scope of the analysis was expanded by using a novel refinement to MFA modelling to track ATP and NAD(P)H production and utilisation. This new approach allowed determination of the statistical confidence limits of the estimates of coenzyme fluxes and quantification of the proportions of ATP and NAD(P)H required for growth and available for maintenance. This represents a technical improvement on the approaches typically employed to estimate resource allocation in bacterial MFA, which are restricted to analysis of best-fit flux estimates without any indication of the statistical reliability of the calculated values (see Long and Antoniewicz, 2019b; Dahle *et al.,* 2022; Oates and Antoniewicz, 2022 for recent examples).

7.1 Effect of low temperature on the CCM

Chapter 4 shows that decreasing the growth temperature of cell suspension to 17°C or 12°C slowed the growth rate and altered the biomass composition of the cultures. Decreased temperatures also induced a significant change in the relative fluxes of some reactions in the OxPPP and glycolysis. Interestingly, there was no significant change in the allocation of ATP and reductant between growth and maintenance processes. These results suggest that the flux distribution in the CCM may not be as sensitive to decreased temperature as has been previously suggested (Kaplan *et al*., 2004).

7.2 Effect of mannose supplementation on the CCM

Mannose is readily absorbed by *Arabidopsis* cells and phosphorylated to mannose 6-phosphate. It was anticipated that mannose 6-phosphate would inhibit phosphoglucoisomerase, thus slowing glycolysis and decreasing the growth rate. Chapter 5 shows that mannose supplementation did slow the growth rate and alter the biomass composition of cultures, but that this was likely due to sequestering inorganic phosphate as mannose 6-phosphate. This phosphate deprivation induced a significant rearrangement of the flux distribution throughout the CCM, likely as part of a response to limited ATP levels. Mannose supplementation also induced altered allocation of ATP and NAD(P)H between growth and maintenance. Presumably this altered resource allocation was related to decreased demand of resources for biosynthetic processes as the growth rate slowed.

7.3 The relationship between growth rate and flux distribution

Two facets of the relationship between growth and the CCM flux distribution were identified:

Firstly, a decreased growth rate did not necessarily require a change in the allocation of ATP and reductant between growth and maintenance. Although altered resource allocation between growth and maintenance processes could accompany a change in the growth rate, reallocation of resources was not a prerequisite for an alteration in growth. Thus, cultures supplemented with mannose had a slowed growth rate and an altered resource allocation, while the cultures grown at decreased temperatures had a slowed growth rate without altered resource allocation. This suggests that the decreased metabolic demands for co-enzymes and biosynthetic precursors associated with growth at lowered temperatures were accompanied by an equivalent proportional decrease in the demands associated with maintenance processes

Secondly, The change in growth rate was associated with a change in the partitioning of G6P between glycolysis and the OxPPP. Cultures with a slower growth rate (irrespective of the experimental perturbation), partitioned a smaller proportion of the G6P pool into the OxPPP via G6P dehydrogenase and a greater proportion was metabolised through glycolysis via phosphoglucoisomerase. Further research is required to understand the mechanism that underlies this correlation, and its biological relevance.

This correlation between growth rate and G6P partitioning has not previously been observed in plant metabolism, and provides an interesting new insight into the functioning of the CCM. A similar effect of slowed growth rate on G6P partitioning has been noted in bacteria (Nanchen *et al.,* 2005; Tännler *et al.,* 2008). However these studies were not able to assess the allocation of resources between growth and maintenance.

The conclusion that growth rate and resource allocation are related to different alterations in flux distribution in the CCM raises an important consideration about metabolic investigations of cells under stress or alternative growth regimes. MFA is often used to compare flux distributions in cells under different conditions to investigate the response to a specific stressor, which often slows the growth rate. While specific metabolic effects of stressors are clearly evident, the insight provided here suggests that it is also necessary to differentiate between specific stress-induced effects and the effects related to changes in growth rate. In an energetic sense ‘stress’ has been defined as anything that causes an increase in the maintenance costs of a cell (Cheung *et al*., 2013). When investigating metabolic effects of certain stressors in future MFA studies, it may be necessary to include a control, that grows at a reduced rate but is not exposed to the same stress as the experimental treatment. This would allow identification of reactions that are truly stress responsive and those that are simply associated with a slowed growth rate. For MFA studies in *Arabidopsis* suspension cultures a mild decrease in growth temperature could be a useful way to slow the rate of growth without inducing stress.

7.4 Future work

7.4.1 Building on the conclusions of this thesis

There are several lines of enquiry which would be logical next steps for validating, and building on the conclusions of this thesis are suggested.

Firstly, an investigation of labelled CO_2 production. MFA allows an estimation of the rate of CO_2 production based the fluxes through various decarboxylation reactions in the network. INCA contains a tracer simulation function which predicts the labelling pattern of metabolites assuming a given label source and flux distribution. The simulated labelling of CO_2 could be compared to labelling of CO_2 produced from cultures grown in MS medium containing positionally radiolabelled glucose. This would allow an assessment of the validity of the calculated flux distributions (Masakapalli *et al.*, 2013).

A second parameter that can be calculated from the flux distribution is the respiratory quotient (oxygen uptake/ CO_2 release). A Clark oxygen electrode could be used to measure the oxygen uptake and the corresponding CO_2 release could be monitored directly by infra-red gas analysis to permit experimental determination of the respiratory quotient, which could then be compared to the corresponding value predicted by the flux distributions.

Thirdly, additional analytical techniques could be used to validate some conclusions. Chapter 5 suggests that supplementation of cultures with mannose induced a significant change in the flux distribution, growth rate and biomass composition because mannose 6-phosphate accumulated and sequestered inorganic phosphate. This proposal could be tested using *in vivo* ^{31}P nuclear magnetic resonance spectroscopy, which provides a useful technique for quantifying the accumulation of mannose 6-phosphate and sequestration of inorganic phosphate, and assessing the impact on intracellular ATP levels (Ratcliffe and Shachar-Hill, 2001). It may also be useful to include mannose metabolism in the model in INCA. Mannose metabolism was not included in this project to make comparison between the flux maps feasible, but it could account for any potential dilution of labelling in F6P and

6 carbon cell wall carbohydrates derived from M6P. Comparison of different model structures could help to identify which pathways of mannose metabolism improve the fit of the data, and thus are significantly active in *Arabidopsis* suspension cultures.

This project also made the assumption that the amino acid composition in *Arabidopsis* would not be significantly different from that of *E.coli*. However, this may not be the case. Although the results in chapter 3 suggest that a change in the amino acid composition has an insignificant effect on flux through the CCM, it would be ideal to have the most accurate amino acid composition data possible. The amino acid quantification method used by Masakapalli *et al*. (2013, 2014a) could be refined by the use of internal isotopic standards using an approach similar to that described by Long and Antoniewicz (2014) and the resulting composition used for future flux maps.

7.4.2 Further studies

This project notes a relationship between the growth rate and partitioning of G6P between glycolysis and the OxPPP. However, the existing data do not reveal the mechanism underlying this relationship. It might be possible to examine the relationship between G6P partitioning and growth more directly by applying MFA to cultures which are supplemented with specific compounds that perturb G6P metabolism. This approach would avoid the complicating secondary consequences of the perturbations employed in this thesis.

G6P dehydrogenase could be inhibited by polydatin, which has been shown to inhibit the enzyme *in vivo* in human tumour cells (Mele *et al*., 2019). However it is unclear whether polydatin will be taken up by *Arabidopsis* cells. An alternative G6P dehydrogenase inhibitor is 6-aminonicotinamide (Köhler *et al*., 1970), which has been used to block the OxPPP in *Arabidopsis* suspension cultures previously (Garlick *et al*., 2002; Smith *et al*., 2019). However, 6-aminonicotinamide operates by generating an analogue of $NADP^+$, which may interfere with multiple $NADP^+$ dependent reactions, thus potentially obscuring the specific effect of limited flux through the G6P dehydrogenase reaction. Phosphoglucoisiomerase

has been shown to be inhibited by fructose 1-phosphate or E4P *in vitro* (Zalitis and Oliver, 1966; Backhausen *et al*., 1997; Preiser *et al*., 2020). It is unlikely that sugar phosphates will be absorbed by the cells, but cultures could be supplemented with erythrose and fructose on the assumption that they will be phosphorylated. A negative control could be provided by using mannoheptulose to inhibit hexoskinase, thus preventing G6P production (Pego *et al*., 1999).

There are few other obvious perturbations that could be used to slow the growth rate of the cultures. Initially it was postulated that the growth rate of cell suspension cultures could be restricted by culturing in MS medium containing a limiting concentration of glucose. However, early work in this project, not presented in the thesis. showed that growing *Arabidopsis* suspensions at lower glucose concentrations did not slow the growth rate throughout the main phase of the culture cycle. Rather, the cultures depleted the available glucose and entered a stationary phase sooner.

This suggests that glucose uptake only becomes a limiting factor in growth at very low concentrations. Steady state MFA would not be suitable for studying cultures in decreased glucose concentrations. This is because by the time the glucose concentration was low enough to limit the growth rate the cultures would not be able to maintain a metabolic steady state for long enough to allow MFA, since the concentration of glucose would keep decreasing, further constraining metabolism. However, isotopically non-stationary MFA might provide a viable strategy for investigating the metabolic response to glucose limited conditions. Non-stationary MFA is based on labelling time courses from minutes to hours, rather than label distribution at steady state. Therefore non-stationary MFA could be used to investigate the effects of conditions in which the metabolic state of the system changes faster than the time taken to reach an isotopically steady state.

Using non-stationary MFA to understand the effects of limited glucose concentration on CCM, would be complicated because lowering the concentration of glucose will alter the water potential of the growth medium. The effects of increased osmotic pressure have been

investigated using MFA previously (William *et al*., 2010), but investigating the effect of a decreased osmotic pressure could also be interesting. One option for investigating glucose deprivation and decreased osmotic pressure would be to perform non-stationary MFA on *Arabidopsis* cultures grown in variations of MS media. One culture could be grown in regular MS medium, another in MS medium with all the components in the same ratio as regular MS but a lower overall concentration, a third in regular medium with some of the glucose replaced with mannitol (as an osmotic control) and a fourth in a reduced concentration medium with some glucose replaced with mannitol. These different MS media would show the effect of limited glucose availability independently of decreased osmotic pressure, of decreased osmotic pressure and the effect of both combined.

7.5 Summary

This thesis presents an investigation into the relationship between growth rate and flux distribution in the CCM of *Arabidopsis* suspension cultures. Two perturbations were used to slow the growth rate: decreased growth temperature and supplementation of the growth medium with mannose. A novel modelling approach was used to quantify the requirement for ATP, reductant and precursors for biosynthesis and assess the potential ATP and reductant available for other processes all with associated confidence intervals.

The results provide insights into the specific effects of mildly decreased growth temperature and mannose supplementation on flux distribution in the CCM. Furthermore, this project identified the lack of a clear correlation between the growth rate and the allocation of ATP and reductant between growth and maintenance processes as well as a novel correlation between growth rate and G6P partitioning between the OxPPP and glycolysis. These results could be used to inform the design of future MFA experiments and introduces a potential new line of investigation into the role of G6P partitioning in growth and metabolism.

References

Allen, D.K., Laclair, R.W., Ohlrogge, J.B., Shachar-Hill, Y., (2012) Isotope labelling of Rubisco subunits provides in vivo information on subcellular biosynthesis and exchange of amino acids between compartments. Plant, Cell & Environment *35,* 1232–1244.

Allen, D.K., Young, J.D., (2013) Carbon and nitrogen provisions alter the metabolic flux in developing soybean embryos. Plant Physiology *161*, 1458–1475.

Amthor, J.S., (2000) The McCree–de Wit–Penning de Vries–Thornley respiration paradigms: 30 years later. Annals of Botany *86*, 1–20.

Antoniewicz, M.R., (2021) A guide to metabolic flux analysis in metabolic engineering: Methods, tools and applications. Metabolic Engineering. *63,* 2-21.

Antoniewicz, M.R., (2013) ^{13}C metabolic flux analysis: optimal design of isotopic labelling experiments. Current Opinion in Biotechnology, *24*, 1116–1121.

Antoniewicz, M.R., Kelleher, J.K., Stephanopoulos, G., (2011) Measuring deuterium enrichment of glucose hydrogen atoms by gas chromatography/mass spectrometry. Analytical Chemistry. *83*, 3211–3216.

Antoniewicz, M.R., Kelleher, J.K., Stephanopoulos, G., (2007a). Elementary metabolite units (EMU): A novel framework for modelling isotopic distributions. Metabolic Engineering *9,* 68–86.

Antoniewicz, M.R., Kelleher, J.K., Stephanopoulos, G., (2007b) Accurate Assessment of Amino Acid Mass Isotopomer Distributions for Metabolic Flux Analysis. Analytical Chemistry. 79, 7554–7559.

Antoniewicz, M.R., Kelleher, J.K., Stephanopoulos, G., (2006) Determination of confidence intervals of metabolic fluxes estimated from stable isotope measurements. Metabolic Engineering *8,* 324–337.

Antoun, M., Ouellet, F., (2013) Growth temperature affects inflorescence architecture in *Arabidopsis thaliana*. Botany *91,* 642–651.

ap Rees, T., Burrell, M.M., Entwhistle, T.G., Hammond, J.B.W., Kirk, D., Kruger, N.J., (1989) Effects of low temperature on the respiratory mechanism of carbohydrates by plants. In: Plants and temperature. Symposia of the Society for Experimental Biology 42 , S.P. Long & F.I. Woodward, eds. Society for Experimental Biology, Cambridge. pp. 377-393.

Aslam, M., Fakher, B., Ashraf, M.A., Cheng, Y., Wang, B., Qin, Y., (2022) Plant low-temperature stress: signalling and response. Agronomy *12,* 702-724.

Atkin, O.K., Bruhn, D., Hurry, V.M., Tjoelker, M.G., (2005) The hot and the cold: unravelling the variable response of plant respiration to temperature. Functional Plant Biology. *32,* 87–105.

Atkin, O.K., Tjoelker, M.G., (2003) Thermal acclimation and the dynamic response of plant respiration to temperature. Trends in Plant Science *8,* 343–351.

Backhausen, J.E., Jöstingmeyer, P., Scheibe, R., (1997) Competitive inhibition of spinach leaf phosphoglucose isomerase isoenzymes by erythrose 4-phosphate. Plant Science *130,* 121–131.

Bahaji, A., Sánchez-López, Á.M., Diego, N.D., Muñoz, F.J., Baroja-Fernández, E., Li, J., Ricarte-Bermejo, A., Baslam, M., Aranjuelo, I., Almagro, G., Humplík, J.F., Novák, O., Spíchal, L., Doležal, K., Pozueta-Romero, J., (2015) Plastidic phosphoglucose isomerase is an important determinant of starch accumulation in mesophyll cells, growth, photosynthetic capacity, and biosynthesis of plastidic cytokinins in *Arabidopsis*. PLoS ONE *10*, e0119641.

Banaś, A.K., Krzeszowiec, W., Dobrucki, J., Gabryś, H., (2010) Mannose, but not glucose or sucrose, disturbs actin cytoskeleton in *Arabidopsis thaliana* leaves. Acta Physiologiae Plantarum *32,* 773–779.

Baskin, T., Remillong, E., Wilson, J., (2001) The impact of mannose and other carbon sources on the elongation and diameter of the primary root of *Arabidopsis thaliana*. Functional Plant Biology *28,* 481-488.

Borsani, O., Valpuesta, V., Botella, M.A., (2001) Evidence for a role of salicylic acid in the oxidative damage generated by NaCl and osmotic stress in *Arabidopsis* seedlings. Plant Physiology *126*, 1024–1030.

Boyer, J.S., (1982) Plant productivity and environment. Science *218,* 443–448.

Breeze, V., Elston, J., (1983) Examination of a model and data describing the effect of temperature on the respiration rate of crop plants. Annals of Botany *51,* 611–616.

Brouquisse, R., James, F., Raymond, P., Pradet, A., (1991). Study of glucose starvation in excised maize root tips. Plant Physiology *96,* 619–626.

Bunn, H.F., Higgins, P.J., (1981) Reaction of monosaccharides with proteins: possible evolutionary significance. Science *213,* 222–224.

Büttner, M., Truernit, E., Baier, K., Scholz-Starke, J., Sontheim, M., Lauterbach, C., Huss, V. a. R., Sauer, N., (2000) AtSTP3, a green leaf-specific, low affinity monosaccharide-H^+ symporter of *Arabidopsis thaliana*. Plant, Cell & Environment *23,* 175–184.

Bykova, N.V., Rasmusson, A.G., Igamberdiev, A.U., Gardeström, P., Møller, I.M., (1999) Two separate transhydrogenase activities are present in plant mitochondria. Biochemical and Biophysical Research Communications *265*, 106-111.

Challa, H., (1976). An analysis of the diurnal course of growth, carbon dioxide exchange and carbohydrate reserve content of cucumber. Agricultural Research Report 861. Wageningen: Centre for Agrobiological Research.

Cheng, Y.-S., Zheng, Y., VanderGheynst, J.S., (2011) Rapid quantitative analysis of lipids using a colorimetric method in a microplate format. Lipids *46,* 95–103.

Cheung, C.Y.M., Williams, T.C.R., Poolman, M.G., Fell, D.A., Ratcliffe, R.G., Sweetlove, L.J., (2013) A method for accounting for maintenance costs in flux balance analysis improves the prediction of plant cell metabolic phenotypes under stress conditions. The Plant Journal *75,* 1050–1061.

Chiba, Y., Mineta, K., Hirai, M.Y., Suzuki, Y., Kanaya, S., Takahashi, H., Onouchi, H., Yamaguchi, J., Naito, S., (2013) Changes in mRNA stability associated with cold stress in *Arabidopsis* cells. Plant Cell Physiology 54, 180–194.

Chubukov, V., Uhr, M., Le Chat, L., Kleijn, R.J., Jules, M., Link, H., Aymerich, S., Stelling, J., Sauer, U., (2013) Transcriptional regulation is insufficient to explain substrate-induced flux changes in *Bacillus subtilis*. Molecular Systems Biology *9,* 709.

Ciereszko, I., Kleczkowski, L.A., (2002) Glucose and mannose regulate the expression of a major sucrose synthase gene in *Arabidopsis* via hexokinase-dependent mechanisms. Plant Physiology and Biochemistry *40,* 907–911.

Cocucci, S.M., Morgutti, S., Abruzzese, A., Alisi, C., Yahye, A.H., Espen, L., (1993) Response of seedlings of radish (*Raphanus sativus*) to osmotic shock and external hydrostatic pressure. Physiologia Plantarum *87*, 609-615.

Cook, D., Fowler, S., Fiehn, O., Thomashow, M.F., (2004) A prominent role for the CBF cold response pathway in configuring the low-temperature metabolome of *Arabidopsis.* Proceedings of the National Academy of Sciences of the USA *101,* 15243–15248.

Cosgrove, D.J., (2005) Growth of the plant cell wall. Nature Reviews of Molecular Cell Biology *6,* 850–861.

Crown, S.B., Antoniewicz, M.R., (2013) Publishing ^{13}C metabolic flux analysis studies: A review and future perspectives. Metabolic Engineering *20,* 42–48.

Dahle, M.L., Papoutsakis, E.T., Antoniewicz, M.R., (2022) ^{13}C-metabolic flux analysis of *Clostridium ljungdahlii* illuminates its core metabolism under mixotrophic culture conditions. Metabolic Engineering *72,* 161–170.

de Witt, T., Brouwer, R., (1969) The simulation of photosynthetic systems In: Productivity of photosynthetic systems: models and methods Setlik I, eds. Trebon, Czechoslovakia: International Biological programme, Intersectional Photosynthesis Liaison Group, Czeckoslovak National Committee (Czechoslovak Academy of Sciences: Institute of Microbiology, Laboratory of Algology), 16-32.

Denison, R.F., Nobel, P.S., (1988) Growth of *Agave deserti* without current photosynthesis. Photosynthetica (Praha) *22,* 51–57.

Draeger, C., Ndinyanka Fabrice, T., Gineau, E., Mouille, G., Kuhn, B.M., Moller, I., Abdou, M.-T., Frey, B., Pauly, M., Bacic, A., Ringli, C., (2015) *Arabidopsis* leucine-rich repeat extensin (LRX) proteins modify cell wall composition and influence plant growth. BMC Plant Biology *15,* 155.

Dyson, J.E.D., Noltmann, E.A., (1969) Conformational states of native and denatured phosphoglucose isomerase. I. Titration of exposed and buried amino acid residues. Biochemistry *8,* 3533–3543.

El-Khatib, R.T., Good, A.G., Muench, D.G., (2007) Analysis of the *Arabidopsis* cell suspension phosphoproteome in response to short-term low temperature and abscisic acid treatment. Physiologia Plantarum *129,* 687–697.

Fernie, A.R., Stitt, M., (2012) On the discordance of metabolomics with proteomics and transcriptomics: coping with increasing complexity in logic, chemistry, and network interactions. Plant Physiology. *158,* 1139–1145.

Fünfgeld, M.M.F.F., Wang, W., Ishihara, H., Arrivault, S., Feil, R., Smith, A.M., Stitt, M., Lunn, J.E., Niittylä, T., (2022) Sucrose synthases are not involved in starch synthesis in *Arabidopsis* leaves. Nature Plants *8,* 574–582.

Garlick, A.P., Moore, C., Kruger, N.J., (2002) Monitoring flux through the oxidative pentose phosphate pathway using [1-^{14}C] gluconate. Planta *216*. 265-272.

Geigenberger, P., Fernie, A.R., (2014) Metabolic control of redox and redox control of metabolism in plants. Antioxidants & Redox Signalling *21,* 1389–1421.

Gilmour, S.J., Sebolt, A.M., Salazar, M.P., Everard, J.D., Thomashow, M.F., (2000) Overexpression of the *Arabidopsis* CBF3 transcriptional activator mimics multiple biochemical changes associated with cold acclimation. Plant Physiology *124,* 1854–1865.

Goldsworthy, A., Street, H.E., (1965) The carbohydrate nutrition of tomato roots VIII. The mechanism of the inhibition by D-mannose of the respiration of excised roots. Annals of Botany *29*, 45–58.

Guy, C.L., Huber, J.L.A., Huber, S.C., (1992) Sucrose phosphate synthase and sucrose accumulation at low temperature. Plant Physiology *100,* 502–508.

Haldar, D., Sen, D., Gayen, K., (2017) Development of spectrophotometric method for the analysis of multi-component carbohydrate mixture of different moieties. Applied Biochemistry & Biotechnology *181,* 1416–1434.

Hannah, M.A., Wiese, D., Freund, S., Fiehn, O., Heyer, A.G., Hincha, D.K., (2006) Natural genetic variation of freezing tolerance in *Arabidopsis*. Plant Physiology *142,* 98–112.

Hansen, L.D., Thomas, N.R., Arnholdt-Schmitt, B., (2009) Temperature responses of substrate carbon conversion efficiencies and growth rates of plant tissues. Physiologia Plantarum *137,* 446–458.

Harper, A.D., Bar-Peled, M., (2002) Biosynthesis of UDP-Xylose. Cloning and characterization of a novel *Arabidopsis* gene family, UXS, encoding soluble and putative membrane-bound UDP-glucuronic acid decarboxylase isoforms. Plant Physiology *130,* 2188–2198.

Harwood, J.L., (1988) Fatty acid metabolism. Annual Review of Plant Physiology and Plant Molecular Biology *39,* 101–138.

Hasdai, M., Weiss, B., Levi, A., Samach, A., Porat, R., (2006) Differential responses of *Arabidopsis* ecotypes to cold, chilling and freezing temperatures. Annals of Applied Biology *148,* 113–120.

He, M., Qin, C.-X., Wang, X., Ding, N.-Z., (2020) Plant unsaturated fatty acids: biosynthesis and regulation. Frontiers in Plant Science *11,* 390.

Herold, A., Lewis, D.H., (1977) Mannose and green plants: Occurrence, physiology and metabolism, and use as a tool to study the role of orthophosphate. The New Phytologist *79,* 1–40.

Herold, A., Lewis, D.H., Walker, D.A., (1976) Sequestration of cytoplasmic orthophosphate by mannose and its differential effect on photosynthetic starch synthesis in C3 and C4 species. New Phytologist *76,* 397–407.

Herrmann, H.A., Dyson, B.C., Miller, M.A.E., Schwartz, J.-M., Johnson, G.N., (2021) Metabolic flux from the chloroplast provides signals controlling photosynthetic acclimation to cold in *Arabidopsis thaliana*. Plant, Cell & Environment *44,* 171–185.

Higgins, T.J.C., Easterby, J.S., (1974) Wheatgerm hexokinase: Physical and active-site properties. European Journal of Biochemistry *45,* 147–160.

Hirsche, J., García Fernández, J.M., Stabentheiner, E., Großkinsky, D.K., Roitsch, T., (2017) Differential effects of carbohydrates on *Arabidopsis* pollen germination. Plant and Cell Physiology *58,* 691–701.

Hou, F.-Y., Huang, J., Yu, S.-L., Zhang, H.-S., (2007) The 6-phosphogluconate dehydrogenase genes are responsive to abiotic stresses in rice. Journal of Integrative Plant Biology *49,* 655–663.

Irving, D.E., Silsbury, J.H., (1988) The respiration of mature field bean (*Vicia faba L.*) leaves during prolonged darkness. Annals of Botany *62,* 473–479.

Iyer, V.V., Sriram, G., Fulton, D.B., Zhou, R., Westgate, M.E., Shanks, J.V., (2008) Metabolic flux maps comparing the effect of temperature on protein and oil biosynthesis in developing soybean cotyledons. Plant Cell & Environment *31,* 506–517.

Izard, J., Limberger, R.J., (2003) Rapid screening method for quantitation of bacterial cell lipids from whole cells. Journal of Microbiological Methods *55,* 411–418.

Jang, J.C., Sheen, J., (1994) Sugar sensing in higher plants. Plant Cell *6,* 1665–1679.

Jiang, Z., Wang, M., Nicolas, M., Ogé, L., Pérez-Garcia, M.-D., Crespel, L., Li, G., Ding, Y., Le Gourrierec, J., Grappin, P., Sakr, S., (2022) Glucose-6-phosphate dehydrogenases: The hidden players of plant physiology. International Journal of Molecular Sciences *23,* 16128-16144.

Junker, B.H., Lonien, J., Heady, L.E., Rogers, A., Schwender, J., (2007) Parallel determination of enzyme activities and in vivo fluxes in *Brassica napus* embryos grown on organic or inorganic nitrogen source. Phytochemistry, Dynamic Metabolic Networks 68, 2232–2242.

Kaplan, F., Kopka, J., Haskell, D.W., Zhao, W., Schiller, K.C., Gatzke, N., Sung, D.Y., Guy, C.L., (2004) Exploring the temperature-stress metabolome of *Arabidopsis.* Plant Physiology *136,* 4159–4168.

Kaplan, F., Kopka, J., Sung, D.Y., Zhao, W., Popp, M., Porat, R., Guy, C.L., (2007) Transcript and metabolite profiling during cold acclimation of *Arabidopsis* reveals an intricate relationship of cold-regulated gene expression with modifications in metabolite content. The Plant Journal *50,* 967–981.

Kazemi-Shahandashti, S.-S., Maali-Amiri, R., (2018) Global insights of protein responses to cold stress in plants: Signaling, defence, and degradation. Journal of Plant Physiology *226,* 123–135.

Khavari-Nejad, R.A., Shekaste Band, R., Najafi, F., Nabiuni, M., Gharari, Z., (2013) The role of Pro-P5C cycle in chs mutants of *Arabidopsis* under cold stress. Russian Journal of Plant Physiology *60,* 375–382.

Kleijn, R.J., van Winden, W.A., van Gulik, W.M., Heijnen, J.J., (2005) Revisiting the ^{13}C-label distribution of the non-oxidative branch of the pentose phosphate pathway based upon kinetic and genetic evidence. FEBS Journal 272, 4970–4982.

Knight, J.A., Anderson, S., Rawle, J.M., (1972) Chemical basis of the sulfo-phospho-vanillin reaction for estimating total serum lipids. Clinical Chemistry *18,* 199–202.

Knol, M.J., Pestman, W.R., Grobbee, D.E., (2011) The (mis)use of overlap of confidence intervals to assess effect modification. European Journal of Epidemiology *26,* 253–254.

Knudson, L., (1917) The toxicity of galactose and mannose for green plants and the antagonistic action of other sugars toward these. American Journal of Botany *4,* 430–437.

Köhler, E., Barrach, H.J, Neubert, D., (1970) Inhibition of NADP dependent oxidoreductases by the 6-aminonicotinamide analogue of NADP. FEBS letters *6*, 225-228.

Krasavina, M.S., Burmistrova, N.A., Raldugina, G.N., (2014) The role of carbohydrates in plant resistance to abiotic stress. In: Ahmed, P., Rasool, S. eds. Emerging technologies and management of crop stress tolerance. San Diego CA: Academic Press, pp. 229 – 270.

Kruger, N.J., (2009) The Bradford method for protein quantitation. In: Walker, J.M. ed. The Protein Protocols Handbook 3rd edition. Totowa NJ: Humana Press, pp. 17-24.

Kruger, N.J., Masakapalli, S.K., Ratcliffe, R.G., (2012) Strategies for investigating the plant metabolic network with steady-state metabolic flux analysis: lessons from an *Arabidopsis* cell culture and other systems. Journal of Experimental Botany *63,* 2309–2323.

Kruger, N.J., Ratcliffe, R.G., (2015) Fluxes through plant metabolic networks: measurements, predictions, insights and challenges. Biochemical Journal *465,* 27–38.

Laidler, K.J., (1984) The development of the Arrhenius equation. Journal of Chemical Education. *61,* 494-498.

Laine, R.A., Sweeley, C.C., (1973) O-methyl oximes of sugars. Analysis as O-trimethylsilyl derivatives by gas-liquid chromatography and mass spectrometry. Carbohydrate Research *27,* 199–213.

Laine, R.A., Sweeley, C.C., (1971) Analysis of trimethylsilyl O-methyloximes of carbohydrates by combined gas-liquid chromatography-mass spectrometry. Analytical Biochemistry *43,* 533–538.

Landi, S., Capasso, G., Esposito, S., (2021) Different G6P dehydrogenase isoforms show specific roles in acclimation to cold stress at various growth stages of barley (*Hordeum vulgare*) and *Arabidopsis thaliana*. Plant Physiology and Biochemistry *169,* 190–202.

Le, X.H., Millar, A.H., (2022) The diversity of substrates for plant respiration and how to optimize their use. Plant Physiology *191,* 2133-2149.

Leakey, A.D.B., Xu, F., Gillespie, K.M., McGrath, J.M., Ainsworth, E.A., Ort, D.R., (2009) Genomic basis for stimulated respiration by plants growing under elevated carbon dioxide. Proceedings of the National Academy of Sciences of the USA *106,* 3597–3602.

Lei, D., Lin, Y., Luo, M., Zhao, B., Tang, Honglan, Zhou, X., Yao, W., Zhang, Yunting, Wang, Y., Li, M., Chen, Q., Luo, Y., Wang, X., Tang, Haoru, Zhang, Yong, (2022) Genome-wide investigation of G6P dehydrogenase gene in strawberry: Evolution and expression analysis during development and stress. International Journal of Molecular Science *23,* 4728-4742.

Levenberg, K., (1944) A method for the solution of certain non-linear problems in least squares. Quarterly of Applied Mathematics *2,* 164–168.

Li, B., Takahashi, D., Kawamura, Y., Uemura, M., (2020) Plasma membrane proteome analyses of *Arabidopsis thaliana* suspension-cultured cells during cold or ABA treatment: Relationship with freezing tolerance and growth phase. Journal of Proteomics *211*, 103528.

Li, B., Takahashi, D., Kawamura, Y., Uemura, M., (2012) Comparison of plasma membrane proteomic changes of *Arabidopsis* suspension-cultured cells (T87 Line) after cold and ABA treatment in association with freezing tolerance development. Plant and Cell Physiology *53,* 543–554.

Li, H., Su, J., Ma, W., Guo, A., Shan, Z., Wang, H., (2015) Metabolic flux analysis of *Saccharomyces cerevisiae* in a sealed winemaking fermentation system. FEMS Yeast Research *15*, 10.

Lin, Y., Lin, S., Guo, H., Zhang, Z., Chen, X., (2013) Functional analysis of PsG6PDH, a cytosolic glucose-6-phosphate dehydrogenase gene from *Populus suaveolens*, and its contribution to cold tolerance improvement in tobacco plants. Biotechnology Letters *35,* 1509–1518.

Liu, K., Zou, W., Gao, X., Wang, X., Yu, Q., Ge, L., (2019) Young seedlings adapt to stress by retaining starch and retarding growth through ABA-dependent and -independent pathways in *Arabidopsis*. Biochemical and Biophysical Research Communications *515,* 699–705.

Long, C.P., Antoniewicz, M.R., (2019a) High-resolution ^{13}C metabolic flux analysis. Nature Protocols *14*, 2856–2877.

Long, C.P., Antoniewicz, M.R., (2019b) Metabolic flux responses to deletion of 20 core enzymes reveal flexibility and limits of *E. coli* metabolism. Metabolic Engineering *55,* 249–257.

Long, C.P., Antoniewicz, M.R., (2014) Quantifying biomass composition by gas chromatography/mass spectrometry. Analytical Chemistry *86,* 9423–9427.

Loughman, B.C., Ratcliffe, R.G., Schwabe, J.W.R., (1989) Galactose metabolism in *Zea mays* root tissues observed by ^{31}P-NMR spectroscopy. Plant Science *59,* 11–23.

Maleszewski, S., Ciereszko, I., Skowrońska, A., Mieczejko, E., Kozłowska-Szerenos, B., (2004) Changes induced by low oxygen concentration in photosynthetic and respiratory CO_2 exchange in phosphate-deficient bean leaves. Biologia Plantarum *48,* 401–405.

Maruta, T., Yonemitsu, M., Yabuta, Y., Tamoi, M., Ishikawa, T., Shigeoka, S., (2008) *Arabidopsis* phosphomannose isomerase 1, but not phosphomannose isomerase 2, is essential for ascorbic acid biosynthesis. Journal of Biological Chemistry *283,* 28842–28851.

Masakapalli, S.K., Bryant, F.M., Kruger, N.J., Ratcliffe, R.G., (2014a) The metabolic flux phenotype of heterotrophic *Arabidopsis* cells reveals a flexible balance between the cytosolic and plastidic contributions to carbohydrate oxidation in response to phosphate limitation. The Plant Journal *78,* 964–977.

Masakapalli, S.K., Ritala, A., Dong, L., van der Krol, A.R., Oksman-Caldentey, K.M., Ratcliffe, R.G., Sweetlove, L.J., (2014b) Metabolic flux phenotype of tobacco hairy roots engineered for increased geraniol production. Phytochemistry *99*, 73-85.

Masakapalli, S.K., Kruger, N.J., Ratcliffe, R.G., (2013) The metabolic flux phenotype of heterotrophic *Arabidopsis* cells reveals a complex response to changes in nitrogen supply. The Plant Journal *74,* 569–582.

Masakapalli, S.K., Le Lay, P., Huddleston, J.E., Pollock, N.L., Kruger, N.J., Ratcliffe, R.G., (2010) Subcellular flux analysis of central metabolism in a heterotrophic *Arabidopsis* cell suspension using steady-state stable isotope labelling. Plant Physiology *152,* 602–619.

May, M.J., Leaver, C.J., (1993) Oxidative stimulation of glutathione synthesis in *Arabidopsis thaliana* suspension cultures. Plant Physiology *103,* 621–627.

McCleary, B.V., Matheson, N.K., (1976) Galactomannan utilization in germinating legume seeds. Phytochemistry *15,* 43–47.

McCormick, A.J., Kruger, N.J., (2015) Lack of fructose 2,6-bisphosphate compromises photosynthesis and growth in *Arabidopsis* in fluctuating environments. The Plant Journal *81,* 670–683.

McCree, K.J., (1974) Equations for the rate of dark respiration of white clover and grain sorghum, as functions of dry weight, photosynthetic rate, and temperature. Crop Science *14,* 509-514.

McCree, K.J., (1970) An equation for the rate of respiration of white clover grown under controlled conditions. Prediction and measurement of photosynthetic productivity. Proceedings of the IBP/PP Technical Meeting, Trebon, [Czechoslovakia], 221-229.

McCree, K.J., Troughton, J.H., (1966a) Prediction of growth rate at different light levels from measured photosynthesis and respiration rates. Plant Physiology. *41,* 559–566.

McCree, K.J., Troughton, J.H., (1966b) Non-existence of an optimum leaf area index for the production rate of white clover grown under constant conditions. Plant Physiology *41,* 1615–1622.

McMahon, A., Lu, H., Butovich, I.A., (2013) The spectrophotometric sulfo-phospho-vanillin assessment of total lipids in human meibomian gland secretions. Lipids *48,* 513–525.

Mele, L., Paino, F., Papaccio, F., Regad, T., Boocock, D., Stiuso, P., Lombardi, A., Liccardo, D., Aquino, G., Barbieri, A., Arra, C., Coveney, C., La Noce, M., Papaccio, G., Caraglia, M., Tirino, V., Desiderio, V., (2018) A new inhibitor of glucose 6-phosphate dehydrogenase blocks pentose phosphate pathway and suppresses malignant proliferation and metastasis *in vivo.* Cell Death and Disease *9*, 1-12.

Millar, A.H., Whelan, J., Soole, K.L., Day, D.A., (2011) Organization and regulation of mitochondrial respiration in plants. Annual Review of Plant Biology *62*, 79–104.

Minami, A., Fujiwara, M., Furuto, A., Fukao, Y., Yamashita, T., Kamo, M., Kawamura, Y., Uemura, M., (2009) Alterations in detergent-resistant plasma membrane microdomains in *Arabidopsis thaliana* during cold acclimation. Plant and Cell Physiology. *50,* 341–359.

Monroe, J.D., Storm, A.R., Badley, E.M., Lehman, M.D., Platt, S.M., Saunders, L.K., Schmitz, J.M., Torres, C.E., (2014) β-Amylase1 and β-Amylase3 are plastidic starch hydrolases in *Arabidopsis* that seem to be adapted for different thermal, pH, and stress conditions. Plant Physiology *166,* 1748-1763.

Moore, J.P., Vicré-Gibouin, M., Farrant, J.M., Driouich, A., (2008) Adaptations of higher plant cell walls to water loss: drought vs desiccation. Physiologia Plantarum *134,* 237–245.

Morgan, J.M., (1984) Osmoregulation and water stress in higher plants. Annual Review of Plant Physiology *35*, 299-319.

Moser, L.E., Volenec, J.J., Nelson, C.J., (1982) Respiration, carbohydrate content, and leaf growth of tall fescue. Crop Science *22,* 237-245.

Nägele, T., Kandel, B.A., Frana, S., Meissner, M., Heyer, A.G., (2011) A systems biology approach for the analysis of carbohydrate dynamics during acclimation to low temperature in *Arabidopsis thaliana.* FEBS Journal. *278,* 506–518.

Nanchen, A., Schicker, A., Sauer, U., (2006) Nonlinear dependency of intracellular fluxes on growth rate in miniaturized continuous cultures of *Escherichia coli.* Applied Environmental Microbiology *72,* 1164–1172.

Noor, E., Eden, E., Milo, R., Alon, U., (2010) Central carbon metabolism as a minimal biochemical walk between precursors for biomass and energy. Molecular Cell *39,* 809–820.

Oates, E.H., Antoniewicz, M.R., (2022) Coordinated reprogramming of metabolism and cell function in adipocytes from proliferation to differentiation. Metabolic Engineering. 69, 221-230.

O'Leary, B.M., Asao, S., Millar, A.H., Atkin, O.K., (2019) Core principles which explain variation in respiration across biological scales. New Phytologist *222,* 670–686.

Olsen, R.W., DeLorey, T.M., (1999) GABA synthesis, uptake and release. In: Siegel GJ, Agranoff BW, Albers RW, eds. Basic Neurochemistry: Molecular, Cellular and Medical Aspects. 6th edition. Philadelphia: Lippincott-Raven.

Pathirana, R., West, P., Hedderley, D., Eason, J., (2017) Cell death patterns in *Arabidopsis* cells subjected to four physiological stressors indicate multiple signalling pathways and cell cycle phase specificity. Protoplasma *254,* 635–647.

Pego, J.V., Weisbeek, P.J., Smeekens, S.C.M., (1999) Mannose inhibits Arabidopsis germination via a hexokinase-mediated step. Plant Physiology *119,* 1017–1024.

Penning De Vries F. W. T., (1975) The cost of maintenance processes in plant cells. Annals of Botany *39,* 77–92.

Penning De Vries F. W. T., (1974) Substrate utilization and respiration in relation to growth and maintenance in higher plants. Netherlands Journal of Agricultureal Science *22,* 40-44.

Penning De Vries F. W. T., (1972) Respiration and growth, in: Rees, A.R., Cockshull, K. E, Hand, D. W., Hurd, R. J. Eds. Crop Processes in Controlled Environments, Applied Botany. Academic Press, London pp. 327-347.

Plaxton, W.C., Podestá, F.E., (2006) The functional organization and control of plant respiration. Critical Reviews in Plant Sciences *25,* 159–198.

Plaxton, W.C., Tran, H.T., (2011) Metabolic adaptations of phosphate-starved plants. Plant Physiology *156,* 1006–1015.

Polko, J.K., Kieber, J.J., (2019) The regulation of cellulose biosynthesis in plants. Plant Cell *31,* 282–296.

Preiser, A.L., Banerjee, A., Weise, S.E., Renna, L., Brandizzi, F., Sharkey, T.D., (2020) Phosphoglucoisomerase is an important regulatory enzyme in partitioning carbon out of the Calvin-Benson cycle. Frontiers in Plant Science *11,* 580726.

Press, W.H., Teukolsky, S.A., Vetterling, W.T., Flannery, B.P., (1992) Numerical recipes in C: The art of scientific computing. Cambridge University Press, Cambridge pp. 304-316.

Price, N.P.J., (2004) Acylic sugar derivatives for GC-MS analysis of ^{13}C-enrichment during carbohydrate metabolism. Analytical Chemistry. *76,* 6566–6574.

Qian, W., Yu, C., Qin, H., Liu, X., Zhang, A., Johansen, I.E., Wang, D., (2007) Molecular and functional analysis of phosphomannomutase (PMM) from higher plants and genetic evidence for the involvement of PMM in ascorbic acid biosynthesis in *Arabidopsis* and *Nicotiana benthamiana.* The Plant Journal *49,* 399–413.

Quick, P., Siegl, G., Neuhaus, E., Feil. R., Stitt, M., (1989) Short-term water stress leads to a stimulation of sucrose synthesis by activating sucrose-phosphate-synthase. Planta *177*, 535-546.

Quirós, M., Martínez-Moreno, R., Albiol, J., Morales, P., Vázquez-Lima, F., Barreiro-Vázquez, A., Ferrer, P., Gonzalez, R., (2013) Metabolic flux analysis during the exponential growth phase of *Saccharomyces cerevisiae* in wine fermentations. PLoS ONE *8,* e71909.

R Core Team (2020). R: A language and environment for statistical computing.

Rasmusson, A.G., Geisler, D.A., Møller, I.M., (2008) The multiplicity of dehydrogenases in the electron transport chain of plant mitochondria. Mitochondrion *8,* 47–60.

Ratcliffe RG, Shachar-Hill Y. (2001) Probing plant metabolism with NMR. Annual Review of Plant Physiology and Plant Molecular Biology. *52:* 499-526.

Ratcliffe, R.G., Shachar-Hill, Y., (2006) Measuring multiple fluxes through plant metabolic networks. The Plant Journal *45,* 490–511.

Reed, J., Privalle, L., Powell, M.L., Meghji, M., Dawson, J., Dunder, E., Sutthe, J., Wenck, A., Launis, K., Kramer, C., Chang, Y.-F., Hansen, G., Wright, M., (2001) Phosphomannose isomerase: An efficient selectable marker for plant transformation. *In Vitro* Cellular and Developmental Biology - Plant *37,* 127–132.

Reid, J.S.G., (1971) Reserve carbohydrate metabolism in germinating seeds of T*rigonella foenum-graecum L. (Leguminosae)*. Planta *100,* 131–142.

Rhoads, D.M., Umbach, A.L., Subbaiah, C.C., Siedow, J.N., (2006) Mitochondrial reactive oxygen species. Contribution to oxidative stress and interorganellar signalling. Plant Physiology *141,* 357–366.

Robson, M.J., Parsons, A.J., (1981) Respiratory efflux of carbon dioxide from mature and meristematic tissue of Uniculm Barley during eighty hours of continuous darkness. Annals of Botany *48,* 727–731.

Rontein, D., Dieuaide-Noubhani, M., Dufourc, E.J., Raymond, P., Rolin, D., (2002) The metabolic architecture of plant cells. Stability of central metabolism and flexibility of anabolic pathways during the growth cycle of tomato cells. Journal of Biological Chemistry *277,* 43948–43960.

Sadava, D., Hillis, D.M., Heller, H.C., Berenbaum, M.R., (2013). Life: The Science of Biology, Tenth Edition. Sinauer Associates, Sunderland, MA.

Saha, B., Borovskii, G., Panda, S.K., (2016) Alternative oxidase and plant stress tolerance. Plant Signalling Behaviour *11,* e1256530.

Saltman, P., (1953) Hexokinase in higher plants. Journal of Biological Chemistry *200,* 145–154.

Sasaki, Y., Takahashi, K., Oono, Y., Seki, M., Yoshida, R., Shinozaki, K., Uemura, M., (2008) Characterization of growth-phase-specific responses to cold in *Arabidopsis thaliana* suspension-cultured cells. Plant, Cell & Environment *31,* 354–365.

Satyakam, Zinta, G., Singh, R.K., Kumar, R., (2022) Cold adaptation strategies in plants—An emerging role of epigenetics and antifreeze proteins to engineer cold resilient plants. Frontiers in Genetics *13.* 1664-8021

Schulte, C.C.M., Borah, K., Wheatley, R.M., Terpolilli, J.J., Saalbach, G., Crang, N., de Groot, D.H., Ratcliffe, R.G., Kruger, N.J., Papachristodoulou, A., Poole, P.S., (2021) Metabolic control of nitrogen fixation in rhizobium-legume symbioses. Scientific Advances *7,* 2375-2548

Schwender, J., Goffman, F., Ohlrogge, J.B., Shachar-Hill, Y., (2004) Rubisco without the Calvin cycle improves the carbon efficiency of developing green seeds. Nature *432,* 779–782.

Schwender, J., Ohlrogge, J.B., Shachar-Hill, Y., (2003) A flux model of glycolysis and the oxidative pentosephosphate pathway in developing *Brassica napus* embryos. Journal of Biological Chemistry. *278,* 29442–29453.

Seifter, S., Dayton, S., Novic, B., Muntwyler, E., (1950) The estimation of glycogen with the anthrone reagent. Archives of Biochemistry. *25,* 191–200.

Sharma, V., Ichikawa, M., Freeze, H.H., (2014) Mannose metabolism: More than meets the eye. Biochemical and Biophysical Research Communications *453,* 220–228.

Sharp, R.E., Poroyko, V., Hejlek, L.G., Spollen, W.G., Springer, G.K., Bohnert, H.J., Nguyen, H.T., (2004) Root growth maintenance during water deficits: physiology to functional genomics. Journal of Experimental Botany *55,* 2343–2351.

Sheu-Hwa, C.-S., Lewis, D.H., Walker, D.A., (1975) Stimulation of photosynthetic starch formation by sequestration of cytoplasmic orthophosphate. New Phytologist *74,* 383–392.

Skirycz, A., De Bodt, S., Obata, T., De Clercq, I., Claeys, H., De Rycke, R., Andriankaja, M., Van Aken, O., Van Breusegem, F., Fernie, A.R., Inzé, D., (2009) Developmental stage specificity and the role of mitochondrial metabolism in the response of *Arabidopsis* leaves to prolonged mild osmotic stress. Plant Physiology *152,* 226–244.

Slein, M.W., Cori, G.T., Cori, C.F., (1950) A comparative study of hexokinase from yeast and animal tissues. Journal of Biological Chemistry *186,* 763–780.

Smith, A.M., Stitt, M., (2007) Coordination of carbon supply and plant growth. Plant, Cell & Environment *30,* 1126–1149.

Smith, A.M.O., Ratcliffe, R.G., Sweetlove, L.J., (2004) Activation and function of mitochondrial uncoupling protein in plants. Journal of Biological Chemistry *279,* 51944–51952.

Smith, E.N., McCullagh, J.S.O., Ratcliffe, R.G., Kruger, N.J., (2019) Limitations of deuterium-labelled substrates for quantifying NADPH metabolism in heterotrophic *Arabidopsis* cell cultures. Metabolite *9.* 205-223.

Smith, E.N., Ratcliffe, R.G., Kruger, N.J., (2023) Isotopically non-stationary metabolic flux analysis of heterotrophic *Arabidopsis thaliana* cell cultures. Frontiers in Plant Science *13.* 1049559.

Smith, I.K., (1985) Stimulation of glutathione synthesis in photorespiring plants by catalase inhibitors. Plant Physiology *79,* 1044–1047.

Sols, A., Cadenas, E., Alvarado, F., (1960) Enzymatic basis of mannose toxicity in honey bees. Science *131,* 297–298.

Sriram, G., Fulton, B.D., Shanks, J.V., (2007) Flux quantification in central carbon metabolism of *Catharanthus_roseus* hairy roots by ^{13}C labelling and comprehensive bondomer balancing. Phytochemistry *68*, 2243-2257.

Sriram, G., González-Rivera, O., Shanks, J.V., (2006) Determination of biomass composition of *Catharanthus roseus* hairy roots for metabolic flux analysis. Biotechnology Progress *22,* 1659–1663.

Sriram, G., Shanks, J.V., (2004) Improvements in metabolic flux analysis using carbon bond labelling experiments: bondomer balancing and Boolean function mapping. Metabolic Engineering. *6,* 116–132.

Stein, J.C., Hansen, G., (1999) Mannose induces an endonuclease responsible for DNA laddering in plant cells. Plant Physiology *121,* 71–80.

Steinhardt, R.G., Calvin, A.D., Dodd, E.A., (1962) Taste-structure correlation with α-D-mannose and β-D-mannose. Science *135,* 367–368.

Stenlid, G., (2006) Toxic effects of D-mannose, 2-deoxy-d-glucose, and D-glucosamine upon respiration and ion absorption in wheat roots. Physiologia Plantarum *7,* 173–181.

Stenlid, G., (1971) The effect of some inhibitory sugars upon the content of adenosine triphosphate in wheat roots. Physiologia Plantarum *25,* 397–401.

Stenlid, G., (1959) Species differences between plant roots in the reaction to inhibitory sugars. Physiologia Plantarum *12,* 218–235.

Stenlid, G., (1957) A comparison of the toxic effects of some sugars upon growth and chloride accumulation in young wheat roots. Physiologia Plantarum *10,* 807–823.

Stephanopoulos, G., Vallino, J.J., (1991) Network rigidity and metabolic engineering in metabolite overproduction. Science *252,* 1675–1681.

Stevenson, C.C., Harrington, G.N., (2009) The impact of supplemental carbon sources on *Arabidopsis thaliana* growth, chlorophyll content and anthocyanin accumulation. Plant Growth Regulation *59,* 255–271.

Steward, F.C., (1965) Plant Physiology. A Treatise. Vol. 4A. Metabolism : Organic Nutrition and Nitrogen Metabolism. Cambridge, MA.

Stewart, R.A., Carrico, C.K., Webster, R.L., Steinhardt, R.G., (1971) Physicochemical stereospecificity in taste perception of α-D-mannose and β-D-mannose. Nature *234,* 220–220.

Stitt, M., Hurry, V., (2002) A plant for all seasons: alterations in photosynthetic carbon metabolism during cold acclimation in *Arabidopsis*. Current Opinion in Plant Biology *5,* 199–206.

Street, H.E., Lowe, J.S., (1950) The carbohydrate nutrition of tomato roots: II. The mechanism of sucrose absorption by excised roots. Annals of Botany *14,* 307–329.

Sweetlove, L.J., Beard, K.F.M., Nunes-Nesi, A., Fernie, A.R., Ratcliffe, R.G., (2010) Not just a circle: flux modes in the plant TCA cycle. Trends in Plant Science *15,* 462–470.

Sweetlove, L.J., Lytovchenko, A., Morgan, M., Nunes-Nesi, A., Taylor, N.L., Baxter, C.J., Eickmeier, I., Fernie, A.R., (2006) Mitochondrial uncoupling protein is required for efficient photosynthesis. Proceedings of the National Academy of Sciences of the USA *103,* 19587–19592.

Tännler, S., Decasper, S., Sauer, U., (2008) Maintenance metabolism and carbon fluxes in *Bacillus* species. Microbial Cell Factories *7,* 1–13.

Taymaz-Nikerel, H., Borujeni, A.E., Verheijen, P.J.T., Heijnen, J.J., van Gulik, W.M., (2010) Genome-derived minimal metabolic models for *Escherichia coli* MG1655 with estimated *in vivo* respiratory ATP stoichiometry. Biotechnology and Bioengineering *107*, 369-381.

Thalmann, M., Pazmino, D., Seung, D., Horrer, D., Nigro, A., Meier, T., Kölling, K., Pfeifhofer, H.W., Zeeman, S.C., Santelia, D., (2016) Regulation of leaf starch degradation by abscisic acid is important for osmotic stress tolerance in plants. The Plant Cell *28,* 1860–1878.

Thalmann, M., Santelia, D., (2017) Starch as a determinant of plant fitness under abiotic stress. New Phytologist *214,* 943–951.

Thomashow, M.F., (1999) Plant cold acclimation: freezing tolerance genes and regulatory mechanisms. Annual Review of Plant Physiology and Plant Molecular Biology. *50,* 571–599.

Thompson, M.R., Douglas, T. J., Obata-Sasamoto, H., Thorpe, T,A., (1986) Mannitol metabolism in cultured plant cells. Physiologia Plantarum *67*, 365-369.

Thornley, J.H.M., (1971) Energy, respiration, and growth in plants. Annals of Botany *35,* 721–728.

Tian, Y., Peng, K., Bao, Y., Zhang, D., Meng, J., Wang, D., Wang, X., Cang, J., (2021) Glucose-6-phosphate dehydrogenase and 6-phosphogluconate dehydrogenase genes of winter wheat enhance the cold tolerance of transgenic *Arabidopsis*. Plant Physiology and Biochemistry *161,* 86–97.

Todd, R., Tague, B.W., (2001) Phosphomannose isomerase: A versatile selectable marker for *Arabidopsis thaliana* germ-line transformation. Plant Molecular Biology Reports *19,* 307–319.

Töpfer, N., Caldana, C., Grimbs, S., Willmitzer, L., Fernie, A.R., Nikoloski, Z., (2013) Integration of genome-scale modelling and transcript profiling reveals metabolic pathways underlying light and temperature acclimation in *Arabidopsis*. Plant Cell *25,* 1197–1211.

Truernit, E., Stadler, R., Baier, K., Sauer, N., (1999) A male gametophyte-specific monosaccharide transporter in *Arabidopsis*. The Plant Journal *17,* 191–201.

Truong, Q., Koch, K., Yoon, J.M., Everard, J.D., Shanks, J.V., (2013) Influence of carbon to nitrogen ratios on soybean somatic embryo (cv. Jack) growth and composition. Journal of Experimental Botany *64,* 2985–2995.

Turgeon, R., Wolf, S., (2009) Phloem transport: Cellular pathways and molecular trafficking. Annual Review of Plant Biology *60,* 207–221.

Uemura, M., Warren, G., Steponkus, P.L., (2003) Freezing sensitivity in the *sfr4* mutant of *Arabidopsis* is due to low sugar content and is manifested by loss of osmotic responsiveness. Plant Physiology *131,* 1800–1807.

Valerio, C., Costa, A., Marri, L., Issakidis-Bourguet, E., Pupillo, P., Trost, P., Sparla, F., (2011) Thioredoxin-regulated β-amylase (BAM1) triggers diurnal starch degradation in guard cells, and in mesophyll cells under osmotic stress. Journal of Experimental Botany *62,* 545-555.

Valgepea, K., Adamberg, K., Vilu, R., (2011) Decrease of energy spilling in *Escherichia coli* continuous cultures with rising specific growth rate and carbon wasting. BMC Systems Biology *5,* 106-117.

van Dongen, J.T., Gupta, K.J., Ramírez-Aguilar, S.J., Araújo, W.L., Nunes-Nesi, A., Fernie, A.R., (2011) Regulation of respiration in plants: A role for alternative metabolic pathways. Journal of Plant Physiology *168,* 1434–1443.

Wahl, S.A., Dauner, M., Wiechert, W. (2004) New tool for mass isotopomer data evaluation in ^{13}C flux analysis: Mass isotope correction, data consistency checking, and precursor relationships. Biotechnology and Bioengineering *85*, 259-268.

Wang H.L., Lee, P.D., Chen W.L., Huang, D.J., Su, J.C., (2000) Osmotic stress-induced changes of sucrose metabolism in cultured sweet potato cells. Journal of Experimental Botany *51*, 1991-1999.

Warren Wilson, J., (1967) Ecological data on dry-matter production by plants and plant communities, in: Collection and Processing of Field Data, E.F. Bradley and O.T. Denmead Eds. John Wiley, New York pp. 77–123.

Wiechert, W., (2001) ^{13}C metabolic flux analysis. Metabolic Engineering. *3,* 195–206.

Wiechert, W., de Graaf, A.A., (1997) Bidirectional reaction steps in metabolic networks: I. Modelling and simulation of carbon isotope labelling experiments. Biotechnology and Bioengineering *55,* 101–117.

Williams, T.C.R., Miguet, L., Masakapalli, S.K., Kruger, N.J., Sweetlove, L.J., Ratcliffe, R.G., (2008) Metabolic network fluxes in heterotrophic *Arabidopsis* cells: stability of the flux distribution under different oxygenation conditions. Plant Physiology *148,* 704–718.

Williams, T.C.R., Poolman, M.G., Howden, A.J.M., Schwarzlander, M., Fell, D.A., Ratcliffe, R.G., Sweetlove, L.J., (2010) A genome-scale metabolic model accurately predicts fluxes in central carbon metabolism under stress conditions. Plant Physiology *154,* 311–323.

Wohl, K., James, W.O., (1942) The energy changes associated with plant respiration. The New Phytologist *41,* 230–256.

Wu, Y., Cosgrove, D.J., (2000) Adaptation of roots to low water potentials by changes in cell wall extensibility and cell wall proteins. Journal of Experimental Botany *51,* 1543–1553.

Yang, Y., Fu, Z., Su, Y., Zhang, X., Li, G., Guo, J., Que, Y., Xu, L., (2014) A cytosolic glucose-6-phosphate dehydrogenase gene, ScG6PDH, plays a positive role in response to various abiotic stresses in sugarcane. Scientific Reports *4,* 7090.

Young, J.D., (2014) INCA: a computational platform for isotopically non-stationary metabolic flux analysis. Bioinformatics *30,* 1333–1335.

Zalitis, J., Oliver, I.T., (1967) Inhibition of glucose phosphate isomerase by metabolic intermediates of fructose. Biochemistry Journal *102,* 753–759.

Zamboni, N., Fendt, S.-M., Rühl, M., Sauer, U., (2009) ^{13}C-based metabolic flux analysis. Nature Protocols *4,* 878–892.

Zanella, M., Borghi, G.L., Pirone, C., Thalmann, M., Pazmino, D., Costa, A., Santelia, D., Trost, P., Sparla, F., (2016) β-amylase 1 (BAM1) degrades transitory starch to sustain proline biosynthesis during drought stress. Journal of Experimental Botany *67,* 1819–1826.

Zhang, Yunting, Luo, M., Cheng, L., Lin, Y., Chen, Q., Sun, B., Gu, X., Wang, Y., Li, M., Luo, Y., Wang, X., Zhang, Yong, Tang, H., (2020) Identification of the cytosolic glucose-6-phosphate dehydrogenase gene from strawberry involved in cold stress response. International Journal of Molecular Science *21,* 7322.

Zhao, X., Tan, H.J., Liu, Y.B., Li, X.R., Chen, G.X., (2009) Effect of salt stress on growth and osmotic regulation in *Thellungiella* and *Arabidopsis* callus. Plant Cell, Tissue and Organ Culture *98*, 97-103.

Zhu, J., Alvarez, S., Marsh, E.L., LeNoble, M.E., Cho, I.-J., Sivaguru, M., Chen, S., Nguyen, H.T., Wu, Y., Schachtman, D.P., Sharp, R.E., (2007) Cell wall proteome in the maize primary root elongation zone. II. Region-specific changes in water soluble and lightly ionically bound proteins under water deficit. Plant Physiology *145,* 1533–1548.